ASSESSMENT OF WATER BALANCE COMPONENTS IN THE KRISHNA RIVER BASIN: A PERSPECTIVE OF CLIMATE AND LAND USE LAND COVER CHANGE

Submitted in partial fulfillment of the requirement for the award of the degree of

Doctor of Philosophy

In

CIVIL ENGINEERING

by

Suram Anil

Roll No. 718109

Under the Supervision of

Prof. P Anand Raj

DEPARTMENT OF CIVIL ENGINEERING

NATIONAL INSTITUTE OF TECHNOLOGY

WARANGAL-506004 INDIA

DECEMBER 2023

APPROVAL SHEET

This thesis entitled **"Assessment of Water Balance Components in the Krishna River Basin: A Perspective of Climate and Land Use Land Cover Change"** by **Mr. S Anil** is approved for the degree of Doctor of Philosophy.

Examiners

_____

_____

_____

Supervisor

Prof. P Anand Raj

Department of Civil Engineering, NIT Warangal

Chairman

Professor & Head

Department of Civil Engineering, NIT Warangal

Date:

NATIONAL INSTITUTE OF TECHNOLOGY WARANGAL

CERTIFICATE

This is certify that the thesis entitled "**Assessment of Water Balance Components in the Krishna River Basin: A Perspective of Climate and Land Use Land Cover Change**" being submitted by **Mr. S Anil** for award of the degree of Doctor of Philosophy to the Faculty of Engineering and Technology of National Institute of Technology Warangal is a record of bonafide research work carried out by her under my supervision and this thesis has not been submitted elsewhere for award for any other degree.

(P. ANAND RAJ)
Thesis supervisor
Emeritus Professor
Department of Civil Engineering
National Institute of Technology Warangal

DECLARATION

This is to certify that the work presented in the thesis entitled "**Assessment of Water Balance Components in the Krishna River Basin: A Perspective of Climate and Land Use Land Cover Change**" is a bonafide work done by me under the supervision of **Prof. P. Anand Raj** and was not submitted elsewhere for the award of any degree.

I declare that this written submission represents my ideas in my own words and where others' ideas or words have been included, I have adequately cited and referenced the original sources. I also declare that I have adhered to all principles of academic honesty and integrity and have nor misrepresented or fabricated or falsified any idea/data/fact/source in my submission. I understand that any violation of the above will be a cause for disciplinary action by the Institute and can also evoke penal action from sources which have thus not been properly cited or from whom proper permission has not been taken when needed.

Suram Anil
Roll No. 718109
Date:

ACKNOWLEDGEMENTS

The research work and the current thesis are outcomes of constant inspiration and help from a number of persons at various spheres of my association. I would like to convey my sincere gratitude to each and every one for their respective assistances.

With great pleasure and proud privilege, I express my deepest gratitude to my thesis Guide and Supervisor **Prof P. Anand Raj**, for his encouragement, constructive criticisms, timely advice, and patience throughout the course of this research work. Your keen interest and concern towards the successful completion of this research work, made me to overcome all the obstacle and proceed with the work. You always made me realise my strengths and capabilities which made me more responsible towards the work. I thank you for distilling the thesis to get a more refined one, even at the far end. **Thanks a lot sir.**

I am very much thankful to **Prof. T D Gunneswara Rao** Head, Department of Civil Engineering for his constant support and encouragement.

I take immense pleasure to thank all the members of my Doctoral Scrutiny Committee, **Prof. N. V. Umamahesh, Prof. K Venkata Reddy** and **Prof. D. Srinivasacharya** for their detailed review, constructive suggestions and excellent advice during the course of this research work.

I am sincerely thankful to my faculties Dr. Vema Vamsi Krishna, Prof K.V. Jayakumar, Shri. V. N. Kameswara Rao, Dr. Litan Kumar Ray for their support in my PhD course.

I would like to my deepest gratitude to our team including my friends, especially Mr. V Manikanta and Mr. V Manohar Reddy for all the useful insights and assistance and offered during the course of work. Throughout the ups and downs, there are some close friends and my cricket team who have stood my side, offering words of motivation, understanding my moments of stress, and celebrating each milestone achieved. I would like to express my deepest gratitude to Mr. T. Aravind Rao, Mr. M. Sagar Kumar, Mr. Aadi Naresh, Mr. M. Rafi, Mr. G. V. Sai Krishna Reddy, Mr. Kandula Srikanth and Mr. Amgoth Ashok for their constant support during my journey.

I place on record my special thanks to my brother **Mr. Suram Ashok** and my friend **Mr. Arram Viay Kumar Reddy** for providing constant encouragement and moral support throughout my life. I acknowledge their love and affection towards me.

The affection and prayer of my parents, especially my father, mother and my brother-in-law's can never be forgotten at this juncture. Above all, I humbly acknowledge the grace and blessings of God Almighty, which enlightened my path throughout.

(Suram Anil)

CONTENTS

LIST OF TABLES x
LIST OF FIGURES xi
ABBREVIATIONS xiv
ABSTRACT xv
CHAPTER 1 INTRODUCTION 1
1.1 General 1
1.2 Studies on Climate Change 2
1.3 Ranking of GCMs 3
1.4 Climate Change on Precipitation 4
1.5 Climate Extremes 5
1.6 Climate Change Impact on Hydrological Modelling 6
1.7 Impact of Climate and LULC Change on Hydrology 6
1.8 Motivation for Research and Problem Formulation 7
1.9 Scope and Objectives of the Study 9
1.10 Research Gaps Identified 9
1.11 Organisation of Thesis 10
CHAPTER 2 LITERATURE REVIEW 11
2.1 General 11
2.2 Global Climate Models (GCMs) 12
2.3 Bias Correction Techniques 13
2.4 GCM Ranking Procedure 13
2.5 Climate Extremes Effects 16
2.6 Hydrological Modelling and Impact Studies 20
2.7 Research Gaps Identified From Literature and Summary 25
CHAPTER 3 METHODOLOGY 27
3.1 General 27
3.2 Study Area 30
3.2.1 General 30
3.2.2 India 30
3.2.3 Krishna River Basin 30
3.3 Data used in the study 31
3.3.1 Indian Meteorological Department (IMD) data 33
3.3.2 CMIP6-GCM data 33
3.3.3 Hydrological data 33
3.3.4 Geo-Spatial data 34
3.4 Procedure Involved in Subjectivity of GCM Rankings 36
3.4.1 Payoff Matrix 37
3.4.2 Objective Weights of Criteria 38
3.4.3 MCDM Techniques 39
3.4.3.1 Fuzzy TOPSIS (FTOPSIS) 39
3.4.3.2 Compromise Programming (CP) 40
3.5 Precipitation Projection across KRB 40
3.5.1 Quantile Mapping Bias Correction 41
3.5.2 Symmetric Uncertainty (SU) for Selection of GCMs 42
3.5.3 GCMS Ranking Using MCDM 43

3.5.4 Reliability Ensemble Averaging (REA) 43
3.6 Precipitation Extremes Calculation 45
3.6.1 Trend analysis 45
3.6.2 Correlation Analysis 47
3.7 Hydrological Model Set Up 47
3.7.1 LULC change under SSP-RCP scenarios 49
3.8 Summary 50
CHAPTER 4 RESULTS AND DISCUSSIONS 51
4.1 General 51
4.2 Ranking of CMIP6-GCMs for T_{max} and T_{min} 51
4.2.1 Ranking Pattern with IMD Dataset 51
4.2.2 Ranking Patterns with CPC Dataset 54
4.2.3 Sensitivity Analysis of Ranking Patterns 56
4.2.4 Conclusions 59
4.3 Projections of Precipitation in the KRB 60
4.3.1 Generation of Multi Model Ensemble (MME) 62
4.3.2 Changes in Annual Precipitation 63
4.3.3 Changes in Seasonal Precipitation 65
4.3.4 Discussions 67
4.3.5 Conclusions 68
4.4 Climate Extremes Analysis in KRB 69
4.4.1 GCMs Selection 69
4.4.2 Trend Analysis 72
4.4.3 Correlation Analysis 74
4.4.4 Analysis of Inter-annual Variation 75
4.4.5 Future Changes in Extremes Precipitation Indices 77
4.4.6 Projected Changes in Future Discharge 81
4.4.7 Conclusions 83
4.5 SWAT Application for Hydrological Modelling in KRB 84
4.5.1 SWAT Model Performance Evaluation 84
4.5.2 Climate Change Impact on WBC in the KRB 88
4.5.3 Climate Change Impact on ISMR Season in the KRB 99
4.5.4 Climate Change Impact on Mean Monthly Flows 102
4.5.5 Discussion 103
4.5.6 Conclusions 104
4.6 Coupled Impact of Climate and LULC Change on WBC of TRB 105
4.6.1 SWAT Performance on TRB Hydrological Modelling 106
4.6.2 LULC Change under SSP-RCP Scenarios 108
4.6.3 Projections of WBCs 110
4.6.4 Seasonal Flow Variation Under Both Climate and LULC Change 115
4.6.5 Conclusions 117
4.7 Closure 117

CHAPTER 5 **SUMMARY AND CONCLUSIONS** 118
5.1 Summary 118
5.2 Conclusions 120
5.3 Contributions From the Study 124
5.4 Limitations of the Study 125
5.5 Scope of further Studies 125
REFERENCES 126
PUBLICATIONS FROM RESEARCH 147

LIST OF TABLES

Table No.	Title	Page No.
3.1	CMIP6 climate models and their sources used for the research study	35
3.2	Model performance evaluation metrics with respective equations, range and ideal values	37
3.3	Extreme precipitation indices and seasonal precipitation indices and their definitions (PP = Precipitation).	45
4.1	Grids with invariant rankings for each individual component with the combinations	58
4.2	Ensemble of GCMs for each climate zone over India	59
4.3	Calibrated Parameters of SWAT model	85
4.4	Performance evaluation values for calibration and validation at Vijayawada gauge station for monthly simulations	86
4.5	Performance evaluation values for calibration and validation at different stations	87
4.6	Comparison of WBC for 9 GCMs and the observed data during the baseline period (1973-2003) for annual period	93
4.7	Comparison of annual average historical precipitation of 9 GCMs with respect to same GCM for the future period scenarios (GCM 1 to 9 represents, BCC-CSM2-MR, EC-Earth3, EC-Earth3-Veg, GFDL-ESM4, IPSL-CM6A-LR, MPI-ESM1-2-HR, MPI-ESM1-2-LR, NorESM2-LM and NorESM2-MM respectively	94
4.8	Impact of climate change on the annual average WBC for KRB with uncertainty bounds	95
4.9	Effect of climate change on the WBC of the KRB (The value in the bracket represents relative change between the GCM historical ensemble average and future scenarios	96
4.10	The expected absolute values for the annual period due to climate change impact (The values in the brackets represents the +/-1 standard deviation values of expected absolute values)	98
4.11	Impact of climate change on the WBC for KRB with prediction bounds for annual average ISMR	99
4.12	Percentage deviation (in brackets) of WBC due to climate change over KRB for ISMR season	100
4.13	The expected absolute values for the annual ISMR period due to climate change impact (The values in the brackets represents the +/-1 standard deviation values of expected absolute values)	101
4.14	Calibrated Parameters used in the TRB study for the SWAT model	107
4.15	Performance evaluation at Mantralayam discharge location	108
4.16	LULC variation from 2015 to 2100 in percent change	109
4.17	Climate and LULC impact on the WBC for TRB with uncertainty bounds	113

LIST OF FIGURES

Figure No.	Title	Page No.
3.1	Overall Methodology of research work	28
3.2	Proposed methodology to rank GCMs using various combinations	29
3.3	Location map of the Study area	32
3.4	Geographical distribution of precipitation over KRB for mean Annual (left), Monsoon (middle) and Pre-monsoon (right) prepared from IMD data for 1985-2014	33
3.5	DEM, LULC and soil maps for Krishna and Tungabhadra river basins	34
3.6	Quantile Mapping bias correction of a grid point in KRB	41
3.7	Geographical location along with model set up of KRB	49
3.8	Soil map and watershed delineation of the TRB	49
4.1	Gridwise ranking of GCMs for Maximum Temperature (T_{max}) for IMD	52
4.2	Gridwise ranking of GCMs for Minimum Temperature (T_{min}) for IMD	52
4.3	Spatial distribution of GCMs with constant ranking patterns using 8 different ranking procedures for IMD, T_{max} (left) and T_{min} (right) dataset	53
4.4	Gridwise ranking of GCMs for Maximum Temperature (T_{max}) for CPC	54
4.5	Gridwise ranking of GCMs for Minimum Temperature (T_{min}) for CPC	55
4.6	Spatial distribution of GCMs with constant ranking patterns using 8 different ranking procedures for CPC, T_{max} (left) and T_{min} (right) dataset	55
4.7	KRB with different climate classification zones	60
4.8	The spatial ranking positions of GCMs at 1st, 2nd and 3rd place using SU over KRB gird locations for precipitation	60
4.9	Histogram of Total Ranking Weight and final ranking positions of models used	61
4.10	Scatter plot of IMD and individual GCMs, and REA estimated MME mean rainfall averaged over KRB for the period 1985–2014	62
4.11	Boxplot displaying statistical metrics derived at various grid positions for individual GCM precipitation and MME mean precipitation in relation to IMD precipitation	63
4.12	Variations (%) in the annual mean precipitation in four SSP scenarios and three future periods in various KRB regions at a 95% confidence level	64
4.13	Change (%) in annual average precipitation in KRB for different SSPs for three future periods, 2015-2040, 2041-2010 and 2071-2100	65
4.14	Projected monthly rainfall changes (%) at different climate zones in KRB for three future periods	66
4.15	Change (%) in average monsoon precipitation in KRB for different SSPs for three future periods, 2015-2040, 2041-2010 and 2071-2100	67
4.16	Ranking of each GCM based Total Ranking Weight (TRW)	70
4.17	Spatial distribution of the top ranked GCMs	70
4.18	Average annual spatial distribution of precipitation extremes during baseline period (1973-2003) in the KRB	71
4.19	Precipitation percentage contributions of RX1day and RX5day to TOTPR during baseline period (1973-2003) in the KRB	72

4.20	Number of grid points exhibiting different trends for ETCCDI indices	73
4.21	Grid-wise trend analysis for different extreme indices in the KRB during baseline period	73
4.22	Correlation between precipitation extremes and AADD and MADD	75
4.23	Anomalies of the different precipitation extremes in the KRB. ((g) represents the absolute ratios in percentage	76
4.24	Comparison of inter-annual variation of precipitation extremes for NF, and FF under SSP1-2.6 (Shaded region represents the ranges of selected climate models and solid line represents the MME average of the GCMs) with the baseline period	78
4.25	Comparison of inter-annual precipitation extremes variations in the NF, FF period under SSP2-4.5 with the baseline period	78
4.26	Comparison of inter-annual precipitation extremes variations in the NF, FF period under SSP3-7.0 with the baseline period	79
4.27	Comparison of inter-annual precipitation extremes variations in the NF, FF period under SSP5-8.5 with the baseline period	79
4.28	Relative changes (in percentage) of precipitation extremes of MME mean with respect to base period	80
4.29	Spatial distribution of relative changes in extreme indices under SSP5-8.5 scenario for FF (2065-2095)	81
4.30	Comparison of AADD of observed and historical climate models and their MME in the baseline period 1973-2003	82
4.31	Variations of inter-annual AADD estimated from TOTPR of selected climate models and their MME under four SSP scenarios	83
4.32	Depiction of simulated and observed streamflow for calibration and validation period	86
4.33	Depiction of simulated and observed streamflow for calibration and validation period at different gauge stations	87
4.34	Average annual precipitation under different SSP scenarios in comparison with observed IMD data	89
4.35	Average annual surface runoff under different SSP scenarios in comparison with observed IMD data	90
4.36	Average annual water yield under different SSP scenarios in comparison with observed IMD data	91
4.37	Average annual streamflow under different SSP scenarios in comparison with observed IMD data	92
4.38	Simulated mean monthly streamflow under different SSP scenarios in the future periods	103
4.39	Correlation between simulated and observed discharge	107
4.40	LULC fluctuation for three future periods under both SSP1-2.6 and SSP5-8.5 scenarios in comparison to the base year map (2015)	109
4.41	Projected annual precipitation variability under scenarios SSP1-2.6 and SSP5-8.5	110
4.42	Projected mean annual temperature variability under scenarios SSP1-2.6 and SSP5-8.5	110
4.43	Relative change in the average annual precipitation in the future periods	111
4.44	Mean annual precipitation variation under different GCMs compared to IMD data	112

4.45	Simulated mean annual WBC comparison i.e. (a) Surface runoff (SurQ), (b) Water Yield (WY), (c) Groundwater (GWq), (d) Evapotranspiration (ET) and Soil moisture (SW) with reference to baseline (1980–2010) due to combined impact climate and LULC change	115
4.46	Streamflow variation at month scale for the IMD period (1981–2010) and the future period (2026 to 2100) for both SSP1-2.6 and SSP5-8.5 scenarios due to combined impact climate and LULC change	116

LIST OF ABBREVIATIONS

AADD	Average Annual Daily Discharge
BD	Bhattacharya Distance
BS	Brier Score
CDF	Cumulative Distribution Function
CMIP3	Couple Model Intercomparison Project phase 3
CMIP5	Coupled Model Intercomparison Project 5
CMIP6	Coupled Model Intercomparison Project 6
CP	Compromise Programming
CRITIC	Criteria Importance Through Intercriteria Correlation
CWC	Central Water Commission
DEM	Digital Elevation Model
ESGF	Earth System Grid Federation
ETCCDI	Expert Team of Climate Change Detection Indices
FAO	Food and Agriculture Organisation
FoM	Figure of Merit
GCM	Global Climate Model
GHG	Green House Gases
IMD	Meteorological Department
IPCC	Intergovernmental Panel on Climate Change
IRBs	Indian River Basins
KGE	Kling Gupta Efficiency
MADD	Maximum Annual Daily Discharge
MAE	Mean Absolute
MCDM	Multi-Criteria Decision Making
MI	Mutual Information
MME	Multi Model
NSE	Nash Sutcliff Coefficient
OA	Overall Accuracy
PBIAS	Percentage of Bias
PDF	Probability Density Function
QM	Quantile Mapping
R4MS4	Fourth Root Mean Square Error
RCP	Representative Concentration Pathway
REA	Reliability Ensemble Averaging
RCMs	Regional Climate Models
SSPs	Shared-Socioeconomic Pathways
SU	Symmetric Uncertainty
SUFI-2	Sequential Uncertainty Fitting
SWAT	Soil and Water Assessment Tool
SVM	Support Vector Machine
TOPSIS	Technique for Order Preference by Similarity to an Ideal Solution
WBC	Water Balance Components
WRIS	Water Resources

ABSTARCT

Natural resources like water have a direct or indirect impact on the ecological and socioeconomic development of a region. In a given location, variations in the land cover, weather, geology, morphological factors such as basin slope and topography, climate change and human activity all contribute to changes in the water budget both spatially and temporally. A worldwide phenomenon, climate change affects different regions to differing degrees. The assessment of climate change effects across a river basin has become essential for effective water resource management due to the accelerating rate of climate change. With this climate change, the changes in Land Use Land Cover (LULC) over a long period in a regional scale is also plays a key role for the availability of water resources. Several Global Climate Models (GCMs) have been generated to forecast the earth's climate in a variety of conceivable futures. GCMs are numerical simulations of distinct physical processes that reflect the seas, land surface, atmosphere, cryosphere and among other components of the global climate system. Policymakers can create recommendations and mitigation plans by using the future climate projections to comprehend the possible effects of climate change. However, the direct use GCMs for the climate change projections in a regional scale may lead to large uncertainty in the results due to their larger spatial resolution. And performance of GCMs are region specific due their coarser resolution, structure, parameterization, boundary conditions and so on. The GCMs are need to be bias corrected and selection of suitable GCMs are necessary before using in the regional scale climate change studies. The need for water is growing worldwide due to population growth and the expansion of cities, industries and agriculture, all of which are causing a decline in the amount of freshwater resources available. Consequently, it is necessary to look into the hydrological changes linked to climate change in order to secure water availability and promote sustainable development, particularly in an agricultural nation like India.

In this study, the GCMs of Coupled Modelled Intercomparison Project 6 (CMIP6) phase repositories are considered for climate change projections in a river basin. This study used Tier-1 Shared-Socioeconomic Pathways (SSPs) scenarios that include SSP1-2.6, SSP2-4.5, SSP3-7.0 and SSP5-8.5 to provide a full range of forcing targets similar in both magnitude and distribution to the RCPs used in CMIP5. In the present work the comprehensive analysis of climate change and their extremes in a river basin is analysed using Multi Model Ensemble (MME) of CMIP6-GCMs.

Initial phase of research work is devoted to investigate the subjectivity involved in the ranking of CMIP6-GCMs using maximum and minimum temperature (T_{max} and T_{min}) across India. Different ranking procedures are employed, encompassing a variety of components in the process, such as model evaluation criteria, criteria weight allocation methods, Multi-Criteria Decision Making (MCDM) techniques and reference gridded datasets. The effect of each individual component on the ranking pattern is systematically analysed and the spatial distribution of grids with same ranking patterns across all the combinations are considered as grids with same ranking. The performance of best performing GCMs are attributed to homogenous climatic zones of India and its corresponding topological features. An ensemble of frequently performing top five GCMs among 16 different ranking procedures are extracted for each climate zone as the most suitable set of GCMs.

The second part of the study work, focused on climate change impact on a river basin in India. The Krishna River Basin (KRB), which is heavily exploited and extremely vulnerable to climate change, was studied to assess the effects of climate change under several forcing scenarios. The concept of Symmetric Uncertainty (SU) is employed on monthly scale to select the top five GCMs. Reliability Ensemble Averaging (REA) approach is used to allocate the weights of selected GCMs to analyse the spatio-temporal analysis of precipitation variation across the KRB. The MME mean of the chosen GCMs showed significant changes in precipitation projection that occurs for a far future period (2071–2100) over the KRB. The projection changes of precipitation range from -36.72 to 83.05% and -37.68 to 95.75% for the annual and monsoon periods, respectively, for various SSPs. Monsoon climate projections show higher changes compared with the annual climate projections, which reveals that precipitation concentration is more during the monsoon period over the KRB.

This study draws attention to the better comprehension of spatio-temporal analysis of climate changes based on precipitation extremes and projection of future streamflow for efficient management of water resources in KRB. Grid-wise trend analysis reveals that there are more number of decreasing trends in extreme precipitation indices than increasing trends for the observed period 1973-2003. It is observed that the percentage contributions of maximum one-day (RX1day) and five-day (RX5day) precipitation indices to the annual total precipitation indices are more important. It is found that in future periods, the precipitation extremes based on Expert Team of Climate Change Detection Indices (ETCCDI) are expected to increase. The projection of future streamflow in the KRB is done using a Support Vector Machine (SVM)

and is expected to increase under different SSPs. These precipitation extremes may increase the chance of hydrological calamities in the future across the basin.

This study assesses the impacts of climate change on the water balance of KRB in India. A frequency-based metric, known as SU, is used to select the top 50% of GCMs from a pool of eighteen CMIP6-GCMs for hydrological modelling. The impact of climate change is projected for three future time frames: Near Future (NF: 2026-2050), Mid Future (MF: 2051-2075) and Far Future (FF: 2076-2100) using four scenarios from SSPs: SSP1-2.6, SSP2-4.5, SSP3-7.0 and SSP5-8.5. Soil and Water Assessment Tool (SWAT) model is used to simulate climate change impact on historical and future periods in the basin. The SWAT model was calibrated and validated using the Sequential Uncertainty Fitting (SUFI-2) technique of the SWAT calibration and uncertainty programme (SWAT-CUP). The results show a significant increase in the annual average precipitation, surface runoff, water yield and streamflow in the future under all SSP scenarios. The increase in the projected annual average precipitation is ranged from 12% to 54% for four SSP scenarios compared to the historical ensemble average. The ensemble average of Indian Summer Monsoon Rainfall (ISMR) precipitation is projected to increase in the range of 13.7% to 55% for the future period compared to historical GCMs ensemble average of baseline period. The highest precipitation, water yield, surface runoff and streamflow are projected to increase 54%, 125%, 124% and 114.5% respectively in FF under SSP5-8.5 scenario compared to ensemble average of baseline period. Precipitation change has a significant influence on future streamflow, with projections showing a potential increase of 31 to 114.5%. Future periods show a shift in the monthly peak flows as compared to the baseline period. More availability of water in the future in the KRB can be effectively used for various water management works.

In this research work the combined impact of climate and LULC change over Tungabhadra River Basin (TRB) was analysed. TRB is one of the major tributary of KRB, which is very essential water resource for the Karnataka state in India. The developed future land use dataset based on SSP-RCP framework for the years 2015 to 2100 is used in this investigation. The LULC for the base year 2015 and future periods under two SSP scenarios, SSP1-2,6 and SSP5-8.5 are forced for the hydrological SWAT model. In the calibration period, both coefficient of determination (R^2) and Nash Sutcliff Coefficient (NSE) is obtained as 0.75 and for the validation period these values are obtained as 0.72 and 0.7 respectively. The simulated major land use classes are identified in Tungabhadra basin as water (1.41%), built-up (0.23%), cropland (76.23%), barren land (9.3%), forests (12.8%) and grassland (0.04%) as per the LULC

of the year 2015. The grass land and barren land is totally converted to cropland in the future under SSP585 scenario where as in case of SSP1-2.6 scenario only barren land totally converted to cropland. The grassland is projected to decrease from 8.37% to 1.61%, a reduction of 6.76% in the FF under SSP1-2.6 scenario. The urbanization and cropland are projected to extend up to 0.59% and 87.88% respectively under SSP5-8.5 scenario till 2100. There is no significant change in the forest cover under SSP1-2.6 scenario but under SSP5-8.5 it has shown small decline by 2.92% in the future. By the end of the twenty-first century, the ensemble mean temperature is predicted to increase by 1.56 ^{o}C and 4.65 ^{o}C, respectively, under the SSP1-2.6 and SSP5-8.5 scenarios. The results show that the WBC such as Surface runoff (SurQ), Groundwater (GWq), and Water Yield (WY) are also following the significant increasing trend with the precipitation. Peak streamflow for all the GCMs are varying between months of August and September under both SSP scenarios.

The findings of this study on the Krishna River's climate change impact can be utilised to create appropriate adaptation plans for the management of these basins' water resources. The research work's methodology can be applied to various river basins in India and around the globe.

Keywords: GCM, Performance metrics, MCDM techniques, River basin, Symmetric Uncertainty, Climate Change Impacts, LULC, WBC and Stremflow

CHAPTER 1

INTRODUCTION

1.1 General

India is a historic, tropical nation where the primary industry is agriculture, which requires abundant water to flourish. The primary water sources for home and agricultural usage are groundwater from open wells and surface water from streams, rivers, lakes and man-made ponds to a large extent. The Himalayas are the source of several rivers in the country's north, which deposit a lot of gravel and alluvium as sediments in the northern plains. The region is extremely fruitful because to the good temperature and sufficient water supply in the Ganges and Indus plains, which are dominated by alluvium deposits. The Deccan plateau and central islands of the peninsula are home to the Narmada, Tapti, Mahanadi, Godavari, Krishna and Kaveri rivers, which are the primary water sources in the area. Groundwater is regarded as a primary supply for household and irrigation needs. A water demand is the amount of water needed to meet a particular need. The amount of water needed for crops, percolation losses, canal seepage and evaporation all count towards the agricultural water demand. The availability of water in India, a developing country, undergoes spatial and seasonal variations that impact societal development. Geographical factors like land use, vegetation and topography further contribute to this dynamic situation. Over the last century, the surge in population and the expansion of economic activities have significantly escalated water usage in many regions across the world. The key element in the water cycle, streamflow, is intricately linked to meteorological factors such as precipitation intensity, amount and duration, temperature, evapotranspiration and relative humidity.

Climate refers to the long-term fluctuations in a region's temperature, humidity, air pressure, wind, precipitation and other meteorological factors. Location, air pressure, mountain barriers, height, continental position, ocean currents, wind belts, storms and human activity are the variables that determine climate. The monsoon climate condition dominates the climatic zones of India. In India, the distribution of monsoon precipitation varies greatly in terms of both time and space (Kripalani et al., 2007). Two primary factors that impact climate conditions are temperature and precipitation. In this regard, it is anticipated that by 2050, the annual mean surface temperature will have increased by 3.5 to 5.5°C overall, the winter season will have warmed and the amount of precipitation in central India would have decreased by roughly 10 to 20% which effects the hydrological process (Mall et al., 2006). The South-West monsoon

brings India its highest rainfall between June and September. On the other hand, the North-East monsoon, which occurs between October and November, primarily affects the state of Tamilnadu in south India.

1.2 Studies on Climate Change

The Intergovernmental Panel on Climate Change (IPCC) defines climate change as a shift in the parameters' mean and/or variability over time brought on by both natural and human activity. According to the IPCC (2021), there has been an increase in the frequency of extreme weather occurrences, including powerful heat waves, intense hot extremes, extreme precipitation, floods and droughts in agriculture conditions. The IPCC AR5 study revealed an unparalleled increase in the earth's surface temperature in the past few decades, leading to significant adverse effects on climate parameters, as well as the biological, chemical and hydrological cycles worldwide. A substantial increasing trend has been noticed in the global temperature owing to the accelerating concentration of Green House Gases (GHG) in the atmosphere and it is expected to increase by 1.8 to 4 ^{o}C by the end of the 21st century as per 5th Assessment Report (AR5) of (IPCC, 2013). Due to these effects the changes are expected in the availability of water and associated climate extremes, such as floods and droughts in river basins, as a result of fluctuations in the climatological parameters.

Climate models are instruments for determining how future natural processes and human activity can impact a region's ecosystem. There are two types of tools for the assessment of climate change studies i.e., Global Climate Models (GCMs) and Regional Climate Models (RCMs). GCMs are numerical models that mimic various physical processes that represent different components of the global climate system such as atmosphere, land surface, oceans and cryosphere (Gouda et al., 2018). Gaps exist between the spatial and temporal realisation of hydrological features and GCMs, making it impossible for GCMs to accurately mimic hydro-meteorological processes at a finer scale. The resolution of GCMs is too coarse to be used as an input for studies on climate change and the raw outputs from GCMs are frequently biased with systematic errors when compared to the observed parameters. The future climate projections enables the policymakers to understand the potential impacts of climate change and to form recommendations and mitigation measures (Nashwan & Shahid, 2019). However, the performance of a climate model is region specific due to the uncertainties attributable to the model structure, parametrization, calibration and so on (IPCC, 2013; Mcsweeney & Jones, 2016). Due to these uncertainties, increasing attention has been given to the ranking of GCMs

in simulating the present climate (Kamworapan & Surussavadee, 2019; Khayyun et al., 2020; Raju et al., 2017; Singh et al., 2015).

IPCC continuously releasing many GCMs based on the greenhouse gas emission scenarios as mentioned in the various Assessment Report (AR) from 1992 to 2018. The 5th AR of IPCC generated Representative Concentration Pathways (RCPs) to illustrate the various stages of greenhouse gas emissions as well as additional radiative forcings that could have an impact in the future. There are four routes (2.6, 4.5, 6.0 and 8.5 watt/m^2) that cover a broad range of forcing, but they lack any socioeconomic "narratives." The Shared Socio-economic Pathways (SSPs), based on five narratives that depict major socio-economic patterns that might affect society in the future, are developed by the IPCC 6th Assessment Report (AR6) to connect a wide range of research communities, including those involved in climate change mitigation and adaptation activities. SSP1-2.6, which represents the low end of the range of future forcing pathways with 2.6 W/m^2 radiative forcing, SSP2-4.5, which represents the medium end of the range of future pathways with 4.5 W/m^2 radiative forcing, SSP3-7.0, which represents the medium to high end of the range of future forcing pathways with 7.0 W/m^2 radiative forcing and SSP5-8.5, which represents the high end of the range of future pathways with 8.5 W/m^2 radiative forcing, are the four SSPs. The SSPs took into account the likely concentration of greenhouse gases assuming changes in the population, GDP, GDP growth, educational attainment and land use land cover, as well as the climate mitigation measures from the ScenarioMIP. SSPs are incorporated into the CMIP6 models, enabling improved future effect assessments through improved parametrization. Using Integrated Assessment Models (IAMs) based on both SSPs and RCPs, these climate projections taking into account new emission and land use scenarios are created (O'Neill et al., 2016).

1.3 Ranking of GCMs

Generally, a set of suitable GCMs will be preferred from the large pool of GCMs for the area of interest for performing climate change impact studies by excluding those that have a greater degree of uncertainty (Khan et al., 2018; Lutz et al., 2016). Many studies on ranking of GCMs are reported in India are based on Couple Model Intercomparison Project phase 3 (CMIP3: Anandhi & Nanjundiah, 2015) and phase 5 (CMIP5: Das et al., 2018; Raju et al., 2017). The performance of a climate model is generally assessed by comparing its historical simulation with a reference dataset. It is quite a challenging due to ambiguity in the selection of model evaluation metrics and the reference gridded dataset. Quality of the observed data, spatial

distribution of gauges and varied interpolation techniques employed in the generation of reference gridded datasets is also a source of uncertainty (Khan et al., 2018). Several model evaluation measures have been utilized to analyse the climate models in matching the observed climate variables (Gleckler et al., 2008; Johnson & Sharma, 2009a; Knutti et al., 2010). An array of metrics were used for the variables of interest for validation. Model evaluation measures were segregated into two categories, namely time-domain and frequency-domain based metrics (Rathinasamy et al., 2014). The time-domain category metric such as coefficient of determination, Nash Sutcliff Coefficient (NSE), Root Mean Square Error (RMSE), Fourth Root Mean Square Error (R4MS4E), Kling Gupta Efficiency (KGE) etc. consolidate the error at each time step into a singular metric. The majority of these metrics are highly susceptible to extreme events and outliers. The second category evaluates the similarity between the frequency distributions of observed and simulated variables in order to assess the goodness of fit. This overcomes previous limitations and allows for a more comprehensive assessment of the match between observed and simulated data. Some of the studies used these frequency domain metrics such as Skill Score (SS: Perkins et al., 2007), Brier Score (BS: Ruan et al., 2018), Symmetric Uncertainty (SU: Khan et al., 2018; Salman et al., 2018) in the climate model selection. The major drawback of these metrics is that the loss of timing information about the error terms. Therefore, every performance evaluation metric has its own strengths and weaknesses and there is no universally accepted model evaluation metric that serves all intents and purposes (McMahon et al., 2015). To address these issues, Multicriteria Decision Making (MCDM) techniques were employed to aggregate multiple performance indicators into a single measure.

1.4 Climate Change on Precipitation

Climate change is a multidimensional complex global phenomenon leading to hydro-climatological extreme events, thereby motivating the research community to study it since the past few decades (Ahmed et al., 2019; Cameron, 2011; Sheffield & Wood, 2008). Precipitation is a key climate variable that can influence the characteristics of hydrological cycle and ecological system of a catchments. The changes in precipitation can affect many sectors, including agriculture, hydrological cycle, environment, health and power. Evidence from science indicates that warmer climates cause changes in precipitation patterns and global warming is predicted to increase the frequency of extreme precipitation. Therefore, it is very important to know the spatio-temporal analysis of precipitation over a catchment. Generally, the atmospheric conditions of semi-arid regions are sensitive to the variability of regional

climate, especially for precipitation (Gong et al., 2004; Xing & Wang, 2017; Ye & Chen, 1992). Sometimes, even a slight deficit in rainfall can cause heavy drought, affecting agricultural plants specifically during summertime. Generally, the selected GCMs are employed to develop the Multi Model Ensemble (MME) mean, which can strengthen the prediction reliability by using information from the variable of interest (Knutti et al., 2010). Future fluctuations in rainfall in a river basin can be better understood by looking at the spatial distribution of the rainfall changes.

1.5 Climate Extremes

Climate extremes especially changes in precipitation extremes is expected to become a major issue affecting flood hazards and hydrological regimes in the upcoming decades. Climate extremes are getting an increased attention due to their explosive impacts on climate change (Klein Tank et al., 2006). High intensity or excessive precipitation often becomes hazardous (Choi et al., 2014). Krishnamurthy et al., (2009) have found that a significant increased trend in extreme precipitation over India. The climate extremes associated with heavy multi-day precipitation is the main cause of floods, soil erosion and landslides in river channels (Mishra, 2022; Talchabhadel et al., 2018). One of the most populous and developing nations in the world, India depends heavily on the summer monsoon precipitation, which is sensitive to climate change (Kitoh et al., 2013; Mohan & Rajeevan, 2017). Moreover, the projected increased temperature along with heavy precipitation extremes in summer monsoon periods are likely to lead for the occurring of floods in Indian River Basins (IRBs). The extremely heavy precipitation which is influencing the Indian economy and putting enormous pressure on millions of people across the India region (Ghosh, 2010; Kothawale et al., 2010; Rajeevan et al., 2006; Roy & Balling, 2004). The effects of a number of extreme precipitation events that have happened in recent decades on infrastructure and society make them noteworthy. For example, the extreme precipitation event of 940bmm in 18 hrs that has occurred in Mombai on July 2005 resulted in flooding caused around 1200 deaths along with effecting millions of people. Furthermore, in November 2015, 483 mm of precipitation fell on Chennai in 48 hours, causing a disastrous loss of almost $3 billion in economic value (Gupta & Nair, 2011). Apart from localised flooding, which is primarily brought on by excessive precipitation, additional factors related to watershed characteristics and extreme precipitation may also contribute to flooding at the river basin scale. More recently, around 440 individuals lost their lives as a result of extensive flooding brought on by excessive precipitation in August 2018 in Kerala and initial assessment of economic damage surpasses $3 billion (Mishra et al., 2018). The

warming climate in India is expected to increase the likelihood of both extreme precipitation events and flooding increasing the risk of financial loss and infrastructure damage (Mukherjee et al., 2018). According to research by Dottori et al., (2018) a 1.5 °C rise in the global mean temperature above preindustrial levels may result in a 70–80% increase in human casualties from flooding, with South Asia being at higher risk. Analysing precipitation extreme indices is crucial for understanding the future climate of a region, especially for areas developing countries like India.

1.6 Climate Change Impact on Hydrological Modelling

A portion of the hydrologic cycle is conceptually and simplistically represented by hydrologic models. These replicate every aspect of the natural flow of water, including stream flow, evapotranspiration and evaporation, soil moisture, groundwater recharge, sediment transport, microbe development in water bodies and sediment transport, etc. Both spatial and temporal derivatives are involved in the hydrologic processes. Depending on whether they take space derivatives into account (lumped) or not (distributed), the hydrologic models fall into one of two categories. Semi-distributed models are categorised based on the presumption that certain processes account for spatial variances. Most of these hydrological models will provide hydrograph with peak values at a specified location of a catchment. The efficiency with which the assumptions and procedures used to estimate various hydrological components account for the applied approaches on spatial scales determines which hydrological model is best. Typically, hydrologic models function at the watershed or river basin scale. They serve a broad purpose in providing knowledge on numerous issues pertaining to water resources and hydrologic extremes at the watershed scales. The inputs needed for utilising hydrologic fashions vary according on the purpose of the models construction. The inputs for a river float simulation version include precipitation, catchment parameters (such as soil type, catchment slope, plant life type, land use type, temperature, solar radiation, groundwater contribution and so on. This kind of model typically produces river flow at a location at a specific point in time (a day, a week, or a month), as well as soil moisture and evapotranspiration throughout the duration. This type of model thus yields valuable data for determining the effects of changes in climate and land use.

1.7 Impact of Climate and LULC Change on Hydrology

Natural resources, such land and water, are the primary drivers of the nation’s economic growth as well as the development of human and environmental services. However, because of the

rapid growing of human population, urbanisation and industry are putting enormous demand on these resources. The amount of rainfall and temperature variations have a significant impact on streamflow and the availability of water. Therefore, assessing the effects of climate change on streamflow and water balance patterns will be useful in developing and overseeing the water resources system in an effective manner. Over the past century, comprehensive climate observations at both regional and global scales have revealed a significant increase in extreme climate events, marked by alterations in temperature, precipitation patterns and energy levels. These changes have directly impacted hydrological processes, leading to consequential effects on local and regional water resources. Therefore, the evaluation of water resource availability in light of climate change at both regional and global levels has been a significant topic of interest to the hydrologic research community in recent years. Worldwide, numerous studies have been reported that the impact of climate change on watershed hydrology (Chen et al., 2020; Givati et al., 2019; Reshmidevi et al., 2018; Wang et al., 2016). For instance, the impacts of climate change on runoff in the Upper Jordan basin were evaluated by Givati et al., (2019), they reported a significant 44% decline in streamflow under the RCP8.5 scenario. Moreover, these studies collectively contribute to our knowledge of the diverse influence of climate change on watershed hydrology across different geographical regions.

Both changes such as climate change and changes in both climate and land use have a major influence on the hydrological processes in the watershed (Pandey et al., 2021). Recent years some of the studies are focused on coupled effect of future climate and LULC changes on a catchment scale (Ahiablame et al., 2017; Woldesenbet et al., 2018). For instance, the future response of streamflow in the region is expected to intensify due to combined change of climate and land use, resulting in a potential increase of 13 to 60% (Ahiablame et al., 2017).. Assessing the impacts of future climate and LULC changes on rivers and water resources is essential for effective water resource management in developing countries like India.

1.8 Motivation for Research and Problem Formulation

Climate change alters the global water cycle by changing the temperature, precipitation and its spatiotemporal distribution. These modifications have an impact on the regional water budget and the biotic environment (IPCC, 2013). The risks that could arise from the 1.5 ^{o}C increase in temperature over pre-industrial levels are described in the IPCC Special Report (IPCC, 2018). When temperatures rise and precipitation patterns shift, it can have a negative impact on streamflow, soil moisture, water availability, the frequency of floods and droughts.

Fluctuations in LULC throughout a catchment can disrupt the hydrological cycle and cause droughts and floods when combined with climate change. To manage the water resource effectively, particularly developing countries like India, it is essential to study and analyse the isolated and coupled effect of changes in future climate and LULC on the water availability of a catchment with reduced uncertainty.

A thorough study of the literature (given in chapter 2) found that numerous studies have been conducted with success in the literature to examine the impact of changing climates on the hydrology of various rivers and watersheds in various aspects. Several CMIP phases GCMs have been used throughout India to evaluate and quantify future forecasts of the water resources. Various types of uncertainties associated with impact of climate change on a watershed scale and choice of GCMs is most important one (Crosbie et al., 2011). However the GCM performance is region specific and depends on many factors such as, performance indices, reference gridded dataset, weighting techniques and MCDM methods. But it is necessary to investigate the subjectivity of GCM ranking and careful selection of GCMs are necessary for climate change impact studies. CMIP6 has an improvised parameterisation that can efficiently model climate projections (Eyring et al., 2016). A study by (Gusain et al., 2020) showed that CMIP6 GCMs are more efficient compared to CMIP5 GCMs in simulating the Indian summer monsoon.

Based on above research studies. It has been exposed that, as water demand rises in tandem with an increase in the spatial and temporal fluctuations of water availability, the need for basin-level research on the impact of climate change has grown to analyse the availability of water resources, water quality, etc., in different rivers of India. Furthermore, research must be done to determine how the changing LULC and climate change may affect ecosystems and water resources. Only few studies have completed successfully across IRBs on climate change impact on water resources of a catchment in various aspects using CMIP6 based climate models by selecting the GCMs. Many studies have not considered ensemble of GCMs. Based on above research studies it is noticed that to investigate the climate change impact on water resources of various catchment using latest AR6 climate change scenarios. For that it necessary to understand the ranking behaviour of the GCM based different factors. Hence, this study an attempt to comprehensive analysis of GCMs ranking procedures, climate and LULC changes impact on water resources of watershed for effective water management and mitigation studies.

1.9 Scope and Objectives of the Study

The main aim of the research is to understand the impact of climate change in the Krishna River Basin (KRB) in India. The broad idea is to systematically investigate the subjectivity involved in the ranking of GCMs, selection of GCMs over KRB and using of these GCMs for the further climate change impact assessment. Additionally, a coupled approach is utilized to simulate the impact of both land use dynamics and climate change scenarios on hydrological responses in the KRB. This methodology allows for a comprehensive knowledge of the effects of both climate and land use changes on the region. The prime objective of the study has been distributed into the subsequent minor objectives.

i. To analyse the role of subjectivity on ranking patterns of CMIP6 GCMs.
ii. To choose the CMIP6 GCMs for projections of spatio-temporal variations in precipitation over KRB.
iii. To assess the changes in projected extreme precipitation indices in KRB using selected CMIP6 GCMs.
iv. To evaluate the effects of climate change on WBC in KRB through the use of a CMIP6 GCM ensemble.
v. To assess the coupled impact of future climate and LULC changes on WBC over Tungabhadra River Sub-Basin (TRB) in KRB.

1.10 Research Gaps Identified

Based on the literature study, the following Gaps were identified:

i. There is no universally accepted ranking procedure to address the region-specific performance of climate models. Hence, the ranking procedure is prone to subjectivity. No study had been reported so far in the literature to address the influence of subjectivity on ranking patterns of climate models.
ii. A set of best performing GCMs is necessary for generating the MME to study the impact of climate change. And no study was conducted on CMIP6 based climate models for assessing the suitability of GCMs over Indian River Basins for climate change impact studies especially for KRB.
iii. Very meagre studies were conducted on analysis of extreme precipitation indices due to climate change in KRB using CMIP5 GCMs especially using CMIP6 GCMs.

iv. No study had been reported so far to assess the impact of climate change in KRB using CMIP6 GCM outputs.

v. Very meagre studies were conducted on coupled effects of future climate and LULC changes over Indian River Basins especially for KRB.

1.11 Organisation of Thesis

Chapter 1 begins with an introduction to the study problem and a discussion of its importance and set up the objectives of the study. A detailed review about GCM ranking procedures, the selection of GCMs for climate change impact studies, rainfall-runoff modelling approaches and climate and LULC change impact studies are presented in chapter 2.

In Chapter 3, the methods pertaining to the GCM ranking procedure, hydrological modelling and the combined effects of climate and LULC change on hydrology are presented. Additionally, this Chapter includes a description of the study area as well as the data required and accessible for the study area.

Chapter 4 describes the results of the various objectives performed in the research works such as GCM ranking subjectivity across India, selection of GCMs for KRB to assess the climate extremes and impact of climate and LULC changes for future periods for efficient management of water resources.

Chapter 5 presents the summary of the study, the conclusions arrived, recommendation from the study and suggestions for further research activities. This Chapter also reports the contribution from this study.

CHAPTER 2

LITERATURE REVIEW

2.1 General

Climate change impacts the hydrological cycle, agricultural output, sea levels and sea surface temperature patterns. In India the increased frequency and severity of extreme events like droughts and floods can be linked to shifts in global climate patterns (IPCC, 2013). Around 70% of the country's precipitation comes from the monsoon, making it highly dependent on this seasonal pattern. This reliance on monsoon rains leaves the country vulnerable to changes in precipitation patterns. According to a 2018 report by Niti Aayog, groundwater wells are depleting and approximately 50% of India's population is experiencing a severe water shortage. The droughts of 2016 had a significant impact, affecting millions of people and causing substantial economic losses. Moreover, between 1950 and 2015, floods have affected an estimated 825 million individuals. During this period, the frequency of flood events in central India has tripled (Kumar et al., 2021; Mishra, 2020). These findings underscore the pressing need to incorporate assessments of climate variability and land use changes to improve the accuracy of predictions regarding water availability. In India, there are 19 major river basins, as reported by (Amarasinghe et al., 2005, 2007). Their findings indicate that water demand is influenced by several factors, including future growth in domestic, industrial, environmental water demand, as well as internal and international trade. Within the 19 basins in India, the Krishna River stands out as a water-scarce river where 20-40% of irrigation relies heavily on groundwater. The level of development in this basin exceeds 60%, resulting in an anticipated depletion of water resources by 50-75% by the year 2050. Due to these concerns, the Krishna river basin has been chosen as a focal area for evaluating water availability under various climate change scenarios. moreover, most of the Krishna river basin is semi-arid in nature and experiencing high vunerability to even small cliamte change. Hence, it is necesaary to understand the climate change impact on hydrology of KRB in comprensive manner.

For longterm projectictions of the water avaialbility the Intergovernmental Panel on Climate Change (IPCC) is continuously putting progressive efforts to understand the climate change behaviour from the past century and releasing different Coupled Modelled Intercomparison Project (CMIP), Assessment Reports (AR) which provides various types of Global Climate

Models (GCMs). Studies on the effects of climate change heavily rely on the examination and selection of climate models.

2.2 Global Climate Models (GCMs)

Global Climate Models (GCMs), as physically-based models, are widely regarded as reliable and practical tools for forecasting changes in atmospheric variables within the context of climate change scenarios. These models encompass the dynamics of both the atmosphere and the oceans (Ghosh & Mujumdar, 2008). GCM projections, while well-suited for continental and hemispherical scales, often lack the finer resolution needed for regional impact analysis, particularly when examining changes in extreme events (Fowler et al., 2007). This limitation is due to their high spatial resolution, typically around 100-250 km. To overcome this challenge and assess the impact of climate change at a regional level, it is necessary to link large-scale climate variables to hydrologic variables at a finer scale. Downscaling methods are commonly employed to derive local to regional scale information from these large-scale climate projections. These methods can be broadly categorized as dynamic or statistical. Dynamic downscaling involves generating finer resolution output based on atmospheric physics over a specific region, using GCMs boundary conditions (Teutschbein & Seibert, 2012). On the other hand, statistical downscaling methods establish empirical relationships between GCM outputs and observed climate data (Fan et al., 2021). By employing these downscaling techniques, researchers can bridge the gap between large-scale climate projections and the finer resolution needed for regional impact studies, thus enabling a more comprehensive analysis of climate change impacts on local and regional hydrology.

Giorgi & Mearns (1991) compared the empirical and GCM nested limited area modelling techniques and discussed the advantages, disadvantages, limitations and variability of their use. They observed that, though GCMs are capable of encompassing the wide range of climate variability and atmospheric phenomenon, they are complex and expensive. Here some of the statistical downscaling literature across the globe were discussed.

Statistical downscaling, unlike the computationally intensive dynamical downscaling, offers a simpler approach by developing empirical connection between local climate and GCM climate variables. These relationships do not involve the complex mass and energy exchange between the land and atmosphere. The statistical downscaling methods can be grouped into weather generators, transfer function and weather typing, each with its own approach to linking large-scale and local-scale climate data (Ghosh & Mujumdar, 2008).

Lin et al., (2017) used the KNN algorithm to develop a novel spatio-temporal downscaling method for hourly rainfall data. Tabari et al., (2021) compared four statistical downscaling techniques such as Change Factor of Mean (CFM), Bias correction (BC), an event-based Weather Generator (WG) and Quantile Perturbation (QP) to assess the impact of climate alteration on drought in the future (2071-2100) compared to a baseline period (1971-2000) for the Uccle region of Belgium. The study used ensemble CMIP6-GCMs for downscaling, considering four future scenarios: SSP1-2.6, SSP2-4.5, SSP3-7.0 and SSP5-8.5. Among these methods, the QP technique demonstrated superior performance in replicating the amplitude and monthly pattern of the reported drought indicators.

2.3 Bias Correction Techniques

Systematic model errors in GCMs or RCMs can result in inherent biases, stemming from imperfect conceptualization, discretisation and spatial averaging within grid cells. These biases are not limited to precipitation but also extend to temperature (Ines & Hansen, 2006). Common biases include an overabundance of wet days with low-intensity rainfall, inaccurate predictions of extreme temperatures, general over or underestimation of precipitation and improper seasonal fluctuations in rainfall (Teutschbein & Seibert, 2012). To address these biases, various bias correction approaches have been established for downscaling climate variables from both GCMs and RCMs (Chen et al., 2011; Chen et al., 2019; Mishra et al., 2020). These strategies vary from straightforward scaling methods to more intricate ones that use weather generators or probability mapping.

These possible biases make GCM simulations difficult to apply, even if their usage in hydrological impact assessments due to climate change is growing. Before being employed in impact studies, the output of climate models is frequently pre-processed using bias correction techniques (Ngai et al., 2017; Piani et al., 2010; Wood et al., 2004).

2.4 GCM Ranking Procedure

Progressive efforts have been documented to evaluate the GCMs performance of ever since their development (Xu, 1999) for climate change impact studies. Different studies are used various types of metrics for ranking of GCMs.

Perkins et al., (2007) assessed daily precipitation, minimum and maximum temperature simulations for 12 Australian locations using the fourth AR of the IPCC coupled climate

models. Probability density functions were employed in the assessment to gauge how well the models represented the observed data.

Fu et al., (2013) evaluated the effectiveness of GCMs at the regional level using a multi-criteria score-based approach based on Relative Error (RE), Normalised Root Mean Squared Error (NRMSE), Brier Score (BS), Skill Score (SS), Correlation Coefficient (CC), Mann-Kendall test Z and Trend magnitude. Applying it to 25 GCM simulations of monthly air temperature, Mean Sea Level Pressure (MSLP) and annual precipitation in south-eastern Australia during period of 1960 to 2000. They revealed that GCMs generally simulate the temperature more accurately than MSLP and monthly rainfall.

Raju & Kumar (2014) used five performance indicators namely, Correlation Coefficient (CC), NRMSE, Absolute Normalised Mean Bias Error (ANMB), Average Absolute Relative Error (AARE) and SS to assess 11 GCMs for India that included 73 2.5° x 2.5° grid locations in terms of precipitation. The weights of each indicator were computed using the entropy technique. The GCMs were ranked using the Preference Ranking Organisation Method of Enrichment Evaluation (PROMETHEE-2) and Multi Criteria Decision-Making (MCDM) methods. Additionally, they stated that the suggested methodology can be expanded to rate GCMs for additional locations.

Anandhi & Nanjundiah (2015) evaluated the 19 CMIP3 GCMs for India in order to simulate daily rainfall using SS. The assessment is carried out on a 2.5° x 2.5° grid and contrasted with the gridded dataset from the Indian Meteorological Department (IMD). They came to the conclusion that no GCM is operating effectively in India.

Jena et al., (2015) evaluated the performance of CMIP5 GCMs for precipitation in India using CC. They revealed that some models, like HadGEM2-AO and MIROC-ESM-CHEM, perform well for the summer monsoon while, for winter monsoon MPI-ESM-LR, MRI-CGCM3 and INM-CM4 performing well.

Raju & Nagesh Kumar (2015) evaluated the 11 GCMs for India in a different study by employing SS as the temperature performance metric. The GCMs were ranked using the MCDM technique, Technique for Order Preference by Similarity to an Ideal Solution (TOPSIS). It was determined that the combination of GFDL2.0, MIROC3, GFDL2.1, BCCR-BCCM2.0, HadCM3, INGV-ECHAM4 were better for India.

Sarthi et al., 2016 assessed 34 CMIP5-GCMs for their performance in simulating the Indian summer monsoon using Taylor diagrams and indicators such as CC, SS and RMSE. MPI-ESM-MR, CESM1(BGC), CESM1(CAM5), CESM1 (WACCM), BCC-CSM1.1(m) and CCSM4 models were effectively simulated precipitation patterns.

Ahmadalipour et al., (2017) evaluated 20 GCMs performance over the Columbia River Basin (CRB) in the Pacific Northwest of the United States using data from the CMIP5 dataset. They evaluated the models using a statistical multicriteria method that included univariate and multivariate techniques. The univariate techniques included mean, coefficient of variation, standard deviation, relative change, Mann-Kendall test, and Kolmogorov-Smirnov test (KS-test). In order to assess the dependability and character of the models at a regional level, the study was done using unprocessed GCM data for temperature and precipitation climatic variables for the years 1970 to 2000, prior to bias adjustment. Using observational gridded data on multiple temporal scales like daily, monthly and seasonal. They graded each GCM according to how well it performed. The statistical qualities they took into consideration when ranking the GCMs, as well as the advantages and disadvantages of each approach, were revealed by their findings. Furthermore, various sets of gridded observational datasets in the region with the raw GCM simulations.

Raju et al., (2017) evaluated 36 CMIP5-based GCMs were assessed to evaluate their performance in simulating maximum and minimum temperatures for India across 40 grid points using CC, NRMSE and SS. Compromise programming (CP), a distance-based decision-making technique, was employed to rank the GCMs. A group decision-making approach was used to aggregate individual grid point rankings and an ensemble approach was suggested as a simple but effective method. Top 3 GCMs were provided for major river basin in the India.

Khan et al., (2018) used SU as the primary indicator to evaluate 31 GCMs from CMIP5 for precipitation, minimum and maximum temperature in Pakistan. They identified six top-ranked GCMs were MIROC5, HadGEM2-ES, HadGEM2-CC, CMCC-CM, CESM1(BGC) and ACCESS1.3. These models were suggested for inclusion in Multi Model Ensemble (MME).

Abbasian et al., (2019) used Climatic Research Unit (CRU) records from 1901–2005 to assess the effectiveness of 37 CMIP5-GCMs in simulating temperature and precipitation over Iran. The evaluation process uses six performance measures: Sen's slope estimator, mean bias, RMSE, linear correlation coefficient (r), Nash-Sutcliffe efficiency (NSE), Kolmogorov- KS and the Taylor diagram. Based on every data at seasonal and annual time scales, the GCMs are

ranked. The findings show that most GCMs can accurately predict annual and seasonal temperatures over Iran.

Ahmed et al., (2019) evaluated 20 CMIP5-GCMs for precipitation across Pakistan using spatial indicators including Cramer's V, Fractional Skill Score (FSS), Goodman–Kruskal's lambda, Kling–Gupta Efficiency (KGE) and Mapcurves. For multi-model ensemble (MME), they employed GFDL-ESM2G, GFDL-CM3, CESM1(CAM5) and NorESM1-M, with a preference for the RF-based MME. Random Forest (RF) was used in the MME process.

Nashwan & Shahid (2019) Proposed a methodology for choosing GCMs based on their capacity to replicate spatial patterns for different climate variables. GCMs to replicate annual regional patterns of maximum and minimum temperatures as well as rainfall depth was evaluated using the Kling-Gupta efficiency (KGE).

Using six climate variables Pandey et al., (2019) evaluated the performance of 24 CMIP5-GCMs for the Upper Narmada river basin (UNB), India. They used metrics including SS, RMSE and Total Index (TI) for their assessment. MIROC5, CNRM-CM5 and MPI-ESM-LR were found to be appropriate models among these GCMs.

The CMIP5 GCMs for the rainfall over Egypt were assessed by Shiru et al., (2019) using the MCDM technique, which is based on markers for precipitation projection such as entropy gain gain ratio and SU. The goal of the study approach is to create a Multi Model MME comprising the top four GCMs in order to decrease uncertainty in precipitation projections.

Homsi et al., (2020) projected potential changes in precipitation for Syria due to climate change. It uses the SU) and MCDA methods to select the best CMIP5 GCMs for precipitation projections. The study projects annual precipitation changes to decrease by -30 to -85.2% for RCPs 4.5, 6.0 and 8.5 scenarios.

2.5 Climate Extremes Effects

Climate extremes are garnering increased attention due to their explosive impacts on climate change worldwide (Agarwal et al., 2014; Goyal, 2014; Z. Guo et al., 2014; Meehl et al., 2005). Among the vital climate components, precipitation plays a crucial role in affecting economic growth, as well as agricultural and industrial development activities. The precipitation extremes associated with heavy multi-day precipitation are the primary cause of floods, soil erosion and landslides in large river channels, significantly impacting the environment, society and economy (Nanditha & Mishra, 2022; Talchabhadel et al., 2018; Trenberth et al., 2011; van Pelt

et al., 2015). The sixth Assessment Report of the Intergovernmental Panel on Climate Change (IPCC) (AR6) has documented an increase in the observed global mean surface temperature of 1.09 ^{o}C from 2011 to 2020 compared to the pre-industrial revolution era, highlighting the long-term impact of changes in precipitation distribution (Gouda et al., 2018; Masson-Delmotte et al., 2021).

According to Mirza (2003) analysis, developing nations are especially vulnerable to the effects of extreme weather and climate change is predicted to make matters worse. These nations' ability to adapt to climate change will rely on the development models they choose and their current level of adaptability. They also reported that the developing countries' long-term sustainable development strategies must incorporate disaster management, adaptation and susceptibility to extreme weather occurrences.

Roy & Balling (2004) used seven different indices: total precipitation, largest 1, 5 and 30-day totals, and the number of daily events that exceeded the 90th, 95th and 97.5th percentiles of all precipitation at each station in India between 1910 and 2000 to quantify extreme precipitation events. A significant rising trend was seen in 114 out of 903 time series (seven variables for 129 stations), whereas a significant downward trend was seen in 61 of them; an upward trend was seen in 61% of the time series. The network-wide standard regression coefficients, which show the trend's strength and direction, have a high degree of correlation.

Klein Tank et al., (2006) used data from 116 meteorological stations to evaluate daily precipitation and temperature extremes in central and south Asia from 1961 to 2000. They came to the conclusion that because of inconsistent spatial trend coherence and varying negative and positive at various stations, the majority of regional indices of wet extremes for precipitation exhibit little variation.

Rajeevan et al., (2008) evaluated the variability and long-term trends of extreme precipitation occurrences over central India for 104 years from 1901–2004. There are statistically significant long-term trends of 6% per decade combined with large inter-annual and inter-decadal variability in the frequency of intense rainfall events. Sea Surface Temperature (SST) changes over the tropical Indian Ocean are responsible for these variations and trends, according to a detailed research.

Deshpande et al., (2016) examined the daily time-series changes in extreme rainfall and temperature characteristics of major river basins of India using high-resolution gridded daily rainfall data from 1951 to 2014 and temperature data from 1951 to 2013. During the southwest

monsoon season (JJAS), they used a rainfall threshold of 10 cm. We used 40 °C as the summertime maximum (MAM) and 10 °C as the wintertime minimum (DJF) as our thresholds for extreme temperature events. In all river basins, an increase in the number of days without rain during the monsoon season has been seen, with the exception of certain regions in the Krishna and Peninsular river basins.

Dubey & Sharma (2018) examined 19 extreme daily precipitation, maximum and miimum temperatures to analyse present and future climate change in the Banas river basin of Rajasthan, India. Utilising ensemble data from three RCMs, CNRM-CM5, CCSM4 and MPI-ESM-LR for historical data from 1971 to 2013 and future forecasts from 2021 to 2050 are used. During these historical periods, there is a significant decline in total annual precipitation (PRCPTOT). It is anticipated that the increasing trend in the Consecutive Dry Days (CDD) index would persist in the future. The indices of R10 mm and R20 mm were exhibited a decreasing trend.

The combined effects of high rainfall and reservoir storage on Kerala floods and climate change were examined by Mishra et al. (2018). They stated that severe flooding struck Kerala, India in August 2018, affecting millions of people and resulting in more than 400 fatalities. Kerala saw rainfall that was 53% over average. For 1, 2 and 3-day durations, the extreme rainfall events that occurred in August 2018 had return periods of 75, 200 and 100 years respectively. By August 8, 2018, six of Kerala's seven major reservoirs were operating at over 90% capacity prior to the intense rainfall. Furthermore, the watershed areas upstream of the three major reservoirs (Idukki, Kakki and Periyar) had significant rainfall episodes spanning one to fifteen days, with return durations reaching 500 years.

Mukherjee et al., (2018) evaluated the extreme precipitation events in India under anthropogenic warming using CMIP5 GCMs. They stated that increased anthropogenic warming has led to a rise in the frequency of extreme precipitation occurrences. Moreover, with human warming, our forecasts indicate a significant increase (10–30%) in 1 to 5 day precipitation maxima at 5 to 500 year return periods. By end of the 21st century, southern and central India are predicted to see much more precipitation extremes on average under the RCP 8.5 scenario.

Ali et al., (2019) evaluated the flood risk on the Indian subcontinent, they discovered that, between 1966 and 2005, the most of the IRBs had an increase in precipitation extremes occurrences. However, these trends were largely not statistically significant at the 5% level. However, for the downscaled and bias-corrected the CMIP5 and the Noah-MP model, the

historic and future climate predictions shown a considerable rise in the frequency of both single and multi-day extreme precipitation and flood events across the region in the future..

Talchabhadel et al., (2021) assessed the precipitation extremes in the West Rapti River basin (WRRB) of Nepal from 1986 to 2015 using 11 ETCCDI indices. For future projections, they used data from three periods and five climate models from the CMIP5 under two RCPs 4.5 and 8.5. Using the Mann-Kendall test and Theil-Sen's slope technique, they conducted a study and revealed that severe precipitation indices associated with very wet days, extremely wet days, maximum 1-day and 5-day precipitation are anticipated to increase drastically in the future.. It was also discovered that a significant indicator of extreme precipitation is the percentage of maximum 1-day and 5-day precipitation that contributes to total annual precipitation. The anticipated increase in rainfall extremes raises concerns about the potential for more frequent hydrological disasters in the WRRB.

Chaubey et al., (2022) analysed the Spatio-temporal analysis in extreme rainfall events over IRBs. They revealed that a notable shift in extreme rainfall events from north-eastern IRBs towards the western IRBs during the period from 1981-2019. Within the IRBs, there are regional differences in the annual maximum rainfall for the 10, 30, and 100 year return levels, they reported statistically significant increasing trends. Furthermore, it is concluded that a shifting and increasing pattern (15% to 58.74%) in extreme rainfall events during wet and dry conditions over the west-flowing river basins in the past decades of the 20^{th} and the present 21^{st} century.

In order to assess the moisture conditions and precipitation features before to high flow events Nanditha & Mishra (2022) developed a novel framework. By comparing observed and predicted future climates, their analysis seeks to quantify the likelihood of flood driver occurrences and their relationship with peak flood magnitudes in IRBs. The main cause of floods in both the observed and predicted future climates, they discovered, is multiday precipitation, which acts as a stand-in for heavy precipitation on moist soil conditions. Remarkably, the findings suggest that in bigger river basins, multiday precipitation plays a more important role in driving floods than extreme soil moisture levels, whereas in smaller river basins, extreme precipitation plays a more significant role in controlling flooding. High flow days, days with heavy precipitation and days with several days of precipitation are expected to increase significantly.

2.6 Hydrological Modelling and Impact Studies

Anthropogenic activities have significantly altered the global climate, posing threats to regional natural resources. Climate change impacts various sectors such as agriculture, environment, water availability, ecosystems and socio-economics. The IPCC AR5 highlighted a rapid global temperature rise, which will affect climatic, ecological, chemical and hydrological processes globally. These changes are expected to influence water availability and related climatic extremes in river basins, particularly in countries like India with significant agricultural reliance (Nilawar & Waikar, 2019). Simulating hydrological responses based on climate conditions is crucial for understanding hydrological phenomena. This approach provides insights into the spatio-temporal changes of hydrological variables and their future interplay with climate. By employing water balance modelling, a qualitative assessment of changes in water resources can be conducted considering both climate and human interventions. Hydrological models are valuable tools to assess the impact of climate change, as they can simulate probable changes in streamflow for specific river basins. Climate and LULC changes are key factors affecting hydrological regimes. Accurately quantifying their effects on streamflow within a watershed is essential, given the diverse range of impacts. Based on the model's capacity to conceptualise input variables with the catchment features, such as LULC, soil type, slope, etc., conceptual hydrological models are generally divided into three types: semi-distributed, lumped and deterministic. Hydrological models that are spatially distributed and physically based cannot only evaluate the geographical fluctuation of hydrological parameters but also make the simulation of external flows and state variables easier. Numerous studies were conducted to evaluate the climate change impact on streamflow. These studies included the Variable Infiltration Capacity (VIC) model (Liang et al., 1994), Hydrologiska Byråns Vattenbalansavdelning (HBV) model (Bergström, 2006) and MIKE 11 (Gaur et al., 2021). The following sections evaluate many hydrologic models and their applicability to impact studies:

Chien et al., (2013) used a combination of hydrologic models and GCM forecasts to model the possible effects of a river basin. They used multi-site calibration and validation using SWAT to show the temporal and spatial fluctuations of the future stream flow. In all the watersheds, future predictions indicate a decrease in the variability of streamflow, both annually and intra annually. The study's findings offer fundamental information for creating adaptation plans intended to lessen the effects of climate change on aquatic ecosystems and resources.

Li et al., (2014) investigated the impact of climate change on streamflow patterns in the Yarlung Tsangpo river (YTR) basin, a region with significant hydro-meteorological influence on southern and eastern Asia. They employed two hydrological models, SIMHYD and GR4J, to analyse monthly and annual streamflow patterns at the watershed scale. Additionally, the study analysed the basin's hydro-meteorology using outputs from 20 GCMs. Their findings suggested an increase in mean annual precipitation and runoff across the region in the future. Specifically, the middle reaches of the YTR and its two tributaries exhibited increasing tendencies in streamflow.

Meenu et al., (2013) studied how climate change is affecting the hydrology of the Tunga-Bhadra River Basin (TRB) in India. Prior to hydrological modelling, they initially used a linear regression-based statistical downscaling model (SDSM) to downscale daily precipitation, maximum and minimum temperature. The Hadley Centre Coupled Model version 3 under A2 and B2 scenarios provided the large-scale climate variables for the three future periods (2021–2040, 2041–2070 and 2071–2099) that were used in the forecasts. The authors used the Hydrologic Modelling System version 3.4 (HEC-HMS 3.4) from the Hydrologic Engineering Centre to evaluate the possible climate change impacts over TRB. In all scenarios, their assessment of the water balance under climate change revealed a rise in runoff and rainfall together with a decline in the rate of real evapotranspiration loss.

Narsimlu et al., (2013) used the SWAT model to study how climate change is affecting the water resources in the upper Sind river basin, India. They used measures such the p-factor, d-factor, NSE and R^2 to evaluate the model's correctness. The results of the study showed that average streamflow rose along with surface runoff and base flow towards the end of the century.

Pankaj & Asis (2013) used the HEC-HMS model, attempted to evaluate the river runoff in the flood-prone systems of India's Eastern and North Eastern river basins. For the A2, A1B and B2 scenarios, the study was conducted using continuous time slices data for the years 2010–2040, 2041–2070, based on the PRECIS model with the baseline years 1961–1990 without the sulphur cycle. A2 and B2 scenarios are more vulnerable than A1B scenario, according to the river runoff of the three scenarios' climate vulnerable scale. Water sequestration by predicted water availability, water footprint, green water availability and virtual water availability were all analysed.

Kulkarni et al., (2014) used RCM (PRECIS) data in SWAT to study potential changes in the water balance components of the Krishna river basin, India. Without altering the LULC data, the simulations were run for the control and two future scenarios. The findings indicate that there will be an increase in surface runoff, base flow and annual discharge in comparison to the current situation. This study's shortcoming stemmed from the fact that model simulations were run with the same LULC while accounting for potential future climate changes.

Abbaspour et al., (2015) did a work to create and improve the SWAT hydrological model in order to examine the various aspects of managing water resources in light of climate change. The model provided a thorough and in-depth investigation of system behaviour by simulating several water resource components at monthly time intervals. This involved applying large-scale, high-resolution water resource models in both physically based and data-driven simulations. The paper offered a comprehensive explanation of the methods utilised for modelling uncertainty, the calibration procedure and the availability of data.

Zhang et al., (2016) evaluated the streamflow regime in the China's Xin river basin by integrating SWAT and SDSM. Under three RCPs, the effects of climate change were examined using downscaled GCMs (BCC-CSM1.1, CanESM2 and NorESM1-M). According to the study, the hydrological characteristics on a yearly, daily and monthly basis were accurately represented by the SWAT model. It was demonstrated that even while rising temperatures are predicted in the future, estimates of precipitation will be more imprecise and differ significantly between GCMs under various RCPs.

Chanapathi et al., (2018) used the SWAT model to assess how climate change may affect the water balance components of the semi-arid Krishna river basin in Peninsular India. A shift in the maximum amount of long-term mean Indian Summer Monsoon Rainfall (ISMR) and surface runoff, an increasing trend in rainfall during October and November and some extreme rainfall events outside of the monsoon season were among the insights observed from the analysis. According to one of the climate models (CNRM-CM5), there would be mild drought episodes in 25% of cases, excessive rainfall in 7% of cases (> 25%) and extreme rainfall in 5% of cases (> 50%).

Das & Nanduri (2018) evaluated the effects of streamflows over the Wainganga river basin due to climate change using the VIC model. Utilising REA, uncertainties related to bias corrected GCMs were addressed. Using the Metropolis-Hastings method and Bayesian analysis, associated uncertainties in flood return levels were simulated while taking anticipated

streamflows into account. Moreover, as the forcings of climate change shift from RCP4.5 to RCP8.5, uncertainty rises. The temporal fluctuation of uncertainty was taken into consideration, suggesting that future scenarios are likely to see an increase in the uncertainty of the anticipated return levels.

The climate change impact on a catchment water balance using Multi Model Ensemble (MME) of five CMIP5 GCMs on Malaprabha river basin India is assessed by Reshmidevi et al., (2018) using SAWT model and reported that irrigation demand is projected to increase by 18.5% due to rise in temperature and evapotranspiration in the future.

Bhatta et al., (2019) measured how climate change affected the Tamor River Basin's water balance in Nepal's eastern Himalayas. The evaluation of SWAT's response involved varying the quantity of sub-basins, HRUs and elevation bands. An ensemble of five linearly bias corrected CMIP5-GCMs and four RCMs under both RCP4.5 and RCP8.5 was used to estimate the future climate over three distinct time frames, namely the 2030s, 2060s and 2080s. This data was then utilised as input SWAT for simulating future streamflows at the watershed scale. According to observations, the latter part of the twenty-first century may see streamflow reductions of more than 8.5% under RCP8.5 scenarios.

Bisht et al., (2020) examined the effects of climate change on the streamflow regime of the Mahanadi river basin while taking into account the projected and bias-corrected climatic scenarios of nine GCMs that were produced from CMIP5 models. The Hirakud and Mundali gauging sites used Integrated MIKE 11 NAM-HD prior to creating the streamflow regimes for the upcoming timeframe. The predicted ensemble mean of the simulated streamflow from various GCMs was used to analyse the streamflow. The mean monthly streamflow for anticipated warming scenarios exhibited increasing tendencies between 2070 and 2099, according to the data. By the end of the twenty-first century, daily high flows likewise demonstrated an increasing tendency in both amplitude and frequency, while low flow occurrences were found to be drastically declining under future climatic scenarios.

Guo et al., (2020) developed an integrated framework to assess the combined impacts of land use/cover and climate variations on streamflow in the Xinanjiang basin, East China. They evaluated the uncertainties using five bias-corrected and downscaled GCM forecasts under three different RCPs. Additionally, they predicted three land use/cover change scenarios based on Cellular Automata - Markov (CA-Markov) modelling, representing different trade-offs between ecological protection (EP) and urban development (UD). These scenarios were input

into SWAT to analyse the combined and isolated impacts of land use/cover and climate on streamflow. The study found that projected streamflow changes due to land use/cover differed from those solely due to climate change. However, the study suggested that land use/cover changes had a greater influence on streamflow patterns compared to climate change, potentially mitigating the impact of land use/cover change.

Sinha et al., (2020) assessed the individual and combined effects of projected LULC and climate change on the Kadalundi river basin in the Western Ghats of India using SWAT model. Using CMIP5 RCMs, Land Change Modeller (LCM) was used to predict the LULC scenarios for 2030 and 2050. The results showed that between 2000 and 2050, there will be a decrease in the amount of forest cover, an increase in grassland and agricultural output and a rise in mean annual surface runoff in metropolitan areas. Concerning the potential for climate change The assessment indicates that in the near, mid and long terms, mean annual surface runoff would decline under both RCP 4.5 and 8.5, with RCP 8.5 implying harsher conditions than RCP 4.5. The combined effects of LULC and climate change pointed to a trend towards less surface runoff in the near and medium term. Furthermore, the projected outcomes indicate that surface runoff will be higher in the summer and winter in both RCP scenarios, with a substantially different pattern during the monsoon season. According to the combined effect estimate, surface runoff would decline under RCP 4.5 and 8.5 more swiftly in the near future than it would in the mid-term.

Pandey et al., (2021) evaluated combined impact of climate and LULC change on the WBC of Upper Narmada Basin, India. The top-performing climate models GFDL-ESM2G, IPSL-CM5A-MR, CNRM-CM5, MPI-ESM-LR and GFDL-ESM-5) at the regional level were chosen using a grading system. To simulate hydrological reactions, these models were then combined with a semi-distributed SWAT hydrological model. The calibrated model was integrated with land use scenarios from the past (1990, 2000, 2010 and 2020) and the future (2030) to assess the hydrological sensitivity to land use change. With an estimated increase in annual mean temperature of 1.79°C and 3.57°C under RCP 4.5 and RCP 8.5 scenarios, respectively and the results point to increased precipitation in the late 21st century. In the basin, annual and monsoon flows are predicted to rise in the 2050s (2041–2070) and 2080s (2071–2100). In order to assess the hydrological sensitivity of the basin to changing climatic circumstances, the study also established correlations between climate variables and elements of the water budget.

Sadhwani et al., (2023) examined how the water balance components of the Periyar river basin, India would be affected by future climatic and LULC changes. Future LULC maps, which are predicted to be created in 2030, 2050, 2075 and 2100, indicate a decrease in forest and plantation lands and an increase in urbanisation and farmland. In evaluating the long-term effects of climate change, the research considers an ensemble of five GCMS with RCP 4.5 and RCP 8.5 scenarios. According to the results, in the near (2041–2040) and mid (2041–2070) futures, climate change is expected to have a bigger influence than LULC change; in the distant (2071–2100) future, however, the opposite is true. The findings offer insightful information about temporal and spatial fluctuations in hydrological components, which can help with decisions about soil permeability, agricultural water demand, irrigation, groundwater recharge and integrated water resource management. The modelling approach developed for this study can be used for comparable assessments with the goal of managing water resources and the environment in other humid tropical river basins.

2.7 Research Gaps Identified From Literature and Summary

Climate change is an important factor to consider when assessing its impact on the hydrological components of a river basin. The planning and management of water resources rely on accurate simulations of future climate and flow using hydrological models. So climate change impact depends up on

1) Availability GCM data
2) Selection of suitable GCMs
3) Selection of Hydrological Model
4) Uncertainty modelling of climate data and hydrological model
5) Climate and LULC change impact on hydrology for future scenarios

From literature it is observed that the GCM selection uncertainty is reduced using GCM ranking in simulating the different climate variables is prone to subjectivity. And the GCM the evaluation metrics can be categorised into two types such as time domain and frequency domain metrics. Every performance evaluation metric has its own strengths and weaknesses and there is no universally accepted model evaluation metric that serves all intents and purposes (McMahon et al., 2015). Various types of performance metrics were used in ranking of GCMs for climate change impact studies across the globe. Efficient and appropriate metrics that represent distinct properties should be chosen as criteria which makes GCM ranking purely

subjective (Randall et al., 2007; Tebaldi & Knutti, 2007). The ranking of newly evolved CMIP6 GCMs across the IRBs for further climate change impacts studies are necessary.

The climate models have a variety of biases, according to literature on climate change and the MME method. These biases must be further rectified using appropriate bias correction procedures. The climate models are related with a number of sources of uncertainty and it is essential to reduce these uncertainties by taking into account an appropriate weightage average technique.

The climate extremes are getting increased from the last century. Especially IRBs becoming more vulnerable to even small changes in climate variables. Numerous studies from literature reported that the IRBs are frequently experiencing floods and droughts due to these changes in climate extremes. The analysis of these climate extremes especially precipitation extremes in IRBs for future scenarios using new projections of CMIP6 GCMs are needed.

Hydrological modelling has become an essential component of climate change assessment, which takes into account a region's physical characteristics, according to the literature on the subject. It is therefore possible to simulate the water balance components and streamflow using physically based hydrological models that include high resolution meteorological data. The SWAT model was developed as a physically distributed model that can simulate different hydrological parameters effectively and maintaining the characteristics of the basin through the use of the SUFI-2 algorithm for uncertainty modelling and sensitive analysis. However most of these studies were considered different CMIP phase GCMs by considering single or multiple GCMs randomly and not considered the water storage structures in hydrological modelling. Limited studies were conducted based CMIP6-GCMs across different basins for the climate change impact, especially IRBs. The coupled impact of future LULC and climate change will provides the clear idea about the future projections of water balance components along with streamflow. In recent years some of the studies were conducted the combined the impact of climate and LULC change in the IRBs by predicting the future LULC using different techniques.

CHAPTER 3

METHODOLOGY

3.1 General

In the present chapter the overall methodology of research work is explained. The various datasets required for GCMs ranking subjectivity across India and climate change impact in Krishna River Basin are presented. In the first phase this study aims to explore the of subjectivity on GCMs rankings, particularly focusing on the past performance of GCMs from the CMIP6 phase in replicating maximum and minimum temperatures across India. Different ranking procedures are employed, encompassing a variety of components in the process, such as model evaluation criteria, criteria weight allocation methods, MCDM techniques and reference gridded datasets The grids with invariant rakings are find out and the top five GCMs are provided for each climate zone in India. In second phase, the concept of SU technique is employed to select the top five GCMs to analyse the spatio-temporal analysis of the precipitation over KRB. The empirical quantile mapping method was utilised to eliminate the biases present in the climate projections. Using the Reliability Ensemble Averaging (REA) technique, the MME mean of projections was produced and the spatiotemporal variations in precipitation under various SSPs are examined. In the third phase the selected top five GCMs used to analyse eleven (11) Expert Team on Climate Change Detection and Indices (ETCCDI) precipitation extremes indices and four seasonal precipitation indices across the KRB. In the fourth phase, the study explores the climate change impacts on the WBC of KRB for three future periods using SWAT model. To improve the model performance and reduce the uncertainty in the output, 13 major reservoirs were considered based on the data availability from Central Water Commission (CWC) for setting up the model. The selected GCMs under four scenarios such as SSP1-2.6, SSP2-4.5, SSP3-7.0 and SSP5-8.5 are used to find the impact future climate change in precipitation, surface runoff, water yield, evapotranspiration and streamflow in the KRB using top 50% GCMs from eighteen (18) GCMs. In the fifth phase, this the study incorporated future LULC from 1-km future global LULC (Chen et al., 2022) datasets along with the selected GCMs in the SWAT model in the Tungabhadra River Basin (TRB) a major tributary of the KRB. A large portion of Karnataka depends on the TRB for water supply, irrigation and hydropower production. Therefore, it is crucial to evaluate how future LULC changes will interact with the basin's shifting climate scenarios. The overall proposed

methodology of research work is represented in Figure 3.1 and Figure 3.2 represents the methodology for the 1st objective of in GCM ranking across India.

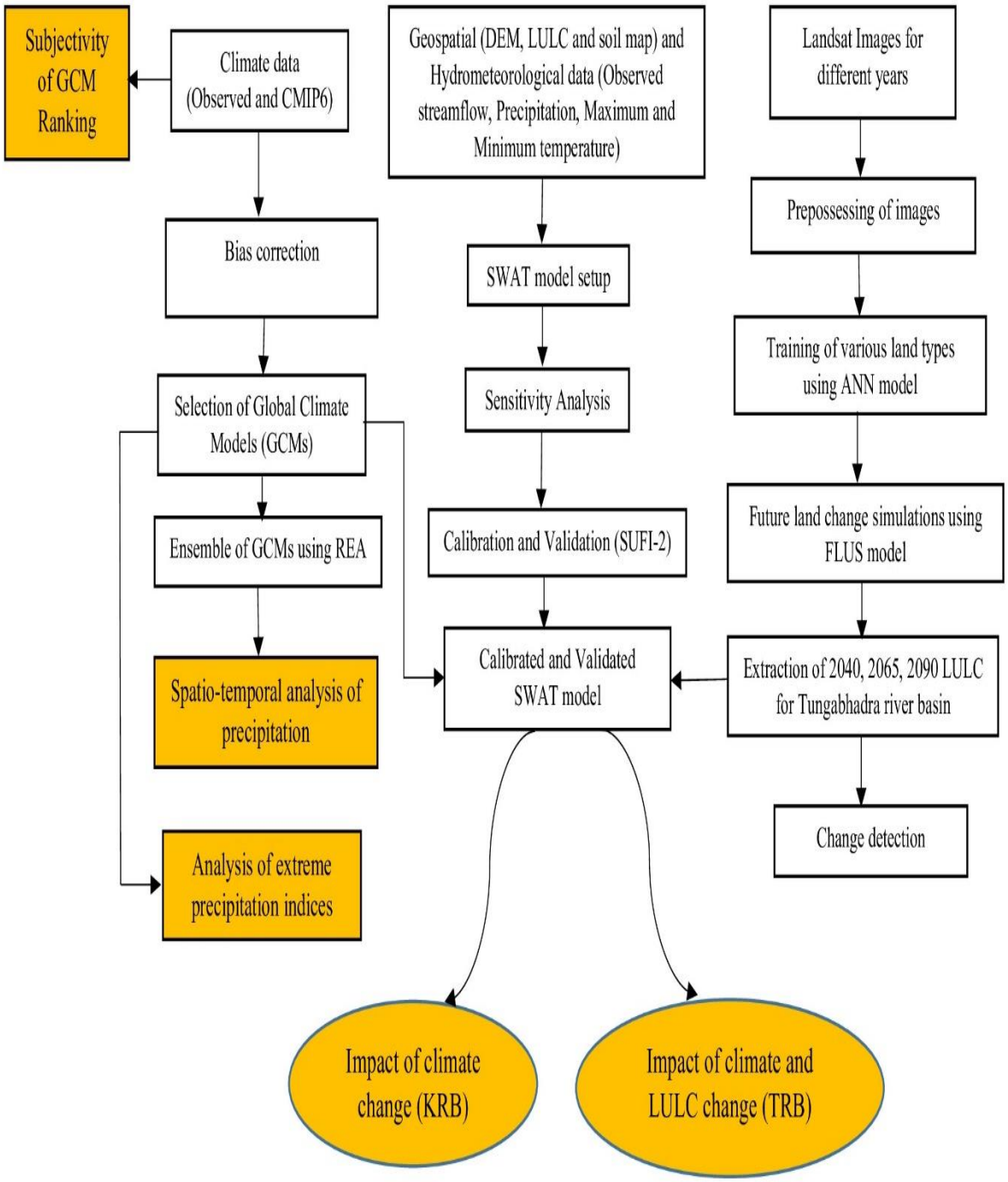

Figure 3.1 Overall Methodology of research work

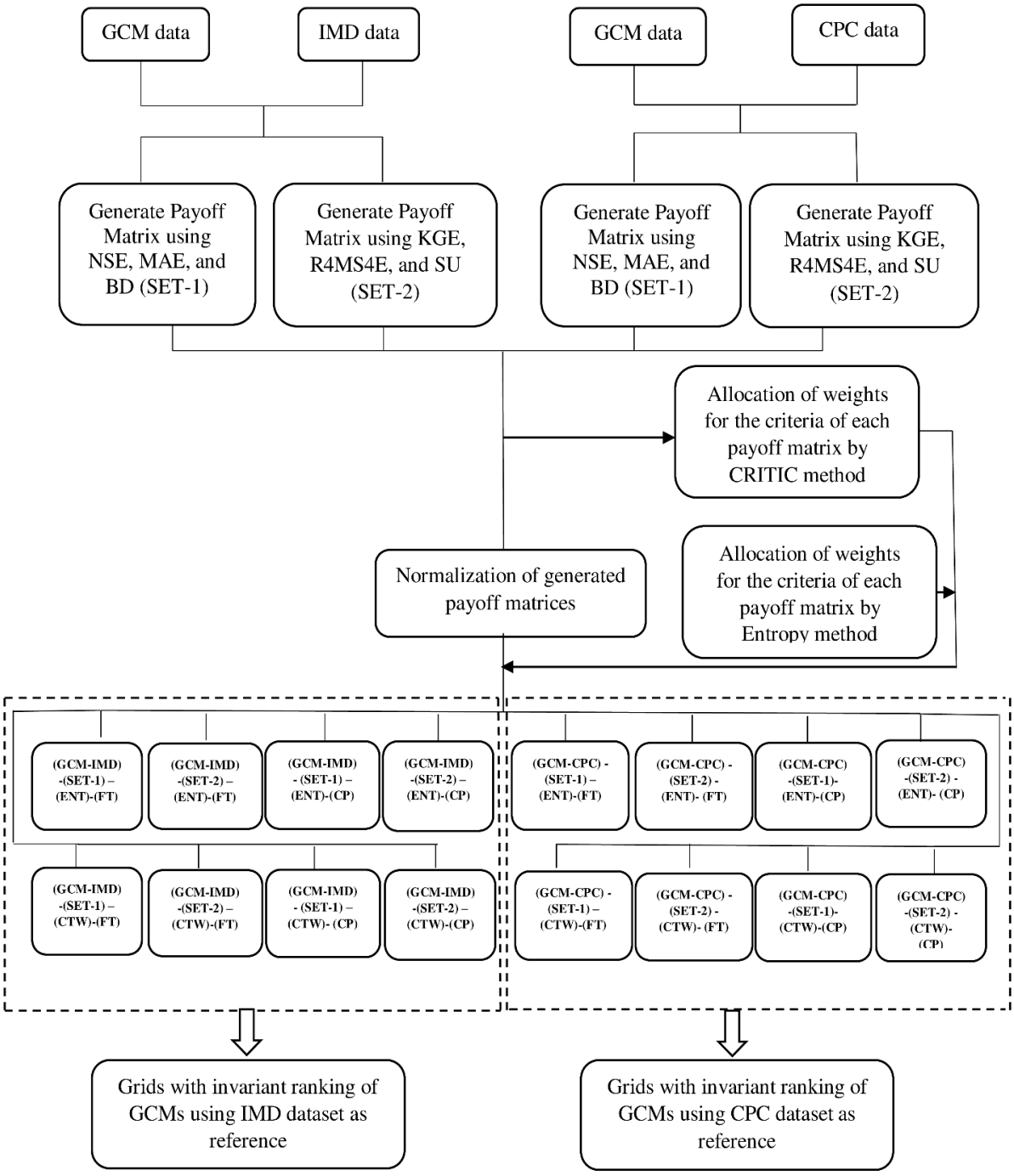

Figure 3.2 Proposed methodology to rank GCMs using various combinations

3.2 Study Area

3.2.1 General

Two study areas are considered in the proposed methodology. To meet the 1st objective i.e., for the analysis of subjectivity involved in ranking of the CMIP6-GCMs the country India is used. And for the 2nd, 3rd and 4th objectives i.e., for the comprehensive analysis of climate change impact on WBC in various aspects the whole KRB was used. Finally, to meet the 5th objective i.e., to investigate the coupled impact future climate and LULC change the TRB which is major tributary of KRB is used.

3.2.2 India

India is a tropical monsoon country that lies between 6°44'N to 35°30'N latitude and 68°7'E to 97°25'E longitude with a geographical area of 3,287,263 km^2. Large range of weather conditions exists in India making generalizations really difficult. To facilitate generalizations, the study area is delineated into eight major homogenous climatic regions by employing Koppen-Geiger climate classification as shown in Figure 3.3.

3.2.3 Krishna River Basin

The Krishna River Basin (KRB) is the fifth largest river basin in the Indian subcontinent and one of the most significant. The KRB covering a geographical area of about 2, 59,000 km^2 (almost 8% of the total geography of India) is the second (2nd) largest river basin in peninsular India between 73°20' and 81°E longitude 13°5'–19°24'N latitude. The Krishna river originates in the Western Ghats near Mahabaleshwar in the state of Maharashtra and extends in Karnataka, Telangana and Andhra Pradesh states with a total length of 1400 km and finally flows into the Bay of Bengal. It has a number of tributaries, with Bhima, Musi and Munneru joining the primary tributaries on the left and Ghatprabha, Malprabha and Tungabadhra joining on the right. The KRB is divided into seven subbasins: Tungabadhra Upper and Lower, Bhima Upper, Bhima Lower, Krishna Upper, Krishna Middle and Krishna Lower. The majority of the basin is composed of level land with a semi-arid climate (Koppen Classification), with the southwest monsoon rains accounting for about 90% of the total precipitation. Between 1985 and 2014, the basin's average annual precipitation varied from 403 mm in the south-east to 3,108 mm in the south-west, with an average of 960 mm, as illustrated in Figure 3.4. The basin's average lowest and maximum temperatures are 20.73˚C and 32.2˚C respectively. There are about 47 hydro-meteorological stations in the basin and streamflow has been observed to be

more on August to November and less in March to May. Fourteen land use categories are present across the KRB with the 76% of agriculture land is dominating. Five soil classifications are observed in KRB with main types of soil are laterite soils, salty and alkaline soils, mixed soils, red soils, alluvium and black soils. According to the 2011 census, there were 74.2 million people living in the basin and over 68% of the people are rural dwellers who rely mostly on agriculture for their living (Sarma et al., 2011). Population growth causes a significant demand for water for industrial and residential uses, placing stress on the basin's water resources. The large-scale water rights projects that have been created in every state cause disputes between states. The basin is experiencing water stress as a result of using more water than is available (Biggs et al., 2007). Additionally, they contend that in order to formulate a policy for the allocation of water for future usage, it is imperative to evaluate the monthly variations in climate factors and their impact on runoff. The semi-arid condition of the KRB and its impending physical water scarcity make it extremely vulnerable to fluctuations in the climate, particularly when it comes to precipitation. (WWAP, 2012). The Tunga (147 km) and Bhadra (178 km) rivers converge to form the Tungabhadra River, which is the principal tributary of the Krishna River. At an altitude of 1,198 meters above mean sea level (MSL), in Varahaparvatha highlands of the Western Ghats, these rivers originate separately from Gangamoola. They eventually combine to form the Tungabhadra River, which originates in the "Shivamogga" district. The interstate multipurpose project called the Tungabhadra dam is situated near Hosapete in Munirabad, in the "Koppala" district of Karnataka state. The TRB spans 13°8'60 N to 16°13'35 N latitude and 74°46'52 E to 78°01'29 E longitude. The region is vital to the whole hydrology, with a catchment area of 63,916 km^2 up to its mantralyam gauge point and converging in the Krishna River at Bavapuram. The southwest monsoon is major water resource for the TRB with the annual average precipitation is about 1100 mm (Bisht et al., 2018). The location map of the study area considered to meet the all the objectives is shown in Figure 3.3.

3.3 Data used in the study

The various sources and their data types that are required for the investigation are included in this section. The data includes Indian Meteorological Department (IMD), Climate Prediction Centre (CPC) data, CMIP6-GCMs, as well as geographical data such as soil maps, Digital Elevation Models (DEMs) and maps of LULC. These are explained in the sections that follow.

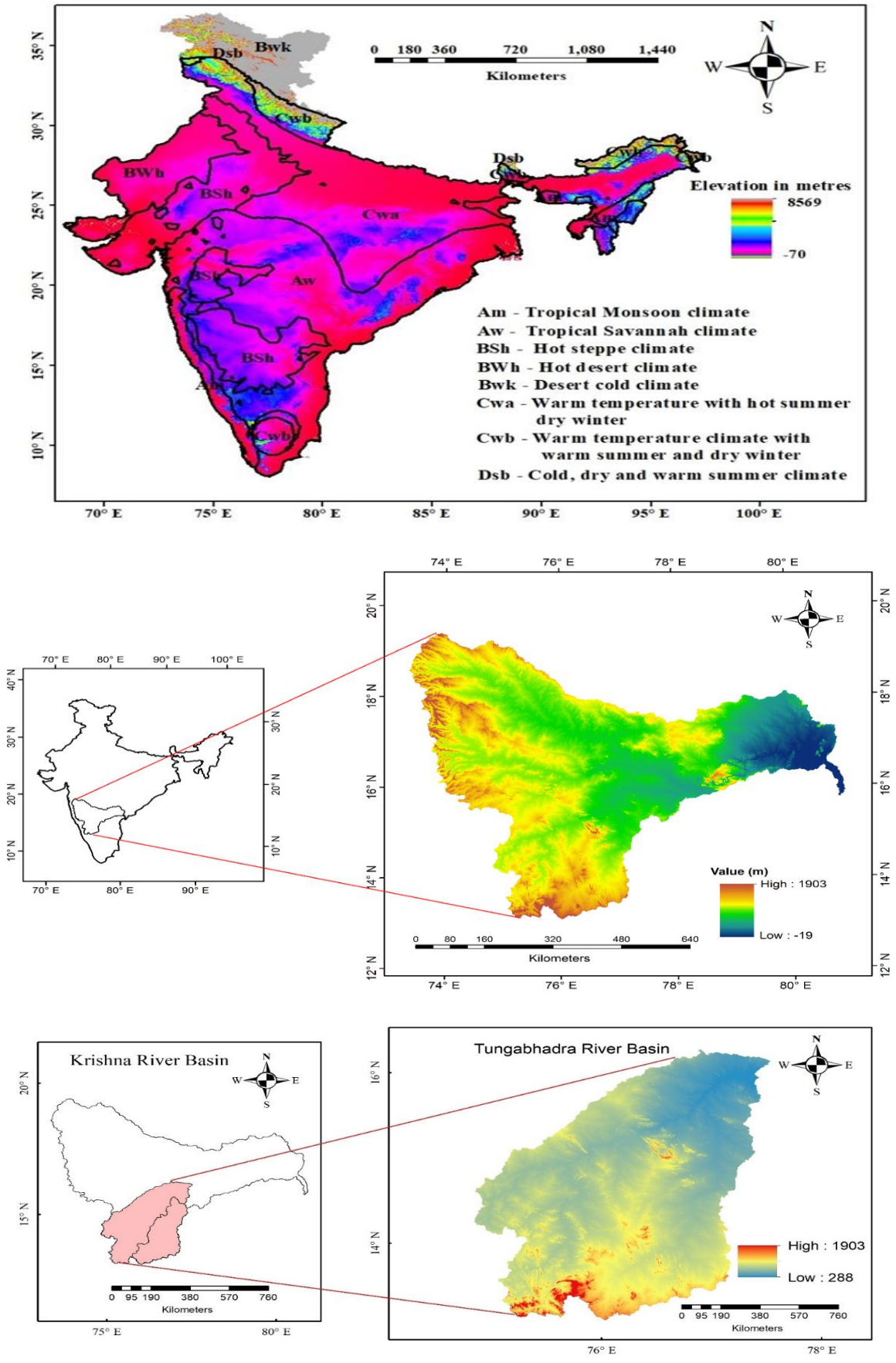

Figure 3.3 Location map of the Study area

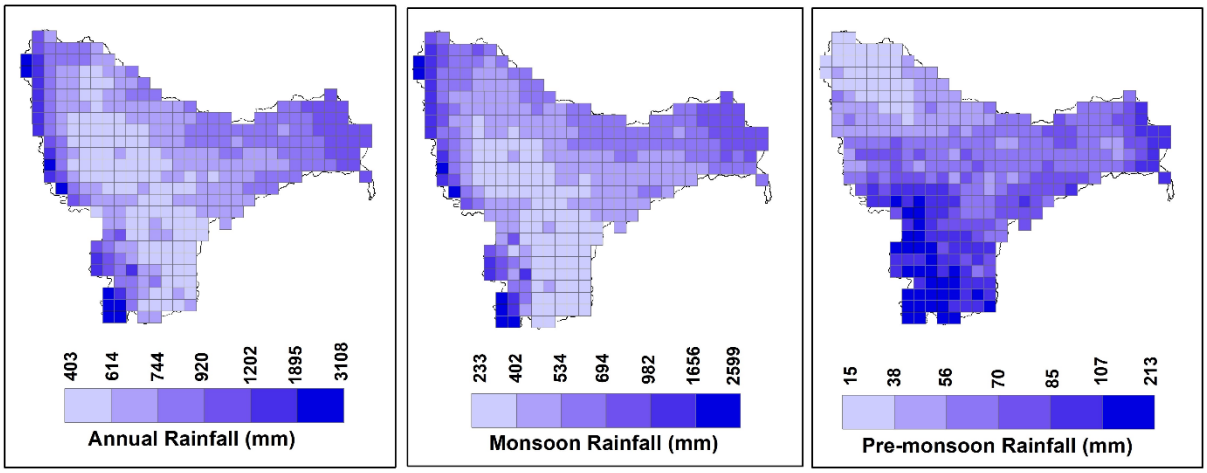

Figure 3.4 Geographical distribution of precipitation over KRB for mean Annual (left), Monsoon (middle) and Pre-monsoon (right) prepared from IMD data for 1985-2014

3.3.1 Indian Meteorological Department (IMD) data

In India, the hydro-meteorological stations are maintained by CWC. Daily gridded precipitation of 0.25^{o} X 0.25^{o}, minimum and maximum temperature of 0.5^{o} X 0.5^{o} are obtained from Indian Metrological Department (IMD; https://www.imdpune.gov.in/). The precipitation dataset has no missing values and developed from 6,955-gauging stations distributed all over India (Pai et al., 2014). And this data is performed better than other global gridded datasets such as National Centres for Environment Predictors (NCEP), Coordinated Regional Climate Downscaling Experiment (CORDEX) and Global Precipitation Climatology Project (GPCP) (Bandyopadhyay et al., 2018).

3.3.2 CMIP6-GCM data

Daily precipitation, maximum and minimum temperature data from GCMs of CMIP6 phase repositories are considered in this study to meet the objectives. This study used Tier-1 SSPs scenarios, which comprise SSP1-2.6, SSP2-4.5, SSP3-7.0 and SSP5-8.5, to offer a complete set of forcing objectives that are comparable to the RCPs used in CMIP5 in terms of both amplitude and dispersion. (Gidden et al., 2019) as shown in Table 3.1. Various GCMs downloaded based on their availability for different objectives. The GCMs data can be accessed from Earth System Grid Federation (ESGF) portal (https:/esgf-node.llnl.gov/search/cmip6).

3.3.3 Hydrological data

Daily streamflow data for six gauging stations such as Mantralayam, T.Ramapuram, Yadagir, Keesara, Dameracherla, Vijayawada (mouth of KRB) were obtained CWC for the period 1970

to 2010. The information regarding monthly storage, volume, area, effective and gross storage capacity of the hydraulic structures and spillway designed capacities are downloaded from Water Resources Information System (WRIS-India) (https://indiawris.gov.in/wris/).

3.3.4 Geo-Spatial data

The primary geo-spatial datasets utilised as input for the SWAT model include soil, slope, LULC and DEM maps. A 30 m spatial resolution of DEM available form Shuttle Radar Topography Mission (SRTM) is used to delineate KRB and TRB. The required LULC of water base land use data contains crop specific digital layers of 400 m resolution, suitable for use in GIS is taken from water base (http://www.waterbase.org/) and digital soil map is taken from Food and Agriculture Organization (FAO), with a scale of 1:5,000,00 for KRB. The future LULC maps under SSP-RCP scenario for the respected three future time periods i.e., 2040, 2065 and 2090 were extracted and is forced along with future climate data for the hydrological modelling of TRB (Chen et al., 2022). All these spatial maps represent heterogeneity of the catchment and are converted into required projected coordinate system. The DEM, LULC and soil maps for the KRB and TRB are shown in Figure 3.5.

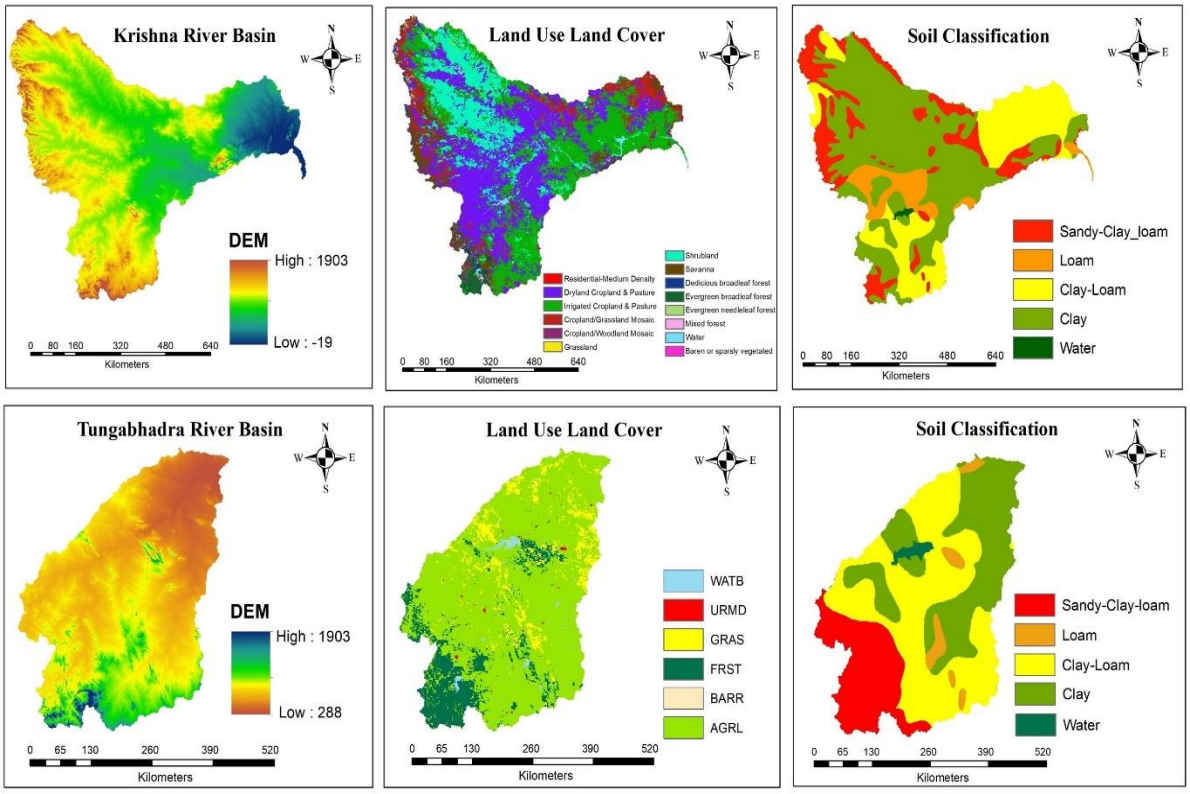

Figure 3.5 DEM, LULC and soil maps for Krishna and Tungabhadra river basins

Table 3.1 CMIP6 climate models and their sources used to meet all the objectives in this study

S.NO	GCM Name	Model Source	Resolution (Lat. X Lon.)	Objective-1	Objective-2	Objectives 3,4,5
1	ACCESS-CM2	Commonwealth Scientific and Industrial Research Organisation, Australia	1.25º X 1.875º	✓	✓	✓
2	ACCESS-ESM1-5	Commonwealth Scientific and Industrial Research Organisation, Australia	1.25º X 1.875º	✓	✓	✓
3	AWI-CM1-1-MR	Alfred Wegener Institute, Helmholtz Centre for Polar and Marine Research, Germany	0.94º X 0.94º	✓	×	×
4	BCC_CSM2-MR	Beijing Climate Center, China	1.12º X 1.13º	✓	✓	✓
5	BCC_ESM1	Beijing Climate Center, China	1.12º X 1.13º	✓	×	
6	CanESM5	National Center for Atmospheric Research, Climate and Global Dynamics Laboratory, USA	2.79º X 2.81º	✓	✓	✓
7	CESM2	National Center for Atmospheric Research, Climate and Global Dynamics Laboratory, USA	0.94º X 1.25º	×	✓	×
8	CESM2-WACCM	National Center for Atmospheric Research, Climate and Global Dynamics Laboratory, USA	0.94º X 1.25º	×	✓	✓
9	EC-EARTH3	EC-EARTH consortium published at Irish Centre for High-End Computing, Netherlands /Ireland	0.7º X 0.7º	✓	✓	✓
10	EC-EARTH3-Veg	EC-EARTH consortium published at Irish Centre for High-End Computing, Netherlands /Ireland	0.7º X 0.7º	✓	✓	✓
11	FGOALS-f3-L	Beijing Climate Center, China	1º X 1.3º	×	✓	×
12	GFDL-CM4	NOAA Geophysical Fluid Dynamics Laboratory, USA	1º X 1.25º	✓	✓	×
13	GFDL-ESM4	NOAA Geophysical Fluid Dynamics Laboratory, USA	1º X 1.25º	✓	✓	✓
14	GISS-E2-1-G	NASA/GISS Goddard Institute for Space Studies, USA	2º X 2.5º	✓	✓	×
15	IITM	Centre for Climate Change Research, Indian Institute of Tropical Meteorology Pune, Maharashtra, India	1.88º X 1.88º	×	✓	✓
16	INM-CM4-8	Institute for Numerical Mathematics, Russia	1.5º X 2º	✓	✓	✓
17	INM-CM5-0	Institute for Numerical Mathematics, Russia	1.5º X 2º	✓	✓	✓
18	IPSL-CM6A-LR	Institute Pierre Simon Laplace, France	1.27º X 2.5º	✓	✓	✓
19	MIROC6	Atmosphere and Ocean Research Institute, University of Tokyo, Japan	1.4º X 1.4º	✓	✓	✓
20	MPI-ESM-1-2-HAM	Max Planck Institute for Meteorology, Germany	1.87º X 1.88º	✓	×	×
21	MPI-ESM1-2-HR	Max Planck Institute for Meteorology, Germany	0.94º X 0.94º	✓	✓	✓
22	MPI-ESM1-2-LR	Max Planck Institute for Meteorology, Germany	1.85º X 1.88º	✓	✓	✓
23	MRI-ESM2-0	Meteorological Research Institute, Japan	1.12º X 1.13º	✓	✓	✓
24	NESM3	Nanjing University of Information Science and Technology, China	1.87º X 1.88º	✓	×	×
25	NorCPM1	Center for International Climate and Environmental Research, Norway	1.89º X 2.5º	✓	✓	×

26	NorESM2-LM	Center for International Climate and Environmental Research, Norway	1.89° X 2.5°	✓	×	✓
27	NorESM2-MM	Center for International Climate and Environmental Research, Norway	0.94° X 1.25°	✓	✓	✓
28	SAM0-UNICON	Seoul National University, Republic of Korea	0.94° X 1.25^0	✓	×	×

3.4 Procedure Involved in Subjectivity of GCM Rankings

Two gridded datasets from IMD and CPC are used as reference datasets to evaluate CMIP6 models for India study area. Based on the availability of the T_{max} and T_{min} data at daily temporal resolution for a longer period, the selection of these datasets are made. IMD gridded dataset is obtained at a spatial resolution of 0.5° x 0.5°, whereas the CPC dataset is developed using 30,000 stations data (Xie et al., 2010) for the same spatial resolution. In order to rank these 24 GCMs , they are re-gridded to a common spatial resolution raging from 2°X2° to 3°X3° (Ahmed , et al., 2019; Jiang et al., 2019; Johnson & Sharma, 2009; Khan et al., 2018; Lutz et al., 2016; Noor et al., 2019; Salman et al., 2018; Raju et al., 2017; Raju & Kumar, 2015; Woldemeskel et al., 2014). To regrid the data to the spatial resolution of reference gridded datasets (Hassan et al., 2020; Pour, Shahid, & Chung, 2018; Tiwari et al., 2014), all the acquired GCMs are regridded to a spatial resolution of 0.5°x0.5° using bilinear interpolation. Six indicators, namely, NSE, KGE, MAE, Fourth Root Mean Quadrupled Error (R4MS4E), BD and SU are considered among the numerous performance indicators available. Two sets of criteria are prepared with each set consisting of three chosen model evaluation metrics. NSE, MAE and BD are enveloped as first set of criteria and KGE, R4MS4E and SU are fixed as the second set of criteria. The first metric in each set will be a dimensionless coefficient that assess the strength of linear dependence between modelled and observed values with accepted standards. NSE and KGE are chosen for this purpose as they are globally accepted and extensively used for model evaluation. The second metric in each set will be based on residual error between observed and simulated time series in respective variables. MAE and R4MS4E are selected for this purpose, where the former allocates equal weights to all the residual errors and the latter allocates higher weights to the errors with higher magnitudes due to a higher power function used in it. MAE yields information about overall match between observed and simulated variables, whereas R4MS4E informs the match between extreme events. The third metric is a frequency-domain based metric and BD and SU are employed in it. BD measures the closeness between the Probability Density Functions (PDFs) of the simulated and observed values, while SU is computed based on information entropies of the observed and simulated data in SET-2.

The amount of common information entropies between two time series are quantified using Mutual Information (MI). SU normalizes the MI in order to overcome the biasedness of MI with higher number of values. The formulation of all the six metrics are tabulated in Table 3.2

Table 3.2 Model performance evaluation metrics with respective equations, range and ideal values

S.No	Performance Evaluation Metric	Equation	Range	Ideal value
1	Nash Sutcliff Efficiency (NSE)	$1 - \frac{\sum_{i=1}^{n}(P_i - O_i)^2}{\sum_{i=1}^{n}(O_i - \bar{O_i})}$	-∞ to 1	1
2	Bhattacharyya Distance (BD)	$-ln\left(\sum_{i=1}^{nb}\sqrt{f_{P_i} f_{O_i}}\right)$	0 to ∞	0
3	Mean Absolute Error (MAE)	$\frac{\sum_{i=1}^{n}\lvert(O_i - P_i)\rvert}{n}$	0 to ∞	0
4	Fourth Root Mean Quadrupled Error (R4MS4E)	$\sqrt[4]{\frac{\sum_{i=1}^{n}(P_i - O_i)^4}{n}}$	0 to ∞	0
5	Kling Gupta Efficiency (KGE)	$1 - \sqrt{(r-1)^2 + (\frac{\mu_{sim}}{\mu_{obs}} - 1)^2 + (\frac{\sigma_{sim}}{\sigma_{obs}} - 1)^2}$	-∞ to ∞	0
6	Symmetric Uncertainty (SU)	$2\,\frac{MI\,(O_i, P_i)}{H(O_i) + H(P_i)}$; $MI\,(O_i, P_i) = \sum_{i=1}^{nb} p(O_i, P_i)\, log\, \frac{p(O_i, P_i)}{p(O_i)\,.\,p(P_i)}$	0 to 1	1

Where, P_i, O_i represent the GCM predicted and reference (observed) values at ith time respectively; $\bar{O_i}$represents the mean of reference value and n represents the number of data points. f_p, f_o represent the probabilities calculated from the frequencies of predicted and reference values at a given bin respectively and "nb" represents the total number of bins chosen to study the match between PDF's observed and simulated values. $H(O_i), H(P_i)$ represent entropies of observed and predicted values respectively. $p(O_i)$, $p(P_i)$ represent observed and simulated probabilities at ith bin respectively and $p(O_i, P_i)$ represents the joint probability.

3.4.1 Payoff Matrix

A payoff Matrix (M) is generated at each grid with GCMs as rows and performance criteria representing columns. The payoff matrix may have a range of values and are brought to a

common range, i.e. 0 to 1, by linear sum normalization technique. The normalized element of a payoff matrix N_{ij} is given in Eqn. 3.1.

$$N_{ij} = \frac{M_{ij}}{\sum_{i=1}^{G} M_{ij}} \quad (3.1)$$

Where M_{ij} is the value of j^{th} model evaluation metric of i^{th} GCM and G is the total number of GCMs.

3.4.2 Objective Weights of Criteria

Two objective weighting methods are employed namely Entropy method and Criteria Importance Through Intercriteria Correlation (CRITIC) method. Entropy method is based on the concept of entropy which measures the uncertainty in the context of probability theory; larger the entropy lesser the information quantity. The linear sum normalization is opted so that all the normalized values in each column acts a probabilities. By measuring the relative intensities of criteria, weights are allocated. The weights for each criteria are calculated using Eqns. 3.2 to 3.4.

$$E_j = -\frac{1}{G}\sum_{j=1}^{G} N_{ij}\, log_e\, N_{ij} \quad (3.2)$$

$$d_j = 1 - E_j \quad (3.3)$$

$$w_j = \frac{d_j}{\sum_{j=1}^{J} d_j} \quad (3.4)$$

Where, E_j, d_j, w_j are respectively entropy, divergence and weight of j^{th} indicator; and J is total number of criteria in the payoff matrix.

As Entropy method uses logarithmic transforms to compute weights of each criteria, negative values should be avoided. For instance, logarithm transform function in entropy fails when the values of NSE or KGE are less than or equal to zero. Hence, to resolve this issue, 1-NSE and 1-KGE are used in the payoff matrix to avoid negative values and facilitate the computation of criteria weightage through entropy method. Instead of using SU, 1-SU is tabulated in the payoff matrix to make the ideal solution of both sets to (0,0,0). In CRITIC method the values of payoff matrix M_{ij} are transformed to the interval [0, 1] based on the concept of ideal point. The

transformed value C_{ij}, the quantity of information (Q_j) and the objective weights (w_j) of each criteria are computed using Eqns 3.5 to 3.7.

$$C_{ij} = \frac{M_{ij} - M_j^{**}}{M_j^{*} - M_j^{**}} \tag{3.5}$$

$$Q_j = \sigma_j * \sum_{k=1}^{J} (1 - r_{jk}) \tag{3.6}$$

$$w_j = \frac{Q_j}{\sum_{j=1}^{J} Q_j} \tag{3.7}$$

Where, M_j^{*}, M_j^{**} represent the ideal and anti-ideal values of j[th] criteria of payoff matrix respectively. Standard deviation of each column (σ_j) is computed which indicates the contrast intensity of each criterion. A symmetric matrix ($J \times J$) with element r_{jk} is formulated, where the value of r_{jk} is linear correlation coefficient between j[th] column and k[th] column.

3.4.3 MCDM Techniques

Two MCDM techniques, TOPSIS and CP are preferred among several MCDM techniques. TOPSIS method determines the alternative with shortest distance to ideal and longest distance to anti-ideal solutions. CP ranks the conflicting alternatives by an acceptable compromise formula.

3.4.3.1 Fuzzy TOPSIS (FTOPSIS)

FTOPSIS has an added advantage due to its potential to address imprecision induced by interpolation techniques in the calculated metrics and Triangular membership function for criteria are adopted in this study. The membership function of N_{ij} (normalised performance criteria), their ideal ($N_j{}^{*}$) and anti-ideal ($N_j{}^{**}$) are defined as $\widetilde{N}_{ij}(x_{ij}, y_{ij}, z_{ij})$, $\widetilde{N}_j{}^{*}(x_j{}^{*}, y_j{}^{*}, z_j{}^{*})$ and $\widetilde{N}_j{}^{**}(x_j{}^{**}, y_j{}^{**}, z_j{}^{**})$ respectively; where x, y and z represent lower, middile and upper values of the triangular membership function. The spread of the triangle is equally distributed on either sides and the spread is determined as $\min\{(1 - max(N_j), min(N_j)\}$. The proximity of an alternative (i) from the Fuzzy Positive Ideal Solution {FPIS(0,0,0)} and Fuzzy Negative Ideal Solution {FNIS(1,1,1)} are represented by DS_i^{+} and DS_i^{-} respectively. Relative closeness (CR_i) of each alternative is calculated using Eqns. 3.8 to 3.10 and higher CR_i values are preferred.

$$DS_i^+ = \sum_{j=1}^{J} w_j \times d\left(\widetilde{N}_{ij}, \widetilde{N}_j^{\,*}\right) = \sum_{j=1}^{J} w_j \times \sqrt{\frac{\left(x_{ij} - x_j^*\right)^2 + (y_{ij} - y_j^*)^2 + (z_{ij} - z_j^*)^2}{3}} \quad (3.8)$$

$$DS_i^- = \sum_{j=1}^{J} w_j \times d\left(\widetilde{N}_{ij}, \widetilde{N}_j^{\,**}\right) = \sum_{j=1}^{J} w_j \times \sqrt{\frac{\left(x_{ij} - x_j^{**}\right)^2 + (y_{ij} - y_j^{**})^2 + (z_{ij} - z_j^{**})^2}{3}} \quad (3.9)$$

$$CR_i = \frac{DS_i^-}{(DS_i^- + DS_i^+)} \quad (3.10)$$

3.4.3.2 Compromise Programming (CP)

Compromise Programming (CP) is a distance based MCDM technique that aggregates multiple criteria into a distance metric called L_p and identifies the solution that has minimal distance from the ideal solution and is computed using Eqn. 3.11.

$$L_p(i) = \left[\sum_{j=1}^{J} w_j \left|N_j^* - N_j(i)\right|^p\right]^{\frac{1}{p}} \quad (3.11)$$

Where, $N_j(i)$is the normalized value of indicator j for ith GCM , N_j^* is the normalized ideal value of indicator j, w_j is weight assigned to indicator j and p is parameter (1 for linear and 2 for squared Euclidean distance). The GCM with lower Lp metric value is as the most prefered one. The proposed methodology to rank GCMs is dipicted in Figure 3.2.

3.5 Precipitation Projection across KRB

The procedure involving the selection of GCMs and spatiotemporal projections of the precipitation changes are outlined below.

Precipitation simulations of 21 GCMs are re-gridded to reference dataset of IMD spatial resolution at 0.25^o x 0.25^o using bilinear interpolation technique and bias corrected using quantile mapping method.

2. The performance of 21 GCMs is evaluated against IMD as reference data by applying SU at 348 grid points covering KRB, for the period of 1951-2014.

3. GCM rankings are estimated based on the aggregated score at all grids obtained using pattern of ranking scores using MCDA over KRB.

4. Top five GCMs were selected based on the aggregated score and future precipitation simulations for different SSPs are bias corrected using same quantile method.

5. Development of MME of top five GCMs using REA method to reduce the uncertainty in projections.

6. Evaluation of spatiotemporal changes of precipitation over KRB during 2015-2040, 2041-2070 and 2071-2100.

The procedure used for the section of GCMs using SU is given below

3.5.1 Quantile Mapping Bias Correction

However, GCMs are extracted and re-gridded to the spatial resolution of observed dataset of 0.25º x 0.25º, there will be bias in the extreme events. Hence this bias should be corrected before GCM performance assessment for better matching of simulations with the observed dataset. In present study a non-parametric Quantile Mapping (QM) method (Cannon, 2016; Cannon et al., 2015; Gudmundsson et al., 2012*)* is employed to remove the bias in each month of GCMs. QM technique adopts the Cumulative Distribution Function (CDF) of simulated data to that of observed data. The transformed function for correcting the bias in simulated data is shown in eqn. 3.12.

$$R_o = F_o^{-1}(F_m(R_m)) \quad (3.12)$$

Where, R_m and R_o are the modelled and observed rainfall, F_m denotes CDF of R_m and F_o^{-1} denotes the inverse CDF (quantile function) corresponding to R_o. The empirical CDF of simulated and observed data is estimated and is applied for simulated GCM data. Figure 3.6 displays the quantile plot that compares the precipitation data of a grid point that has been before and after bias corrected. For every climate model at 348 grid points, the same bias correction process is used.

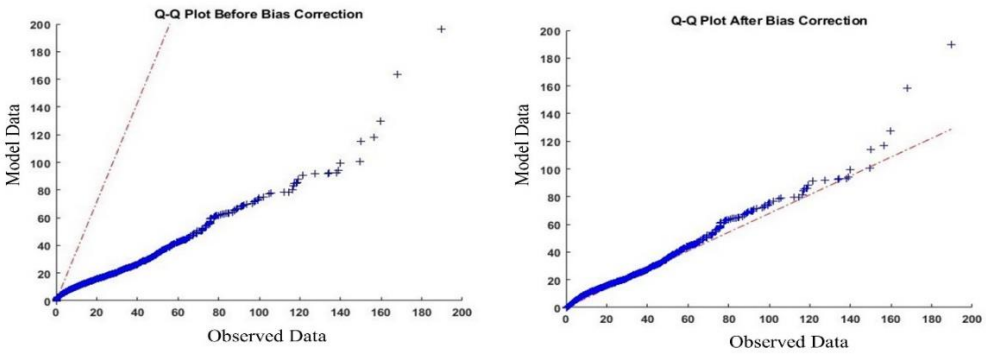

Figure 3.6 Quantile Mapping bias correction of a grid point in KRB

3.5.2 Symmetric Uncertainty (SU) for Selection of GCMs

The selection of relevant GCMs for climate studies becoming major challenge in projecting the climate. SU is an information entropy theoretical filter-based method which is computes similarity between the observed and simulated time series in terms of MI entropies. If P(A) and P(B) denotes the Probability Density Functions (PDF) of observed and simulated variables, the joint PDF will be P(A,B) then the MI between A and B can be quantified as Eqn. 3.13.

$$MI(A;B) = \sum P(A,B)\, log \frac{P(A,B)}{P(A)\,.P(B)} \quad (3.13)$$

From the properties of MI, it can be written as differences in the sum of individual entropies and joint entropy using Eqn. 3.14.

$$MI(A;B) = H(A) + H(B) - H(A,B) \quad (3.14)$$

Where, $H(A), H(B)\ and\ H(A,B)$, represents entropies of A, B and joint entropy of A, B, respectively.

The SU can overcome the drawback of the MI which is biased to higher number of values by normalising the MI with the entropies of two variables is given in Eqn. 3.15. Therefore, SU is an unbiased estimation of similarity between two time series with the range between 0 to 1. Furthermore, without requiring knowledge of the nature of the underlying distributions and conditional dependencies, the SU offers a generic measure that connects dependent and independent variables. Additionally, SU performs well when selecting features from large datasets. When rating GCMs, the SU filter is a helpful alternative to using traditional statistical criteria like coefficient of determination and normalised root mean square error. (Homsi et al., 2020; Pour et al., 2018; Press et al., 1996; Salman et al., 2018; Wu & Zhang, 2004).

$$SU = 2 \times \frac{MI(A;B)}{H(A)+H(B)} \quad (3.15)$$

The SU between two variables is 0 means no agreement between two random variables and this occurs if and only if the two variables are statistically independent. If the SU value is 1 means perfect agreement between two variables (Shreem et al., 2016).

3.5.3 GCMS Ranking Using MCDM

Aggregation of information from different sources using MCDM is found to efficient in selecting the alternatives (Raju et al., 2017; Salman et al., 2019). At a single grid point ranking of GCM can be assessed easily. When multiple grids involve it is difficult to select the GCMs, because of distinct results will be given by GCMs at different grid points. MCDM techniques will be effectively used to overcome this complexity and used for GCMs ranking for KRB. The following steps involved in the MCDM technique.

i) GCMs are ranked 1st 2nd 3rd etc. at each grid point using score obtained by using SU. ii) Specified weight (w_i) is given to each GCM such way that inverse weight is applied to ranking of GCMs. iii) the frequency(Fr_i) of each GCMs for each rank was calculated. And Total Ranking Weight (TRS) of each GCM calculated using MCDM given in Eqn. 3.16

$$TRW = \sum_{i=1}^{5} Fr_i * w_i \quad (3.16)$$

iv) The GCMs final ranking was find out by sorting the Total Ranking Weight (TRW) in descending order. In the present study the GCMs rankings up to 5th position in each grid only considered and remaining are ignored because it is assumed that they cannot simulate the precipitation well at that grid point.

3.5.4 Reliability Ensemble Averaging (REA)

With more number of GCMs the projections will vary from one GCM to other because of structural differences (Sachindra et al., 2014). The Multi-model Ensemble Mean (MME) will reduce the uncertainty involved in the individual GCM and can enhance accuracy of projections (Iqbal et al., 2020; Pour, Shahid, Chung, et al., 2018; Tebaldi & Knutti, 2007; H. Zhang & Huang, 2013). Generally MME approaches are divided in to two types. (i) Simple Ensemble average (SEM) and (ii) Weighted Ensemble Method (WEM). Equal weightage is allotted to each GCM in SEM whereas, in WEM the weights are allocated by based on historical relationship between observations and GCMs (Sanchez-Gomez et al., 2009). REA method is used to find the weights of the selected five GCMs and projections of different SSP scenarios. REA can be used to quantify uncertainty of multiple GCMs prior to hydrological modelling that reduces the vagueness of using projections of multi models (Chandra et al., 2015). REA method incorporates two reliability criteria to assign weights to GCMs such as "model performance" where the capability of the model to capture the original data series and "model convergence" where model simulation is converging to a specified forcing scenario.

Procedure involved in REA method to get the weighted GCM projection time series is as follows:

1. The RMSE is estimated by considering Cumulative Distribution Function (CDF) deviations for the observed precipitation and all the GCM simulations for control time period. The inverse of the RMSE values are treated as weight proportionality and weighted sum across all the GCMs is equal to 1.The higher weights assigned to best performing GCMs. The initial weight of GCMs computed using Eqn. 3.17.

$$W_i = \frac{1/RMSE_i}{\sum_{i=1}^{n} 1/RMSE_i} \qquad i = 1,2,3,\ldots\ldots\ldots\ldots,n \tag{3.17}$$

2. The weights which are obtained through the model performance criteria treated as initial weights which can be used for performing respective GCM model convergence.
3. The weighted mean CDF (CDF_M^F) for future scenario is estimated by multiplying the corresponding initial weight(W_i) with CDF of the future simulation of ith GCM (CDF_i^F) using Eqn.3.18.

$$CDF_M^F = \sum_{i=1}^{n} W_i * CDF_i^F \tag{3.18}$$

4. Now, RMSE will be computed between CDF of individual GCMs projections and future weighted mean CDF.
5. Next, the mean of the inverse of RMSE estimated using steps 1 and 4 is averaged, therefore the new weights are allocated to GCMs proportionally used, such that the new weights sum will become 1 for all the GCMs.
6. To satisfy the model convergence conditions, repeat steps 2 through 5 until the old weight and the new weight are equal.

The procedure which is explained above is applied at 348 grid points over the KRB for the variable rainfall and the final weights obtained are multiplied with respective scenario in a grid therefore the summation of the weighted values will be considered as ensemble average for that specified grid.

The spatiotemporal variations of rainfall was evaluated from the MME precipitation projections and analysed near future 2015 – 2040, against historical period 1989-2014, mid future (2041 – 2070) and end future (2071-2100) against 1985- 2014 to find changes in the KRB.

3.6 Precipitation Extremes Calculation

To meet this objective the top five GCMs were considered based on daily data after applying SU concept as mentioned in the section 3.5.2 and 3.5.3. The present study used eleven (11) ETCCDI extreme precipitation indices (TOTPR, R95P, R99P, RX1day, RX5day, R10, R20, R50, CWD, CDD and SDII) which are widely used across the globe (Alsarmi & Washington, 2014; John et al., 2022; X. Zhang et al., 2011) and four seasonal precipitation indices (Winter, Post-monsoon, Monsoon, Pre-monsoon) whose definitions are presented in Table 3.3.

Table 3.3 Extreme precipitation indices and seasonal precipitation indices and their definitions (PP = Precipitation).

Name of Indice	Index	Definitions	Units
Total annual-wet day PP	TOTPR	daily PP sum > 1.0mm	mm
very heavy wet days	R95p	Total annual PP when PP > 95th percentile	mm
extremely wet days	R99p	Annual total PPR when PP> 99th percentile	mm
Max 1-day PP	RX1day	Yearly maximum 1-day PP	mm
Max 5-day PP	RX5day	Yearly maximum consecutive 5-day PP	mm
Count of slightly heavy PP days	R10	Annual number of days where PP ≥ 10 mm	Days
Count of heavy PP days	R20	Annual number of days where PP ≥ 20 mm	Days
Count of very heavy PP days	R50	Annual number of days where PP ≥ 50 mm	Days
Consecutive Wet Days	CWD	Maximum count of consecutive days with PP ≥1 mm	Days
Consecutive Dry Days	CDD	Maximum number of consecutive days with PP < 1 mm	Days
Simple Daily Intensity Index	SDII	Total annual PP divided by the number of wet days (PP ≥ 1.0 mm) in the year	mm/day
Total winter PP	Winter	Total winter PP in wet days	mm
Total post-monsoon PP	Post-monsoon	Total post-monsoon PP in wet days	mm
Total monsoon PP	Monsoon	Total monsoon PP in wet days	mm
Total pre-monsoon PP	Pre-monsoon	Total pre-monsoon PP in wet days	mm

3.6.1 Trend Analysis

Non-parametric Mann-Kendall (MK) test (Kendall 1975; Mann 1945) is employed to analyse the temporal trends of precipitation extremes in the KRB for the IMD observed period (1973-2003). The MK test is independent, not effected by outliers and missing data to detect the trend in variables such as precipitation, temperature and streamflow. (Longobardi and Villani 2010; Asfaw *et al.* 2018; Ali *et al.* 2019). The slope of the trend line was determined using Sen's method (Sen, 1968; Theil, 1992) at a 5% level of significance. The MK statistic (S) indicates

the direction of the trend and is computed as

$$S = \sum_{i=1}^{r-1} \sum_{j=i+1}^{r} \operatorname{sgn}(t_j - t_i) \tag{3.19}$$

Where, t_j and t_i refers to observations with j > i and r is the length of the dataset

$$\operatorname{sgn}(t_j - t_i) = \begin{cases} 1 & \text{if } (t_j - t_i) > 0 \\ 0 & \text{if } (t_j - t_i) = 0 \\ -1 & \text{if } (t_j - t_i) < 0 \end{cases} \tag{3.20}$$

In the case of large datasets (r > 10), MK statistic (S) is approximately normally distributed with mean zero and variance σ_s is given by

$$\sigma_s = \frac{t(t-1)(2t+5) - \sum_{i=1}^{x} o_i(o_i-1)(2o_i+5)}{18} \tag{3.21}$$

Where, x = count of tied groups, o_i denotes the number of tied data of extent i, tied group represents a set of data with the same value.

The standard normal test statistic Z_s is estimated as:

$$Z_s = \begin{cases} \dfrac{S-1}{\sqrt{\sigma_s}} & \text{if } S > 0 \\ 0 & \text{if } S = 0 \\ \dfrac{S+1}{\sqrt{\sigma_s}} & \text{if } S < 0 \end{cases} \tag{3.22}$$

Negative and positive values of Z_s indicates decreasing and increasing trends respectively.

The slope estimator of the trend (Q) is computed using Theil–Sen Approach (TSA) as follows

$$Q = \frac{(t_j - t_i)}{(j-i)} \quad \text{For } j>i \tag{3.23}$$

Sen's slope (Y) is computed from the median of the slope as

Sen (Y) = Median (Q)

3.6.2 Correlation Analysis

The daily discharge data at Vijayawada gauge station, the terminal outlet of the KRB downstream is used in this study. Daily discharge data available from 1973-2003 is used to compute Average Annual Daily Discharge (AADD) and Maximum Annual Daily Discharge (MADD). Pearson correlation coefficient (r) is used to analyse the association between the discharge with extreme precipitation indices and among the extremes in the KRB. The Support Vector Machine (SVM) regression is developed between Annual TOTal PRecipitation (TOTPR) and (AADD) to predict the future streamflow. For the detailed methodology of this SVM technique, the readers can refer to (Ghosh and Mujumdar 2008; Ghosh 2010). Finally the spatial distribution of the future precipitation extremes were analysed.

3.7 Hydrological Model Set Up

Among the availble18 CMIP6-GCMs, SU is used to identify the top 50% of GCMs for hydrological modelling. For the current investigation, SWAT has been selected to simulate the hydrological fluxes of TRB and KRB. The SWAT model has the capability to simulate the impacts of the long term climate and LULC variations on the hydrology in the large complex catchments (Arnold et al., 2012; Neitsch et al., 2011; Wang et al., 2008). SWAT model divides the entire catchment into sub-catchments, based on topography and then segregates into Hydrological Response Units (HRUs) using the unique combinations of slope, LULC and soil classes. The HRUs are split vertically divided into various control volumes, such as surface layer, root zone, shallow aquifer and deep aquifer. By using climate data and LULC patterns, SWAT model can estimate anticipated watershed scenarios. Moreover, it has the ability to evaluate streamflow variability by taking into account forecasted climate variables for the future. Two sub-basins such as KRB and TRB are considered for the SWAT application of hydrological modelling. KRB is used for the climate change impact assessment of WBC for four SSP scenarios namely, SSP1-2.6, SSP2-4.5, SSP3-7.0 and SSP5-8.5. The TRB is used for the investigation of the coupled impact of future climate and LULC for two SSP scenarios namely, SSP1-2.6 and SSP5-8.5. The entire KRB is divided into 85 sub-basins after delineation process and 5% overlap of LULC, soil and slope is provided to define HRUs resulting into 1490 HRUs as shown in Figure 3.7. The water storage structures in any basin will significantly influence the performance of the model which shows impact on the WBC (Chanapathi & Thatikonda, 2020; Sahoo et al., 2018). To improve the model performance and reduce the uncertainty in the output, thirteen (13) major reservoirs such as Bhadra, Tungabhadra,

Nagarjunasagar, Srisailam, Almatti, Koyana, Narayanapura, P.D. Jurala, Ujjaini, Malaprabha, Pulichintala, Hidkal and Vaanivilas are considered based on the data availability from CWC for setting up the model. Various details of reservoirs are provided such as, area, volume, principal, gross storage, live capacity, principle volume, emergency, principle surface area, design flood, maximum, minimum monthly outflows, target storage capacities and consumptive storages. The model set observed data for thirty-four years (1970-2003) was considered for the calibrating and validating the SWAT model. The first 3 years (1970-1972) data is taken as warmup period. Using the Sequential Uncertainty Fitting (SUFI-2) technique in the SWAT-CUP, the SWAT model is validated and calibrated (Abbaspour et al., 2015). Prior to calibration, the sensitivity of the model parameters influencing streamflow is estimated in the SWAT-CUP. The p-values and t-stat values are used to identify the sensitive parameters, which can influence the model output. Smaller p-values with larger t-stat represents higher sensitivity for the optimization function and thus the observed variable i.e., discharge. Relative significance is represented by t-stat, while p-value represents the significance of sensitivity (Sinha et al., 2020).

The TRB is split into 25 sub-basins after the SWAT delineation of the basin. The sub-basin discretization for the SWAT model is shown in Figure 3.8. The model was simulated from 1978-2010, with first 3 years considered as warmup period. The 20 year period from 1981 to 2000 is used to calibrate the model and remaining 10 year period from 2001 to 2010 is used to validate the model using SUFI-2 algorithm in the SWAT-CUP.

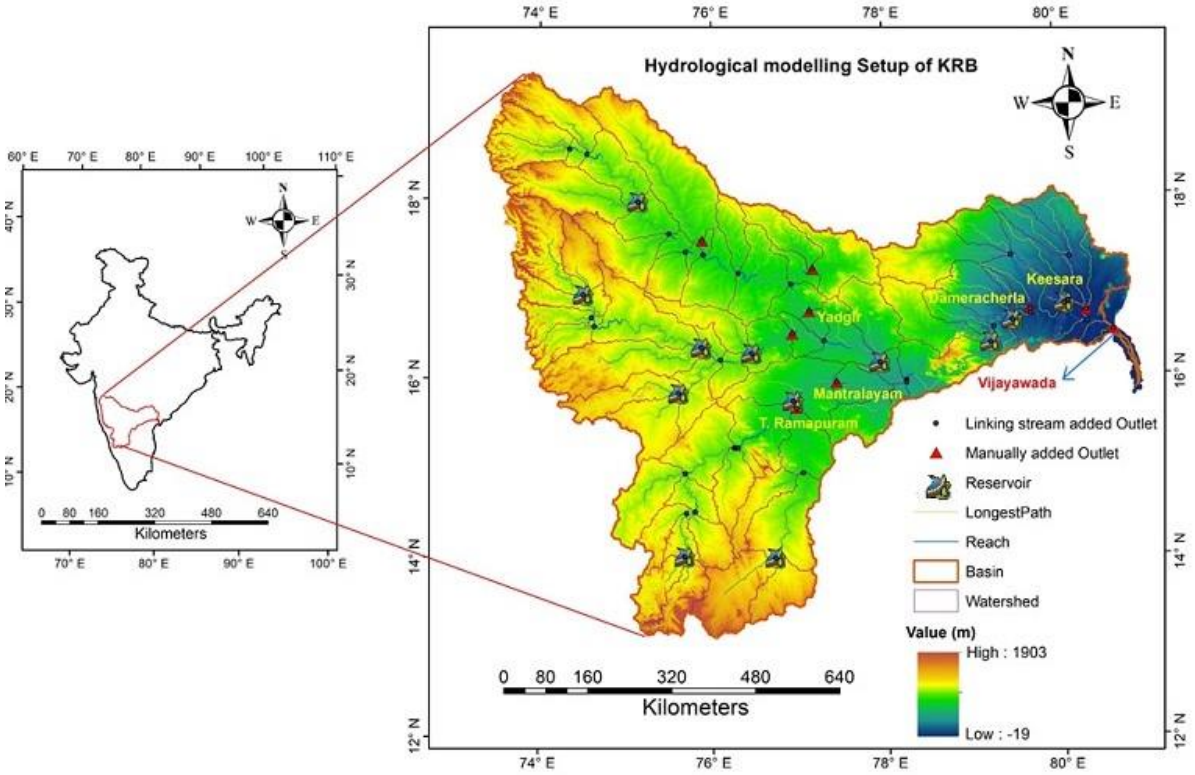

Figure 3.7 Geographical location along with model set up of KRB

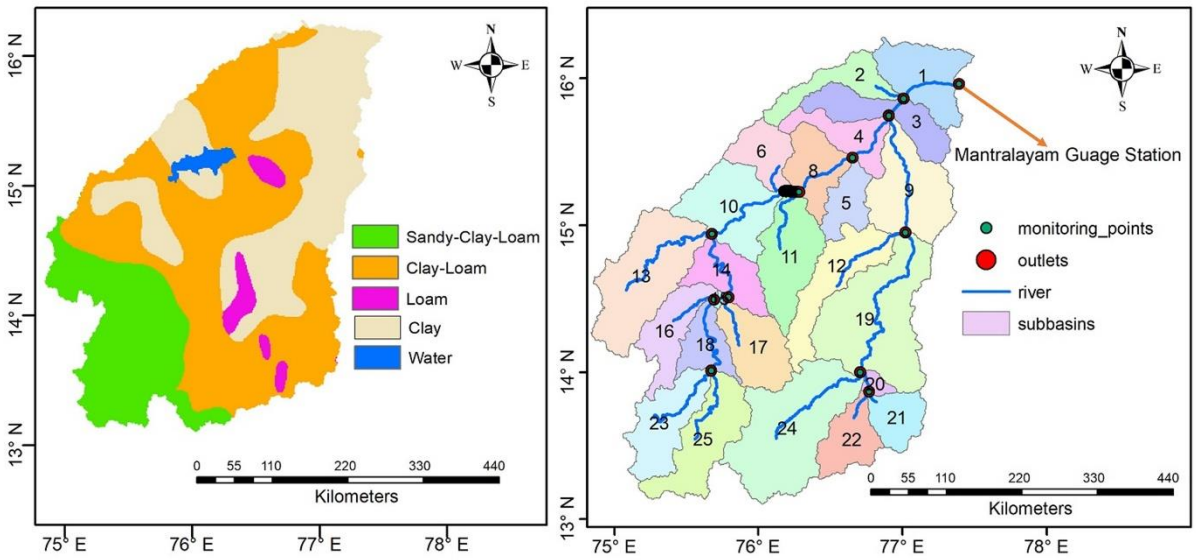

Figure 3.8 Soil map and watershed delineation of the TRB

3.7.1 LULC change under SSP-RCP scenarios

The future LULC maps under SSP-RCP scenario for the respected three future time periods i.e 2040, 2065 and 2090 are extracted and is forced along with future climate data for the hydrological modelling.

3.8 Summary

This chapter describes the quantitative and qualitative assessment on climate and LULC change impact on the KRB. Sensitivity analysis of GCM rankings were analysed using different ranking procedures. A popular method called SU is employed at each grid location to select suitable GCMs for projecting the climate change impact study. Spatio-temporal variation precipitation extreme indices were analysed across KRB. SWAT model is used to find the temporal variation of WBC along with streamflow using top 9 GCMs and their ensemble in KRB and TRB.

CHAPTER 4

RESULTS AND DISCUSSIONS

4.1 General

Approaches to fulfil the goals of the research outlined in Chapter 3 are implemented in the research domain. This chapter provides an overview of the findings related to the study's several goals. The first objective applies to all of India, as was previously discussed, whereas objectives 2, 3 and 4 are applicable to KRB and the fifth objective is applicable to TRB. A comprehensive explanation follows the presentation of the results in the form of tables, graphs and box plots.

4.2 Ranking of CMIP6-GCMs for T_{max} and T_{min}

The main aim of this study is to systematically analyse the uncertainties in the selection of climate models. For this purpose, various combinations are employed by changing MCDM techniques (FTOPSIS and CP), performance evaluation metrics (NSE, MAE, BD, KGE, R4MS4E and SU), weightage allocation methods (Entropy and CRITIC) and reference gridded datasets (IMD and CPC gridded datasets). For each variable namely, T_{max} and T_{min} the skill of CMIP6 based GCMs in replicating the reference values is evaluated using 16 combinations. The variability of ranking patterns is assessed by keeping same reference dataset with different evaluation methods (MCDM techniques, performance evaluation metrics and criteria weighting methods).

4.2.1 Ranking pattern with IMD dataset

The spatial ranking patterns of T_{max} and T_{min} are plotted in Figure 4.1 and 4.2 with IMD reference dataset. With the spatial distribution of top ranked GCMs, it can be observed that the GCM rankings are invariant at some of the grids irrespective of the evaluation methods. The number of grids with invariant ranking patterns using 8 different ranking procedures with IMD as reference dataset for T_{max} and T_{min} are 455 and 280 respectively. It can also be noticed that the scatter in spatial ranking patterns of T_{min} are high in comparison to that of T_{max}. The grids with stable performance of GCMs in simulating T_{max} and T_{min} across all the chosen evaluation methods are identified and plotted in Figure 4.3.

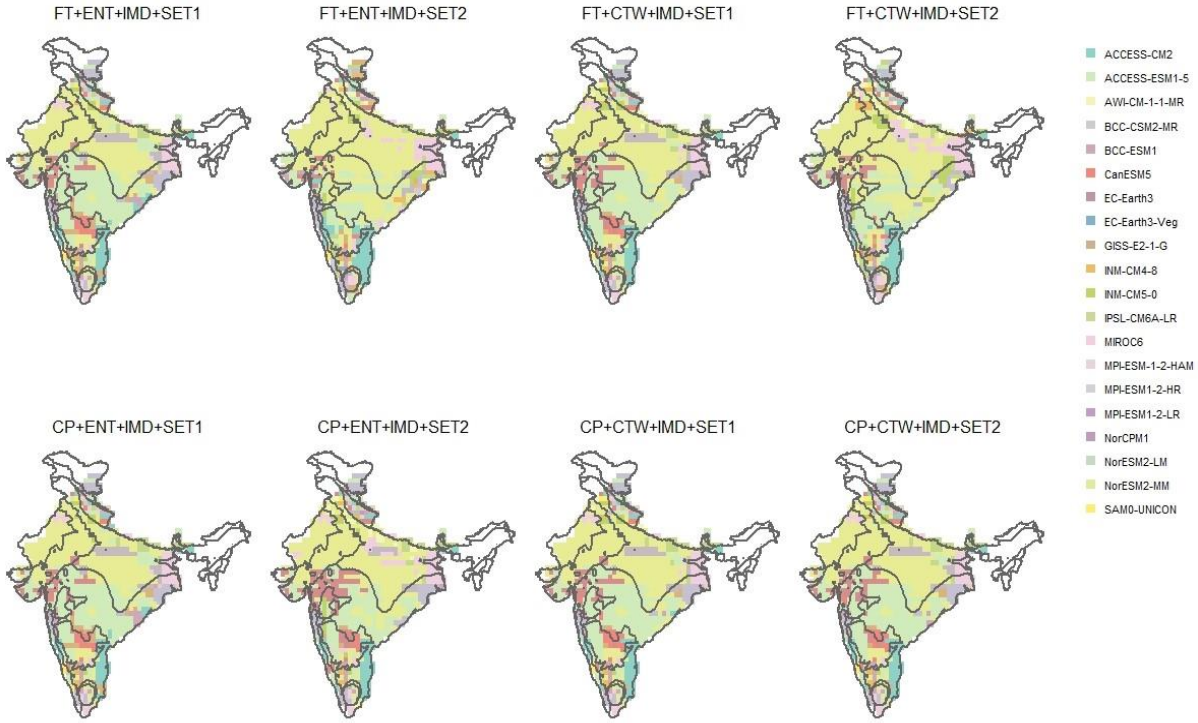

Figure 4.1 Gridwise ranking of GCMs for Maximum Temperature (T_{max}) for IMD

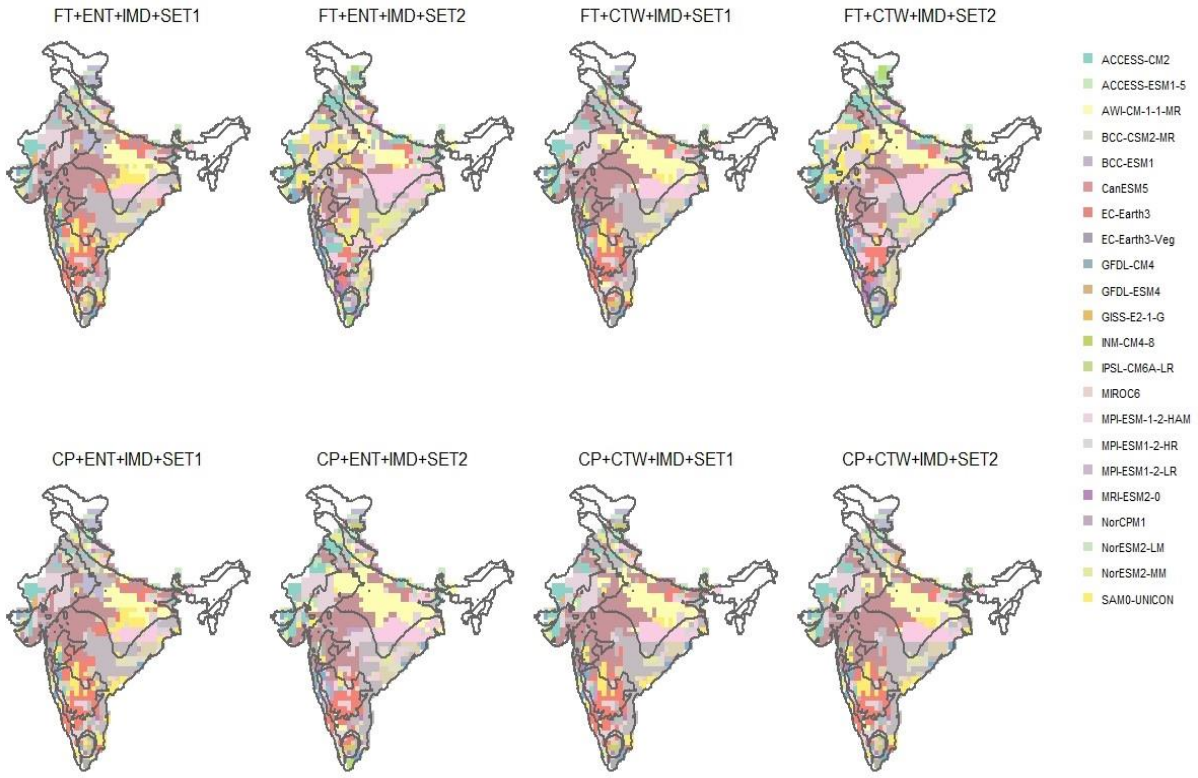

Figure 4.2 Gridwise ranking of GCMs for Minimum Temperature (T_{min}) for IMD

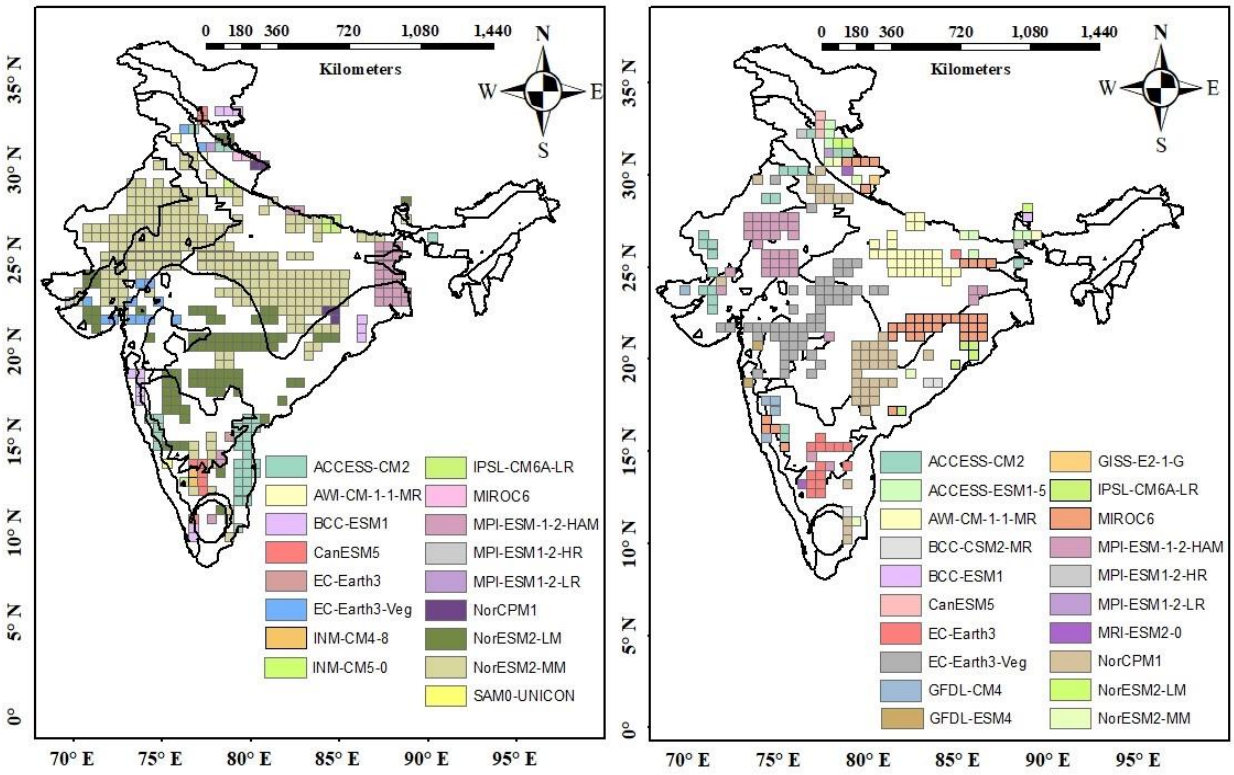

Figure 4.3 Spatial distribution of GCMs with constant ranking patterns using 8 different ranking procedures for IMD, T_{max} (left) and T_{min} (right) dataset

The stable performance of GCMs at those grids is attributed to homogenous climatic zones which are delineated using Koppen-Geiger climate classification. As the temperature depends upon the geographical and topographical features, such as latitude and elevation of the location, the performance of GCM is also attributed to the elevation and latitude. To facilitate this, the whole study area is classified into low (0-20th percentile), medium (20-80th percentile) and high (80-100th percentile) elevation zones. From Figure 4.1 for T_{max}, it can be noticed that NorESM2-MM is performing well in all parts of BSh, BWh zones which are arid and Cwa with warm temperatures at all elevation zones. MPI-ESM1-2-HAM is performing well in the low elevation zones of Aw, with high summer temperatures near Tropic of Cancer, and Cwa zone. ACCESS-CM2 is reasonably good in the low elevation zones of Aw in the southern parts of India. NorESM2-MM is performing well in the medium range elevation zones of Aw. For T_{min}, the following conclusions are drawn. EC-Earth3- Veg is performing well in the high elevation zones of Aw, BSh and Cwa. The performance of AWI-CM-1-1-MR is found to be good in low elevation zones of Cwa and NorCPM1 is performing well in the low elevation zones of Aw. In the medium range elevation zones of Cwa and Aw, MIROC6 is found to be performing well.

In the high and medium range elevation zones of BSh and BWh, MPI-ESM-1-2-HAM is reasonably good.

4.2.2 Ranking patterns with CPC Dataset

Grid wise ranking patterns of T_{max} and T_{min} for CPC reference dataset are shown in Figure 4.4 and 4.5. The number of grids with constant ranking patterns using 8 different ranking procedures with CPC as reference dataset for T_{max} and T_{min} are 314 and 201 respectively. The grids with stable performance of GCMs in simulating T_{max} and T_{min} across all the chosen evaluation methods are identified and plotted in Figure 4.6.

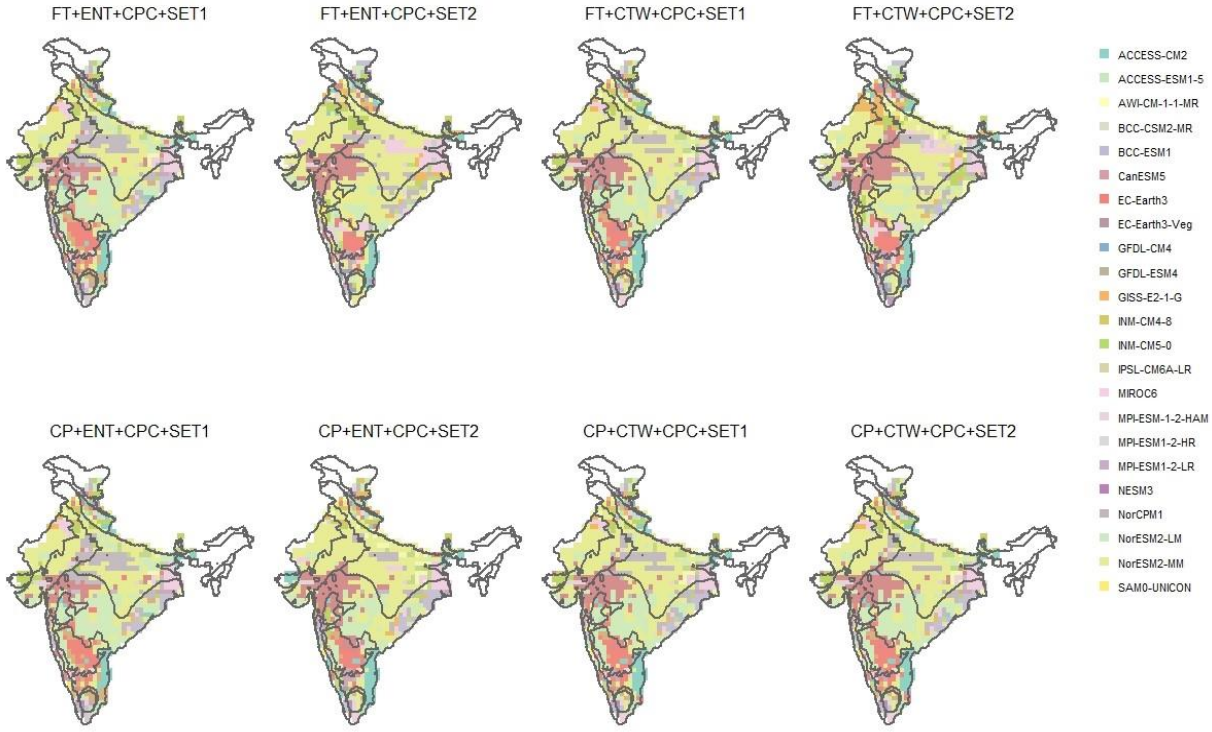

Figure 4.4 Gridwise ranking of GCMs for Maximum Temperature (T_{max}) for CPC

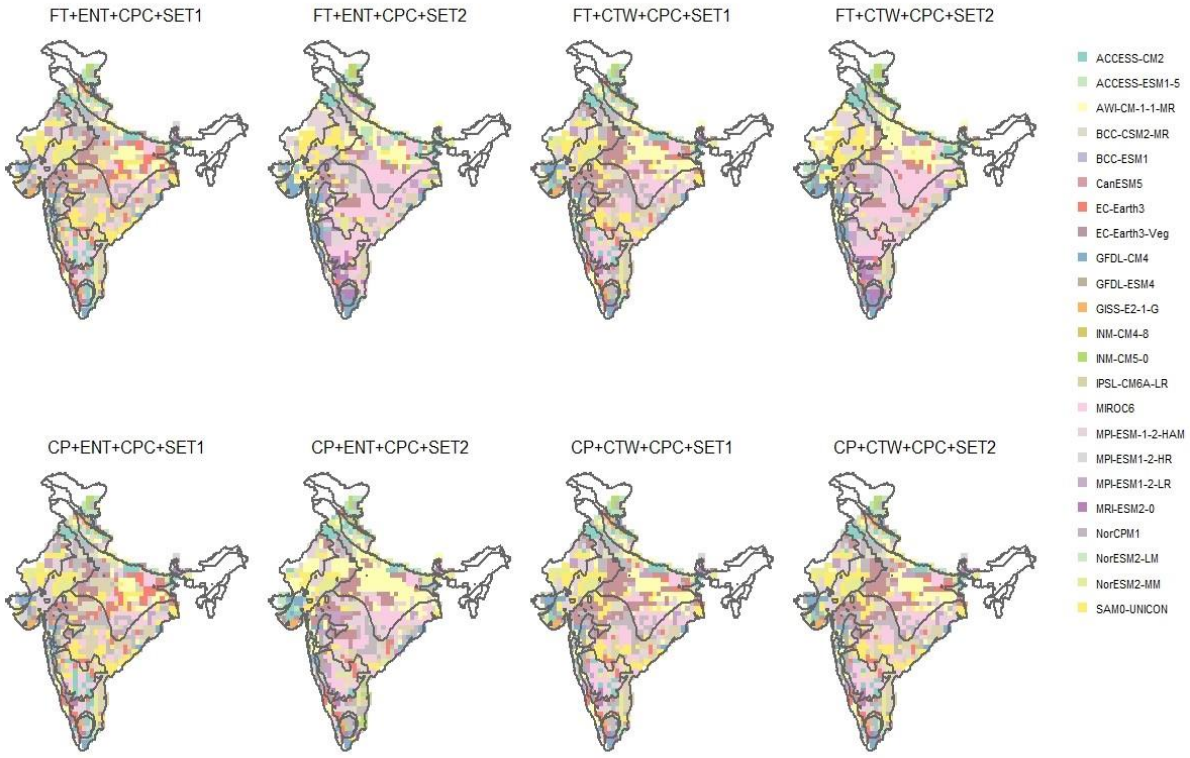

Figure 4.5 Gridwise ranking of GCMs for Minimum Temperature (T_{min}) for CPC

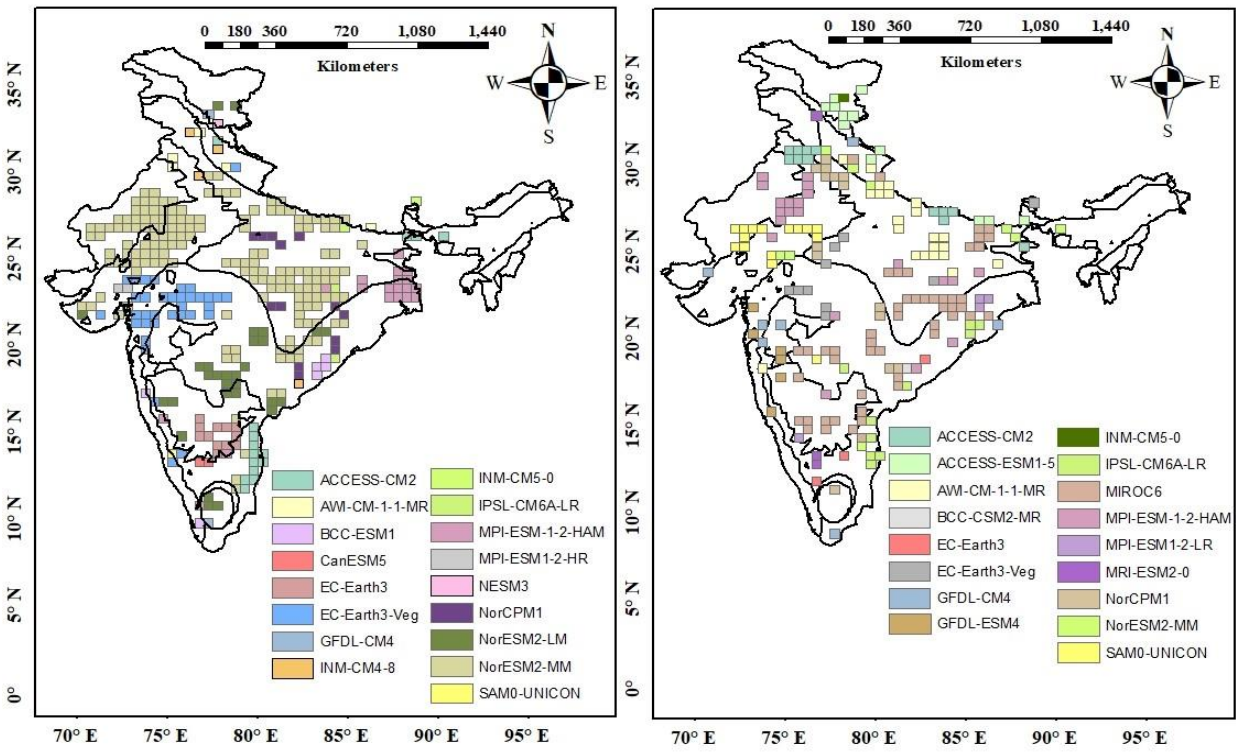

Figure 4.6 Spatial distribution of GCMs with constant ranking patterns using 8 different ranking procedures for CPC, T_{max} (left) and T_{min} (right) dataset

By seeing the spatial distribution of top ranked GCMs for T_{max}, it can be observed that except in high elevation zones of BSh and Aw, the ranking patterns are approximately similar to the ranking patterns obtained with IMD as reference dataset. For T_{min}, it can be observed that the ranking of GCMs with CPC dataset are highly scattered while rankings with IMD dataset are clustered. This shows the significance of reference dataset in ranking procedure.

4.2.3 Sensitivity Analysis of Ranking Patterns

The sensitivity of ranking patterns to each individual components of ranking procedure (MCDM technique, input criteria, weighting technique and reference gridded dataset) is studied to understand the significance of each component. For example, the effect of MCDM technique on ranking procedure is analysed by just altering the MCDM technique (FTOPSIS and CP) alone with all the other components unaltered. Similarly, the impact of every single component on the ranking patterns is analysed by counting the number of grids with invariant rankings which are tabulated in Table 4.1.

The number of grids with invariant ranking patterns due to alteration of reference gridded datasets is less than 600 for T_{max} and less than 400 for T_{min}. The ranking patterns are sensitive to reference datasets and accounts for nearly 50% changes in the ranking patterns. Therefore, the reference dataset has a substantial influence on the ranking of GCMs. Even the remaining three components effect the ranking, but they are mutually dependent on each other.

The effect of input criteria is investigated by changing the two sets of criteria. The metrics enveloped in two sets of criteria vary highly and represent the match between various properties of the simulated dataset to that of observed dataset. By observing the number of invariant grids, there is significant change in the ranking pattern except for the combination of CP with CRITIC weighting method where the number of invariant grids are ranging from 921 and 897 for T_{max} and T_{min}. This is due to the fact that CRITIC weighting method considers inter-criteria correlation along with intra-criteria variability, whereas Entropy method completely depends upon the latter. As the SET-2 criteria consists of two highly varying metrics KGE and R4MS4E in comparison to SU, the weights allocation through Entropy method gets biased to the criteria with high variability whereas CRITIC weighting method yields weights that are unbiased to variability. The grids with invariant ranking for combination of FTOPSIS with CRITIC weighting method are ranging from 494 to 609 for T_{max} and for T_{min} from 419 to 490 which are comparatively less to the combination of CP with CRITIC.

The effect of weighting technique highly depends upon the differences between the variability of the input criteria. The number of grids with constant ranking patterns are ranging from 695 to 852 for T_{max} and for T_{min} the range is from 582 to 744. It indicates that there is a decrease in the number of grids with constant rankings out of 946 girds due to the weighting techniques (see Table 4.1). It can also be observed that the number of rank invariant grids decrease from SET-1 to SET-2. As a result of bounded range, the variability in SU is comparatively lower than that of other metrics and this influences entropy method to assign more weights to the highly varying criteria.

The influence of MDCM technique on the ranking is mainly dependent upon the input criteria. From Table 4.1, the number of rank invariant grids for SET-1 are varying from 882 to 930 and for SET-2 the number of grids are ranging from 404 to 597. From this it can be inferred that the rankings change greatly with SET-2 compared to that of SET-1. This is attributed to the spread of triangular fuzzy numbers in FTOPSIS methodology. Since the allocation of spread depends upon the variability of input criteria, the rankings vary highly with SET-2. The low variability of SU due to its bounded range distributes the spread among the criteria in SET-2 disproportionately in FTOPSIS method. However, the spread is more or less uniform in SET - 1, thereby yielding a similar ranking pattern to that of CP. Hence, allocation spread in the fuzzy MCDM techniques is also important in ranking of GCMs.

Table 4.1 Grids with invariant rankings for each individual component with the combinations

Input Criteria			**Weighting Technique**			**Reference Gridded Dataset**			**MCDM Technique**		
Combination	**No of Grids**		**Combination**	**No of Grids**		**Combination**	**No of Grids**		**Combination**	**No of Grids**	
	T_{max}	**T_{min}**		**T_{max}**	**T_{min}**		**T_{max}**	**T_{min}**		**T_{max}**	**T_{min}**
FT+ENT+IMD+SET1 FT+ENT+IMD+SET2	540	350	FT +IMD+SET1+ENT FT+IMD+SET1+ CTW	841	744	FT+ENT +SET1+IMD FT+ENT +SET1+CPC	484	277	ENT+IMD+SET1+ FT ENT+IMD+SET1+ CP	930	904
FT+ENT+CPC+SET1 FT+ENT+CPC+SET2	431	320	FT +IMD+SET2 +ENT FT+IMD+SET2+ CTW	772	703	FT+ENT +SET2+IMD FT+ENT +SET2+CPC	485	361	ENT+IMD+SET2+ FT ENT+IMD+SET2+ CP	597	463
FT+CTW+IMD+SET1 FT+CTW+IMD+SET2	609	490	FT +CPC+SET1 +ENT FT+CPC+SET1+ CTW	764	697	FT+ CTW+SET1+IMD FT+ CTW+SET1+CPC	541	333	ENT+CPC+SET1+ FT ENT+CPC+SET1+ CP	916	899
FT+CTW+CPC+SET1 FT+CTW+CPC+SET2	494	419	FT +CPC+SET2 +ENT FT+CPC+SET2+ CTW	726	698	FT+ CTW+SET2+IMD FT+CTW+SET2+CPC	489	398	ENT+CPC+SET2+ FT ENT+CPC+SET2+ CP	550	416
CP+ENT+IMD+SET1 CP+ENT+IMD+SET2	670	529	CP +IMD+SET1+ENT CP+IMD+SET1+CTW	852	744	CP+ENT +SET1+IMD CP+ENT +SET1+CPC	488	278	CTW +IMD+SET1+FT CTW +IMD+SET1+CP	915	884
CP+ENT+CPC+SET1 CP+ENT+CPC+SET2	559	426	CP +IMD+SET2+ENT CP+IMD+SET2+CTW	743	655	CP+ENT +SET2+IMD CP+ENT +SET2+CPC	568	396	CTW +IMD+SET2+FT CTW +IMD+SET2+CP	593	454
CP+CTW+IMD+SET1 CP+CTW+IMD+SET2	921	897	CP +CPC+SET1 +ENT CP+CPC+SET1+ CTW	769	688	CP+ CTW+SET1+IMD CP+ CTW+SET1+CPC	519	323	CTW +CPC+SET1+FT CTW +CPC+SET1+CP	890	882
CP+CTW+CPC+SET1 CP+CTW+CPC+SET2	919	905	CP +CPC+SET2 +ENT CP+CPC+SET2+ CTW	695	582	CP+ CTW+SET2+IMD CP+ CTW+SET2+CPC	516	319	CTW +CPC+SET2+FT CTW +CPC+SET2+CP	476	404

Since, a single GCM could not address the uncertainty in the future climate prediction, ensemble of top five GCMs are selected that are most frequently performing well among the 16 methods are given as the best suitable GCMs for each climate zone (see Table 4.2).

Table 4.2 Ensemble of GCMs for each climate zone over India

S No	Koppen – Geiger climate zone Classification	Top five ranked GCMs	
		T_{max}	T_{min}
1	Am	EC-Earth3-Veg, EC-Earth3, SAM0-UNICON, CanESM5, BCC-ESM1	MPI-ESM1-2-HR, AWI-CM-1-1-MR, EC-Earth3-Veg, EC-Earth3, GFDL-ESM4
2	Aw	NorESM2-MM, NorESM2-LM, EC-Earth3, EC-Earth3-Veg, NorCPM1	NorCPM1, EC-Earth3, EC-Earth3-Veg, SAM0-UNICON, BCC-CSM2-MR
3	BSh	NorESM2-MM, EC-Earth3-Veg, NorESM2-LM, EC-Earth3, INM-CM5-0	EC-Earth3-Veg, EC-Earth3, MPI-ESM-1-2-HAM, SAM0-UNICON, NorCPM1
4	BWh	NorESM2-MM, INM-CM4-8, EC-Earth3-Veg, INM-CM5-0, NorESM2-LM	MPI-ESM-1-2-HAM, SAM0-UNICON, AWI-CM-1-1-MR, NorCPM1, NorESM2-MM
5	Bwk	BCC-ESM1, INM-CM4-8, NorESM2-LM, INM-CM5-0, NorCPM1	INM-CM4-8, NorESM2-LM, INM-CM5-0, ACCESS-ESM1-5, NorCPM1
6	Cwa	NorESM2-MM, EC-Earth3-Veg, EC-Earth3, NorCPM1, NorESM2-LM	EC-Earth3-Veg, EC-Earth3, AWI-CM-1-1-MR, SAM0-UNICON, NorCPM1
7	Cwb	ACCESS-CM2, NorESM2-MM, EC-Earth3-Veg, EC-Earth3, NorESM2-LM	MRI-ESM2-0, AWI-CM-1-1-MR, NorCPM1, ACCESS-ESM1-5, MIROC6
8	Dsb	ACCESS-CM2, BCC-ESM1, INM-CM5-0, AWI-CM-1-1-MR, IPSL-CM6A-LR	ACCESS-CM2, BCC-ESM1, EC-Earth3-Veg, ACCESS-ESM1-5, EC-Earth3

4.2.4 Conclusions

Ranking of GCMs are highly dependent upon the chosen reference gridded dataset. Selection of input criteria to evaluate the model performance plays a key role in ranking of GCMs. The weights allocated to the criteria and the final aggregated outputs from MCDM techniques is highly dependent upon the chosen evaluation metrics. The variability of metrics is driving factor for allocation of weights in weighting techniques and distribution of spread in fuzzy MCDM techniques. An ensemble of most frequently performing GCMs are extracted for each climate zone as the most suitable set of GCMs for the corresponding climate zone and these GCMs can be used for the downscaling for further climate impact studies.

4.3 Projections of Precipitation in the KRB

The KRB is classified into three major climate zones as per Koppen-Geiger climate classification. The whole KRB is divided into three major elevation zones such as low (-8m to 356.7m), medium (356.8m to 609.7m) and high (609.8m to 1890m) using ArcMap classification for the analysis of results as shown Figure 4.7. The concept SU is applied to rank the GCMs at 348 grid points over the entire KRB. The spatial distribution of the 1st, 2nd and 3rd ranked GCMs in KRB is shown in Figure 4.8.

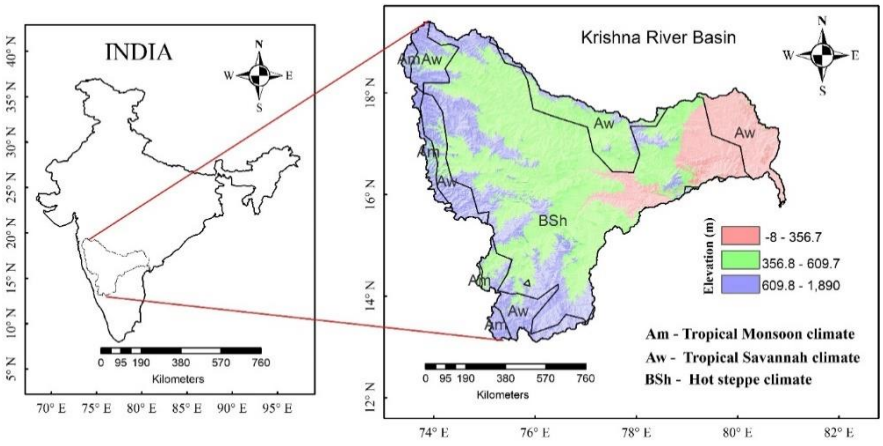

Figure 4.7 KRB with different climate classification zones

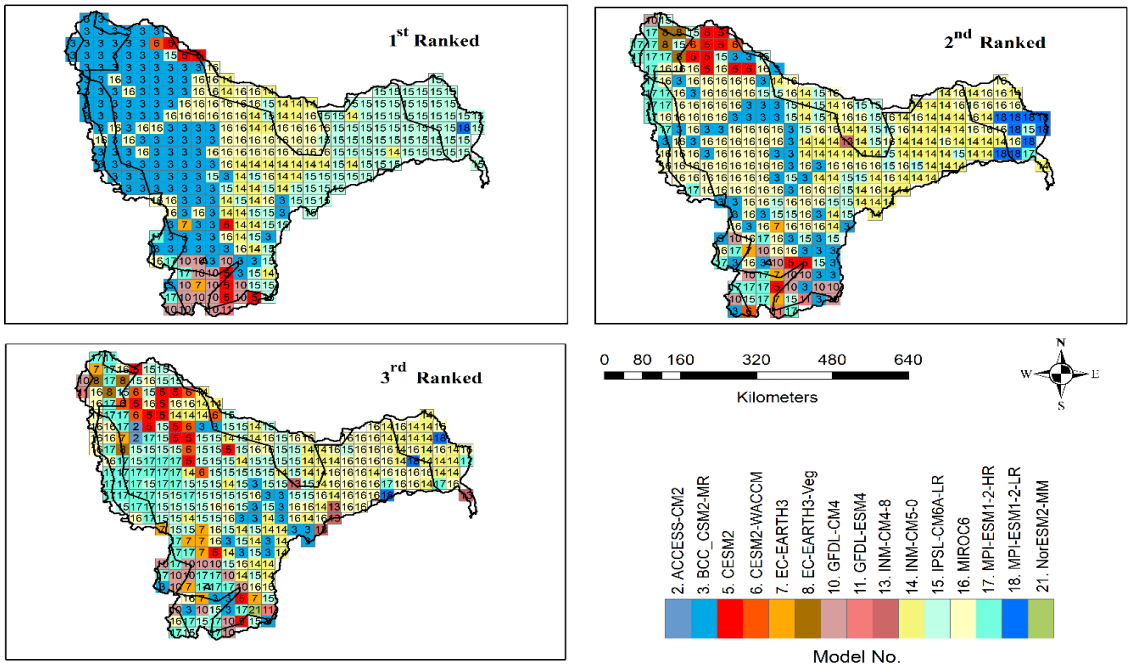

Figure 4.8 The spatial ranking positions of GCMs at 1st, 2nd and 3rd place using SU over KRB gird locations for precipitation

From the figure of 1st ranked GCMs it is revealed that most of the grid points of medium and higher elevations zones in the BSh, Aw and Am climate zones BCC-CSM2-MR is the best ranked GCM followed by IPSL-CM6A-LR in lower elevation zone in Aw and BSh zones, MIROC6 is performing well in medium elevation zone in the central part of the BSh zone. And at higher elevation zone in southern part in BSh, Aw and Am zones at some grid points GFDL-CM4 and CESM2 performing well. From 2nd ranking positions INM-CM5-0, MIROC6 and MPI-ESM1-2-LR performing well in lower elevation of Aw zone. In the medium elevation of BSh zone of central part of the region INM-CM5-0, BCC-CSM2-MR, IPSL-CM6A-LR and MIROC6 is performing well and at higher elevation zones of northwest region MPI-ESM1-2-HR and MIROC6 are best performing GCMs. And at higher elevation zones in southern part there will be mixed results in best performing GCMs. From 3rd ranking positions it can observed that INM-CM5-0, MPI-ESM1-2-HR, BCC-CSM2-MR, IPSL-CM6A-LR and MIROC6 are best GCMs, performing well at most of the grids in different elevation zones of climate zones of the study area. Finally, BCC-CSM2-MR, IPSL-CM6A-LR, MIROC6, INM-CM5-0 and MPI-ESM1-2-HR chosen as top five GCMs over the entire study area after applying the MCDM technique as discussed in methodology. The Total Ranking Weight using MCDM technique and ranks obtained from different GCMs for precipitation is shown in Figure 4.9.

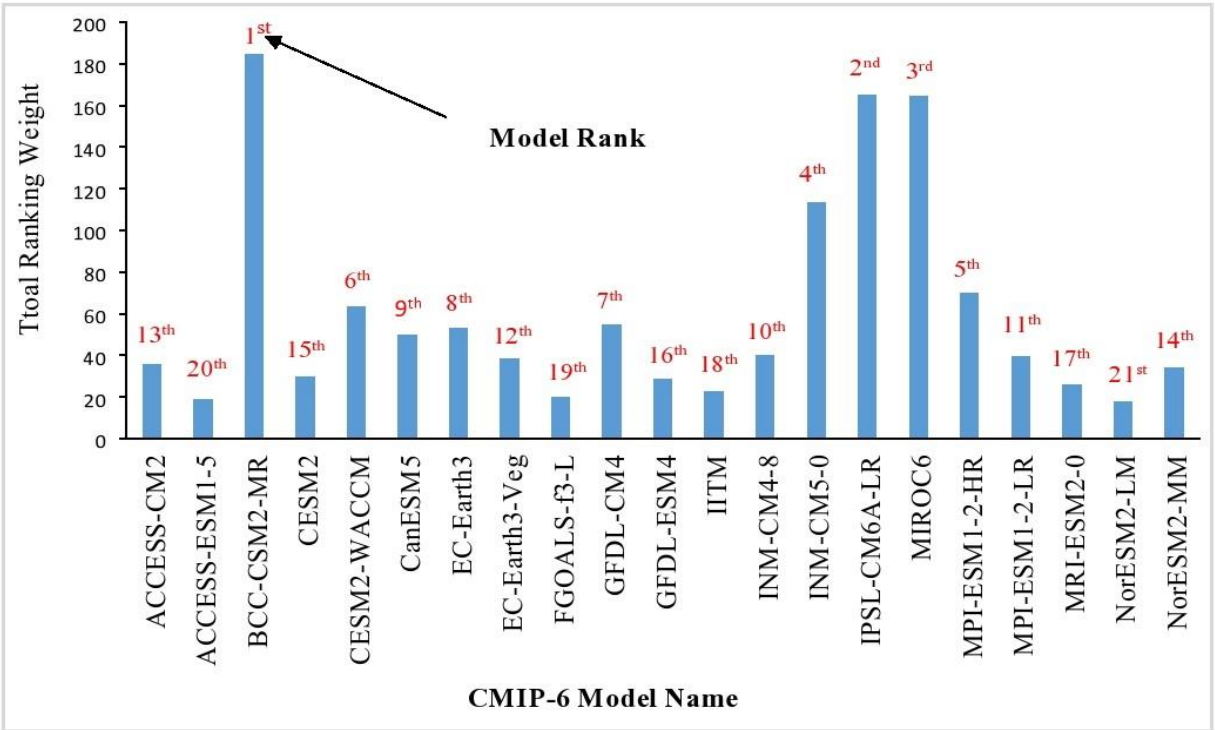

Figure 4.9 Histogram of Total Ranking Weight and final ranking positions of models used

4.3.1 Generation of Multi Model Ensemble (MME)

The MME average of bias corrected precipitation at each grid was developed by using REA method for the selected top five GCMs, for estimating the future possible variations in precipitation over KRB. As there is no regulation to choose the number of GCMs, the top5 GCMs are selected to develop the MME for each SSPs. The ability of REA method to develop MME was assessed by scatter plots of observed spatially averaged monthly rainfall, with individual and MME of GCMs for period 1985-2014 shown in Figure 4.10. the scatter plots shows that the individual GCMs and MME average of GCMs shows satisfactory alignment with the 45-degree line and compared to individual GCMs, MME mean shows better alignment with correlation coefficient 0.605 which is means that MME mean can improve accuracy in precipitation projections by reduce the uncertainty associated in the individual GCMs.

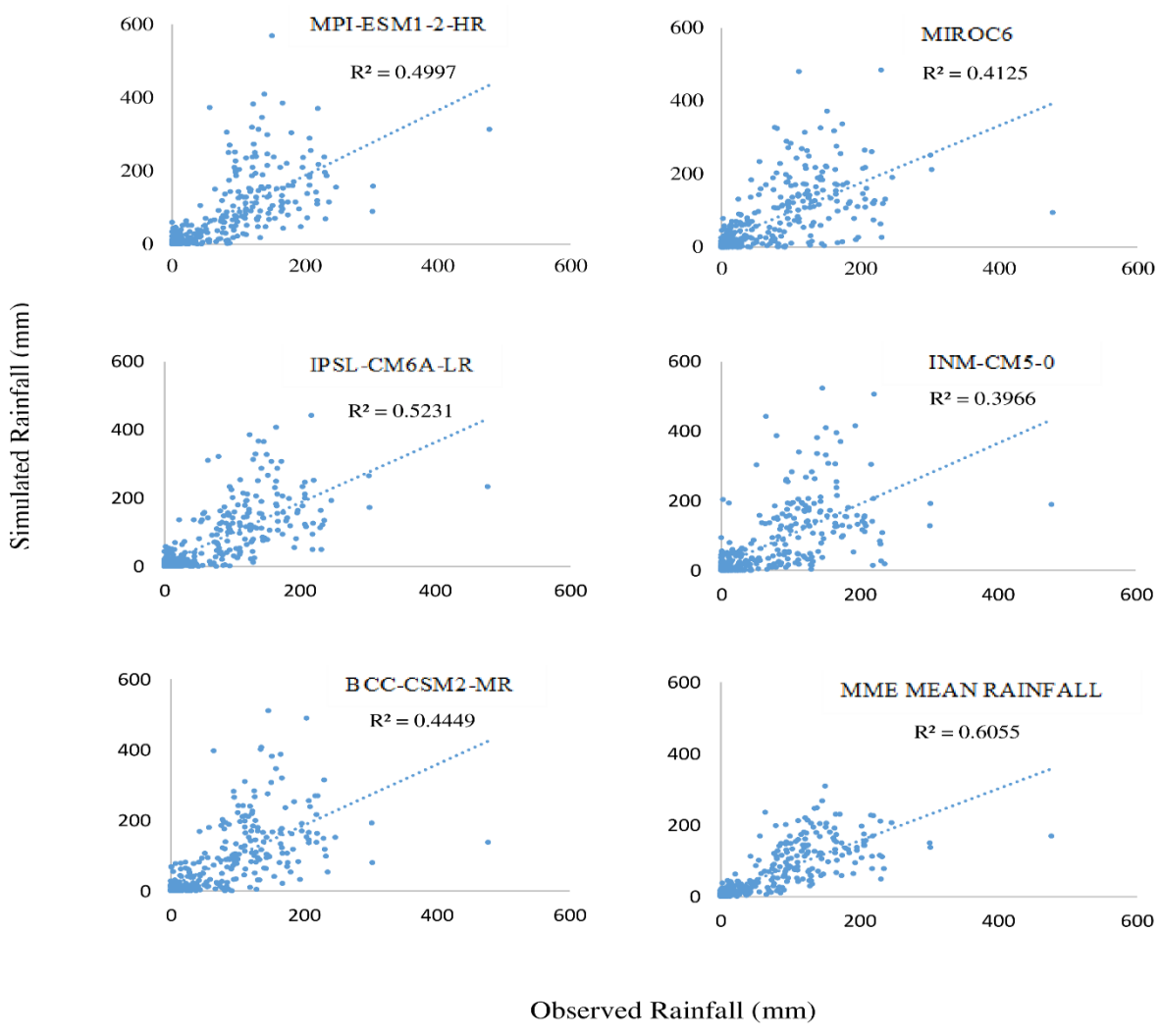

Figure 4.10 Scatter plot of IMD and individual GCMs and REA estimated MME mean rainfall averaged over KRB for the period 1985–2014

The performance of the REA based MME mean was evaluated against the observed precipitation for 1985-2014. Three statistical parameters namely NRMSE, Percentage bias (Pbias) and index of agreement (MD) are calculated at all the grid points and the getting results are represented in boxplots shown in Figure 4.11. It is revealed from the box plots that the median of the MME shows satisfactory improvement with the interquartile range compared to selected individual GCMs for the all the statistics.

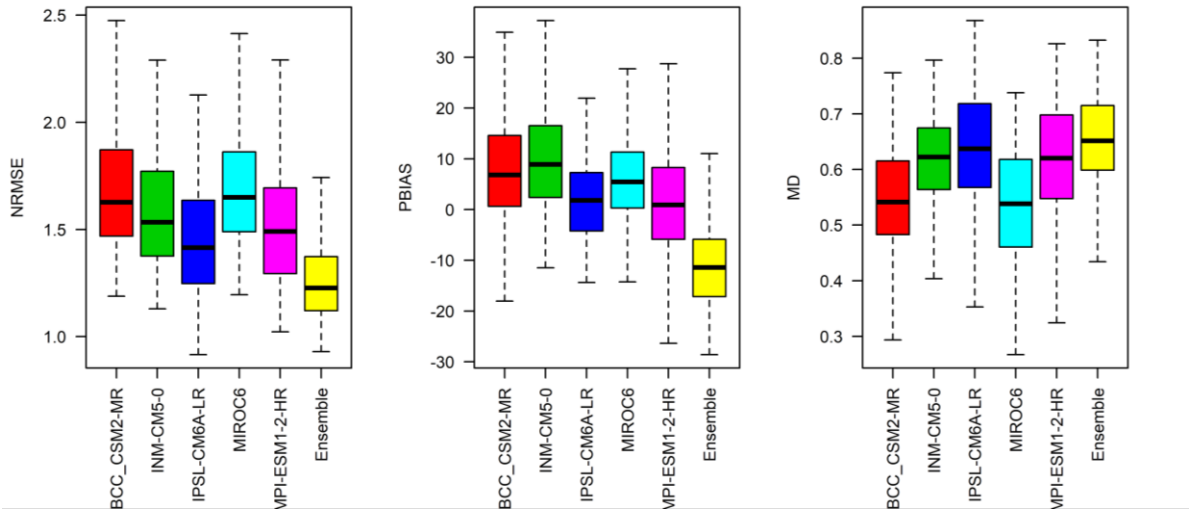

Figure 4.11 Boxplot displaying statistical metrics derived at various grid positions for individual GCM precipitation and MME mean precipitation in relation to IMD precipitation

4.3.2 Changes in Annual Precipitation

The future annual precipitation changes (%) over KRB for three future periods, namely near future (2015-2040), mid future (2041-2070) and end future (2071-2100) were assessed using MME against observed precipitation of 1989-2014 for near future 1985-2014 for rest of the period for four SSP scenarios. The projected precipitation for different periods at all grids points of climate zones were averaged to find out the changes in the precipitation of the region. The projected rainfall is increasing and decreasing in future periods for all SSPs in most regions of KRB. The changes in future precipitation and uncertainty levels were estimated using MME mean and 95% confidence interval band shown in Figure 4.12. It is found that the variation in precipitation changes from zone to zone and period to period under all SSPs. The more changes were occurred in the end period (2071-2100) under SSP5-8.5 followed by other all SSPs. The highest levels of uncertainties were found in Am climate zone which is covering only 10 grids in the entire study area under all SSP scenarios. Under various SSPs, for future periods, the

upper band of uncertainty level was greater than zero while the lower band is lower than zero. At a 95% confidence level, this shows a rise and reduction in precipitation for KRB's various SSPs.

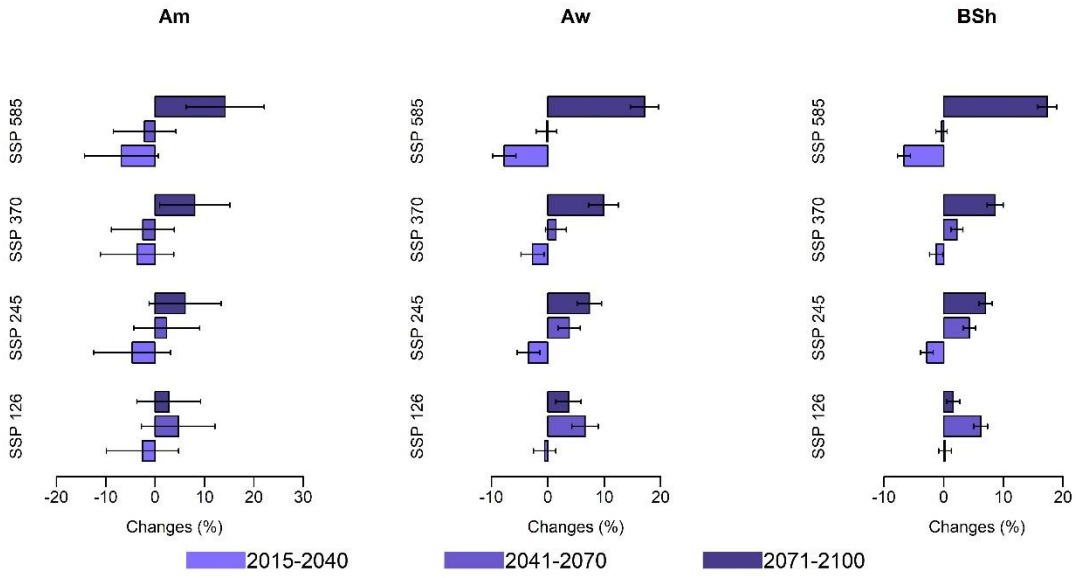

Figure 4.12 Variations (%) in the annual mean precipitation in four SSP scenarios and three future periods in various KRB regions at a 95% confidence level

For clear understanding the changes in annual precipitation the spatial plots were drawn shown in figure 4.13. The change in annual rainfall is gradually increasing and decreasing in ranging from 38.97% to -36.72% during near period (2015 - 2040), 45.24% to -31.61% during mid period (2041-2070) and 83.05% to -30.63% in the end period (2071-2100) for different SSPs. The maximum increase in the rainfall found to be 83.05%, in the end period at higher elevation part in BSh and Aw climate zones and higher decrease of -36.7% found to be in near period in higher elevation of Aw and Am climate zones under SSP5-8.5 respectively. It can be observed from the figure that most of the grid points in the BSh climate zone the change in projections is ranging from -20% to 20% and few grids it is up to 40% during near and mid periods for all SSPs except SSP1-2.6. But in the SSP1-2.6 at most of grids the change in projection is in the range of -20% to 60% during near period. The major changes in the projections were occurred during end period such a way there is a decrease in the rainfall from -31% to -20% in the lower elevations os Aw and medium elevations of BSh climate zone and the increase in the rainfall is in the range of 0 to 20% in medium elevations of Aw and BSh zones under SSP1-2.6 and for SSP2-4.5 there is increase in rainfall from 0 to 60% in the BSh zone. For SSP3-7.0 and SSP5-8.5 similar kind of results were obtained for end period. Most of the grids in medium elevations

the precipitation increasing from 0 to 60% but in higher elevations it is expected increase up to 83%.

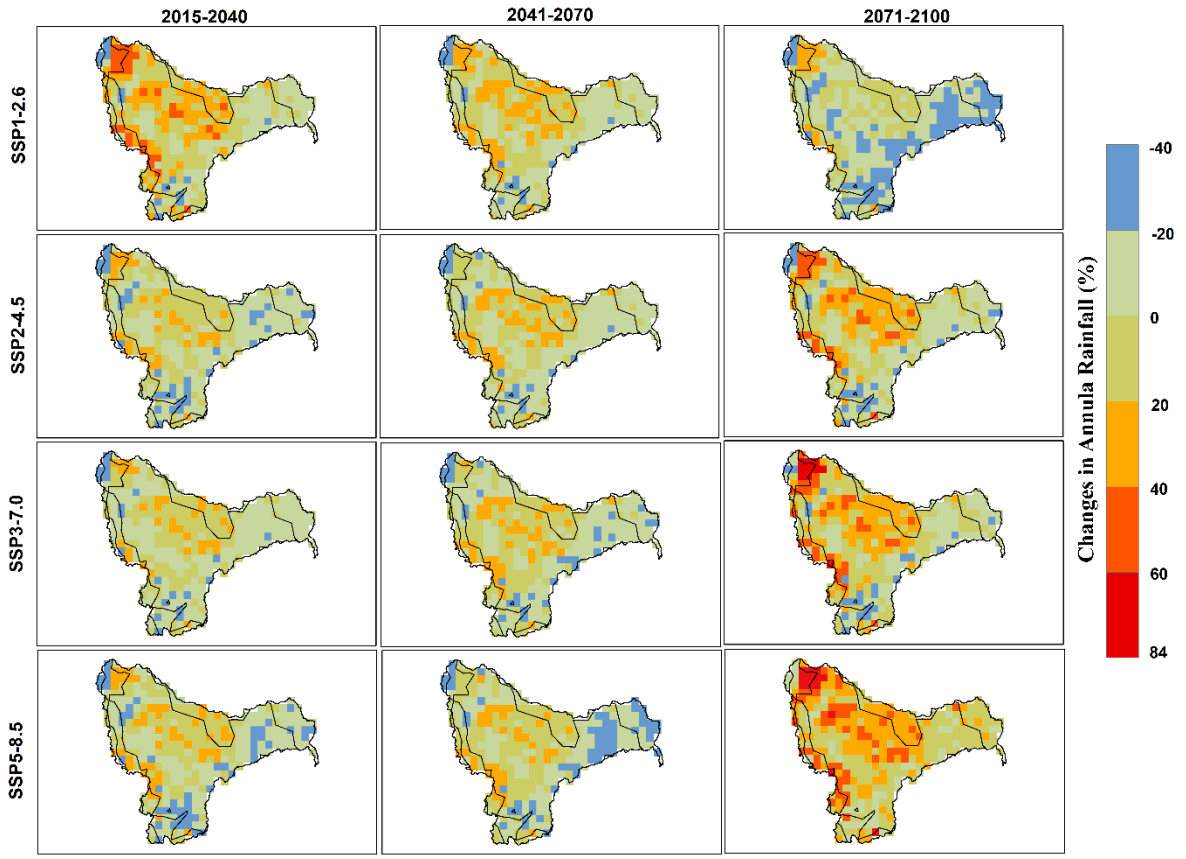

Figure 4.13 Change (%) in annual average precipitation in KRB for different SSPs for three future periods, 2015-2040, 2041-2010 and 2071-2100

4.3.3 Changes in Seasonal Precipitation

As seen in Figure 4.14, the precipitation estimates for each month across all climate zone grid points are averaged to evaluate variations in the seasonal precipitation projections. From the figure it clearly understanding that monsoon period (June-October) is more influencing comparing to other months and future precipitation is underestimating the observed precipitation under all SSPs. As monsoon period is dominating for the occurrence of precipitation (80%) for the study area, the future changes in monsoon period only discussed. The spatial distribution of changes in rainfall for monsoon period for different SSPs were shown in Figure 4.15. There is a significant change in the rainfall is occurred in different climate zones. There is similar kind of trend in the results occurred in monsoon rainfall projections compared to annual change but increasing rate more at some grid points in the BSh climate zone. The projected changes in the monsoon rainfall are in the range of -37.68% to

64.56% during near period, -36.72% to 70.73% during mid period, -37.42% to 95.75% during end period. The most increase 95.75% and decrease 37.66% in projected rainfall occurred in the higher elevation zones of BSh and Aw zones under SSP5-8.5, SSP2-4.5 respectively. The major increases were occurred in the end period under SSP5-8.5 compared to near and mid period and all other SSPs. SSP2-4.5 and SSP1-2.6 shown more influence in the future projections as there is increment up to 80% in most of the grids except end period. And there is a similar kind of increment up to 80% for near period under three future scenarios except SSP5-8.5.

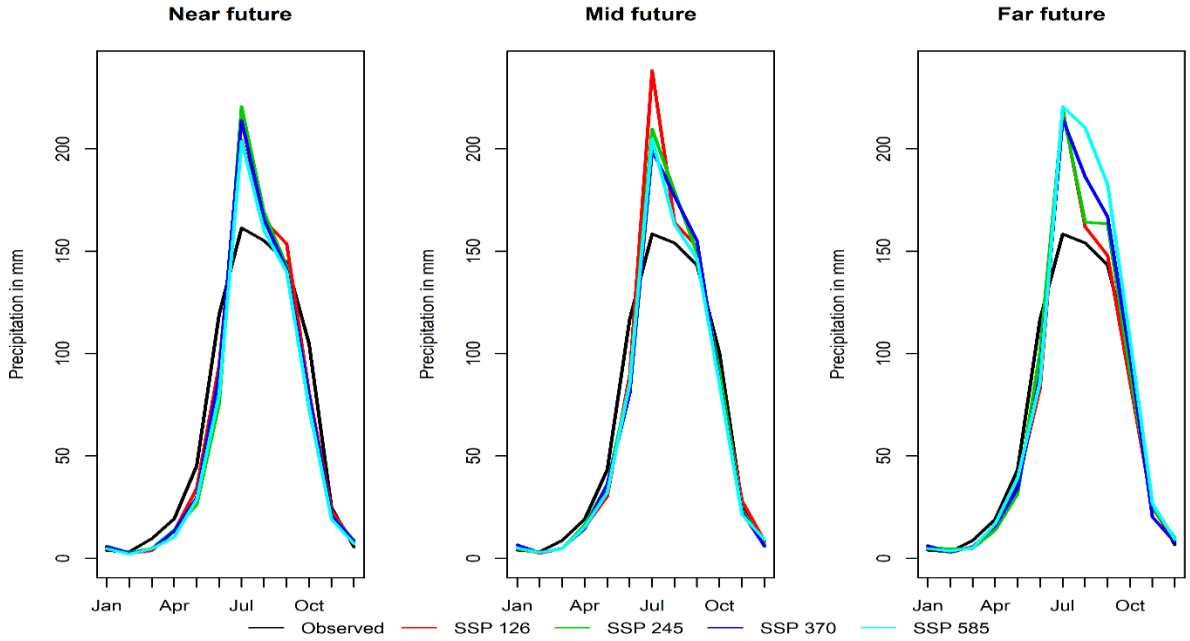

Figure 4.14 Projected monthly rainfall changes (%) at different climate zones in KRB for three future periods

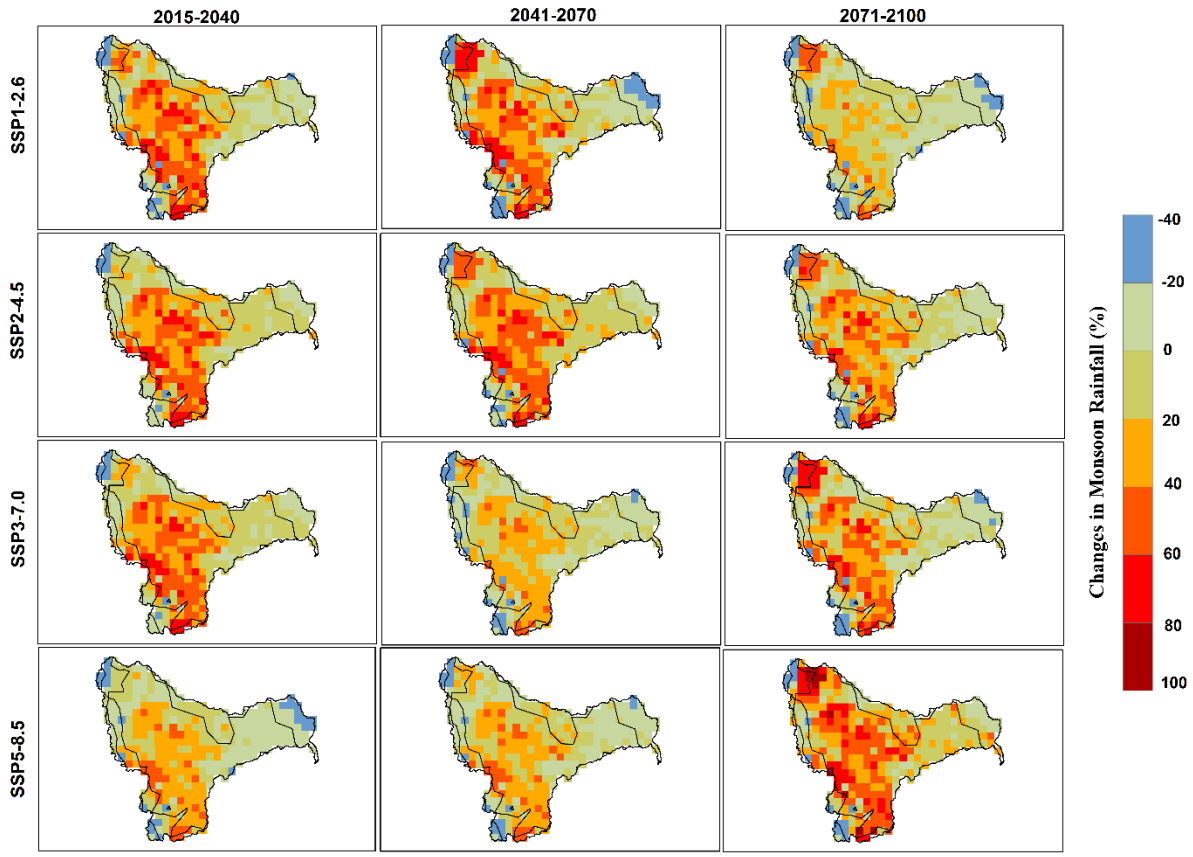

Figure 4.15 Change (%) in average monsoon precipitation in KRB for different SSPs for three future periods, 2015-2040, 2041-2010 and 2071-2100

The major changes either increasing or decreasing were occurring in the BSh and Aw climate zones at medium and higher elevations as the topography influencing the study area and most part of the study area also covering with the BSh and Aw zones.

4.3.4 Discussions

The study over KRB is most significant due to its semi-arid nature and vulnerable to climate change, owing to uneven distribution of precipitation. Generally, GCMs are developed to project the climate variables at global scales, so they show huge uncertainty for climate simulations over various regions. According to earlier research, using appropriate GCMs can help to lower the uncertainty in climate change estimates (Raju & Nagesh Kumar, 2014). The GCMs in this study were chosen using SU, which has been shown to be the most reliable technique for doing so in comparison to the several traditional statistical performance matrices that have been used in recent years to choose GCMs (Pour et al., 2018; Salman et al., 2018; Shiru et al., 2019).

The GCMs which are selected as most skillful for this study can be compared with the previous studies. (Raju & Kumar, 2015) used TOPSIS method for ranking of GCMs over the country India and KRB. From their results, they ranked MIROC3 and BCCR as top ranked GCMs in KRB. Similar kind of results was found in this study in such a way that the same family GCMs are in the top five. (Babar et al., 2015) found that MIROC5 is the best GCM for precipitation projection of India for annual precipitation. The list of the top 5 GCMs for the current study also includes MIROC5, which was determined to be the best GCM for projecting precipitation in India. Using SS, Taylor diagrams and traditional statistical criteria, (Sarthi et al., 2016) determined that, out of 34 GCMs, BCCCSM1.1(m) was the most suitable GCM for projecting precipitation in India. Additionally, the top GCM in the current study is the same family group GCM, BCC-CSM2-MR.The projection of MME shows that there is an uneven distribution of precipitation throughout the basin under four SSP scenarios for future slices. The results of MME mean projections can be compared with the previous studies. From Figures 4.13 and 4.15, the future projections revealed that there is a probability of water scarcity and getting of drought in the future at some of the grid locations of semi-arid BSh climate zone under four SSPs except SSP5-8.5 scenario for the far future. This is due to the reduction of precipitation which agrees with the previous study (Gosain et al., 2006). As per (Kulkarni et al., 2014) who considered only one SRES scenario, the annual precipitation follows for the mid future (20141-2070), follows an increasing trend which is true for some grids in the present study. But for the SSP5-8.5 scenario it can be found the increasing trend in the far period which agrees with past studies (Mishra & Lilhare, 2016).

4.3.5 Conclusions

The objective of the current study was to select the most skillful GCMs for projecting the precipitation over KRB using information based selection method namely SU. 21 (See Table 3.1, Objective 2) GCMs from CMIP6 phase which have precipitation projections for four SSP scenarios are used to select the suitable GCM ensembles over KRB. And the selected top five GCMs are used to generate the MME using the REA method over KRB. The performance of the MME was assessed using statistical matrices such as correlation coefficient, NRMSE, Pbias and MD. The REA method was used to compute MME mean. Following are specific conclusions of the study.

The study area was classified into three major homogeneous climate zones as per Koppen classification for facilitating the realizations. BCC-CSM2-MR, IPSL-CM6A-LR, MIROC6,

INM-CM5-0 and MPI-ESM1-2-HR are selected as the top five GCMs over the entire study area based on their skill in mimicking the observed precipitation. The selected GCMs are found to be matched with obtained GCMs in the previous studies over Indian regions or river basins which conforms to the suitability of SU for GCM ranking. The major changes in precipitation projections occurred in the far future compared to the rest period under different SSP scenarios. The precipitation projections are increasing up to 83% in the higher elevation zone of the northwest region in the BSh climate zone at few grid points under SSP3-7.0 and SSP5-8.5 during the far future. Most of the decrease in projections is up to -36% occurred in the coastal region of the southeast region in BSh climate zone under SSP1-2.6 during far future. Seasonal projection changes show more increment in the near, mid future up to 80% and end future up to 100% at few grids in higher elevations of BSh zone. Particularly, the SSP5-8.5 shows more homogeneous precipitation variation and increasing trend for both annual and seasonal periods during the far future. It is revealed from the results that the higher increase in MME precipitation in the monsoon period compared to the annual period would be indicating that the precipitation in KRB is more concentrated in monsoon season or ISMR period.

4.4 Climate Extremes Analysis in KRB

4.4.1 GCMs Selection

The TRW of the 18 considered GCMs (See Table 3.1 from Objective 3,4 and 5) is shown in Figure 4.16. As mentioned above, the performance of the GCMs was evaluated in all the 348 grids within the KRB using SU. The spatial distribution of the best performing GCMs from rank 1 to rank 5 is shown in Figure 4.17. For the 1st rank, the GCM MPI-ESM1-2HR performed best in 50% of the grids i.e. 165 in terms of the SU value. The output of the MPI-ESM1-2-LR was observed to be best in 60 grid points and was ranked 2. Similarly, the maximum number of grids from a single GCM for rank 3, 4 and 5 were EC-Earth3, NorESM2-LM and GFDL-ESM4. From Figure 4.17 it is evident that as the rank of the GCM is increasing the performance of different GCMs was observed to be comparable resulting in wide variation. The ranking of each of the GCM was computed based on the frequency of occurrence of each GCM from rank 1 to rank 5 and is computed as the TRW. Based on the results, top five (5) suitable GCMs: MPI-ESM1-2-HR, MPI-ESM1-2-LR, GFDL-ESM4, NorESM2-LM, EC-Earth3-Veg, were considered for further analysis.

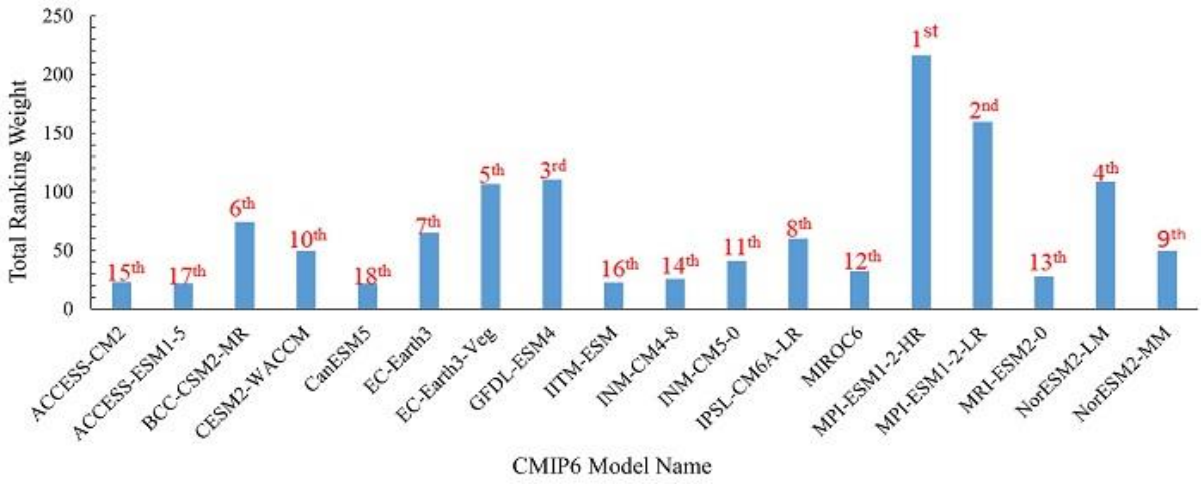

Figure 4.16 Ranking of each GCM based Total Ranking Weight (TRW)

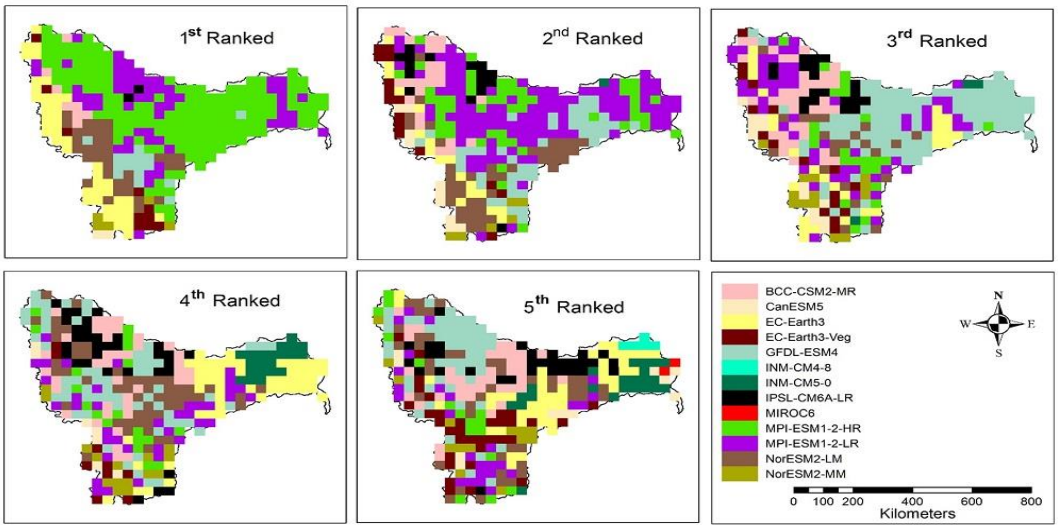

Figure 4.17 Spatial distribution of the top ranked GCMs

The spatial distribution of different average annual precipitation extremes during the baseline period (1973-2003) is shown in Figure 4.18. It is observed that the spatial distribution of Consecutive Dry Days (CDD) ranges from 65 to 147 days. The spell of CDD is more in the northwest region (147 days) compared to the northeast region of the basin. The type of CDD depends on the spatial distribution of the precipitation over the basin. Whereas the spatial distribution of Consecutive Wet Days (CWD) varies from 5 to 47 days, which is more in the western region, the remaining portion of the central and eastern regions are covered by the low length of CWD.

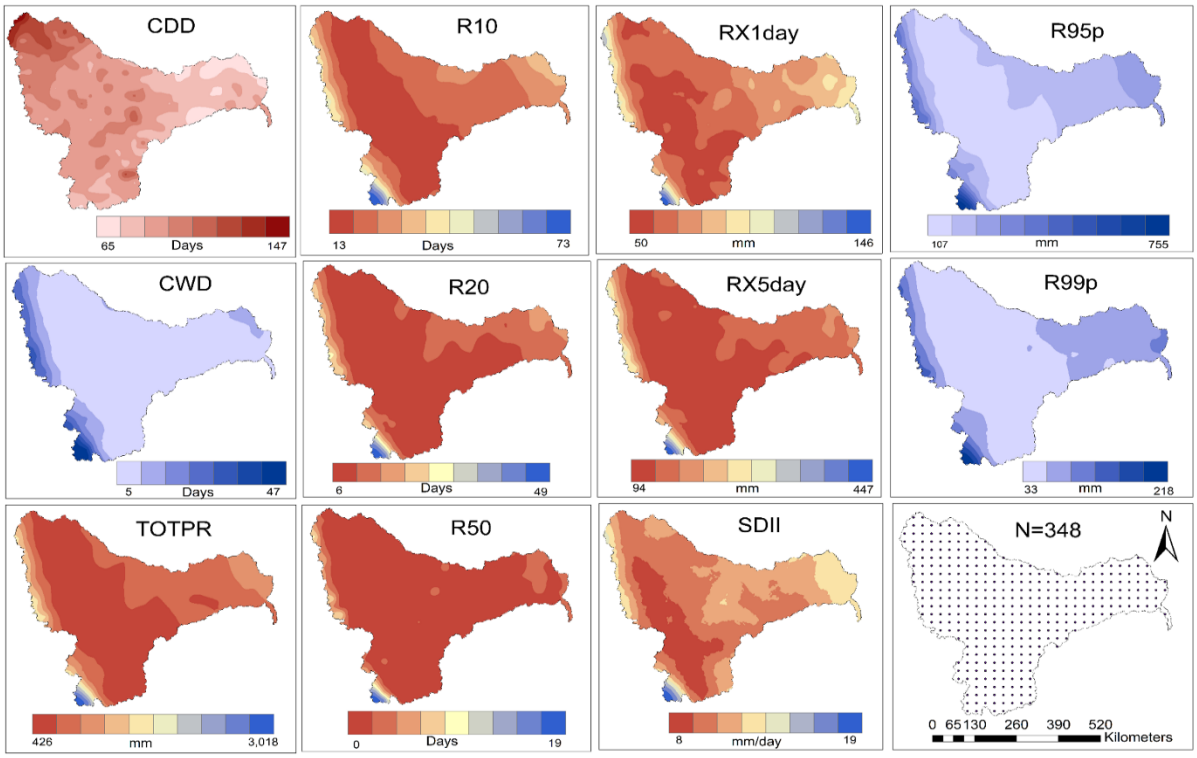

Figure 4.18 Average annual spatial distribution of precipitation extremes during baseline period (1973-2003) in the KRB

Spatial distribution of ToTal annual-wet day PRecipitation (TOTPR), count of slightly heavy precipitation days (R10), count of heavy precipitation days (R20) and count of very heavy precipitation days (R50) are congruous to the drier valley in the basin especially central part of the basin due to its semi-arid nature. Even though the mean annual TOTPR ranges from 426 mm to 3018 mm, the annual average of the basin is about 735 mm indicating the precipitation importance. The mean annual R10, R20 and R50 are about 22, 10 and 2 days respectively. Interestingly, R50 is showing quite a different pattern from its spatial distribution compared to TOTPR, R10 and R20. Moreover, RX5day, R95p and R99p are almost congruous with the TOTPR, R10 and R20 and the spatial distribution of the Simple Daily Intensity Index (SDII) is congruous with RX1day. The average annual values of very heavy wet days (R95p) and extremely wet days (R99p) are 189 mm and 61 mm across the basin and lower values are observed in the central part of the eastern region. A similar tendency is observed in RX1day and RX5day. The average annual values of RX1day and RX5day are 68 mm and 132 mm respectively with spatial standard deviations of 15 mm and 48 mm. The ratios of RX1day and RX5day up on TOTPR provide precise information on precipitation extremes on annual average precipitation (Talchabhadel et al., 2018).

The mean annual ratio of RX1day/TOTPR is about 9.7%, ranging from 4 to 16%. Similarly, the annual average value of RX5day/TOTPR is found to be 18.5% and spatial distribution

varies from 12 to 24% (Figure 4.19). From this analysis, it can be understood that on average 9.7% of total annual precipitation can occur in a single day and 18.5% in 5 consecutive days. On average, the percentage contribution of maximum RX1day and RX5day is about 10-11% and 17-21% of TOTPR respectively in the central part of the basin. Inter annual variations of these indices determine more precise information on precipitation extremes occurrences. For finding the flood warning thresholds in the catchment, R95p, R99p, RX1day, RX5day and information from the ratios of indices are necessary. The spatial distribution of mean annual SDII varies from 8 mm/day to 19 mm/day from the high to low elevation region of the KRB and the mean value is about 10 mm/day. From the spatial pattern of both SDII and TOTOPR, it can be seen that at higher elevations the TOTPR and number of heavy rainy days occurrences are more and SDII is also more. Similarly, at medium and low elevations both TOTPR and the number of heavy rainy days occurrences are less and SDII was also less.

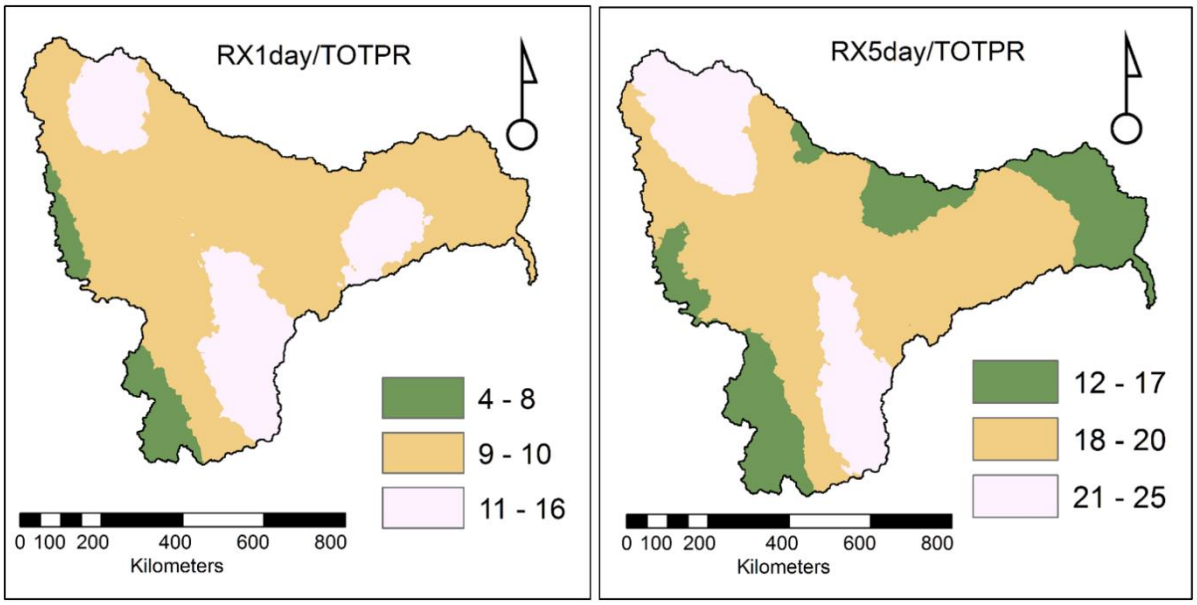

Figure 4.19 Precipitation percentage contributions of RX1day and RX5day to TOTPR during baseline period (1973-2003) in the KRB

4.4.2 Trend Analysis

The grid-wise trends such as decreasing, increasing and no trend conditions of extreme precipitation indices are analysed at a 5% significant level for the baseline period (1973-2003) as shown in Figure 4.20 and their spatial pattern is presented in Figure 4.21 respectively. Figure 4.21 shows that except for grids with no trend condition, all the grids are exhibiting mixed trend conditions of decreasing and increasing for all the extreme precipitation indices.

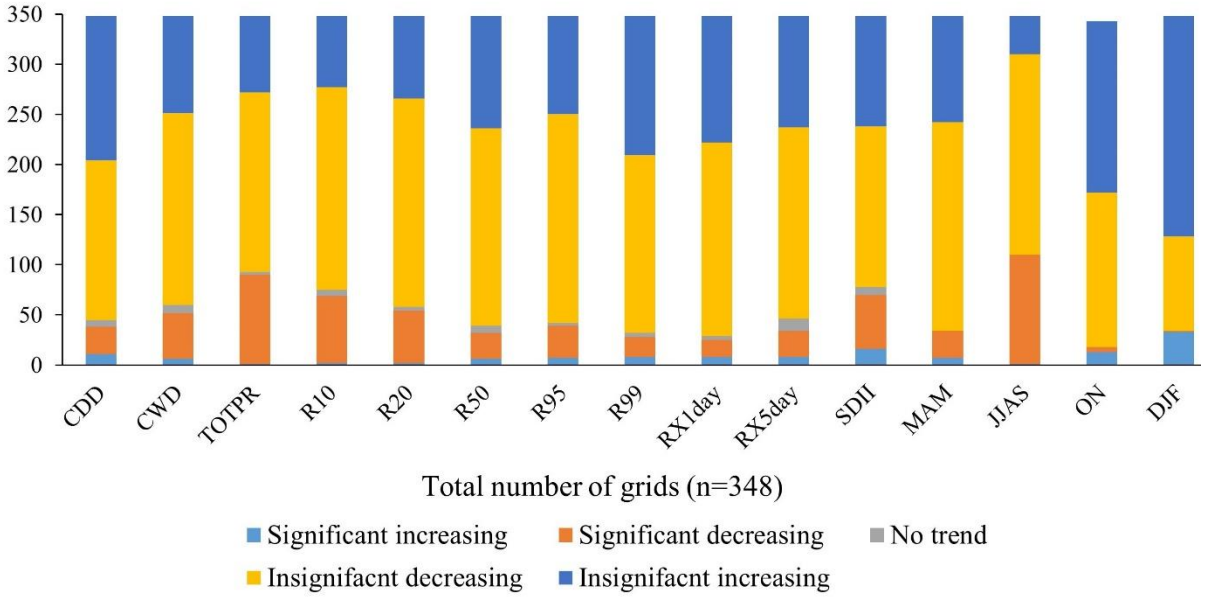

Figure 4.20 Number of grid points exhibiting different trends for ETCCDI indices

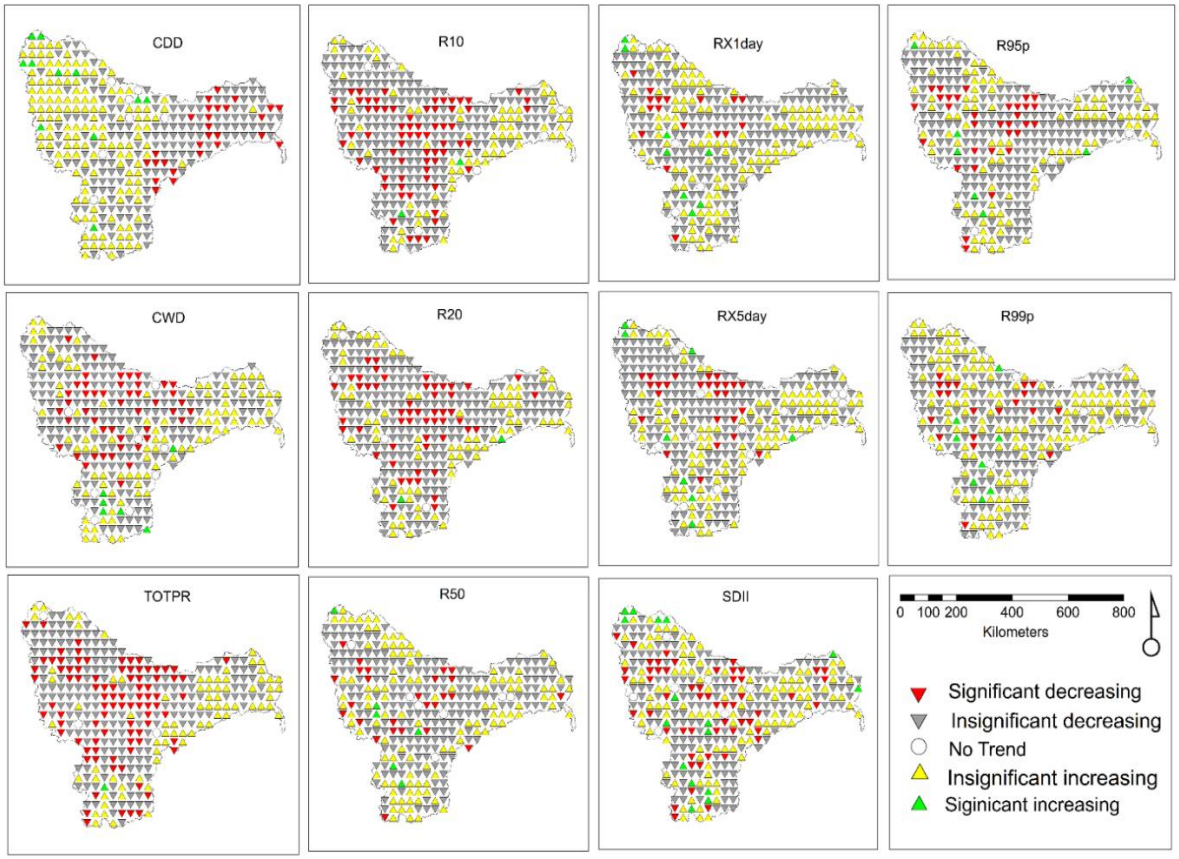

Figure 4.21 Grid-wise trend analysis for different extreme indices in the KRB during baseline period

In the case of CDD, only 5 grids have shown no trend, 10 grids have shown a significant increasing trend at high elevations, 27 grids have shown a significantly decreasing trend at

lower elevations and the remaining 306 grids have exhibited both insignificant increasing and decreasing trends. In contrast, CWD shows decreasing trends in the central region of the basin and only 5 grid points have shown a significant increasing trend in the southern part of the basin. RX5day shows 8 grid points with a significantly increasing trend, 27 grid points have shown a significant decreasing trend, 12 grid points have shown no trend and the remaining grid points exhibited an insignificant decreasing trend (191 grid points) followed by an insignificant increasing trend (111 grid points). It can be observed that TOTPR shows only one grid point as a significant increasing trend and most of the grid points exhibited decreasing trends. A similar pattern is observed for R10, R20 and R50. In the case of R95p and R99p, insignificant decreasing trends can be observed at 208 and 177 grid locations respectively compared to other trend conditions. In all the extreme precipitation indices, few grid points have shown no trend conditions and most of the grid points exhibit a decreasing trend compared to an increasing trend. In the case of SDII, it can be observed that mixed conditions of decreasing and increasing trends and only 17 grid points have shown a significant increasing trend.

4.4.3 Correlation Analysis

The Pearson correlation coefficient (r) is used to compute the association between the discharge and extreme precipitation indices and amongst the extreme indices using IMD data for the baseline period (1973-2003) is shown in Figure 4.22. It can be found that CDD is very weakly and negatively correlated with the other extreme indices due to its drier tendency with rising values. CWD has displayed a moderate correlation with TOTPR, R10, R20, R50, RX5day (0.61 - 0.64) and has shown a lower correlation with R95p, R99p, RX1day and SDII (0.21 - 0.47). TOTPR has shown a good correlation with other indices especially, it has a very strong correlation with R10, R20 and R50 (0.9 - 0.99). And it has a good correlation with very heavy precipitation indices RX1day (0.65), RX5day (0.68) and R99p (0.71) inferring that heavy precipitation may guarantee more precipitation in a year. It can be seen that R10 and R20 are moderate to well correlated (0.55 - 0.68) with RX1day, RX5day and R99p which supports that a slightly heavy precipitation increase has a good association with the existence of very heavy and extreme precipitation. Apart from TOTPR, R50 also has a very strong correlation with RX1day, RX5day R99p and SDII (0.82 - 0.9). On account of seasonal precipitation, only the monsoon season has shown good association with all precipitation extremes excluding CDD. In addition to this, the seasonal precipitation correlations among themselves are also weak.

The strong correlation of AADD can be seen with TOTPR, R10, R20 and R50 (0.7 to 0.75) but a moderate correlation is observed with the heavy extreme indices R99p (0.56), RX5day (0.57) and monsoon precipitation (0.65). A similar kind of pattern can be observed with MADD. The remaining indices showed a weak correlation with AADD.

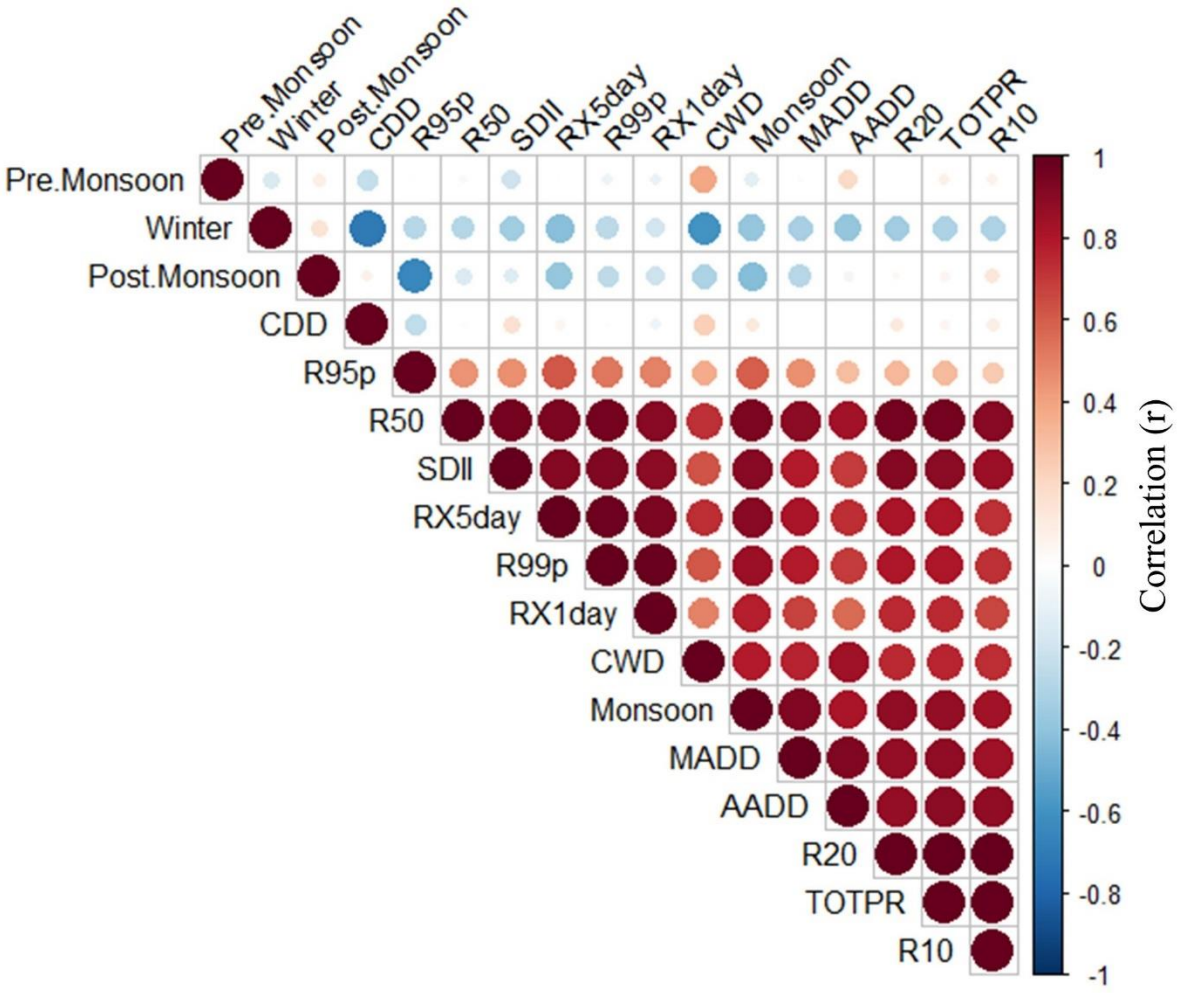

Figure 4.22 Correlation between precipitation extremes and AADD and MADD

4.4.4 Analysis of Inter-annual Variation

Analysis of the variation in extreme precipitation indices including seasonal precipitation and the inter-annual anomalies are computed across the basin and shown in Figure 4.23 (a) to (f). The absolute ratios (in percentage) of RX1day/TOTPR and RX5day/TOTPR are represented by Figure 4.23 (g). Inter-annual fluctuations of extreme indices are similar to slight alterations in the magnitude. Heavy precipitation intensity indices RX1Day, RX5Day, R95p and R99p are exhibiting similar patterns of fluctuations in the basin. These indices have more positive

fluctuations which indicates that the rainfall concentrating in less no of days which may be aggregated to flash floods in the basin.

R99p is the total precipitation on the days having more precipitation than 99th percentile of observed period. The R99p values in 1975 and 1983 are 87.63 mm and 99.76 mm respectively. The highest value of R99p is observed 1983 may lead to highest peak flow in 1983 (20,711 m^3/s) than 1975 (18,512 m^3/s).

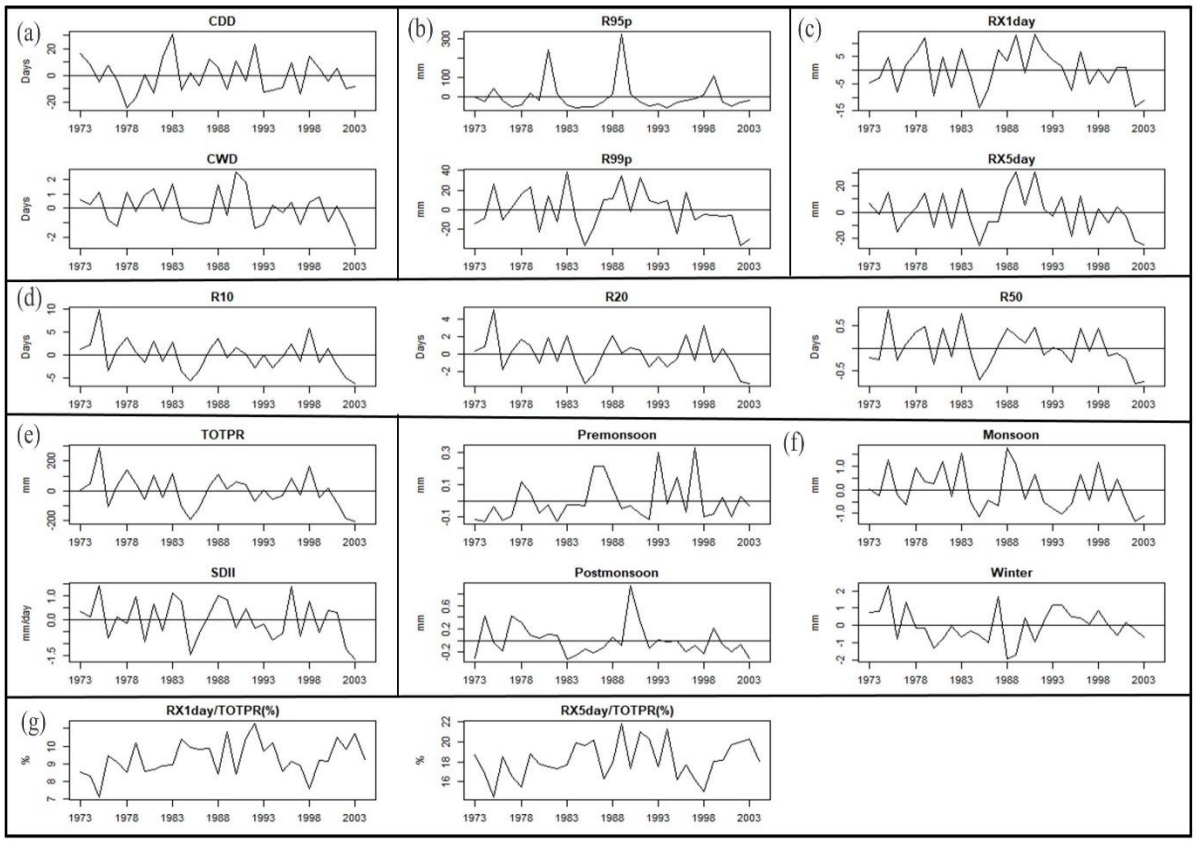

Figure 4.23 Anomalies of the different precipitation extremes in the KRB. ((g) represents the absolute ratios in percentage

So, it can be referred from the analysis that the heavy precipitation is more during that year where the magnitudes of fluctuations are greater. The percentage contributions of RX1day and RX5day to TOTPR were about 7.6% and 15% respectively in the year 1998. The percentage contributions of RX5day is highest (21.83%) in 1989 and the peak flow is about 17,617 m^3/s. This information is useful in the design of drainage network facilities and stream advancement works because the lower-lying regions are inclined to flooding and immersion issues.

The fluctuations of CDD and CWD are opposite and CWD has more increasing fluctuations compared to CDD which results in the accumulation of a high amount of precipitation in the basin. The fluctuations of TOTPR, R10, R20, R50, Monsoon and SDII follow similar kinds of

trends in each year. The precise information of variability in precipitation extremes including seasonal precipitation may act as useful data to various stakeholders.

4.4.5 Future Changes in Extremes Precipitation Indices

Four future warming precipitation scenarios namely, SSP1-2.6, SSP2-4.5, SSP3-7.0 and SSP5-8.5 of CMIP6-based GCMs in two future time frames are used in the present study. These two future frames such as Near Future (NF: 2025-55) and Far Future (FF: 2065-95) extreme precipitation fluctuations are shown in Figures 4.24 to 4.27. The uncertainty variability ranges are more in FF compared to NF and slightly higher in magnitude for high warming scenarios of SSP3-7.0 and SSP5-8.5 compared to other scenarios. The MME average of selected GCMs shows a significant increase in all extreme precipitation indices compared to the baseline period under all SSP scenarios. It can be observed that under SSP5-8.5, the MME average shows a higher increase for FF compared to other SSPs. Figure 4.28 depicts the relative change of MME averages of selected climate models for future periods. The relative change magnitude is anticipated to increment more in future phases (FF > NF) but the extent of change is not substantial. The MME average of CWD and R50 are expected to be doubled with respect observed period, especially in the FF. The heavy extreme precipitation indices such as R99p, R95p, RX5day and RX1day are significantly increasing along with other precipitation extremes indices. R95p and RX5day are increased slightly more in magnitude compared to R99p and RX1day respectively. Significant increment can be seen in annual TOTPR, but low in magnitude compared to heavy extreme indices. The SSP5-8.5 scenario shows significant changes under FF compared to other scenarios for all the extreme indices.

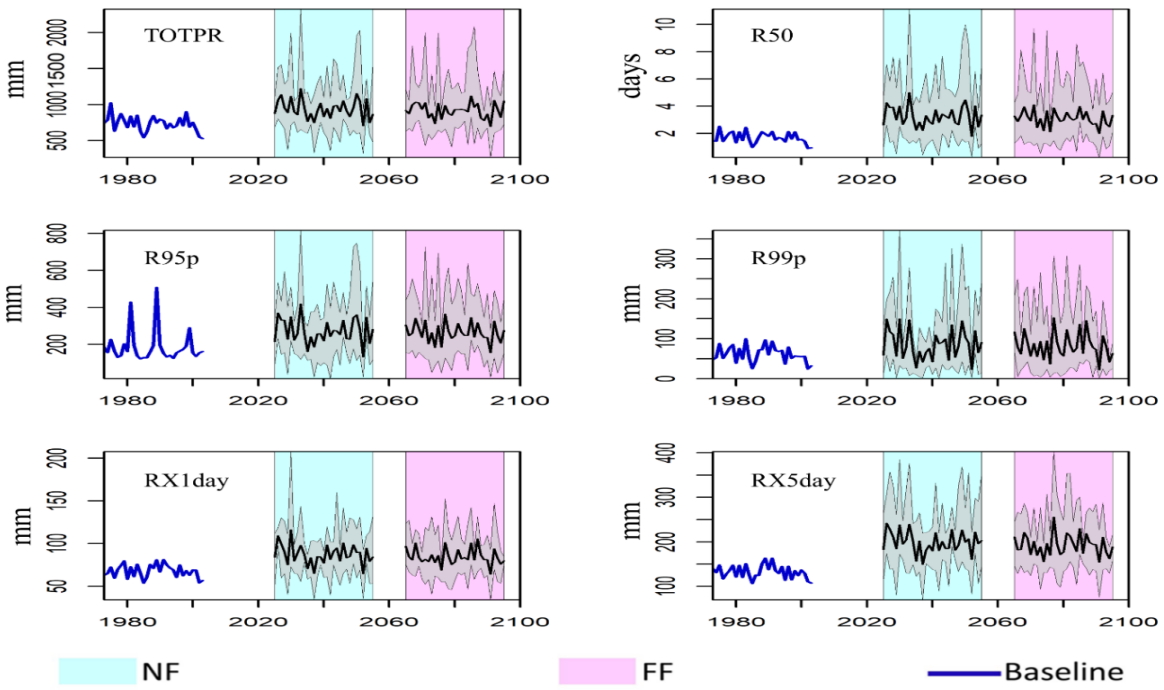

Figure 4.24 Comparison of inter-annual variation of precipitation extremes for NF and FF 847 under SSP1-2.6 (Shaded region represents the ranges of selected climate models and solid line represents the MME average of the GCMs) with the baseline period

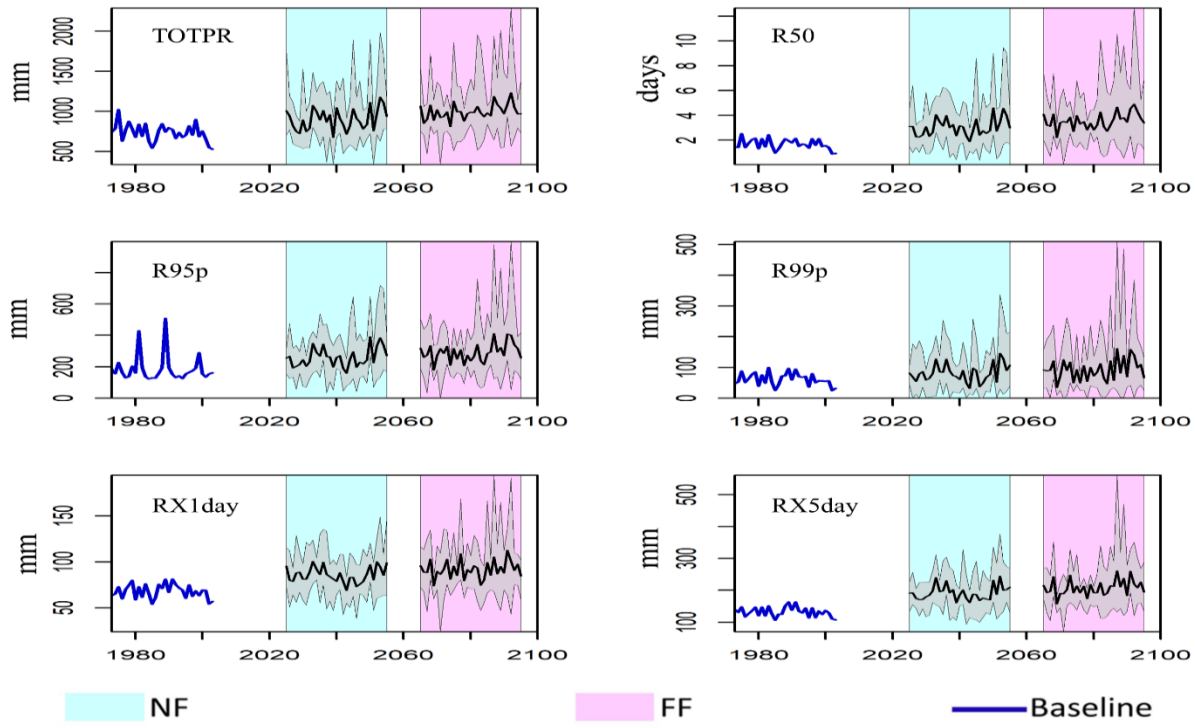

Figure 4.25 Comparison of inter-annual precipitation extremes variations in the NF, FF period under SSP2-4.5 with the baseline period

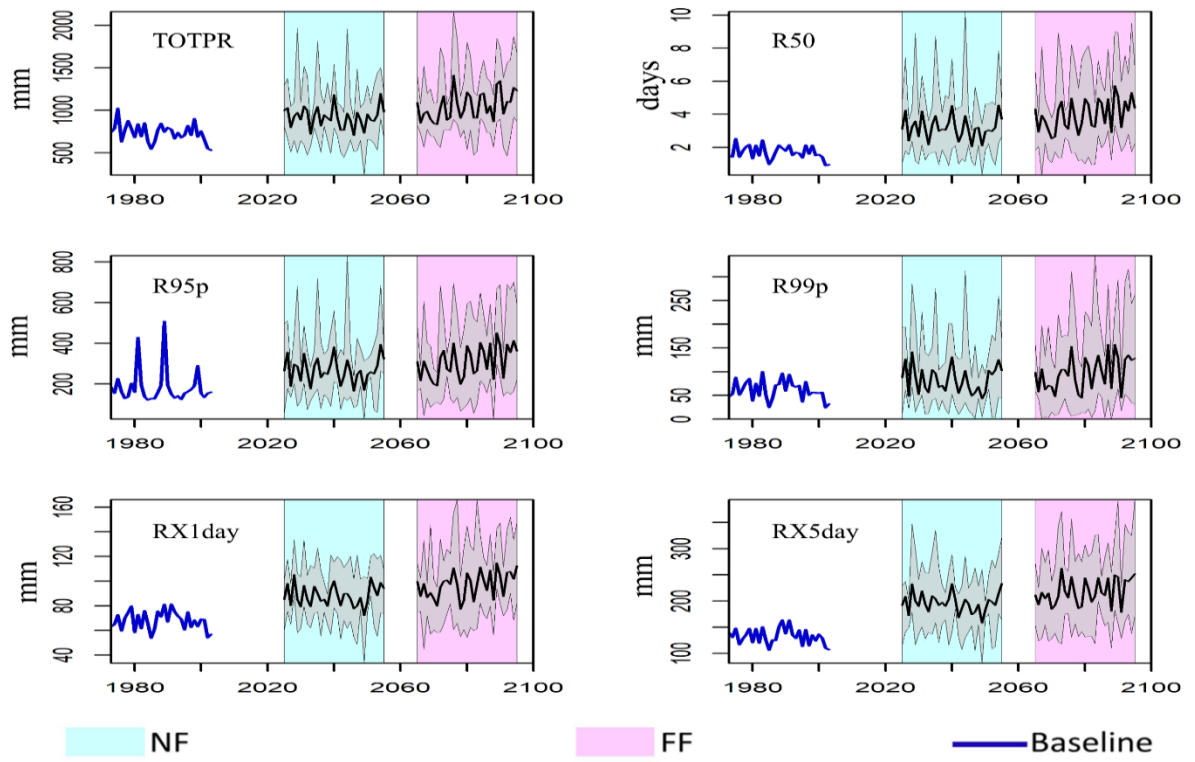

Figure 4.26 Comparison of inter-annual precipitation extremes variations in the NF, FF period under SSP3-7.0 with the baseline period

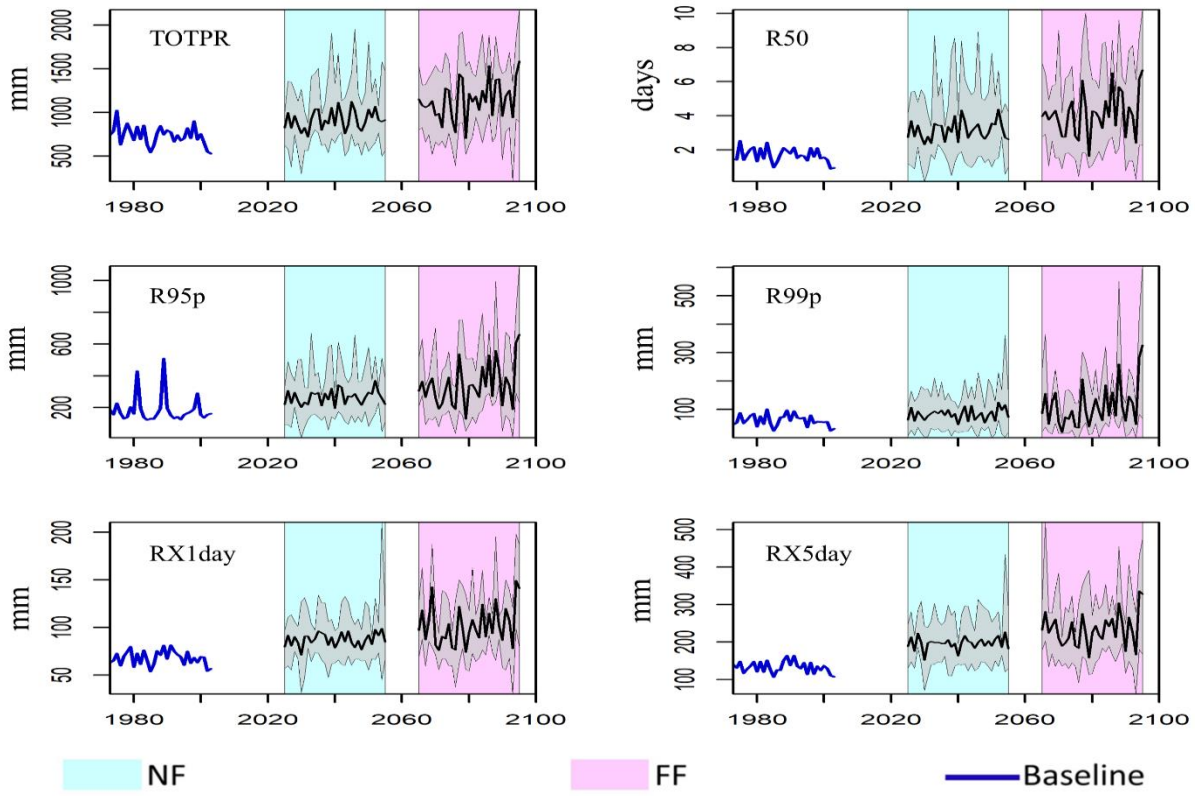

Figure 4.27 Comparison of inter-annual precipitation extremes variations in the NF, FF period under SSP5-8.5 with the baseline period

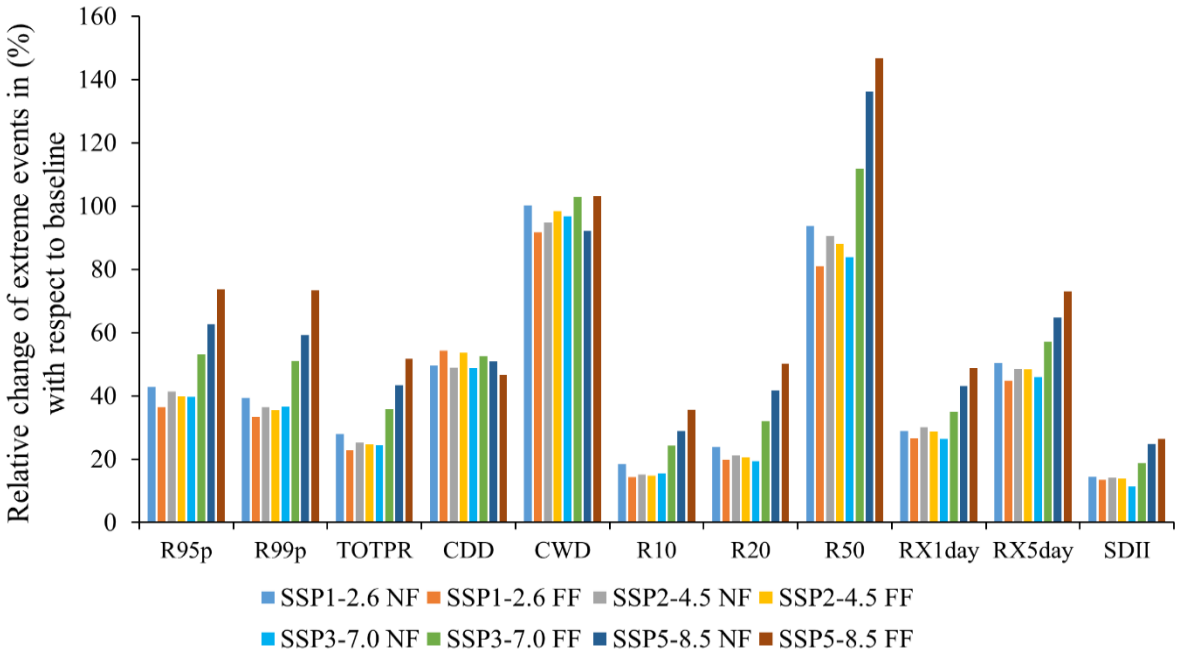

Figure 4.28 Relative changes (in percentage) of precipitation extremes of MME mean with respect to base period

The spatial distribution of relative change under SSP5-8.5 under FF is shown in Figure 4.29. It is observed that R95p and R99p are showing similar trends of increment in magnitude. Compared to RX1day, RX5day increment magnitudes are greater, TOTPR and R20 are more or less following the same trends of increments. R50 and CWD almost doubled in magnitude at most of the grids. Other scenarios also followed similar trends with SSP5-8.5, but less in magnitude. Few gird locations showed a decrement in the extreme indices but these are very less in number.

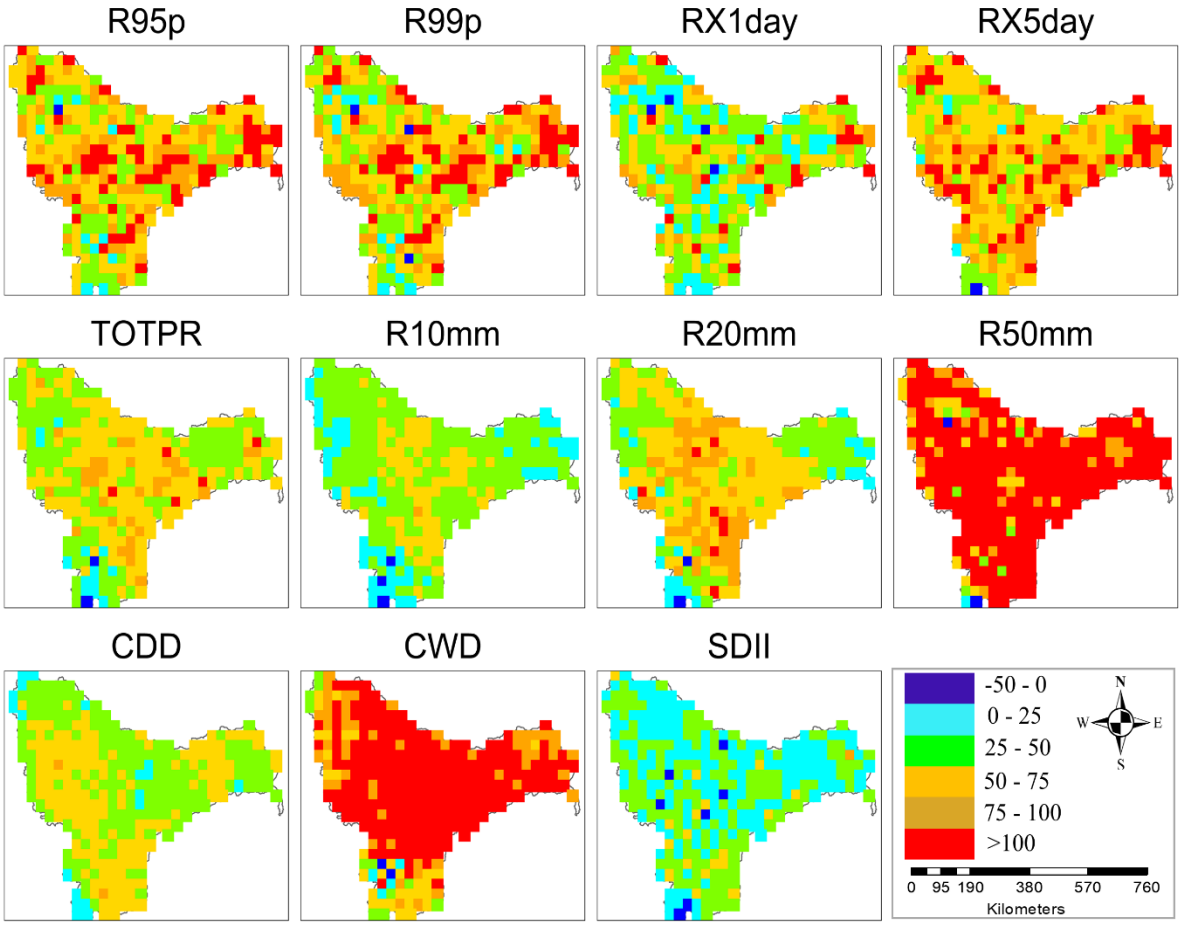

Figure 4.29 Spatial distribution of relative changes in extreme indices under SSP5-8.5 scenario for FF (2065-2095)

4.4.6 Projected Changes in Future Discharge

The present study used SVM regression to quantify the future AADD by establishing the relationship between TOTPR and AADD. The calibration period (1973-1996) is considered in the training for SVM regression and the remaining period from 1997-2003 is taken for testing (validation). The values of coefficient of determination (R^2) and Nash Sutcliff Efficiency (NSE) for training and testing periods are observed as (1, 1) and (0.8, 0.71) respectively and this shows a very good performance. The values of SVM parameters C, γ and ε are obtained as 64, 0.0001 and 0.0001 respectively. The observed AADD between 2000 and 2003 is low when compared to the rest period. The TOTPR for these years was observed as low compared to the rest period, which might be the reason for the low discharges between 2000 and 2003. The variation of simulated AADD of selected GCMs and their ensemble for the baseline scenario (1973-2003) using SVM regression is shown in Figure 4.30.

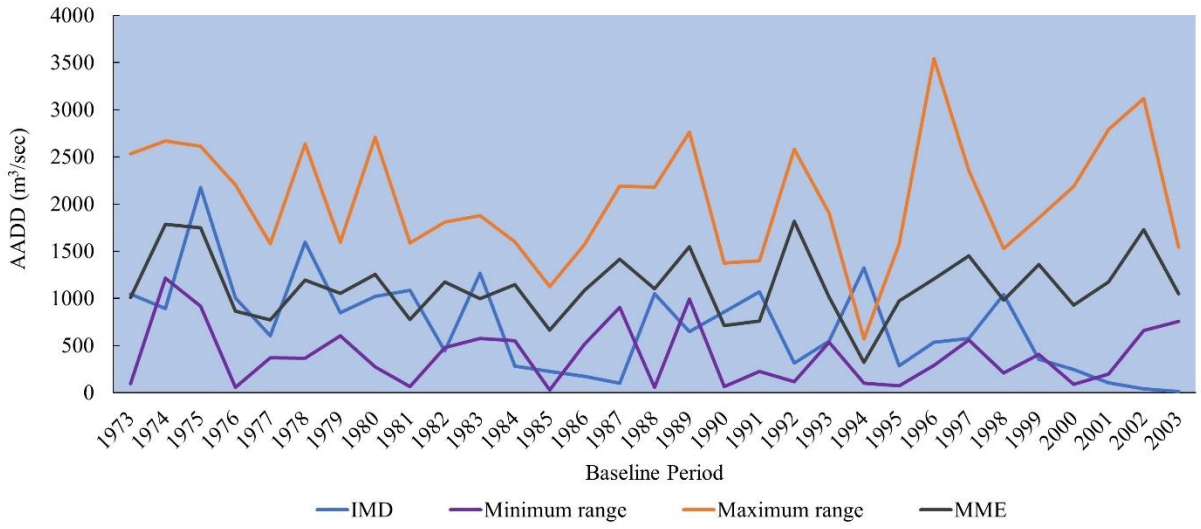

Figure 4.30. Comparison of AADD of observed and historical climate models and their MME average in the baseline period 1973-2003

It can be observed that the maximum range of simulated AADD under selected GCMs is more compared to the observed AADD except in the year 1994. The maximum peak of 3540 m^3/s can be observed in the year 1996 which is 122% higher than the highest peak of observed streamflow (1545 m^3/s). The minimum range of simulated AADD under selected GCMs is almost less compared to the observed AADD. The MME of the simulated historical streamflow is higher than the observed streamflow in the same period suggesting that there is the probability of increasing in the future streamflow. The overall average of MME streamflow during the period 1973-2003 is observed as 1131 m^3/s which is 61.11% more compared to the observed streamflow average (702 m^3/s) in the same period. Figure 4.31 depicts an inter-annual variation of AADD under four SSP scenarios over future periods. The results depict that the MME of future streamflow is expected to increase significantly in the future periods compared baseline period under all SSP scenarios. In the SSP1-2.6 and SSP2-4.5 scenarios, the increasing range of streamflow almost follows a similar pattern during the NF and FF. For the NF under SSP1-2.6 and SSP2-4.5, the highest average streamflow of 2190 m^3/s and 2075 m^3/s are observed in the years 2027 and 2033 respectively.

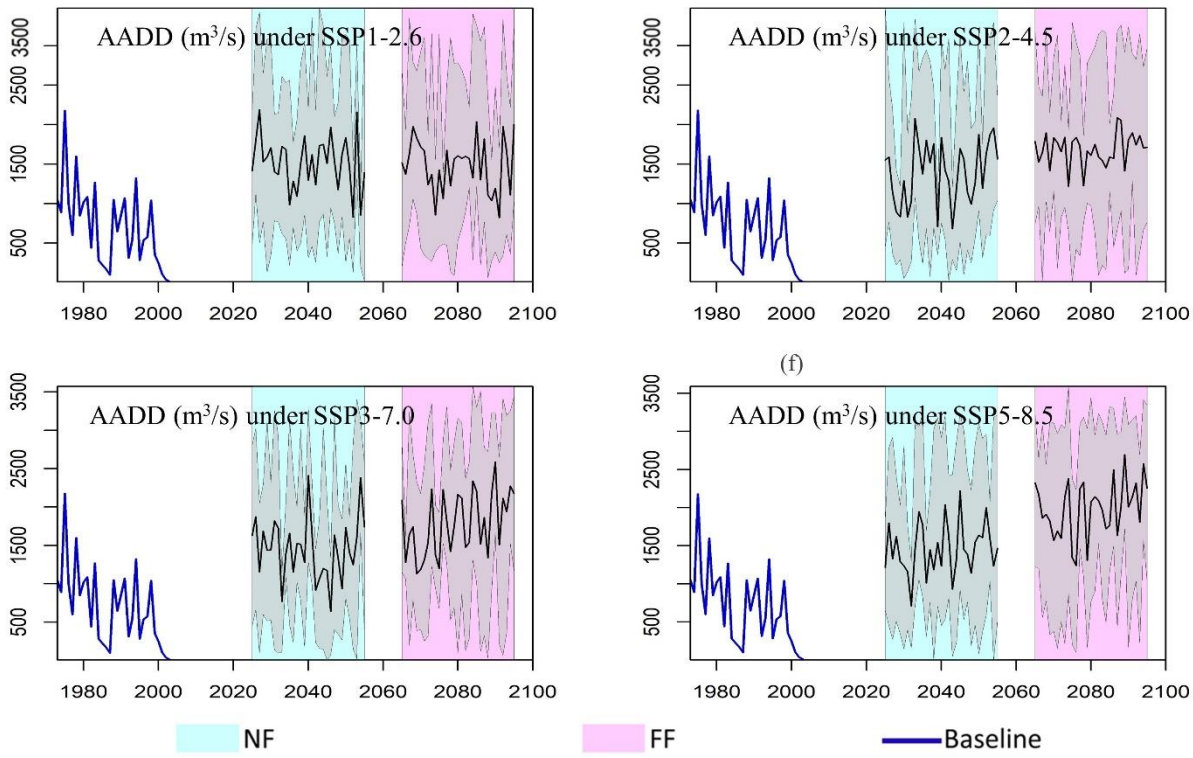

Figure 4.31 Variations of inter-annual AADD estimated from TOTPR of selected climate models and their MME under four SSP scenarios

The maximum shifts in streamflow are observed in the FF under SSP3-7.0 and SSP5-85 scenarios compared to NF. The maximum MME average streamflow of 2588 m^3/s and 2694 m^3/s is observed in the years 2090 and 2089 for the far future under SSP3-7.0 and SSP5-8.5 respectively. It can be observed that the average MME streamflow of all four scenarios is higher than the AADD streamflow (702 m^3/s) during the baseline period 1973-2003 and the increase is in the range of 98.78% to 183.33%. These results infer that the more availability of water and the probability of occurring of floods in the future period in the KRB.

4.4.7 Conclusions

A systematic investigation spatio-temporal analysis of various extreme precipitation indices in KRB, India is done for a baseline period of 31 years (1973–2003) and two future frames of Near Future (NF: 2025–2055) and Far Future (FF: 2065-2095) under four CMIP6 based projected climate scenarios of SSP1-2.6, SSP2-4.5, SSP3-7.0 and SSP5-8.5. A larger number of grid points exhibited decreasing trends (insignificant and significant) followed by increasing (insignificant) trends and a very small number of grid points experienced positive significant trends for extreme precipitation indices across the basin. RX1day and RX5day are major extreme precipitation indices and the mean annual contributions are 9.7% and 18.5%

respectively in the baseline period. It is found that the MME average of extreme precipitation indices is predicted to increase over the future periods. Particularly, in the FF the magnitude of increase is greater under all SSP scenarios over the basin. The heavy extreme precipitation indices R95p and R99p are increased to about 74%, RX1day and RX5day are increased to 49% and 73% respectively in the FF under the high warm SSP5-8.5 scenario. The MME average streamflow is projected to increase in the future under all scenarios but slightly more in the order of magnitude under SSP3-7.0 and SSP5-8.5 compared to other scenarios.

4.5 SWAT Application for Hydrological Modelling in KRB

To meet this objective, SU is used to select the top 50% of GCMs from a pool of 18 CMIP6 GCMs for hydrological modelling using TRW from Figure 4.16. Top nine (9) suitable GCMs: MPI-ESM1-2-HR, MPI-ESM1-2-LR, GFDL-ESM4, NorESM2-LM, EC-Earth3-Veg, BCC-CSM2-MR, EC-Earth3, IPSL-CM6A-LR, NorESM2-MM, were considered for further analysis.

4.5.1 SWAT Model Performance Evaluation

The SWAT model was calibrated and validated at monthly step using the observed discharge at six outlet stations. The sub-basin discretization for the SWAT model along with the locations of reservoirs, gauge points is shown in Figure 3.5. The model was simulated from 1970-2003, with first 3 years considered as warm-up period. The calibration of the model was performed for 21 years i.e. 1973-1993 and validation for 10 years i.e. 1994-2003 using SUFI-2 algorithm in the SWATCUP. Based on the past studies, 12 parameters that influenced the streamflow were selected for the calibration (Table 4.3).

Table 4.3 Calibrated Parameters of SWAT model

Parameter	Range	Fitted value
R__CN2.mgt	-0.1 to 0.1	-0.0946
V__ALPHA_BF.gw	0.2 to 0.8	0.7526
A__GW_DELAY.gw	-30 to 90	-21.960001
A__GWQMN.gw	-1000 to 1000	250
R__SOL_AWC().sol	-0.1 to 0.1	-0.009
A__REVAPMN.gw	-750 to 750	-154.5
A__RCHRG_DP.gw	-0.05 to 0.05	0.0175
V__GW_REVAP.gw	0.02 to 0.2	0.0569
V__CH_N2.rte	0 to 0.2	0.0146
V__CH_K2.rte	0 to 100	81.900002
R__OV_N.hru	-0.2 to 0.2	0.1532
V__ESCO.hru	0 to 0.8	0.1576

Among these parameters, nine (9) parameters, i.e. CN2, GWQMN, ESCO, SOL_AWC, CH_N2, REVAPMN, GW_DELAY, CH_K2 and GW_REVAP, are identified as most sensitive parameters after 500 iterations. The performance of the model during calibration and validation was assessed using the Nash Sutcliff Efficiency (NSE) and coefficient of determination (R^2). A similar R^2 and NSE value of 0.79 was obtained during calibration period, which is considered as good as per the suggestions given in Moriasi et al. (2015). For the validation period the R^2 and NSE values of 0.65 and 0.64 were obtained, which is considered as satisfactory. The good performance of the model during the calibration and validation periods is also observed between the close match in the simulated and observed hydrographs as shown in Figure 4.32.

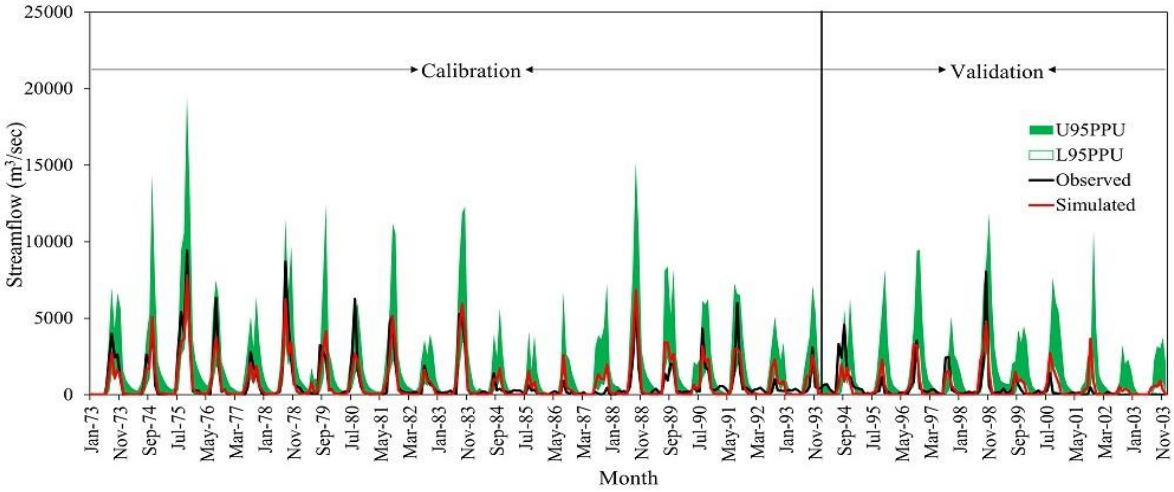

Figure 4.32 Depiction of simulated and observed streamflow for calibration and validation period

The performance of the model was also compared using other statistical performance measures such as PBIAS, p-factor and r-factor as shown in Table 4.4.

Table 4.4 Performance evaluation values for calibration and validation at Vijayawada gauge station for monthly simulations.

Parameter	Calibration	Validation
NSE	0.79	0.65
R^2	0.79	0.64
PBIAS	-0.9	-11.5
p-factor	0.62	0.57
r-factor	1.06	1.29

The p-factor represents the percentage of observed data bracketed by the 95PPU and varies from 0 to 1. For the streamflow the P-factor value > 0.7 is considered as good. The r-factor indicates the width of the 95PPU band and value < 1.5 is considered as desirable. In the present study, the P-factor and R-factor at Vijayawada gauge station are observed as 0.62 and 1.06 respectively and are considered as satisfactory (Abbaspour et al., 2015). The negative values of the PBIAS in both calibration and validation periods indicate that model has under predicted the streamflow as compared to the observed flow. The calibrated and validated model was also evaluated at other gauging locations as shown in Table 4.5 and Figure 4.33.

Table 4.5 Performance evaluation values for calibration and validation at different stations

Sub-basin (station no)	Calibration		Validation		PBIAS	p-factor	r-factor
	R^2	NSE	R^2	NSE			
Mantralayam (66)	0.80	0.78	0.70	0.68	16.8	0.63	0.88
T.Ramapuram (72)	0.67	0.57	0.65	0.58	16.3	0.73	1.37
Yadagir (33)	0.78	0.77	0.67	0.67	6.8	0.8	0.82
Keesara (32)	0.86	0.84	0.61	0.58	2.7	0.77	1.10
Dameracherla (29)	0.54	0.53	0.63	0.45	9.2	0.65	1.9

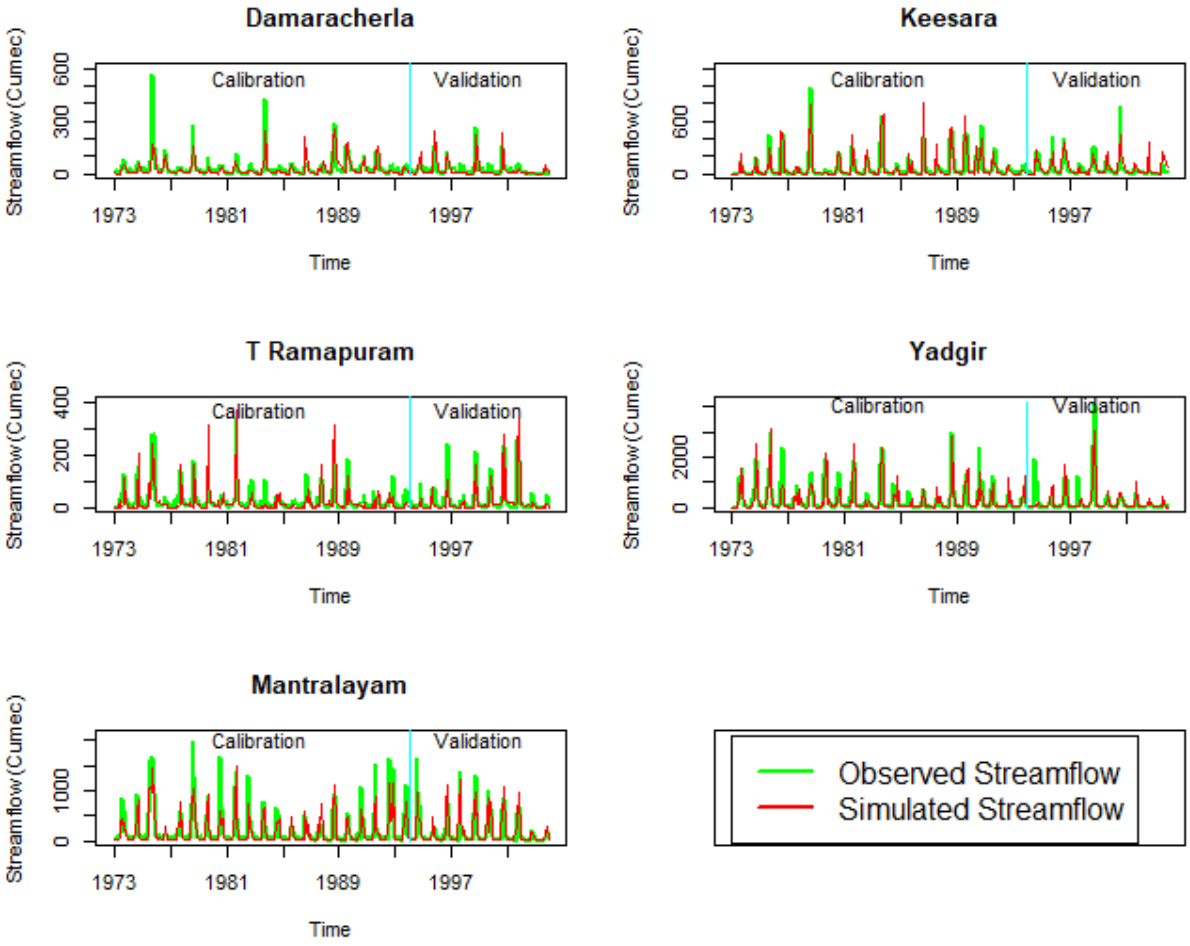

Figure 4.33 Depiction of simulated and observed streamflow for calibration and validation period at different gauge stations

The high values of NSE, R^2 and PBIAS at different gauging locations across the KRB suggest that the model is spatially performing well. The good performance of the calibrated model suggests that the model is able to capture the spatial and temporal variability of the hydrological processes properly within the basin.

4.5.2 Climate Change Impact on WBC in KRB

The impact of climate change on the hydrology of the KRB is assessed using the selected 9 GCMs for the four scenarios of SSP1-2.6, SSP2-4.5, SSP3-7.0 and SSP5-8.5. The analysis was performed for three future time periods i.e. Near Future (NF: 2026-2050), Mid Future (MF: 2051-2075) and Far Future (FF: 2076-2100). The impact of climate change on the water balance components, i.e. precipitation, evapotranspiration, surface runoff, water yield and streamflow at the watershed outlet was assessed. The historical simulations of each of the GCMs were forced through the SWAT model to obtain the historical output and is considered as the baseline for assessing the impacts of climate change for each GCM (Figures. 4.34 to 4.37). A comparison is also made between the WBC simulations obtained from historical GCM and the observed IMD data for the baseline period i.e. 1973-2003. The uncertainty in the future projections is evident from the difference in the projected values from different GCMs as shown in Figures 4.34 to 4.37. During the baseline period 1973-2003, the average annual precipitation projections for the historical GCMs are ranged from 713 mm to 796 mm, compared to the observed precipitation value of 697 mm. Among the 9 GCMs, MPI-ESM1-2-HR, EC-EARTH3, EC-EARTH3-Veg models were observed to have less deviation with observed precipitation in the baseline period whereas, NorESM2-LM, NorESM2-MM models are exhibiting maximum variation compared to other GCMs (see Figure 4.34).

The future projection of precipitation for four SSP scenarios are significantly increasing for each GCM compared to historical GCM, except for MPI-ESM1-2-HR and MPI-ESM1-2-LR. In comparison to the historical period, the EC-EARTH3, EC-EARTH3-Veg models show the highest range in projected precipitation change under all SSP scenarios. It is also observed that the future precipitation increases from NF to FF under all scenarios for all GCM. To understand the variation of precipitation for each GCM, the annual average precipitation changes of the historical period for each GCM with respect to observed IMD data was analysed and is provided in the Table 4.6. Similarly, the percentage changes in the projections of precipitation of each GCM with respect to same GCM in the future is provided in Table 4.7.

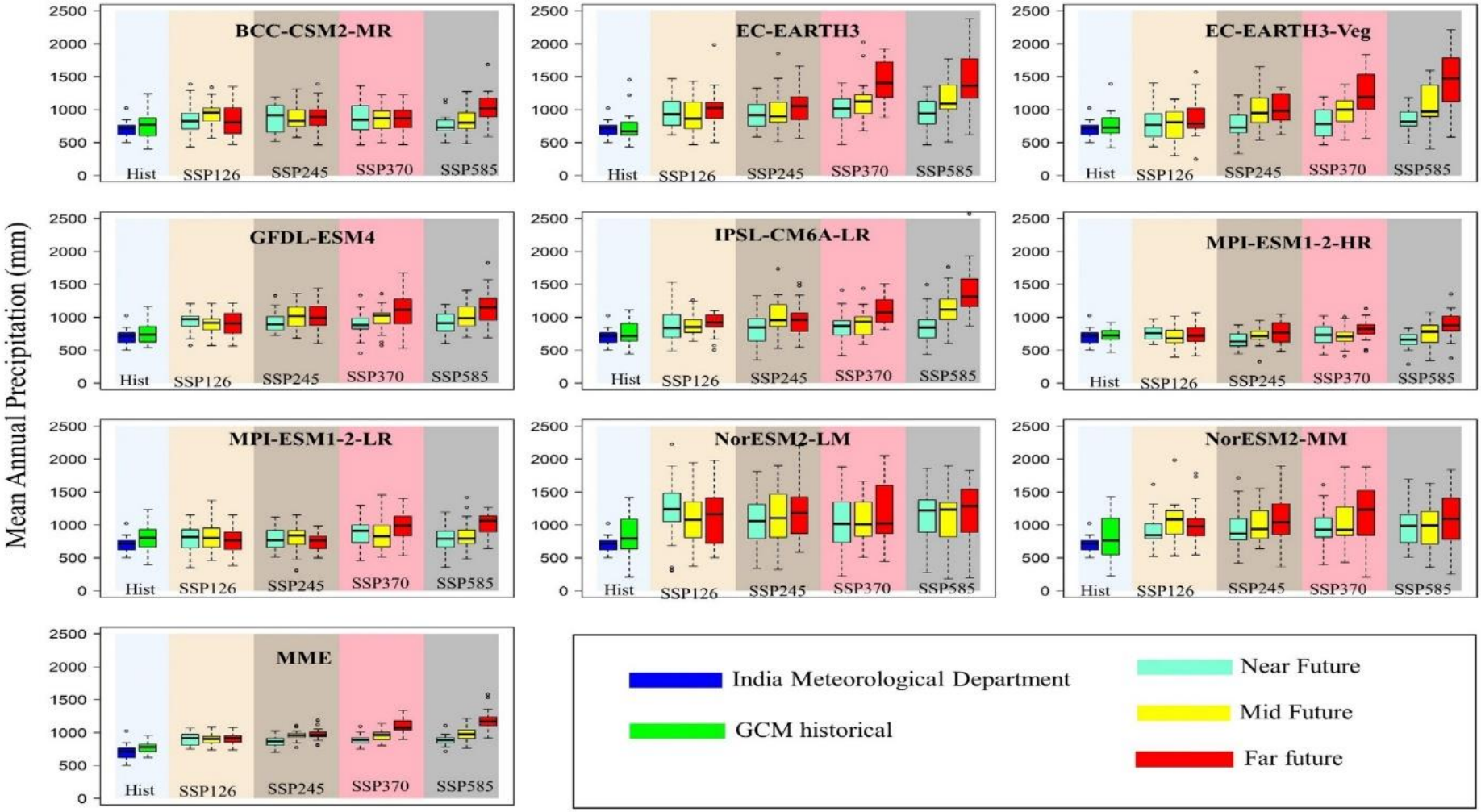

Figure 4.34 Average annual precipitation under different SSP scenarios in comparison with observed IMD data

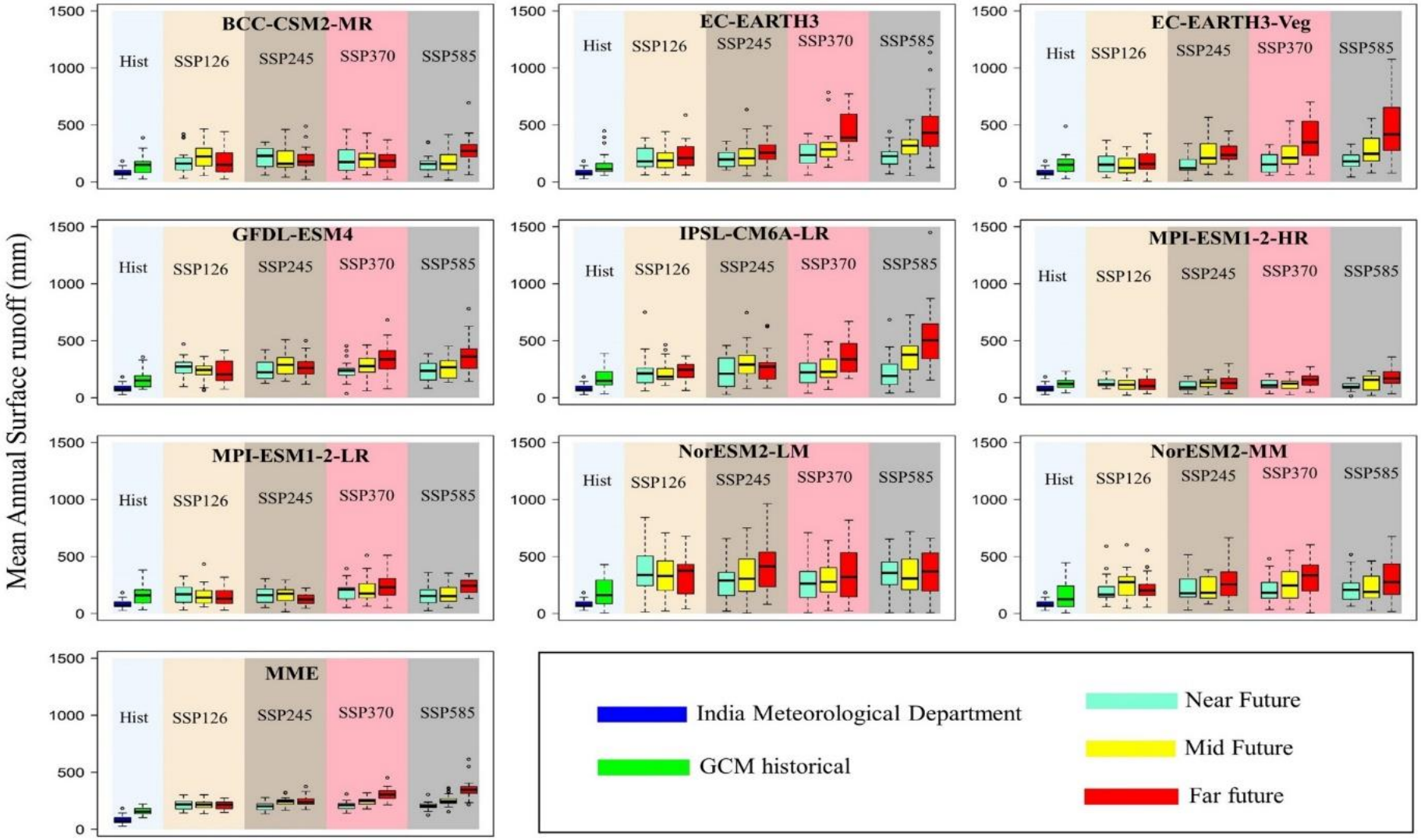

Figure 4.35 Average annual surface runoff under different SSP scenarios in comparison with observed IMD data

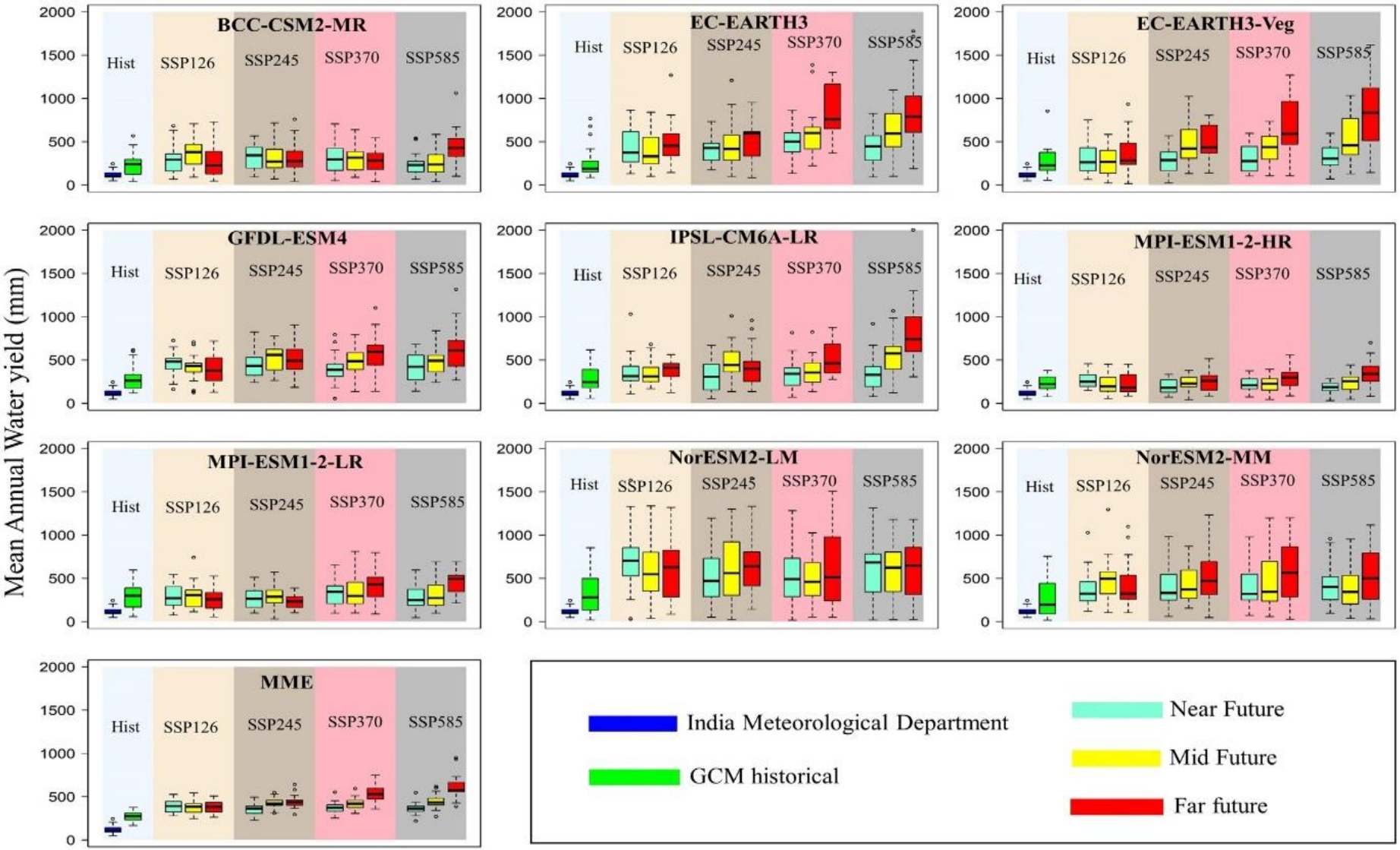

Figure 4.36 Average annual water yield under different SSP scenarios in comparison with observed IMD data

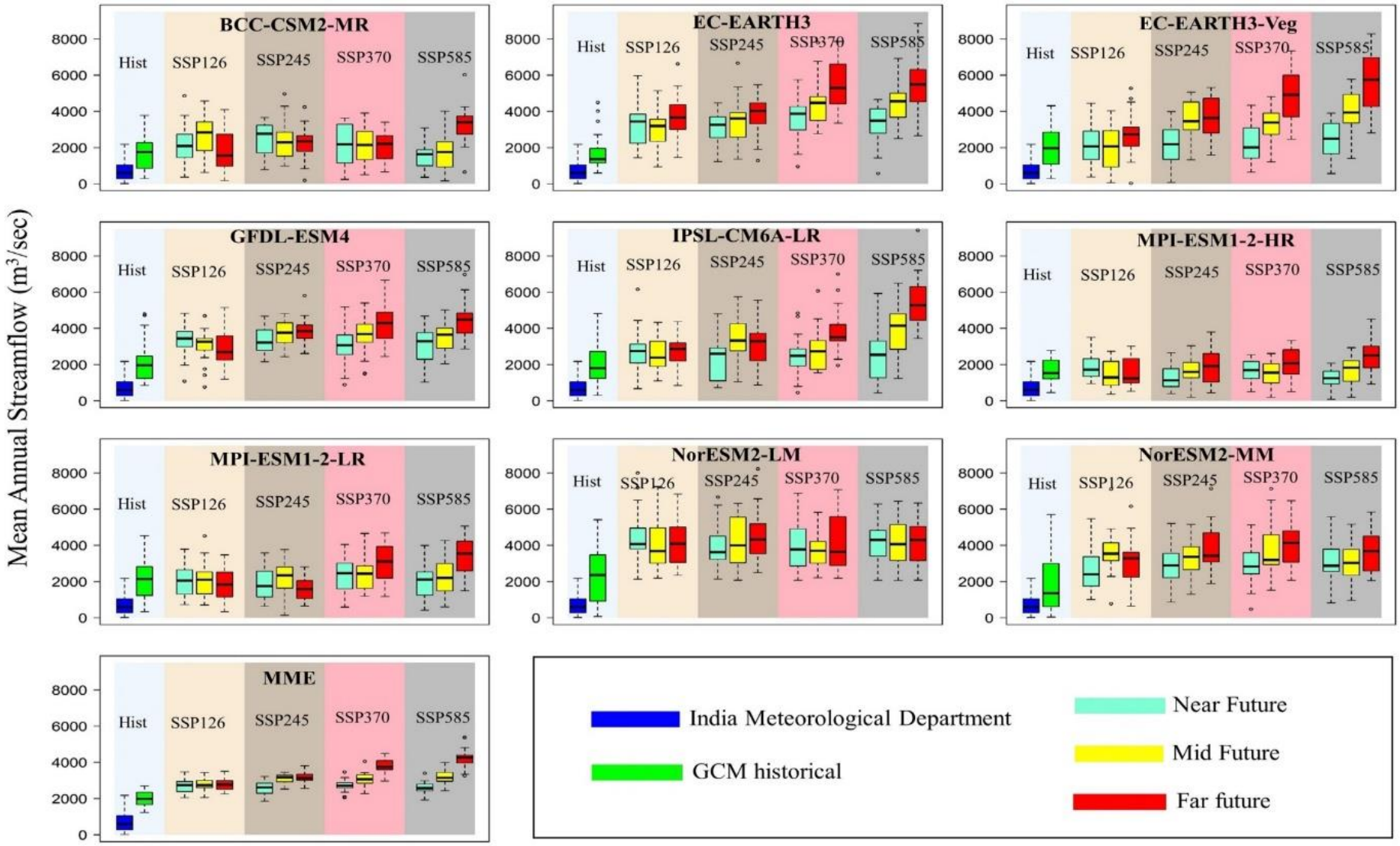

Figure 4.37 Average annual streamflow under different SSP scenarios in comparison with observed IMD data

Table 4.6 Comparison of WBC for 9 GCMs and the observed data during the baseline period (1973-2003) for annual period

Scenario	Precipitation (mm)	ET (mm)	Water Yield (mm)	Surface Runoff (mm)	Streamflow (m^3/sec)
IMD	697	519	119	82	702
BCC_CSM2-MR	767.5 (10.1)	456 (-12.1)	231.3 (94)	146.4 (78)	1674 (138)
EC-EARTH3	739.1 (6.04)	409.5 (-21)	246.7 (107)	143.9 (75)	1708.5 (143)
EC-EARTH3-Veg	771.1 (10.63)	409.5 (-21)	277.2 (132)	155.3 (89)	2033 (189)
GFDL-ESM4	768 (10.18)	396.9 (-23)	285.9 (140)	162.7 (98)	2110.3 (200)
IPSL-CM6A-LR	778 (11.6)	414.6 (-20)	282.3 (137)	181.7 (121)	2077.7 (196)
MPI-ESM1-2-HR	712.8 (2.3)	402.7 (-22)	226.7 (90)	122.3 (49)	1633.5 (132)
MPI-ESM1-2-LR	794.6 (14)	416 (-19)	293.2 (146)	165.2 (101)	2125.6 (202)
NorESM2-LM	819.3 (17.5)	408.9 (-21)	325.9 (173)	190.6 (132)	2380.7 (239)
NorESM2-MM	795.5 (14)	441.6 (-15)	271.2 (127)	154.3 (88)	1986.8 (183)
MME	771.8 (10.7)	417.3 (-19)	271.1 (127)	158 (92)	1970 (180)

The value in the brackets represents percentage change.

The variation in projections of the annual average precipitation compared to historical GCMs are in the range of -5.7% for MPI-ESM1-2-LR to 100.9% for EC-EARTH3 in the future under SSP2-4.5 and SSP5-8.5 respectively. NorESM2-LM and NorESM2-MM models are projecting more precipitation in the future compared to other historical GCMs projections under all SSP scenarios except SSP5-8.5 in the FF. In the FF, EC-EARTH3-Veg model is projecting highest precipitation compared to historical period. The surface runoff and water yield components are also following similar increasing patterns with the precipitation under all GCMs in the historical period. The annual MME average of surface runoff and water yield are projected to increase up to 92% and 127% respectively in comparison to historical period. The significant rise in water yield and surface runoff has led to a corresponding increase in streamflow across all GCMs. The comparison of surface runoff, water yield and streamflow between each GCM for the future periods under four SSP scenarios is also computed.

Table 4.7 Comparison of annual average historical precipitation of 9 GCMs with respect to same GCM for the future period scenarios (GCM 1 to 9 represents, BCC-CSM2-MR, EC-Earth3, EC-Earth3-Veg, GFDL-ESM4, IPSL-CM6A-LR, MPI-ESM1-2-HR, MPI-ESM1-2-LR, NorESM2-LM and NorESM2-MM respectively).

GCM	1	2	3	4	5	6	7	8	9
Historical PR **(mm)**	767.5	739.1	771.1	768	778	712.8	794.6	794.6	795.5
SSP1-2.6 (NF)	856.3 (11.6)	949.6 (28.5)	789 (2.3)	941.5 (22.6)	885.6 (13.8)	759 (6.5)	804 (1.3)	1235.9 (55.5)	905.3 (13.8)
SSP1-2.6 (MF)	923.5 (20.3)	905.2 (22.5)	761.3 (-1.3))	898.7 (17)	885.8 (13.9)	701.3 (-1.6)	808.9 (1.8)	1133 (42.6)	1059 (33.1)
SSP1-2.6 (FF)	826.6 (7.7)	1034.8 (40)	885.6 (14.8)	904.7 (17.8)	915.6 (17.7)	721.7 (1.2)	767 (-3.47)	1129.9 (42.2)	1012.7 (27.3)
SSP2-4.5 (NF)	873.4 (13.8)	930.4 (25.9)	769.8 (-0.2)	921.9 (20)	836.9 (7.6)	655.8 (-8)	788 (-0.83)	1055.8 (32.9)	956 (20.2)
SSP2-4.5 (MF)	890.59 (16)	989 (33.9)	988.8 (28.2)	1007 (31.1)	1016 (30.6)	728.9 (2.3)	814.7 (2.5)	1119.8 (40.9)	1021.5 (28.4)
SSP2-4.5 (FF)	885.3 (15.3)	1027.6 (39)	1021 (32.4)	1015 (32.2)	960.7 (23.5)	762.6 (7)	748.7 (-5.7)	1221.8 (53.8)	1099 (38.2)
SSP3-7.0 (NF)	857.6 (11.7)	1007 (36.2)	786.6 (2)	893 (16.3)	848.3 (9)	727.5 (2.1)	854 (7.4)	1051.9 (32.4)	960 (20.7)
SSP3-7.0 (MF)	863.5 (12.5)	1147.8 (55.2)	965.6 (25.2)	981 (27.7)	914 (17.5)	703 (-1.4)	866.9 (9)	1059 (33.3)	1061 (33.4)
SSP3-7.0 (FF)	856.5 (11.6)	1435.4 (94.2)	1250.6 (62.2)	1081.5 (40.8)	1092 (40.4)	813 (14.1)	986 (24)	1182 (48.8)	1146.6 (44.1)
SSP5-8.5 (NF)	758.3 (-1.2)	961.9 (30.1)	843.2 (9.4)	902.4 (17.5)	881.5 (13.3)	655.7 (-8)	781.2 (-1.68)	1156.8 (45.6)	996.9 (25.3)
SSP5-8.5 (MF)	825.8 (7.6)	1164.2 (57.5)	1065.5 (38.2)	1000.8 (30.3)	1135.8 (46)	751.2 (5.4)	839.2 (5.61)	1110.3 (39.7)	1006.9 (26.6)
SSP5-8.5 (FF)	1033 (34.6)	1484.6 (100.9)	1429 (85.3)	1169.4 (52.3)	1415.6 (82)	888.6 (24.7)	1036.6 (30.45)	1156 (45.5)	1066.5 (34.1)

The values in the brackets represents percentage change in the (PR= precipitation).

A comparison of the future projected precipitation from all GCM's with the historical GCM observed precipitation indicates that the mean precipitation in the basin is increasing in most of the future scenarios. Only few years in all the GCM simulations have shown lower precipitation as compared to the historical GCM precipitation within the basin. It is also observed that the variability in the future projected mean annual precipitation is increasing as evident from the box plots of Figure 4.34. The MPI-ESM1-2-HR and MPI-ESM1-2-LR GCMs are predicting less increment in the future compared to other GCMs, which occupied 1st and

2nd rank in GCM ranking. It can be seen that NorESM2-LM and NorESM2-MM are overestimating the higher extremes and underestimating the lower extremes. Although NorESM2-LM got 4th rank in GCM ranking, it showed more extremes compared to other GCMs in all periods except FF under SSP5-8.5. This could be due to the inherent fundamental uncertainties in the climate change projection of GCMs (Li & Jin, 2017; Ndhlovu & Woyessa, 2020). The Ec-Earth3 and Ec-Earth3-Veg outputs are predicting more precipitation in FF under SSP5-8.5. In the FF the precipitation magnitude increase is more compared to NF and MF under SSP3-7.0 and SSP5-8.5. The high variability in the precipitation for the future projected GCM's suggest that the basin is going to experience climate extremes more frequently in the future. The increase in the total projected precipitation is also evident from the multi-model ensemble average value for the three future periods. The prediction bounds and percentage changes in the future projections is evident from the difference in the projected values from different GCMs (see Table 4.8 and 4.9).

Table 4.8. Impact of climate change on the annual average WBC for KRB with uncertainty bounds

	Precipitation (mm)	ET (mm)	Water Yield (mm)	Surface Runoff (mm)	Streamflow (m^3/sec)
IMD	697	519	119	82	702
GCM historical (MME Average)	771.8	417.3	271.1	158	1970
SSP1-2.6 (NF)	909 (309-2228)	437 (260-630)	385 (30-1633)	216 (14-843)	2733 (370-8001)
SSP1-2.6 (MF)	899 (300-1985)	440 (269-590)	378 (23-1337)	212 (11-708)	2750 (55-7246)
SSP1-2.6 (FF)	910 (247-1984)	448 (252-664)	382 (16-1320)	211 (6-678)	2767 (31- 6839)
SSP2-4.5 (NF)	865 (328-1814)	434 (293-610)	353 (23-1994)	200 (13-657)	2576 (81-6658)
SSP2-4.5 (MF)	953 (310-1901)	449 (267-637)	422 (23-1300)	240 (4-751)	3081 (136-6672)
SSP2-4.5 (FF)	971 (366-2205)	453 (317-583)	436 (43-1657)	246 (23-964)	3163 (188-8220)
SSP3-7.0 (NF)	887 (223-1882)	437(215-575)	371 (16-1281)	210 (8-709)	2718 (246-6890)
SSP3-7.0 (MF)	951 (411-2026)	451 (316-645)	419 (44-1389)	242 (25-787)	3072 (190-7796)
SSP3-7.0 (FF)	1094 (209-2050)	479 (209-686)	532 (25-1507)	308 (7-819)	3762 (500-7861)
SSP5-8.5 (NF)	882 (280-1861)	438 (254-595)	364 (18-1314)	205 (8-683)	2592 (90-6285)
SSP5-8.5 (MF)	989 (183-1898)	460 (185-644)	446 (21-1181)	255 (9-726)	3210 (156-6920)
SSP5-8.5 (FF)	1187 (194-2570)	491 (190-677)	609 (23-2004)	354 (8-1450)	4226 (648-9418)

* The average annual value along with prediction bounds in brackets (minimum and maximum) of considered GCMs

The ensemble mean of projected annual precipitation is projected to increase by 24.1% to 70.3% in future time frames, when compared to the observed IMD data in the baseline period. The maximum average annual precipitation is predicted to rise by 30.56%, 39.31%, 56.96% and 70.30% by the end of the 21st century under SSP1-2.6, SSP2-4.5, SSP3-7.0 and SSP5-8.5, respectively in comparison to the observed IMD data in the baseline period.

Table 4.9 Effect of climate change on the WBC of the KRB (The value in the bracket represents relative change between the GCM historical ensemble average and future scenarios).

	Precipitation (mm)	ET (mm)	Water Yield (mm)	Surface Runoff (mm)	Streamflow (m^3/sec)
GCM historical (MME Average)	771.8	417.3	271.1	158	1970
SSP1-2.6 (NF)	909 (17.7)	437 (4.7)	385 (42)	216 (36.7)	2733 (38.7)
SSP1-2.6 (MF)	899 (16.5)	440 (5.4)	378 (39.4)	212 (34.2)	2750 (39.5)
SSP1-2.6 (FF)	910 (17.9)	448 (7.3)	382 (40.9)	211 (33.5)	2767 (40.5)
SSP2-4.5 (NF)	865 (12.1)	434 (4)	353 (30.2)	200 (27)	2576 (31)
SSP2-4.5 (MF)	953 (23.5)	449 (7.6)	422 (55.6)	240 (52)	3081 (56)
SSP2-4.5 (FF)	971 (25.8)	453 (9.3)	436 (60.8)	246 (55.7)	3163 (61)
SSP3-7.0 (NF)	887 (15)	437(4.7)	371 (36.8)	210 (33)	2718 (38)
SSP3-7.0 (MF)	951 (23.2)	451 (8)	419 (54.5)	242 (53.2)	3072 (56)
SSP3-7.0 (FF)	1094 (41.7)	479 (14.8)	532 (96.2)	308 (95)	3762 (91)
SSP5-8.5 (NF)	882 (14.3)	438 (4.9)	364 (34.3)	205 (29.7)	2592 (35)
SSP5-8.5 (MF)	989 (28.2)	460 (10.2)	446 (64.5)	255 (61.4)	3210 (63)
SSP5-8.5 (FF)	1187 (54)	491 (18)	609 (125)	354 (124)	4226 (114.5)

The increased precipitation in the historical GCMs compared to the observed data is translated to other water balance components such as water yield, surface runoff and streamflow at the catchment outlet. Similarly, the future scenarios of all GCMs are also following similar kind increasing trend in WBC as in the case of historical GCMs. The water yield, surface runoff

and streamflow showed increase for the years in which rainfall is increasing while it is lower than the GCM historical in few years. The increase in the surface runoff, water yield and streamflow at the outlet follows similar trend to the precipitation data. Precipitation change has a significant influence on future streamflow, with projections showing a potential increase of 31 to 114.5%. The maximum ensemble mean changes in average annual streamflow is projected to increase 40.5%, 61%, 91% and 114.5% under SSP1-2.6, SSP2-4.5, SSP3-7.0 and SSP5-8.5 respectively, compared to GCM historical ensemble average of baseline period by the end of 21st century. The variation of mean annual future streamflow shows significantly increasing trends from NF to FF under all SSPs (Figure 4.37) compared to baseline period of historical GCMs. Among the four SSP scenarios the higher increase in projected streamflow is projected to occur under SSP3-7.0 and SSP5-8.5 compared to historical GCM streamflow of the baseline period. In the NF and MF, NorESM1-2-LM is predicting more future streamflow under SSP1-2.6 and SSP2-4.5. For the scenarios of SSP3-7.0 and SSP5-8.5, the maximum average streamflow values are observed for EC-EARTH3 output during the MF. The FF is experiencing higher magnitudes of streamflow, especially under SSP5-8.5 scenario compared other periods. It is also observed that the maximum flow of 8856 m^3/sec has occurred in the FF under SSP5-8.5 scenario for EC-EARHT3 GCM output, which is 1.96 times the maximum flow value (4500 m^3/sec) of the GCM historical. Whereas, the peak flow of ensemble average is predicted in the future as 5381 m^3/sec which is 2 times the peak flow (2692.7 m^3/sec) of ensemble average during baseline period. The highest precipitation, water yield, surface runoff and streamflow are projected to increase 54%, 125%, 124% and 114.5% respectively in FF under SSP5-8.5 scenario compared to ensemble average of baseline period. The higher increase in the water yield, surface runoff and streamflow components as compared to the precipitation may suggest that the precipitation is increasing during the monsoon period leading to saturated conditions resulting in higher runoff generation. The percentage increase in the ET is observed to be in general less for the future periods as compared to the other WBC. The ET is projected to increase in the range of 4% to 18% for the future periods under different SSP scenarios compared to ensemble average. One of the reasons for the lower ET increase is that although the future rise in temperature may accelerate evapotranspiration but, increased CO_2 concentration and increased humidity (caused by increased rainfall intensity) may inhibit transpiration by altering leaf stomata, potentially offsetting the increased rate of evapotranspiration, which is also reported in other studies (Chanapathi et al., 2018; Snyder et al., 2011). The lower ET demand in the future period combined with the higher precipitation is leading to higher runoff generation from the basin. The percentage change of WBC is

continuously increasing from NF to FF under all scenarios except for SSP1-2.6. In case of SSP1-2.6 the percentage change of WBC (except streamflow) is more compared to MF and FF.

The relative change calculated between the GCM historical ensemble average and future GCMs ensemble average is applied to IMD observed values of baseline period to obtain the expected future water balance components (see Table 4.10). The average annual precipitation is expected to increase in the range of 781 mm to 1072 mm for future period under different SSP scenarios based on IMD data. In a similar way, future predictions indicate that surface runoff, water yield, evapotranspiration and streamflow are ranging from 104 to 184 mm, 155 to 268 mm, 540 to 610 mm and 920 to1506 m^3/sec respectively for different scenarios.

Table 4.10 The expected absolute values for the annual period due to climate change impact (The values in the brackets represents the +/-1 standard deviation values of expected absolute values).

	Precipitation (mm)	ET (mm)	Water Yield (mm)	Surface Runoff (mm)	Streamflow (m^3/sec)
IMD	697	519	119	82	702
GCM historical (MME Average)	771.8	417.3	271.1	158	1970
SSP1-2.6 (NF)	820 (737.8902)	543 (517-569)	169 (136-202)	112 (87-136)	974 (844-1103)
SSP1-2.6 (MF)	812 (735-889)	547 (521-572)	166 (135-197)	110 (89-130)	980 (865-1094)
SSP1-2.6 (FF)	822 (751-893)	557 (532-582)	168 (137-199)	109 (90-128)	986 (852-1119)
SSP2-4.5 (NF)	781 (713-849)	540 (525-555)	155 (127-183)	104 (85-122)	920 (795-1044)
SSP2-4.5 (MF)	861 (794-928)	558 (532-584)	185 (160-210)	125 (105-144)	1095 (996-1193)
SSP2-4.5 (FF)	877 (803-950)	567 (549-585)	191 (157-224)	128 (104-151)	1130 (1015-1244)
SSP3-7.0 (NF)	802 (729-875)	543 (522-564)	163 (133-192)	109 (90-128)	969 (854-1083)
SSP3-7.0 (MF)	859 (786-931)	561 (533-588)	184 (154-214)	126 (107-144)	1095 (968-1221)
SSP3-7.0 (FF)	988 (887-1088)	596 (567-625)	233 (190-275)	160 (131-189)	1341 (1197-1485)
SSP5-8.5 (NF)	797 (725-868)	544 (525-562)	160 (132-187)	106 (88-123)	948 (837-1056)
SSP5-8.5 (MF)	894 (799-988)	572 (538-606)	196 (160-232)	132 (105-158)	1144 (1006-1281)
SSP5-8.5 (FF)	1072 (933-1211)	610 (578-642)	268 (210-325)	184 (140-228)	1506 (1321-1691)

4.5.3 Climate Change Impact on ISMR Season in KRB

A further analysis was performed to evaluate the climate change impacts during the Indian Summer Monsoon Rainfall (ISMR: from June-October) period. The prediction ranges of various GCMs and their ensemble average is compared with GCM historical baseline period are given in Table 4.11 and 4.12 respectively.

Table 4.11 Impact of climate change on the WBC for KRB with prediction bounds for annual average ISMR

	Precipitation (mm)	ET (mm)	Water Yield (mm)	Surface Runoff (mm)	Streamflow (m^3/sec)
IMD	600	366	110	79	1659
GCM historical	724	314	259	156	4026
SSP1-2.6 (NF)	857 (186-2148)	329 (155-476)	369 (22-1569)	213 (13-834)	5268 (830 -16592)
SSP1-2.6 (MF)	849 (251-1875)	330 (191-429)	362 (20-1280)	209 (10-707)	5271 (87-14667)
SSP1-2.6 (FF)	862 (220-1811)	336 (176-434)	364 (12-1231)	209 (6-678)	5316 (30- 13401)
SSP2-4.5 (NF)	823 (289-1742)	328 (205-428)	337 (19-1102)	197 (12-617)	4929 (149-12337)
SSP2-4.5 (MF)	907 (129-1846)	334 (116-443)	403 (11-1263)	236 (3-751)	5815 (235-13254)
SSP2-4.5 (FF)	928 (311-2187)	341 (196-464)	418 (40-1588)	243 (23-963)	6062 (407-16467)
SSP3-7.0 (NF)	848 (167-1873)	333(149-435)	357 (12-1231)	208 (7-709)	5221 (536-14045)
SSP3-7.0 (MF)	898 (347-1887)	336 (238-457)	397 (40-1303)	238 (25-760)	5805 (350-15315)
SSP3-7.0 (FF)	1037 (184-1986)	354 (151-459)	505 (16-1474)	303 (7-819)	7155 (828-16236)
SSP5-8.5 (NF)	836 (215-1847)	328 (181-431)	348 (13-1273)	202 (7-683)	4966 (135-12667)
SSP5-8.5 (MF)	937 (137-1745)	338 (114-438)	423 (16-1114)	251 (9-718)	6083 (222-12958)
SSP5-8.5 (FF)	1123 (130-2569)	356 (105-453)	576 (9-1980)	347 (4-1450)	8009 (1323-20382)

Table 4.12 Percentage deviation (in brackets) of WBC due to climate change over KRB for ISMR season

	Precipitation (mm)	ET (mm)	Water Yield (mm)	Surface Runoff (mm)	Streamflow (m^3/sec)
GCM historical	724	314	259	156	4026
SSP1-2.6 (NF)	857 (18.4)	329 (4.8)	369 (42.5)	213 (36.5)	5268 (30.8)
SSP1-2.6 (MF)	849 (17.3)	330 (5.1)	362 (39.7)	209 (34)	5271 (31)
SSP1-2.6 (FF)	862 (19)	336 (7)	364 (40.5)	209 (34)	5316 (32)
SSP2-4.5 (NF)	823 (13.7)	328 (4.5)	337 (30)	197 (26.3)	4929 (22.5)
SSP2-4.5 (MF)	907 (25.3)	334 (6.5)	403 (55.6)	236 (51.3)	5815 (44.2)
SSP2-4.5 (FF)	928 (28.3)	341 (8.6)	418 (61.4)	243 (55.8)	6062 (50.6)
SSP3-7.0 (NF)	848 (17)	333 (6)	357 (37.8)	208 (33.33)	5221 (30)
SSP3-7.0 (MF)	898 (24)	336 (7)	397 (53.3)	238 (52.5)	5805 (44.2)
SSP3-7.0 (FF)	1037 (43)	354 (12.7)	505 (95)	303 (94)	7155 (77.7)
SSP5-8.5 (NF)	836 (15.5)	328 (4.5)	348 (34.4)	202 (29.5)	4966 (23)
SSP5-8.5 (MF)	937 (29.5)	338 (7.6)	423 (63.3)	251 (61)	6083 (51.1)
SSP5-8.5 (FF)	1123 (55)	356 (13.4)	576 (122.4)	347 (122)	8009 (99)

It can be found that nearly 90% of the climate change impact on WBC is occurring in the ISMR period. Mainly this study focused on precipitation, water yield and surface runoff. It can be observed that significant variations in the all WBC from the prediction bound values. The ensemble mean of precipitation is varying from minimum of 129 mm (under GCM: NorESM1-LM) to maximum of 2569 mm (under GCM: IPSL-CM6A-LR) in the future (Table 4.11). From the ensemble average it can be observed that in the near future almost all the scenarios showed similar kind of increase in the precipitation. The ensemble average of ISMR precipitation is projected to increase in the range of 13.7% to 55% for the future period compared to historical GCM ensemble average of baseline period. The maximum increase in the ensemble average precipitation in the percentages are observed as 19, 28.3, 43 and 55 respectively in the far future under SSP1-2.6, SSP2-4.5, SSP3-7.0 and SSP5-8.5. The increases in precipitation is larger under SSP5-8.5 and SSP3-7.0 compared to the other scenarios. The direct response of water yield and surface runoff to the precipitation are also followed same trend with the precipitation. The surface runoff and water yield components are projected to increase up to 175 mm and 245 mm for ISMR period, 184 mm and 268 mm for the annual period respectively and by the end

of 21st century under SSP 5-8.5 scenario after applying the relative percentage of GCMs to the IMD observed values shown in Table 4.13.

Table 4.13 The expected absolute values for the annual ISMR period due to climate change impact (The values in the brackets represents the +/-1 standard deviation values of expected absolute values).

	Precipitation (mm)	ET (mm)	Water Yield (mm)	Surface Runoff (mm)	Streamflow (m^3/sec)
IMD	600	366	110	79	1659
GCM historical	724	314	259	156	4026
SSP1-2.6 (NF)	710 (633-786)	383 (366-400)	157 (125-188)	108 (84-132)	2170 (1093-3247)
SSP1-2.6 (MF)	704 (639-768)	385 (369-401)	154 (125-183)	106 (86-125)	2173(1120-3226)
SSP1-2.6 (FF)	714 (648-780)	392 (376-407)	155 (125-184)	106 (88-124)	2190 (1139-3241)
SSP2-4.5 (NF)	682 (620-744)	382 (370-394)	143 (117-169)	100 (82-118)	2032 (1043-3020)
SSP2-4.5 (MF)	752 (690-814)	390 (372-407)	171 (147-199)	119 (100-138)	2392(1286-3497)
SSP2-4.5 (FF)	770 (702-837)	397 (384-409)	177 (145-209)	123 (100-146)	2498 (1388-3607)
SSP3-7.0 (NF)	702 (636-768)	388 (374-401)	151 (123-179)	105 (86-123)	2156 (1175-3136)
SSP3-7.0 (MF)	744 (682-805)	392 (373-410)	168 (141-195)	120 (102-137)	2392 (1353-3430)
SSP3-7.0 (FF)	858 (764-951)	412 (394-429)	214 (173-254)	153 (124-181)	2948 (1707-4189)
SSP5-8.5 (NF)	693 (627-758)	382 (369-394)	148 (122-174)	102(85-119)	2040 (1039-3041)
SSP5-8.5 (MF)	777 (688-865)	394 (370-418)	179 (144-214)	127 (100-153)	2507 (1391-3623)
SSP5-8.5 (FF)	930 (810-1049)	415 (391-438)	245 (192-297)	175 (133-216)	3301 (1844-4757)

Almost 95% of the annual surface runoff and 92% of annual water yield are occurring during the ISMR period. This is due to a higher occurrence of precipitation during the monsoon period. Generally, the rise in the WBC may indicating that excessive availability of water and high groundwater storage. The streamflow is expected to increase significantly in the future under all the scenarios. The individual streamflow for one of the GCM is projected to increase maximum up to 20,382 m^3/sec under SSP5-8.5 scenario in the FF period. The selected SSP scenarios showed an increase in surface runoff, water yield and streamflow as a result of increasing rainfall. The evapotranspiration is also followed an increasing trend but lesser increase compared with the other WBC under all SSP scenarios. These results were similar to those reported in earlier studies (Chanapathi et al., 2018; Kulkarni et al.,, 2014). The ensemble mean of ISMR future streamflow is ranging from 4929 m^3/sec to 8009 m^3/sec under different SSP scenarios, which is 22.5% to 99% more compared to the historical GCM ensemble

average. The results suggest that more water will be available in the basin in the future period and the basin may experience more floods.

4.5.4 Climate Change Impact on Mean Monthly Flows

The impact of climate change is also assessed by comparing the mean monthly streamflow for the future periods with the baseline period as shown in Figure 4.38. It is clearly observed that compared to baseline period, the future streamflow is significantly higher (especially higher variations from June-October) under all scenarios. During the NF period, the output of NorESM2-LM GCM is projecting higher magnitude of streamflow compared to the other GCM outputs under four SSP scenarios. It is observed that the maximum flow value of 13,213 m^3/sec in the August month for SSP1-2.6 scenario. For the MF period, EC-EARTH3 output is projecting higher magnitude of streamflow under SSP3-7.0 scenario with streamflow value about 13,102 m^3/sec in the August month. Likewise, In the FF period, EC-EARTH3-VEG shows large magnitude of streamflow under SSP5-8.5 scenario with peak flow of 15,166 m^3/sec in the September month.

It can be observed that there is a shift in the occurrence of peak flow value in the future period compared to observed period 1973-2003. In the observed period, the highest recorded flow rate was 2540 m^3/sec, which took place during the month of August. But in the case of future periods the Peak flow values for most of the individual GCMs and MME average is observed in the month of September. For the EC-EARTH3 model, the peak flow value is projected to occur in the month of October in FF under SSP5-8.5 scenario. This shift in peak streamflow in future periods compared to the observed period can be related to the extension of ISMR even up to October month, resulting in an increase in surface runoff. This significant surface runoff in September and October has a negative impact on the Kharif crops in the KRB since most of the crops are in the harvesting stage, particularly rice, maize and cotton. It can be observed that the streamflow increment is more in MF and FF than NF under all SSP scenarios except SSP1-2.6 scenario. Under the SSP1-2.6 scenario, the highest MME average streamflow in the NF is predicted to rise about 3.17 times (i.e., 7942 m^3/sec) in comparison to the historical period (i.e., 2540 m^3/sec). Likewise, the projected increases in maximum MME average streamflow during the MF and FF under SSP5-8.5 are estimated to be 3.52 times (8835.9 m^3/sec) and 4.38 times (10,973 m^3/sec) respectively, compared to the baseline period. These findings align with previous studies by (Chanapathi & Thatikonda, 2020; Nikam et al., 2018).

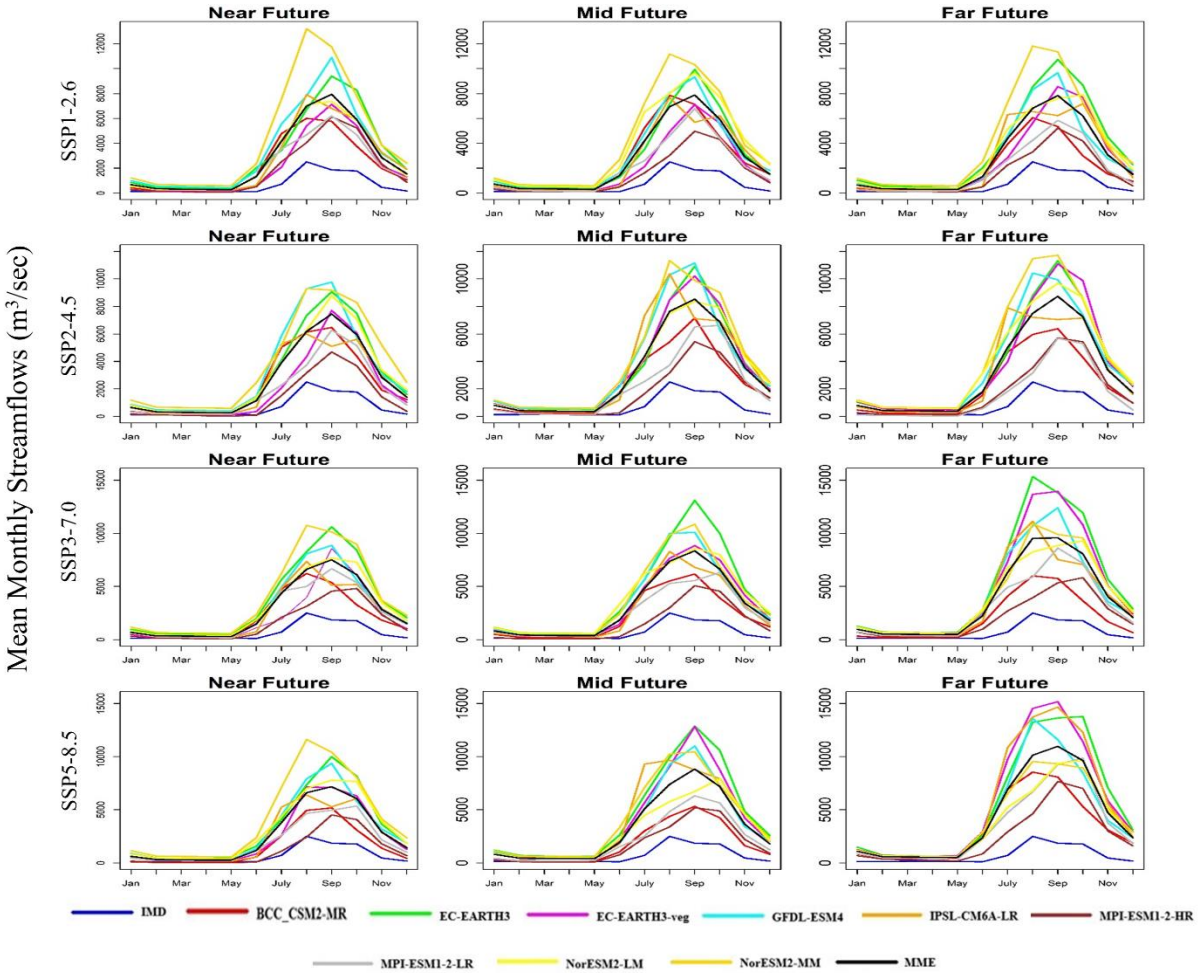

Figure 4.38 Simulated mean monthly streamflow under different SSP scenarios in the future periods

4.5.5 Discussion

The research on the KRB is of utmost importance due to its semi-arid environment and susceptibility to climate change, resulting from an uneven spread of rainfall. Previous research has suggested that choosing appropriate GCMs can help to decrease uncertainties in climate change projections (McSweeney et al., 2015; K S Raju & Nagesh kumar D, 2014). The selected GCMs using SU technique is agreeing of the previous studies of different CMIP phases over the KRB. The NorESM, BCCCSM1.1 (m) family GCM ranked top in evaluating the Indian Summer Monsoon (ISM) rainfall (Babar et al., 2015; Sarthi et al., 2016). The GFDL and BCCR family GCMs were ranked top in the KRB in evaluating the precipitation in the KRB (Raju & Nagesh Kumar, 2015) and IPSL family is performing well for the temperature over India (Raju & Nagesh Kumar, 2016). The same family GCMs are ranked in the top 50% in the present study. However, for the CMIP6 phase climate models, MPI family is performing well compared to other GCMs, which is agreeing with the peninsular India (Anandhi & Nanjundiah,

2015). Therefore, selected top 50% GCMs are utilized to compel the hydrologic SWAT model. The average annual precipitation of MME average along with individual GCM is significantly increasing from IMD precipitation in all three future periods in contrast to the previous study reported that in the NF the precipitation projections are decreasing using the GHG (Gosain et al., 2006), CNRM-CM5, GFDL-ESM2M GCM output (Chanapathi & Thatikonda, 2020).

The increase in the precipitation resulted in the increase of other WBC such as surface runoff, water yield, streamflow and decrease in the evapotranspiration in the future can be observed in the present study. The results are in confirmation to the previous studies (Chanapathi & Thatikonda, 2020; Kulkarni BD, 2014; Kundu et al., 2017; Nikam et al., 2018). For example, the maximum amount of annual average precipitation, was projected to increase about 33.4% under CNRM-CM5 output in FF under high emission RCP 8.5 scenario (Chanapathi & Thatikonda, 2020) compared to baseline period whereas, in the present study MME average is projected to rise about 54% in FF under SSP5-8.5 scenario. Ensemble average precipitation was projected to increase up to 1073 mm under RCP8.5 scenario whereas, in the present study it is projected to increase up to 1187 mm under SSP5-8.5 scenario in the FF. Similarly, the ensemble average values of water yield, surface runoff and streamflow were projected to increase up to 499 mm, 459 mm and 6021 m^3/s whereas, in the current study they are projected to rise up to 609 mm, 354 mm and 4226 m^3/s in the FF respectively. The lower increase of the streamflow and surface runoff could be attributed to the incorporation of the reservoir system within the SWAT model. The results of the study suggest that future policies for cropping pattern, cropping period and reservoir operation must be updated for sustainable water management within the basin.

4.5.6 Conclusions

This study examines the impacts of climate change on the water balance components and hydrology of the Krishna River Basin for three future time frames.Tier-1 scenarios, SSP1-2.6, SSP2-4.5, SSP3-7.0 and SSP5-8.5, which are similar in magnitude and distribution to the RCPs in CMIP 5 were used in the current study. The selected top 50% GCMs future scenarios are forced as input to the well calibrated and validated distributed hydrological model (SWAT) to simulate the WBC and streamflow.

The MPI-ESM1-2-HR and MPI-ESM1-2-LR GCMs closely match observed precipitation data during the baseline period, with no significant changes expected in the future except under the

SSP5-8.5 scenario during the FF period. The outputs of NorESM2-LM and NorESM2-MM GCMs consistently showed an overestimation of future precipitation across all SSP scenarios except in the FF under SSP5-8.5 scenario. It is observed that the ensemble mean of projected mean annual precipitation has significantly increased in the range of 12 to 54% in the future periods under different SSP scenarios compared to GCM ensemble. The fluctuation of these predicted precipitation levels will likely have a significant impact on other water balance components in the basin The ensemble average of annual surface runoff and water yield is projected to increase from 27% to 124% and 30% to 125%, respectively, under different SSP scenarios for future periods. The future streamflow is significantly impacted by changes in future precipitation and the annual MME average is projected to increase from 31 to 114.5% from NF to FF under four SSP scenarios. The ensemble mean of future flows occurred mostly in the month of September and the increase in flows can also be observed even in the months of October and November due to monsoon extension. This shows the adverse effects on Kharif crops as they are under harvesting stage. So, the policymakers can make the decisions on cropping patterns and cultivation for better agricultural productivity. Future streamflow is significantly impacted by the large increases in precipitation, surface runoff and water yield, which may result in major flood events in the KRB. During the monsoon period the maximum peak flows are observed compared to non-monsoon period. It is found that the MPI-ESM1-2-HR model will not experience any extreme flow occurrences in the future. The maximum number of streamflow extremes can be observed for NorESM2-LM and IPSL-CM6A-LR outputs.

4.6 Coupled Impact of Climate and LULC Change on WBC of TRB

In India, the changes in LULC and climate are posing threats to water supply and triggering natural disasters like floods and droughts (Singh et al., 2019; Sinha & Eldho, 2018) . The country heavily relies on monsoon precipitation (about 70%), making it vulnerable to changing precipitation patterns. According to the 2018 Niti Aayog report, groundwater wells are disappearing and 50% of India's population suffers from a severe water deficit. Droughts in 2016 affected millions, resulting in substantial economic losses. Additionally, between 1950 and 2015, floods have impacted approximately 825 million individuals. Furthermore, the frequency of flood events in central India has tripled during this time frame (Kumar et al., 2021; Mishra, 2020). Therefore, it is emphasizing the urgent need to integrate climate variability and land use change assessments for accurate water availability predictions.

The hydrologic cycle's parameters are significantly impacted by both LULC and climate change, which must be taken into consideration when making decisions on how best to use and manage water resources going forward. For the purpose of managing water resources, variations in water balance components such as evapotranspiration, base flow, surface and subsurface runoff regionally and temporally are crucial. Based on these changes, a number of fields have evolved, including irrigation system design and management, hydrologic water balance, crop yield simulation, planning and management of water resources and water loss optimisation through improved agricultural water use.

The Tunga (147 km) and Bhadra (178 km) rivers converge to form the Tungabhadra River, which is the principal tributary of the Krishna River is used to investigate the coupled impact of climate and LULC change WBC.

4.6.1 SWAT Performance on TRB Hydrological Modelling

The long-term climatic and LULC effects on the hydrology of large complex catchments can be simulated by the SWAT model (Bae et al., 2011; S. Wang et al., 2008). The SWAT model uses different combinations of slope, LULC and soil classes to divide the entire catchment into sub-catchments based on topography, which are then classified into Hydrological Response Units (HRUs) (Abbaspour et al., 2015). By using climate data and LULC patterns, SWAT models can estimate anticipated watershed scenarios. Moreover, it has the ability to evaluate streamflow variability by taking into account forecasted climate variables and LULC change for the future. The monthly discharge recorded at the Mantralayam outlet is utilised to calibrate and validate the SWAT model. The model was simulated from 1978-2010, with first 3 years considered as warmup period. The 20 year period from 1981 to 2000 is used to calibrate the model and remaining 10 year period from 2001 to 2010 is used to validate the model using SUFI-2 algorithm in the SWAT-CUP. Based on the past studies, 13 parameters that influenced the streamflow were selected for the calibration (Table 4.14). Among these parameters, 8 parameters, i.e. CN2, SOL_AWC, GWQMN, ESCO, ALPHA_BF.gw, GW_REVAP.gw, CH_K2 and CH_N2 are identified as most sensitive parameters after 500 iterations. NSE abd R^2 are used to evaluate the model performance during calibration and validation. Both the R^2 and NSE value of 0.75 is attained in the calibration period, which is regarded as very good

(Moriasi et al., 2007). During the validation period a very good R^2 and NSE values of 0.72 and 0.70 are obtained respectively. The observed and simulated discharge values using SWAT-CUP is shown in Figure 4.39.

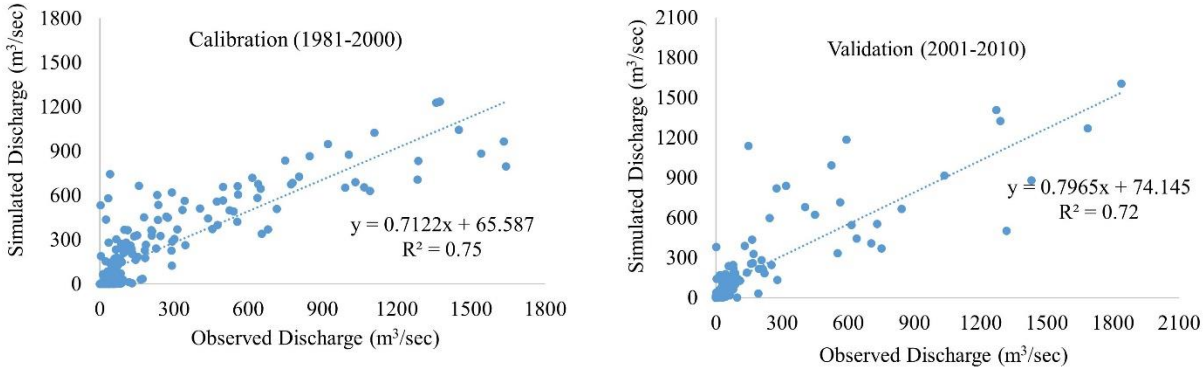

Figure 4.39 Correlation between simulated and observed discharge

Other statistical performance metrics, including PBIAS, p-factor and r-factor are also used to compare the model's performance as shown in Table 4.15. The negative PBIAS values are suggesting that the streamflow has been underestimated by the model compared to the observed flow. The calibrated model strong performance indicates that it can accurately represent the temporal and geographical variability of the hydrological processes occurring within the catchment.

Table 4.14 Calibrated parameters used in the present study for the SWAT model

Parameter	Range	Fitted value
R_CN2.mgt	-0.3 to 0.01	-0.1366
A_GWQMN.gw	-600 to 1645	416.98
A_GW_DELAY.gw	-30 to 100	4.5
V_ALPHA_BF.gw	0 to 0.14	0.12754
R_SOL_AWC().sol	-0.1 to 0.1	-0.0874
A_REVAPMN.gw	-750 to 750	-379.5
A_RCHRG_DP.gw	-0.05 to 0.05	-0.0403
V_GW_REVAP.gw	0.02 to 0.2	0.0569
R_OV_N.hru	-0.2 to 0.2	-0.0708
V_CH_K2.rte	10 to 100	20.53
V_ESCO.hru	0 to 0.5	0.01
V_CH_N2.rte	0.1 to 0.3	0.1266
V_CANMX.hru	0 to 20	9.7

Table 4.15 Performance evaluation at Mantralayam discharge location

Parameter	Calibration	Validation
NSE	0.75	0.72
R^2	0.75	0.70
PBIAS	-3.8	-18.3
p-factor	0.87	0.74
r-factor	1.3	1.6

Using the chosen nine GCMs and projected LULC for the years 2040, 2065 and 2090 under the SSP1-2.6 and SSP5-8.5 scenarios, are employed to assess the coupled impact on the hydrology of the TRB. The analysis is carried out for three future time frames namely, Near Future (NF: 2026–2050), Mid Future (MF: 2051–2075) and Far Future (FF: 2076-2100).

4.6.2 LULC Change under SSP-RCP Scenarios

The future LULC maps under SSP-RCP scenario for the respected three future time periods i.e 2040, 2065 and 2090 were extracted and is forced along with future climate data for the hydrological modelling. Figure 4.40 depicts the LULC variation under different SSP scenarios along with base year map. The simulated major land use classes were identified in Tungabhadra basin as water (1.41%), built-up (0.23%), cropland (77.01%), barren land (0.04%), forests (12.94%) and grassland (8.37%) as per the LULC of the year 2015. To quantitatively assess the accuracy of land simulation, three widely employed indicators namely Kappa coefficient, Overall Accuracy (OA) and Figure of Merit (FoM) were employed. The obtained values for India were 0.918, 0.959 and 0.093 for the Kappa coefficient, OA and FoM respectively. Table 4.16 shows the spatial coverage of each LULC class in the TRB.

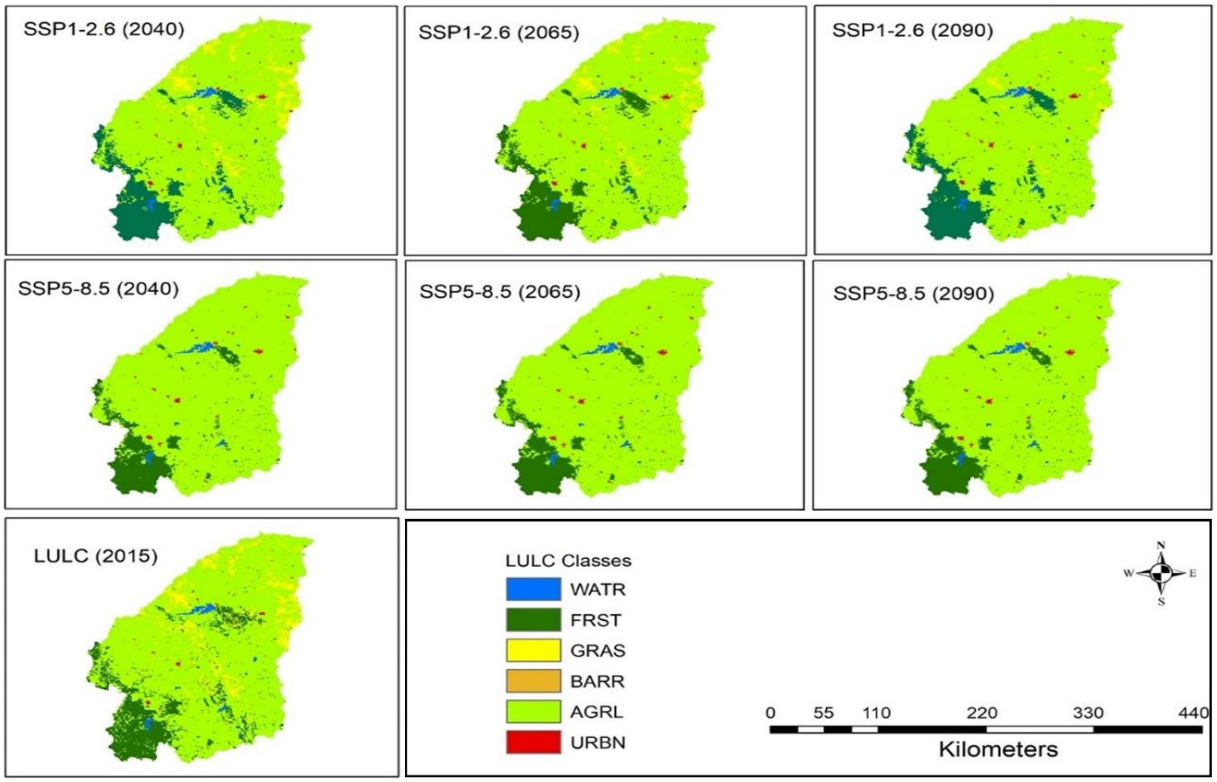

Figure 4.40 LULC fluctuation for three future periods under both SSP1-2.6 and SSP5-8.5 scenarios in comparison to the base year map (2015)

Table 4.16 LULC variation from 2015 to 2100 in percent change

Year	LULC class and change in percentage (%)					
	Water	Forest	Barren land	Grass land	Cropland	Built-up
2015	1.41%	12.94%	0.04%	8.37%	77.01%	0.23%
SSP1-2.6						
2040	1.4 (-0.01%)	13.06 (+0.12%)	(0%)	6.69 (-1.68%)	78.44 (+1.43%)	0.41 (+0.18%)
2065	1.4 (-0.01%)	12.91 (-0.03%)	(0%)	4.7 (-3.67%)	80.48 (+3.47%)	0.51 (+0.28%)
2090	1.4 (-0.01%)	12.84 (-0.1%)	(0%)	1.61 (-6.76%)	83.63 (+6.62%)	0.51 (+0.28%)
SSP5-8.5						
2040	1.41 (0 %)	10.02 (-2.92%)	(0%)	(0%)	87.07 (+10.06%)	0.5 (+0.27%)
2065	1.41 (0 %)	10.12 (-2.82%)	(0%)	(0%)	87.88 (+10.87%)	0.59 (+0.36%)
2090	1.41 (0 %)	10.12 (-2.82%)	(0%)	(0%)	87.88 (+10.87%)	0.59 (+0.36%)

It can be observed that some significant changes were found in future LULC for the two SSP scenarios. The grass land and barren land is totally converted to cropland in the future under SSP585 scenario where as in case of SSP1-2.6 scenario only barren land totally converted to cropland. The grassland is projected to change from 8.37% to 1.61% in the FF under SSP1-2.6

scenario indicating a decrease of 6.76%. The urbanization and cropland are projected to extend up to 0.59% and 87.88% respectively under SSP5-8.5 scenario till 2100. There is no significant change in the forest cover under SSP1-2.6 scenario but under SSP5-8.5 it has shown small decline by 2.92% in the future. It can be concluded from this analysis is that these small changes in future can affect the streamflow and other WBC. These findings contribute to a better comprehension of the evolving dynamics within the river basin, thereby offering valuable insights for strategic planning and effective management.

4.6.3 Projections of WBCs

The annual mean temperature and precipitation for the twenty-first century are projected using an ensemble of models from nine GCMs. A comparison of the ensemble variability in mean precipitation and temperature for the future period under the SSP1-2.6 and SSP5-8.5 scenarios is shown in Figure 4.41 and 4.42 respectively.

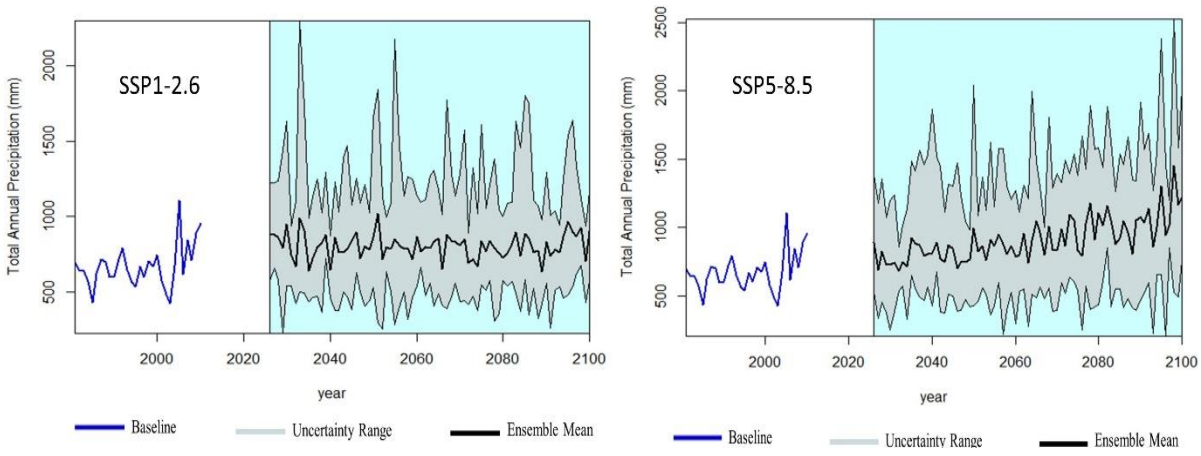

Figure 4.41 Projected annual precipitation variability under scenarios SSP1-2.6 and SSP5-8.5

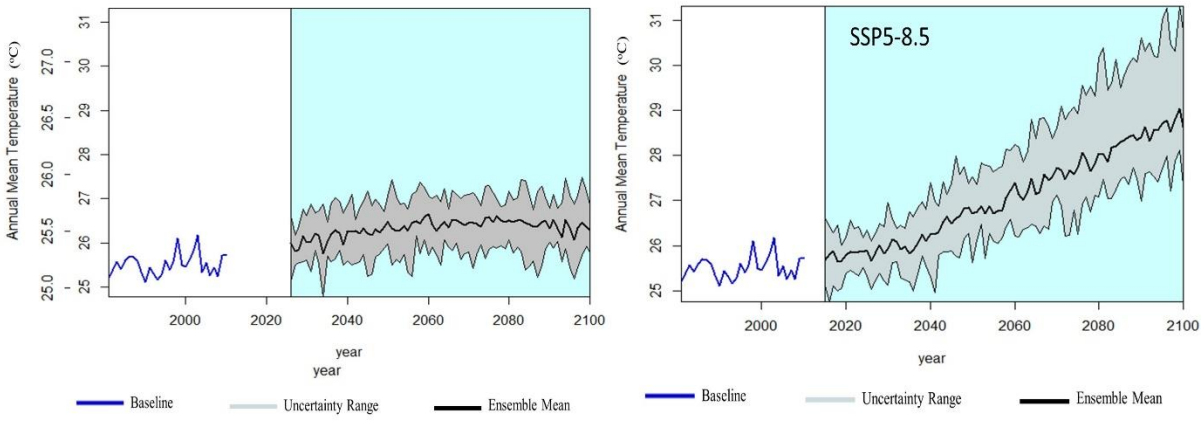

Figure 4.42 Projected mean annual temperature variability under scenarios SSP1-2.6 and SSP5-8.5

It can observed that an increase in the projected annual precipitation under both the scenarios in the future compared to baseline period. The magnitude of increase in precipitation is more in SSP5-8.5 scenario compared to SSP1-2.6 scenario. The more uncertainty range of future precipitation can be observed in the NF and MF compared to FF under SSP1-2.6 scenario. But for the SSP5-8.5 scenario, the uncertainty range is more for FF compared to NF and MF. Figure 4.42 depicts that there is significant linear increment in the mean temperature of ensemble average under both the scenario compared to baseline period. The uncertainty range of mean temperature is more for mid and far future compared to near future under SSP1-2.6 scenario, but in case of SSP5-8.5 scenario clear linearly increasing trend for all the future period. By the end of the 21st century, the ensemble mean temperature is predicted to increase by 1.56 ^{o}C and 4.65 ^{o}C, respectively, under the SSP1-2.6 and SSP5-8.5 scenarios. The relative change of annual precipitation for 9 GCMs under both SSP1-2.6 and SSP5-8.5 scenarios is shown in Figure 4.43. It is noticed that the precipitation is projected to increase up to 61% for the NorESM2-LM output in the NF under SSP1-2.6 scenario. Similarly, it is observed that the precipitation is projected to rise up to 92% under SSP5-8.5 scenario for the FF. MPI-ESM1-2-HR is projected to decrease precipitation under SSP1-2.6 scenario in three future periods and about 20.6% decrement can be observed in NF under SSP5-8.5 scenario.

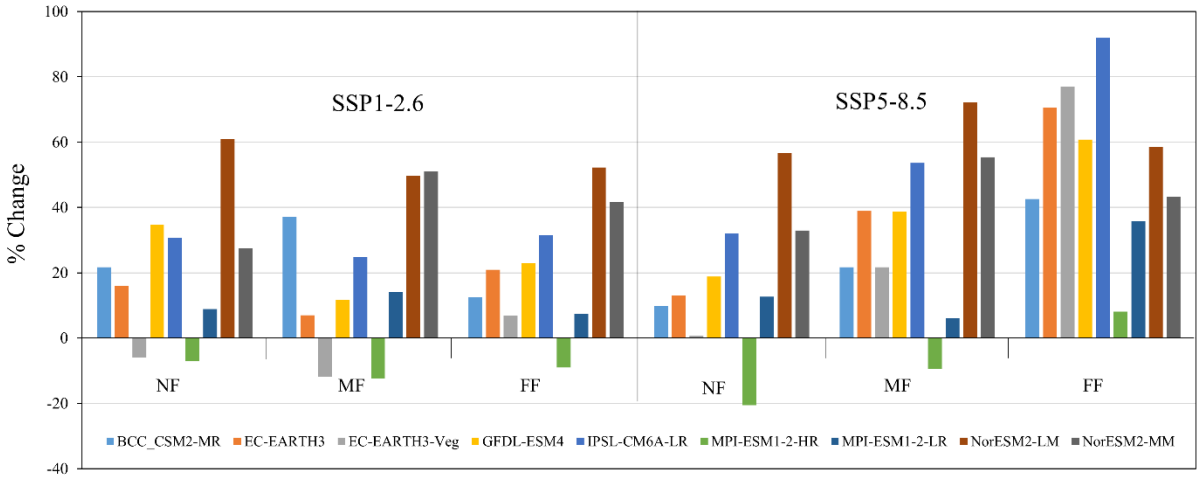

Figure 4.43 Relative change in the average annual precipitation in the future periods

A comparison of the future projected precipitation from all GCM's with the historical observed precipitation indicates that the mean precipitation in the basin is increasing in most of the future scenarios. Only few years in all the GCM simulations have shown lower precipitation as compared to the historical precipitation within the basin. It is also observed that the variability

in the future projected mean annual precipitation is increasing as evident from the box plots of Figure 4.44.

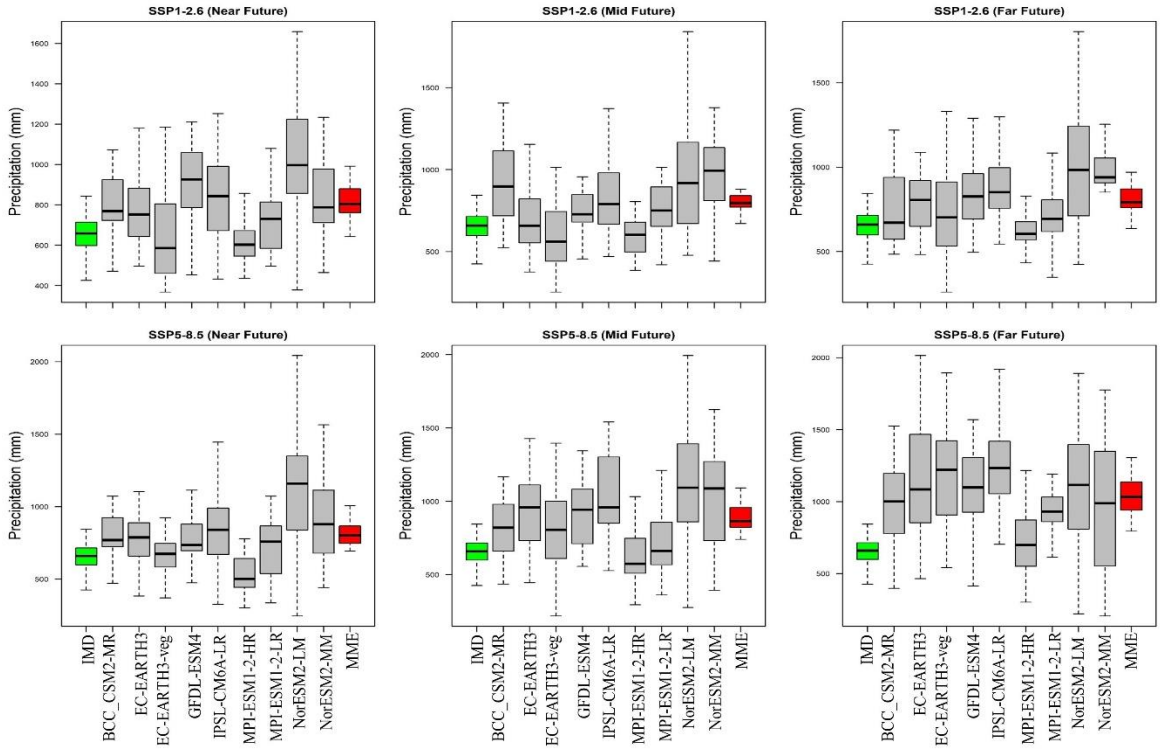

Figure 4.44 Mean annual precipitation variation under different GCMs compared to IMD data

In comparison to the baseline period, the ensemble mean of precipitation is predicted to increase by 19.08% to 20.86% and 19.97% to 55.59% under the SSP1-2.6 and SSP5-8.5 scenarios respectively. The high variability in the precipitation for the future projected GCM's suggest that the basin is going to experience climate extremes more frequently in the future. The increase in the total projected precipitation is also evident from the MME average value for the three future periods. The prediction ranges of various GCMs and their ensemble average of annual WBC is compared with baseline period is given in Table 4.17.

Table 4.17 Climate and LULC impact on the WBC for TRB with prediction bounds

	Precipitation (mm)	ET (mm)	Water Yield (mm)	Surface Runoff (mm)	Soil moisture (mm)	Groundwater (mm)
IMD	671	420	150	116	83	28
SSP1-2.6 (NF)	811 (228-2297)	349 (223-454)	277 (29-1546)	207 (16-1032)	83 (40-122)	61 (10-493)
SSP1-2.6 (MF)	799 (253-2177)	349 (203-479)	270 (31-1258)	201 (17-838)	83 (29-135)	60 (11-428)
SSP1-2.6 (FF)	811 (259-1802)	356 (250-548)	270 (35-1113)	200 (17-675)	83 (30-116)	61 (12-478)
SSP5-8.5 (NF)	805 (245-2041)	350 (245-476)	273 (27-1253)	207 (11-954)	84 (36-121)	60 (10-387)
SSP5-8.5 (MF)	888 (218-1992)	362 (231-507)	325 (31-1058)	242 (16-874)	87 (22-117)	73 (7-391)
SSP5-8.5 (FF)	1044 (205-2524)	384 (231-523)	435 (28-1830)	323 (13-1389)	88 (36-121)	102 (6-422)

The results show that the WBC such as SurQ, GWq and WY are also following the significant increasing trend with the precipitation. Both surface runoff and groundwater recharge are included in water yield and the greater increase in water yield is attributable to the rise in both. This could be mostly due to anticipated increases in precipitation along with increased urbanisation, cropland and decreased forest cover. Similarly, the increasing trend of WBC is projected in some of the studies under different RCP4.5 and RCP8.5 scenarios in Krishna River Basin (Chanapathi et al., 2018; Mishra & Lilhare, 2016). Regardless of increase in precipitation, ET is projected to decrease under all scenarios in the future periods but the reduction percentage of ET is negligible compared to the other WBC. Surface properties, such as variations in Curve Number (CN) values and evapotranspiration properties, are impacted by changes in LULC. The decrease in the forest cover in the future might be the reason to reduce the ET (Getachew et al., 2021). The similar results are observed for ET under CMIP3 and CMIP5 GCMs (Chanapathi et al., 2018; Reshmidevi et al., 2018). It is observed that the ensemble mean of SW shows no variation compared to baseline period under SSP1-2.6 scenario for the future periods. Although the ensemble mean of SW has shown some variation compared baseline period under SSP5-8.5 scenario which is almost negligible but as per GCM wise the some significant variation can be observed. Simulated WBC of 9 climate models and their ensemble mean are compared with the baseline period (1980-2010) shown in Figure 4.45a to 4.45e. It can be observed from the figure that NorESM2-LM is projected to increase more compared to other GCMs in under all WBC except ET in NF and MF under both the scenarios. IPSL-CM6A-LR output shows more variations in the WBC in the FF under both the scenario. The highest annual surface runoff and water yield increase of 309.5% and 328% is projected

respectively under SSP5-8.5 in the FF under IPSL-CM6A-LR. The maximum groundwater increase about 446% is projected for SSP1-2.6 scenario in the NF under NorESM2-LM. MPI-ESM1-2-HR shows very less variation in all the WBC for the future periods. MPI-ESM1-2-HR is projected to decrease the WBC in all the future periods except FF under SSP5-8.5. In the SSP1-2.6 scenario, the ensemble mean of ET decreases by -16.1%, -16.2% and -14.6% in the near, mid and far future situations, whereas in the SSP5-8.5 scenarios, it decreases by -16%, -12.9% and -7.7% respectively. In contrast, groundwater recharge is predicted to rise in the range of 115.6% to 265% in the future, whereas surface runoff and water yield of the ensemble mean are predicted to increase in the very identical ranges of 72.7% to 178.8% and 80% to 189.5%, respectively. Similarly, a rise in soil moisture of 0.5% to 7% is anticipated in the future. The slight rise in soil moisture may be associated with future farmland expansion, which may enhance the soil's porosity and water-holding ability (Sadhwani et al., 2023).

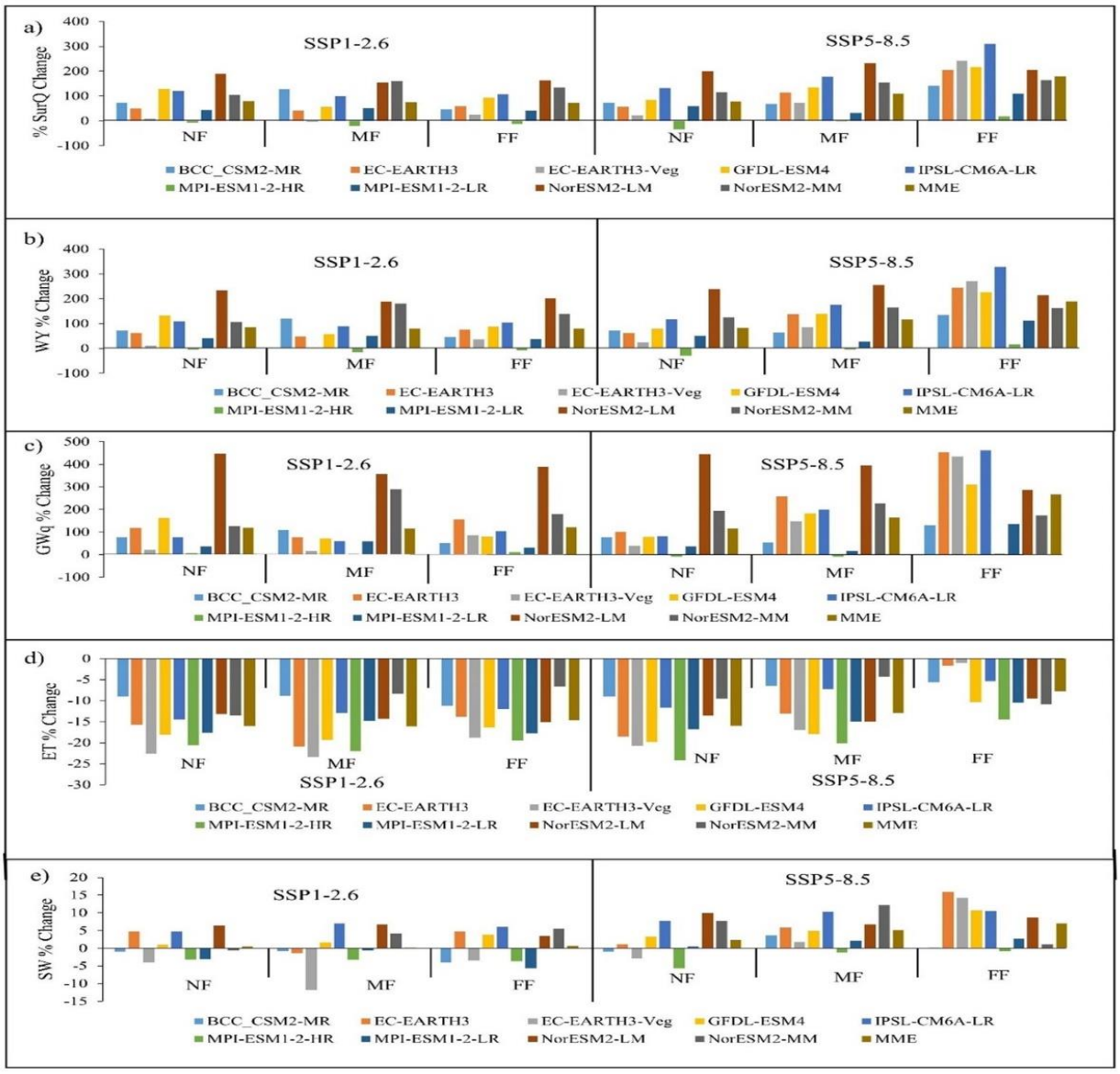

Figure 4.45 Simulated mean annual WBC comparison i.e., (a) Surface runoff (SurQ), (b) Water Yield (WY), (c) Groundwater (GWq), (d) Evapotranspiration (ET) and Soil moisture (SW) with reference to baseline (1980–2010) due to combined impact of climate and LULC change

4.6.4 Seasonal Flow Variation under both Climate and LULC Change

Future streamflow has been compared at monthly scale using ensemble of 9 climate models under both the scenarios using the boxplots shown in Figure 4.46. It can be observed that nominal change in future streamflow in the dry period from January to May for both emission scenarios. However, during the Indian Summer Monsoon Rainfall (ISMR) season (June to October) the significant change can be observed in streamflow in the future under both the scenarios. Moreover, peak streamflow for all the GCMs are varying between months of August and September under both SSP scenarios. The peak streamflow of 2515.14 m^3/sec, 2400 m^3/sec

and 2444 m^3/sec has projected to occur in the month of August in NF, MF and in the month of September in the FF respectively under SSP1-2.6 scenario. Similarly, under the SSP5-8.5 scenario, the peak streamflow of 2296.85 m3/sec is predicted to occur in the NF in September, while the peaks of 2652.2 m^3/sec and 4379.52 m^3/sec are predicted to occur in the MF and FF in August. The highest streamflow of 4379.52 m^3/sec in the FF under SSP5-8.5 scenario is 2.6 times compared to observed period inferring the probability of more water arability and occurring of floods. Since low-lying areas are vulnerable to floods and inundation issues, all of this information is helpful in the design of drainage systems and river development projects.

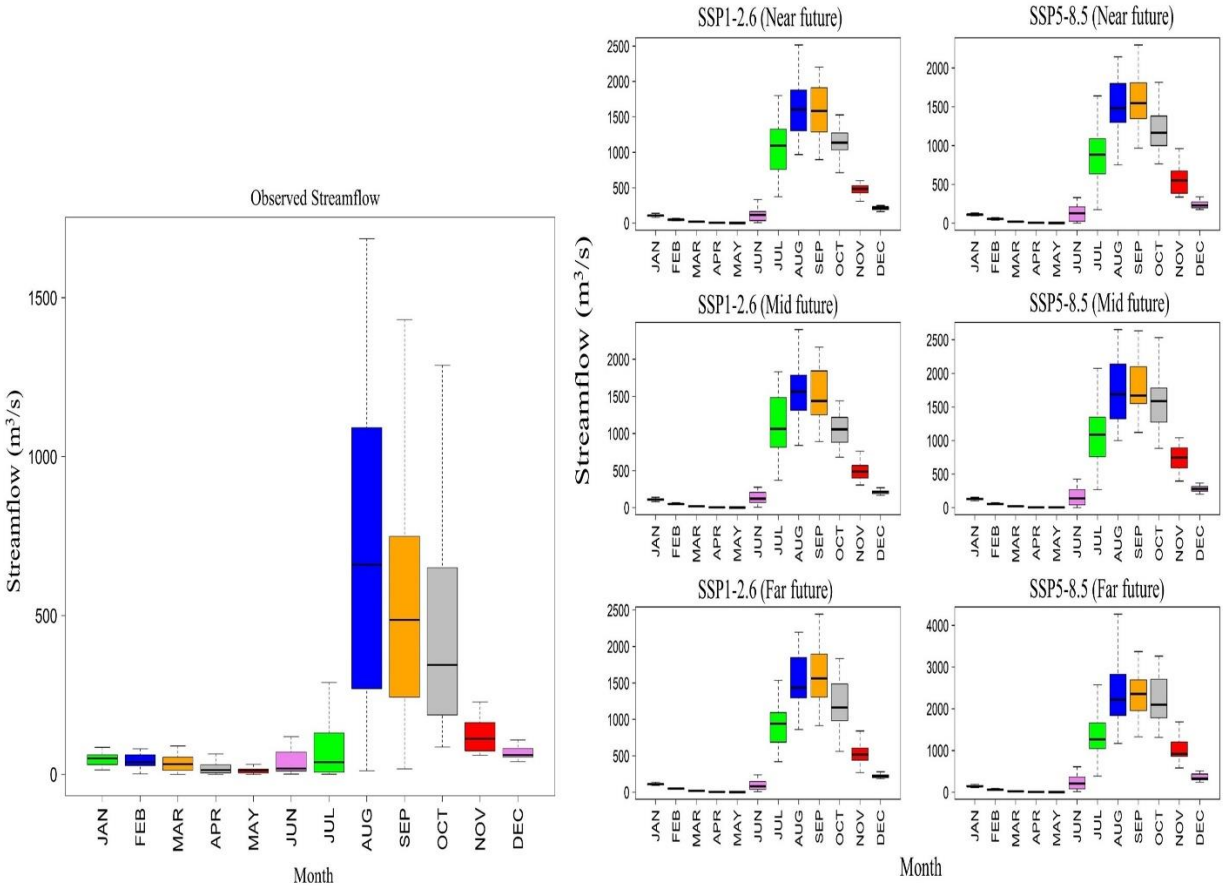

Figure 4.46 Streamflow variation at month scale for the IMD period (1981–2010) and the future period (2026 to 2100) for both SSP1-2.6 and SSP5-8.5 scenarios due to combined impact of climate and LULC change

4.6.5 Conclusions

India's semi-arid regions face escalating vulnerability as population growth drives persistent over-exploitation of natural resources. This is demonstrated by the increase in cropland area, which has been achieved at the cost of deforestation and subsequent urban development. The current study looks into how the hydrological components in the Tungabhadra River Basin, India, might react to changes in the combined effects of climate change and LULC patterns. The future LULC maps under SSP-RCP scenario for the respected three future time frames i.e., 2040, 2065 and 2090 were used and is forced along with future climate data of two SSP scenarios that indicates the most optimistic SSP1-2.6 and pessimistic SSP5-8.5 projections of the future climate to hydrological model. Following are the key findings of the study.

Under both scenarios, it is expected that precipitation and temperature will continue to increase in the future. The ensemble mean temperature is projected to rise by 1.56 ^{o}C and 4.65 ^{o}C under SSP1-2.6 and SSP5-8.5 scenarios respectively by the end of 21st century. The ensemble mean precipitation is projected to increase in the range of 19.07% to 55.67% towards end of 21st century. The findings indicate a future scenario characterized by expanded cropland and urbanization, coupled with a reduction in forest cover, grassland and barren land. The TRB may have more water availability in the future due to the combined effects of climate change and land use variation. The water yield and surface runoff ensemble mean is projected to increase in the nearly same range of 80% to 189.5% and 72.7% to 178.8% respectively in the future. The groundwater recharge is expected to rise in the future, possibly by 115.6% to 265%, as a result of the decrease in ET.

4.7 Closure

In this chapter the results and some of the key findings for each objective is described in detailed manner. The comprehensive analysis of sensitivity of GCMs rankings, climate change impact in various aspects in the KRB and combined impact of climate and LULC change on WBC in the TRB is investigated.

CHAPTER5

SUMMARY AND CONCLUSIONS

5.1 Summary

The hydrological cycle, patterns of sea level and surface temperature and agricultural productivity are all impacted by climate change. Global climate pattern changes may have an impact on the severity, frequency and frequency of extreme events such as droughts and floods (IPCC, 2013). The current study project simulates the effects of climate change for the Krishna and Tungabhadra river basins in both the present and the future. However, for future projections of various water balance components investigation, GCMs are necessary. The CMIP6 GCMs are an improvised versions of CMIP5 GCMs in simulating climate variables. Generally the ranking of GCMs are prone to subjectivity. So, the GCMs subjectivity is analysed in India as a case study in first phase of research. The skill of CMIP6 based GCMs in replicating the T_{max} and T_{min} across India is evaluated using various combinations of input criteria, MCDM techniques, weighting methods and reference gridded datasets. Two sets of input criteria were used in this study that consists of three model evaluation metrics in each set. NSE, MAE, BD, KGE, R4MS4E and SU were used as input criteria. The metrics are chosen in such a way that they differ in capturing distinctive characteristics of dataset. Two MCDM techniques namely FTOPSIS and CP are chosen where both differ in the aggregation of multiple criteria. Entropy and CRITIC weight methods were chosen for weightage allocation. IMD and CPC gridded datasets were used as reference datasets. Various combinations of these alternatives were used to rank the performance of GCMs. These combinations address the uncertainty in the ranking of GCMs due to subjectivity involved in choosing the components of ranking procedures.

For the climate change impact in the KRB, the symmetric uncertainty concept is employed to screen the top CMIP6-GCMs available GCMs to reduce the GCM selection uncertainty. The precipitation of CMIP6-GCMs are re-gridded by employing bilinear interpolation technique to a resolution of 0.25° in order to guarantee compatibility with IMD data. Initially, the precipitation outputs from various GCMs were bias corrected using empirical quantile mapping and ranking was done on monthly basis. Top five GCMs were selected based on total ranking weight obtained for each GCM. Uncertainty of the climate model data is reduced using REA to develop the MME. Spatio-temporal analysis of precipitation across the KRB is investigated using this MME. It is observed that most of the grid location exhibited increase in the

precipitation for annual and ISMR periods. The decrease in the precipitation is projected in the middle Krishna basin grid locations as most of the middle Krishna basin is semi-arid in nature.

It is noticed that very limited studies were conducted in the KRB on the climate extreme point of view using different CMIP phase GCMs. So, in this study the spatio-temporal analysis of precipitation extremes were analysed for present and two future periods under four SSP scenario. This top five GMCs were selected out of 18 CMIP6 GCMs. However the ranking of GCMs are varying based on the daily and monthly data sets. Eleven (11) ETCCDI precipitation extreme indices are considered which are sufficient to understand extreme events behaviour in a basin. The correlation between the annual average daily discharge and precipitation extremes were analysed to know the impact of which extreme indices influencing more on discharge. However, in a basin wise the total precipitation indice most important as a major water resource. The good correlation is observed between the discharge and total precipitation, so an attempt is made to predict the future streamflow using simple nonlinear regression equation is known as support vector regression. However for the extreme event analysis the event based hydrological modelling will provide results with lesser uncertainty, but it is time complex and need lot of input data. The statistical models are simple, takes lesser time and need less input data in predicting any climate variable or streamflow. The established relationship between the discharge and total precipitation for historical period is employed for future streamflow prediction. This spatio-temporal analyse extremes in the KRB provide a valuable information for the policymakers.

For climate change impact on the water balance components in the KRB, top 50% best performed GCMs (nine) are considered. Multi-site calibration and validation of SWAT model has been carried out Krishna river basin to find the spatial performance of the hydrological model. The nine bias corrected GCMs were forced to calibrated and validated hydrological model. The water balance components and streamflow availability is investigated for 9 historical GCMs for the baseline period 1973-2003 and for three future periods of their four SSP scenarios. The streamflow and water balance components are investigated at monthly and annual scale due to climate change. The far future showed more significant projected changes in streamflow and water balance components across the basin based on the 9 GCMs their simple ensemble average. The prediction bounds of minimum and maximum values of all considered GCMs are also shown to know the lower and higher extremes of different water balance components. The mean monthly flows of all 9 GCMs and their ensemble are projected

to increase in the future. Especially, the ISMR season shown a high increase in the streamflow variations.

An attempt is made to investigate the coupled impact of the climate and LULC change in the Tungabhadra river basin for the three future periods. Two Shared Socioeconomic Pathways (SSPs) scenarios namely, SSP1-2.6 and SSP5-8.5 are especially chosen to reflect the most optimistic and pessimistic future climate estimates. The Scenario Model Intercomparison Project defined these SSPs, which integrate different trajectories of greenhouse gas emissions with alternate scenarios of societal expansion in the absence of climate change (O'Neill et al., 2016). According to (Riahi et al., 2017) SSP1 presents an optimistic trajectory for human growth that includes substantial investments in health and education, whereas SSP5 depicts a gloomy society that relies heavily on energy. By the end of the 21st century, the forcing scenarios of both SSP1-2.6 and SSP5-8.5 are intended to stabilise at 2.6 and 8.5 W/m^2, respectively. The future LULC maps under SSP-RCP scenario for the respected three future time periods i.e., 2040, 2065 and 2090 were extracted (Chen 2022) and is forced along with future climate data for the hydrological modelling. A good coefficient determination and Nash Sutcliff Efficiency were observed represents that the SWAT model is performing well in simulating the streamflow. The variability in the future projected mean annual surface runoff, groundwater, soil moisture, evapotranspiration, water yield and monthly streamflow were projected using calibrated and validated SWAT model.

5.2 Conclusions

The following conclusions are arrived based on the study.

- Ranking of GCMs are highly dependent upon the chosen reference gridded dataset. Selection of input criteria to evaluate the model performance plays a key role in ranking of GCMs. The weights allocated to the criteria and the final aggregated outputs from MCDM techniques is highly dependent upon the chosen evaluation metrics.

- At some locations, the ranking pattern of GCMs is not affected by any of the component involved in the ranking procedure across India and hence can be chosen as the best performing GCM irrespective of the subjective decisions. An ensemble of most frequently performing GCMs for maximum and minimum temperatures are extracted for each climate zone as the most suitable set of GCMs for the corresponding climate

zone and these GCMs can be used for the downscaling for further climate impact studies. The IMD dataset was used for the further climate change impact assessment study in the KRB.

- The ability of GCMs to reproduce the observed precipitation on monthly base data is ranked using the concept of SU. BCC-CSM2-MR, IPSL-CM6A-LR, MIROC6, INM-CM5-0 and MPI-ESM1-2-HR, which were the most preferable GCMs for projecting the precipitation in the KRB.

- The REA method was used to develop the MME for the projection of precipitation using above mentioned five GCMs. The results revealed that there is an increase in annual precipitation in almost the entire study area (except 11 grid points) in the far future under the SSP5-8.5 scenario.

- The declination in precipitation projections in the near future can be observed in the range of 56% (192 grid points) to 81% (283 grid points) in the KRB for REA based ensmble, especially in the BSh climate zone under different SSP scenarios. This result suggests the vulnerability of the study area to droughts in the near future in those locations due to the reduction in the precipitation projections based on REA ensemble average.

- SSP5-8.5 shows an increase in precipitation over most of the grids in the basin in the far future. In contrast to the annual precipitation trends projected by the MME, the seasonal precipitation increases in the near future, showing that the precipitation patterns will get intensified in the future over the KRB.

- The same SU concept is employed to screen the suitable GCMs using daily datasets of IMD and GCMs. Based on the results, top nine (9) i.e., 50% of 18 suitable GCMs: MPI-ESM1-2-HR, MPI-ESM1-2-LR, GFDL-ESM4, NorESM2-LM, EC-Earth3-Veg, BCC-CSM2-MR, EC-Earth3, IPSL-CM6A-LR and NorESM2-MM. However it is observed that the ranking of the GCMs are varying based on temporal resolution of the data also.

- The top five GCMs such as MPI-ESM1-2-HR, MPI-ESM1-2-LR, GFDL-ESM4, NorESM2-LM and EC-Earth3-Veg are used to analyse the precipitation extremes in the KRB.

- A larger number of grid points exhibited decreasing trends (insignificant and significant) followed by increasing (insignificant) trends and a very small number of grid points experienced positive significant trends for extreme precipitation indices across the basin for the baseline period (1973-2003).

- RX1day and RX5day are major extreme precipitation indices and the mean annual contributions are 9.7% and 18.5% respectively in the baseline period. Heavy precipitation intensity indices RX1day, RX5day, R95p and R99p have exhibited positive fluctuations which indicate most of the rainfall is concentrated in less number of days which may aggregate to flash floods.

- It is found that the MME average of extreme precipitation indices is predicted to increase over the future periods. Particularly, in the FF the magnitude of increase is greater under all SSP scenarios over the basin.

- The heavy extreme precipitation indices both R95p and R99p are increased to nearly same value about 74% and RX1day and RX5day are increased to 49% and 73% respectively in the FF under the high warm SSP5-8.5 scenario.

- The SVM based streamflow shows that, the SSP1-2.6 and SSP2-4.5 scenarios are expected to follow similar increasing streamflow patterns and the maximum average streamflow is observed as 2190 m^3/s in the year 2027 under SSP1-2.6 in the NF.

- The SVM based streamflow shows that the highest MME average streamflow for FF under SSP5-8.5 was 2694 m^3/s in the year 2089. The prediction bound of maximum flow value is projected to reach up to 3591 m^3/s in FF under the SSP5-8.5 scenario. This study, in conclusion, establishes that the discharges will increase with increased precipitation extremes causing frequent hydrological disasters in the Krishna River Basin in the future.

- The climate impact on the water balance components and streamflow of the KRB was analysed using top 9 GCMs for historical and future periods.

- The MPI-ESM1-2-HR and MPI-ESM1-2-LR GCMs closely match observed precipitation data during the baseline period, with no significant changes expected in the future except under the SSP5-8.5 scenario during the FF period.

- The outputs of NorESM2-LM and NorESM2-MM GCMs consistently showed an overestimation of future precipitation across all SSP scenarios except in the FF under SSP5-8.5 scenario.

- It is observed that the ensemble mean of projected mean annual precipitation has significantly increased in the range of 12.07% to 53.79% in the future periods under different SSP scenarios compared to GCM ensemble.

- The fluctuation of these predicted precipitation levels will likely have a significant impact on other water balance components in the basin. The ensemble average of annual surface runoff and water yield is projected to increase from 27% to 124% and 30% to 125%, respectively, under different SSP scenarios for future periods.

- With the increase in precipitation, ET is also projected to increase under all scenarios in the future periods but the increase percentage of ET is less compared to baseline period ET and the other WBC in the future.

- The future streamflow is significantly impacted by changes in future precipitation and the annual MME average is projected to increase from 31 to 114.5% from NF to FF under four SSP scenarios.

- The ensemble mean of future flows occurred mostly in the month of September and the increase in flows can also be observed even in the months of October and November due to monsoon extension. This shows the adverse effects on Kharif crops as they are under harvesting stage.

- The current study looks into how the hydrological components in the Tungabhadra river basin, India, might react to changes in the combined effects of climate change and LULC patterns for future periods under SSP1-2.6 and SSP5-8.5 scenarios.

- Under both scenarios, it is expected that precipitation and temperature will continue to increase in the future. The ensemble mean temperature is projected to rise by 1.56 ^{o}C and 4.65 ^{o}C under SSP1-2.6 and SSP5-8.5 scenarios respectively by the end of 21st century compared to IMD baseline period 1978-2010

- The ensemble mean precipitation is projected to increase in the range of 19.07% to 55.67% towards end of 21st century compare to observed period.

- The findings indicate a future scenario characterized by expanded cropland and urbanization, coupled with a reduction in forest cover, grassland and barren land.

- The water yield and surface runoff ensemble mean is projected to increase in the nearly same range of 80% to 189.5% and 72.7% to 178.8% respectively in the future. The groundwater recharge is expected to rise in the future, possibly by 115.6% to 265%, as a result of the decrease in ET.

- Future streamflow in TRB is expected to rise significantly during the ISMR season with the other WBC, which may damage kharif crops and cause floods. The highest streamflow of MME is observed as 4379.52 m^3/sec in the FF under SSP5-8.5 scenario which is 2.6 times compared to observed period inferring the probability of more water arability and occurring of floods.

- Therefore, it may be concluded that the more water availability chances in the KRB and TRB under different CMIP6 climate change projections and also has the probability of occurring of floods in the future periods. As a result, this knowledge is highly helpful for sustainable development and improved planning and management of water resources.

5.3 Contributions from the Research

The current study has made the following significant contributions to research:

The present study explores the various GCMs ranking patterns based on the subjectivity for temperature and made some important conclusions to reader that which parameters will affect the ranking patterns more. And provided top five ensemble for maximum and minimum temperature across different climate zones of India. These GCMs can be used directly for the further climate change studies.

This study comprehensively investigated the climate change impact on water resources of the Krishna river basin. This study tried an attempt to reduce the GCM selection uncertainty in climate change impact study in the KRB. The precipitation is projected using REA based ensemble to tackle the GCM uncertainty under four SSP scenarios (SSP1-2.6, SSP2-4.5, SSP3-7.0 and SSP5-8.5). The precipitation extremes are also projected to know the impact of extreme indices across the basin for the future periods.

Furthermore, a semi-distributed hydrological model called SWAT model is used to project the water balance components along with streamflow (hydrological process) of the Krishna and Tungabhadra river basins. The prediction bounds projected water balance components and streamflow of the 9 GCMs and MME average are presented in the current study. This study results offer valuable insights, enhancing comprehension and regarding water availability in the spatially diverse KRB and TRB under anticipated future scenarios.

5.4 Limitations of the Study

- LULC is assumed to be constant during SWAT simulations for periods of 2025-2100 in the KRB. This indicates that the climate is the only factor influencing the water balance components and streamflow variability during future scenarios. The combined impact of LULC and climate could give a better knowledge about the hydrological processes in the entire KRB.

- The work is carried out with data of available resolution. Finer resolution data would have given better results.
- Even though the hydrological model is calibrated and validated, the uncertainty may still exist which can be reduced to some extent by employing ensemble of different hydrological models.

5.5 Scope of Further Studies

Based on research findings, the scope of future studies are identified as:

- Other than REA method, any other weighting technique method can be used for development of MME for climate impact studies.

- The coupled effect of future climate and LULC change analysis can be carried out for other sub-basins in the KRB.

- The event based rainfall-runoff model can be used for better simulations of water budget components and hydrological extremes.

- Ensemble of different hydrological models can be used in simulating the hydrological process to reduce the uncertainty in the future projections.

REFERENCES

Abbasian, M., Moghim, S., & Abrishamchi, A. (2019). Performance of the general circulation models in simulating temperature and precipitation over Iran. *Theoretical and Applied Climatology*, *135*(3), 1465–1483. https://doi.org/10.1007/s00704-018-2456-y

Abbaspour, K. C., Rouholahnejad, E., Vaghefi, S., Srinivasan, R., Yang, H., & Kløve, B. (2015). A continental-scale hydrology and water quality model for Europe: Calibration and uncertainty of a high-resolution large-scale SWAT model. *Journal of Hydrology*, *524*, 733–752. https://doi.org/10.1016/j.jhydrol.2015.03.027

Agarwal, A., Babel, M. S., & Maskey, S. (2014). Analysis of future precipitation in the Koshi river basin, Nepal. *Journal of Hydrology*, *513*, 422–434. https://doi.org/10.1016/j.jhydrol.2014.03.047

Ahiablame, L., Sinha, T., Paul, M., Ji, J. H., & Rajib, A. (2017). Streamflow response to potential land use and climate changes in the James River watershed, Upper Midwest United States. *Journal of Hydrology: Regional Studies*, *14*(November), 150–166. https://doi.org/10.1016/j.ejrh.2017.11.004

Ahmadalipour, A., Rana, A., Moradkhani, H., & Sharma, A. (2017). Multi-criteria evaluation of CMIP5 GCMs for climate change impact analysis. *Theoretical and Applied Climatology*, *128*(1–2), 71–87. https://doi.org/10.1007/s00704-015-1695-4

Ahmed, K., Sachindra, D. A., Shahid, S., Demirel, M. C., & Chung, E.-S. (2019b). Selection of multi-model ensemble of general circulation models for the simulation of precipitation and maximum and minimum temperature based on spatial assessment metrics. *Hydrology and Earth System Sciences*, *23*, 4803. https://doi.org/10.5194/hess-23-4803-2019

Ahmed, K., Shahid, S., Sachindra, D. A., Nawaz, N., & Chung, E.-S. (2019). Fidelity assessment of general circulation model simulated precipitation and temperature over Pakistan using a feature selection method. *Journal of Hydrology*, *573*, 281–298. https://doi.org/10.1016/j.jhydrol.2019.03.092

Ali, H., Modi, P., & Mishra, V. (2019). Increased flood risk in Indian sub-continent under the warming climate. *Weather and Climate Extremes*, *25*, 100212. https://doi.org/1 0.1016 /j.wace.2019.100212

Ali, R., Rashid Abubaker, S., & Othman Ali, R. (2019). Spatio-Temporal Pattern in the Changes in Availability and Sustainability of Water Resources in Afghanistan View project Water resources problem in Huai river basin View project Trend analysis using mann-kendall, sen's slope estimator test and innovative . *International Journal of Engineering &Technology*, *8*(2), 110–119. https://doi.org/10.14419/ijet.v7i4.29591

Alsarmi, S. H., & Washington, R. (2014). Changes in climate extremes in the Arabian Peninsula: Analysis of daily data. *International Journal of Climatology*, *34*(5), 1329–1345. https://doi.org/10.1002/joc.3772

Amarasinghe, U., Shah, T., Turral, H., & Anand, B. K. (2007). *India's water future to 2025-2050: Business-as-usual scenario and deviations* (Vol. 123). IWMI.

Amarasinghe, U., Sharma, B. R., Aloysius, N., Scott, C., Smakhtin, V., & De Fraiture, C. (2005). *Spatial variation in water supply and demand across river basins of India* (Vol. 83). Iwmi.

Anandhi, A., & Nanjundiah, R. S. (2015). Performance evaluation of AR4 Climate Models in simulating daily precipitation over the Indian region using skill scores. *Theoretical and Applied Climatology*, *119*(3), 551–566. https://doi.org/10.1007/s00704-013-1043-5

Arnold, G. J., N. Moriasi, D., W. Gassman, P., C. Abbaspour, K., J. White, M., Srinivasan, R., Santhi, C., D. Harmel, R., van Griensven, A., W. Van Liew, M., Kannan, N., & K. Jha, M. (2012). SWAT: Model Use, Calibration, and Validation. *Transactions of the ASABE*, *55*(4), 1491–1508. https://doi.org/10.13031/2013.42256

Asfaw, A., Simane, B., Hassen, A., & Bantider, A. (2018). Variability and time series trend analysis of rainfall and temperature in northcentral Ethiopia: A case study in Woleka sub-basin. *Weather and Climate Extremes*, *19*(December), 29–41. https://doi.org/10.1016/j.wace.2017.12.002

Babar, Z. A., Zhi, X. F., & Fei, G. (2015). Precipitation assessment of Indian summer monsoon based on CMIP5 climate simulations. *Arabian Journal of Geosciences*, *8*(7), 4379–4392. https://doi.org/10.1007/s12517-014-1518-4

Bae, D.-H., Jung, I.-W., & Lettenmaier, D. P. (2011). Hydrologic uncertainties in climate change from IPCC AR4 GCM simulations of the Chungju Basin, Korea. *Journal of*

Hydrology, *401*(1), 90–105. https://doi.org/10.1016/j.jhydrol.2011.02.012

Bandyopadhyay, A., Nengzouzam, G., Singh, W. R., Hangsing, N., & Bhadra, A. (2018). *Comparison of Various Reanalyses Gridded Data with Observed Data from Meteorological Stations over India*. *3*, 190–180. https://doi.org/10.29007/c1sf

Bergström, S. (2006). Experience from applications of the HBV hydrological model from the perspective of prediction in ungauged basins. *IAHS-AISH Publication*, *307*, 97–107.

Bhatta, B., Shrestha, S., Shrestha, P. K., & Talchabhadel, R. (2019). Evaluation and application of a SWAT model to assess the climate change impact on the hydrology of the Himalayan River Basin. *Catena*, *181*(May), 104082. https://doi.org/10.1016/j.catena.2019.104082

Biggs, T., Gaur, A., Scott, C., Thenkabail, P., Gangadhara Rao, P., Gumma, M. K., Acharya, S., & Turral, H. (2007). *Closing of the Krishna basin: irrigation, streamflow depletion and macroscale hydrology* (Vol. 111). IWMI.

Bisht, D. S., Chatterjee, C., Raghuwanshi, N. S., & Sridhar, V. (2018). Spatio-temporal trends of rainfall across Indian river basins. *Theoretical and Applied Climatology*, *132*(1), 419–436. https://doi.org/10.1007/s00704-017-2095-8

Bisht, D. S., Mohite, A. R., Jena, P. P., Khatun, A., Chatterjee, C., Raghuwanshi, N. S., Singh, R., & Sahoo, B. (2020). Impact of climate change on streamflow regime of a large Indian river basin using a novel monthly hybrid bias correction technique and a conceptual modeling framework. *Journal of Hydrology*, *590*, 125448. https://doi.org/10.10 16/j.jhy drol.2020.125448

Cameron, F. (2011). Guest editorial : Climate change as a complex phenomenon and the problem of cultural governance. *Museum and Society*, *9*(Rosenau 2003), 84–89.

Cannon, A. J. (2016). Multivariate bias correction of climate model output: Matching marginal distributions and intervariable dependence structure. *Journal of Climate*, *29*(19), 7045–7064. https://doi.org/10.1175/JCLI-D-15-0679.1

Cannon, A. J., Sobie, S. R., & Murdock, T. Q. (2015). Bias correction of GCM precipitation by quantile mapping: How well do methods preserve changes in quantiles and extremes? *Journal of Climate*, *28*(17), 6938–6959. https://doi.org/10.1175/JCLI-D-14-00754.1

Chanapathi, T., & Thatikonda, S. (2020). Investigating the impact of climate and land-use land cover changes on hydrological predictions over the Krishna river basin under present and future scenarios. *Science of the Total Environment*, *721*, 137736. https://doi.org/10.1016/j.scitotenv.2020.137736

Chanapathi, T., Thatikonda, S., & Raghavan, S. (2018). Analysis of rainfall extremes and water yield of Krishna river basin under future climate scenarios. *Journal of Hydrology: Regional Studies*, *19*(June), 287–306. https://doi.org/10.1016/j.ejrh.2018.10.004

Chandra, R., Saha, U., & Mujumdar, P. P. (2015). Model and parameter uncertainty in IDF relationships under climate change. *Advances in Water Resources*, *79*(February), 127–139. https://doi.org/10.1016/j.advwatres.2015.02.011

Chaubey, P. K., Mall, R. K., Jaiswal, R., & Payra, S. (2022). Spatio-Temporal Changes in Extreme Rainfall Events Over Different Indian River Basins. *Earth and Space Science*, *9*(3), 1–21. https://doi.org/10.1029/2021ea001930

Chen, C., Haerter, J. O., Hagemann, S., & Piani, C. (2011). On the contribution of statistical bias correction to the uncertainty in the projected hydrological cycle. *Geophysical Research Letters*, *38*(20). https://doi.org/10.1029/2011GL049318

Chen, G., Li, X., & Liu, X. (2022). Global land projection based on plant functional types with a 1-km resolution under socio-climatic scenarios. *Scientific Data*, *9*(1), 125. https://doi.org/10.1038/s41597-022-01208-6

Chen, J., Brissette, F. P., Zhang, X. J., Chen, H., Guo, S., & Zhao, Y. (2019). Bias correcting climate model multi-member ensembles to assess climate change impacts on hydrology. *Climatic Change*, *153*(3), 361–377. https://doi.org/10.1007/s10584-019-02393-x

Chen, Q., Chen, H., Zhang, J., Hou, Y., Shen, M., Chen, J., & Xu, C. (2020). Impacts of climate change and LULC change on runoff in the Jinsha River Basin. *Journal of Geographical Sciences*, *30*(1), 85–102. https://doi.org/10.1007/s11442-020-1716-9

Chien, H., Yeh, P. J.-F., & Knouft, J. H. (2013). Modeling the potential impacts of climate change on streamflow in agricultural watersheds of the Midwestern United States. *Journal of Hydrology*, *491*, 73–88. https://doi.org/10.1016/j.jhydrol.2013.03.026

Choi, W., Tareghian, R., Choi, J., & Hwang, C. sue. (2014). Geographically heterogeneous temporal trends of extreme precipitation in Wisconsin, USA during 1950-2006. *International Journal of Climatology*, *34*(9), 2841–2852. https://doi.org/10.1002/joc.3878

Crosbie, R. S., Dawes, W. R., Charles, S. P., Mpelasoka, F. S., Aryal, S., Barron, O., & Summerell, G. K. (2011). Differences in future recharge estimates due to GCMs, downscaling methods and hydrological models. *Geophysical Research Letters*, *38*(11), 1–5. https://doi.org/10.1029/2011GL047657

Das, J., & Nanduri, U. V. (2018). Assessment and evaluation of potential climate change impact on monsoon flows using machine learning technique over Wainganga River basin, India. *Hydrological Sciences Journal*, *63*(7), 1020–1046. https://doi.org/10.1080/02626667.2018.1469757

Das, L., Dutta, M., Mezghani, A., & Benestad, R. E. (2018). Use of observed temperature statistics in ranking CMIP5 model performance over the Western Himalayan Region of India. *International Journal of Climatology*, *38*(2), 554–570. https://doi.org/10.1002/joc.5193

Deshpande, N. R., Kothawale, D. R., & Kulkarni, A. (2016). Changes in climate extremes over major river basins of India. *International Journal of Climatology*, *36*(14), 4548–4559. https://doi.org/10.1002/joc.4651

Dottori, F., Szewczyk, W., Ciscar, J.-C., Zhao, F., Alfieri, L., Hirabayashi, Y., Bianchi, A., Mongelli, I., Frieler, K., Betts, R. A., & Feyen, L. (2018). Increased human and economic losses from river flooding with anthropogenic warming. *Nature Climate Change*, *8*(9), 781–786. https://doi.org/10.1038/s41558-018-0257-z

Dubey, S. K., & Sharma, D. (2018). Spatio-Temporal Trends and Projections of Climate Indices in the Banas River Basin, India. *Environmental Processes*, *5*(4), 743–768. https://doi.org/10.1007/s40710-018-0332-5

Eyring, V., Bony, S., Meehl, G. A., Senior, C. A., Stevens, B., Stouffer, R. J., & Taylor, K. E. (2016). Overview of the Coupled Model Intercomparison Project Phase 6 (CMIP6) experimental design and organization. *Geoscientific Model Development*, *9*(5), 1937–1958. https://doi.org/10.5194/gmd-9-1937-2016

Fan, X., Jiang, L., & Gou, J. (2021). Statistical downscaling and projection of future temperatures across the Loess Plateau, China. *Weather and Climate Extremes*, *32*, 100328. https://doi.org/10.1016/j.wace.2021.100328

Fowler, H. J., Ekström, M., Blenkinsop, S., & Smith, A. P. (2007). Estimating change in extreme European precipitation using a multimodel ensemble. *Journal of Geophysical Research Atmospheres*, *112*(18), 1–20. https://doi.org/10.1029/2007JD008619

Fu, G., Liu, Z., Charles, S. P., Xu, Z., & Yao, Z. (2013). *A score-based method for assessing the performance of GCMs : A case study of southeastern Australia*. *118*(February), 4154–4167. https://doi.org/10.1002/jgrd.50269

Gaur, S., Bandyopadhyay, A., & Singh, R. (2021). From Changing Environment to Changing Extremes: Exploring the Future Streamflow and Associated Uncertainties Through Integrated Modelling System. *Water Resources Management*, *35*(6), 1889–1911. https://doi.org/10.1007/s11269-021-02817-3

Getachew, B., Manjunatha, B. R., & Bhat, H. G. (2021). Modeling projected impacts of climate and land use/land cover changes on hydrological responses in the Lake Tana Basin, upper Blue Nile River Basin, Ethiopia. *Journal of Hydrology*, *595*(January), 125974. https://doi.org/10.1016/j.jhydrol.2021.125974

Ghosh, S. (2010). SVM-PGSL coupled approach for statistical downscaling to predict rainfall from GCM output. *Journal of Geophysical Research Atmospheres*, *115*(22), 1–18. https://doi.org/10.1029/2009JD013548

Ghosh, S., & Mujumdar, P. P. (2008). Statistical downscaling of GCM simulations to streamflow using relevance vector machine. *Advances in Water Resources*, *31*(1), 132–146. https://doi.org/10.1016/j.advwatres.2007.07.005

Gidden, M. J., Riahi, K., Smith, S. J., Fujimori, S., Luderer, G., Kriegler, E., Van Vuuren, D. P., Van Den Berg, M., Feng, L., Klein, D., Calvin, K., Doelman, J. C., Frank, S., Fricko, O., Harmsen, M., Hasegawa, T., Havlik, P., Hilaire, J., Hoesly, R., … Takahashi, K. (2019). Global emissions pathways under different socioeconomic scenarios for use in CMIP6: A dataset of harmonized emissions trajectories through the end of the century. *Geoscientific Model Development*, *12*(4), 1443–1475. https://doi.org/10.5194/gmd-12-

1443-2019

Giorgi, F., & Mearns, L. O. (1991). Approaches to the simulation of regional climate change: a review. *Reviews of Geophysics*, *29*(2), 191–216. https://doi.org/10.1029/90RG02636

Givati, A., Thirel, G., Rosenfeld, D., & Paz, D. (2019). Climate change impacts on streamflow at the upper Jordan River based on an ensemble of regional climate models. *Journal of Hydrology: Regional Studies*, *21*(December 2018), 92–109. https://doi.org/10.1016/j.ejrh.2018.12.004

Gleckler, P. J., Taylor, K. E., & Doutriaux, C. (2008). Performance metrics for climate models. *Journal of Geophysical Research: Atmospheres*, *113*(D6). https://doi.org/10.1029/2007JD008972

Gong, D. Y., Shi, P. J., & Wang, J. A. (2004). Daily precipitation changes in the semi-arid region over northern China. *Journal of Arid Environments*, *59*(4), 771–784. https://doi.org/10.1016/j.jaridenv.2004.02.006

Gosain, A. K., Rao, S., & Basuray, D. (2006). Climate change impact assessment on hydrology of Indian river basins. *Current Science*, *90*(3), 346–353. https://www.jstor.org/stable/24091868

Gouda, K. C., Nahak, S., & Goswami, P. (2018). Evaluation of a GCM in seasonal forecasting of extreme rainfall events over continental India. *Weather and Climate Extremes*, *21*(September), 10–16. https://doi.org/10.1016/j.wace.2018.05.001

Goyal, M. K. (2014). Statistical Analysis of Long Term Trends of Rainfall During 1901-2002 at Assam, India. *Water Resources Management*, *28*(6), 1501–1515. https://doi.org/10.1007/s11269-014-0529-y

Gudmundsson, L., Bremnes, J. B., Haugen, J. E., & Engen-Skaugen, T. (2012). Technical Note: Downscaling RCM precipitation to the station scale using statistical transformations – A comparison of methods. *Hydrology and Earth System Sciences*, *16*(9), 3383–3390. https://doi.org/10.5194/hess-16-3383-2012

Guo, Y., Fang, G., Xu, Y.-P., Tian, X., & Xie, J. (2020). Identifying how future climate and land use/cover changes impact streamflow in Xinanjiang Basin, East China. *Science of*

The Total Environment, *710*, 136275. https://doi.org/10.1016/j.scitotenv.2019.136275

Guo, Z., Wang, N., Kehrwald, N. M., Mao, R., Wu, H., Wu, Y., & Jiang, X. (2014). Temporal and spatial changes in Western Himalayan firn line altitudes from 1998 to 2009. *Global and Planetary Change*, *118*, 97–105. https://doi.org/10.1016/j.gloplacha.2014.03.012

Gupta, A. K., & Nair, S. S. (2011). Urban floods in Bangalore and Chennai: Risk management challenges and lessons for sustainable urban ecology. *Current Science*, *100*(11), 1638–1645. https://www.jstor.org/stable/24077767

Gusain, A., Ghosh, S., & Karmakar, S. (2020). Added value of CMIP6 over CMIP5 models in simulating Indian summer monsoon rainfall. *Atmospheric Research*, *232*, 104680. https://doi.org/10.1016/j.atmosres.2019.104680

Hassan, I., Kalin, R. M., White, C. J., & Aladejana, J. A. (2020). Selection of CMIP5 GCM ensemble for the projection of Spatio-temporal changes in precipitation and temperature over the Niger Delta, Nigeria. *Water*, *12*(2), 385. https://doi.org/10.3390/w12020385

Homsi, R., Shiru, M. S., Shahid, S., Ismail, T., Harun, S. Bin, Al-Ansari, N., Chau, K.-W., & Yaseen, Z. M. (2020). Precipitation projection using a CMIP5 GCM ensemble model: a regional investigation of Syria. *Engineering Applications of Computational Fluid Mechanics*, *14*(1), 90–106. https://doi.org/10.1080/19942060.2019.1683076

Homsi, R., Shiru, M. S., Shahid, S., Ismail, T., Harun, S. Bin, Al-ansari, N., Chau, K., & Mundher, Z. (2020). *Mechanics Precipitation projection using a CMIP5 GCM ensemble model : a regional investigation of Syria*. *2060*. https://doi.org/10.1080/19942060.2019.1683076

Ines, A. V. M., & Hansen, J. W. (2006). Bias correction of daily GCM rainfall for crop simulation studies. *Agricultural and Forest Meteorology*, *138*(1), 44–53. https://doi.org/10.1016/j.agrformet.2006.03.009

IPCC. (2013). AR5 - Citations. *CLIMATE CHANGE 2013 - The Physical Science Basis, Contribution of Working Group I to the Fifth Assessment Report of the Intergovernmental Panel on Climate Change*, 3. https://doi.org/10.1017/CBO9781107415324.Summary

IPCC, 2018: Global warming of 1.5°C. An IPCC Special Report on the impacts of global

warming of 1.5°C above pre-industrial levels and related global greenhouse gas emission pathways, in the context of strengthening the global response to the threat of climate change, sustainable development, and efforts to eradicate poverty [V. Masson-Delmotte, P. Zhai, H. O. Pörtner, D. Roberts, J. Skea, P.R. Shukla, A. Pirani, W. Moufouma-Okia, C. Péan, R. Pidcock, S. Connors, J. B. R. Matthews, Y. Chen, X. Zhou, M. I. Gomis, E. Lonnoy, T. Maycock, M. Tignor, T. Waterfield (eds.)]. In Press.

Iqbal, Z., Shahid, S., Ahmed, K., Ismail, T., Khan, N., Virk, Z. T., & Johar, W. (2020). Evaluation of global climate models for precipitation projection in sub-Himalaya region of Pakistan. *Atmospheric Research*, *245*, 105061. https://doi.org/10.1016/j.atmosres.2020.105061

Jena, P., Azad, S., & Rajeevan, M. N. (2015). *Statistical Selection of the Optimum Models in the CMIP5 Dataset for Climate Change Projections of Indian Monsoon Rainfall*. 858–875. https://doi.org/10.3390/cli3040858

Jiang, Z., Sharma, A., & Johnson, F. (2019). Assessing the sensitivity of hydro-climatological change detection methods to model uncertainty and bias. *Advances in Water Resources*, *134*(October), 103430. https://doi.org/10.1016/j.advwatres.2019.103430

John, A., Douville, H., Ribes, A., & Yiou, P. (2022). Quantifying CMIP6 model uncertainties in extreme precipitation projections. *Weather and Climate Extremes*, *36*(February), 100435. https://doi.org/10.1016/j.wace.2022.100435

Johnson, F., & Sharma, A. (2009a). Measurement of GCM skill in predicting variables relevant for hydroclimatological assessments. *Journal of Climate*, *22*(16), 4373–4382. https://doi.org/10.1175/2009JCLI2681.1

Johnson, F., & Sharma, A. (2009b). Measurement of GCM skill in predicting variables relevant for hydroclimatological assessments. *Journal of Climate*, *22*(16), 4373–4382. https://doi.org/10.1175/2009JCLI2681.1

Kamworapan, S., & Surussavadee, C. (2019). Evaluation of CMIP5 Global Climate Models for Simulating Climatological Temperature and Precipitation for Southeast Asia. *Advances in Meteorology*, *2019*, 1–18. https://doi.org/10.1155/2019/1067365

Kendall, M. G. (1975). Rank Correlation Methods, Charles Griffin, London (1975). *Google*

Sch.

Khan, N., Shahid, S., Ahmed, K., Ismail, T., Nawaz, N., & Son, M. (2018a). Performance assessment of general circulation model in simulating daily precipitation and temperature using multiple gridded datasets. *Water*, *10*(12), 1793. https://doi.org/10.3390/w10121793

Khayyun, T. S., Alwan, I. A., & Hayder, A. M. (2020). Selection of Suitable Precipitation CMIP-5 Sets of GCMs for Iraq Using a Symmetrical Uncertainty Filter. *IOP Conference Series: Materials Science and Engineering*, *671*(1). https://doi.org/10.1088/1757-899X/671/1/012013

Kitoh, A., Endo, H., Krishna Kumar, K., Cavalcanti, I. F. A., Goswami, P., & Zhou, T. (2013). Monsoons in a changing world: A regional perspective in a global context. *Journal of Geophysical Research Atmospheres*, *118*(8), 3053–3065. https://doi.org/10.1002/jgrd.50258

Klein Tank, A. M. G., Peterson, T. C., Quadir, D. A., Dorji, S., Zou, X., Tang, H., Santhosh, K., Joshi, U. R., Jaswal, A. K., Kolli, R. K., Sikder, A. B., Deshpande, N. R., Revadekar, J. V., Yeleuova, K., Vandasheva, S., Faleyeva, M., Gomboluudev, P., Budhathoki, K. P., Hussain, A., … Spektorman, T. (2006). Changes in daily temperature and precipitation extremes in central and south Asia. *Journal of Geophysical Research Atmospheres*, *111*(16), 1–8. https://doi.org/10.1029/2005JD006316

Knutti, R., Abramowitz, G., Collins, M., Eyring, V., Gleckler, P. J., Hewitson, B., & Mearns, L. (2010). Good Practice Guidance Paper on Assessing and Combining Multi Model Climate Projections. *IPCC Expert Meeting on Assessing and Combining Multi Model Climate Projections*, 15pp.

Kothawale, D. R., Revadekar, J. V, & Rupa Kumar, K. (2010). Recent trends in pre-monsoon daily temperature extremes over India. *Journal of Earth System Science*, *119*(1), 51–65. https://doi.org/10.1007/s12040-010-0008-7

Kripalani, R. H., Oh, J. H., Kulkarni, A., Sabade, S. S., & Chaudhari, H. S. (2007). South Asian summer monsoon precipitation variability: Coupled climate model simulations and projections under IPCC AR4. *Theoretical and Applied Climatology*, *90*(3–4), 133–159. https://doi.org/10.1007/s00704-006-0282-0

Krishnamurthy, C. K. B., Lall, U., & Kwon, H. H. (2009). Changing frequency and intensity of rainfall extremes over India from 1951 to 2003. *Journal of Climate*, *22*(18), 4737–4746. https://doi.org/10.1175/2009JCLI2896.1

Kulkarni BD, D. N. (2014). Assessing Hydrological Response to Changing Climate in the Krishna Basin of India. *Journal of Earth Science & Climatic Change*, *05*(07). https://doi.org/10.4172/2157-7617.1000211

Kumar, N., Kumar Goyal, M., Kumar Gupta, A., Jha, S., Das, J., & Madramootoo, C. A. (2021). Joint behaviour of climate extremes across India: Past and future. *Journal of Hydrology*, *597*, 126185. https://doi.org/10.1016/j.jhydrol.2021.126185

Kundu, S., Khare, D., & Mondal, A. (2017). Individual and combined impacts of future climate and land use changes on the water balance. *Ecological Engineering*, *105*, 42–57. https://doi.org/10.1016/j.ecoleng.2017.04.061

Li, F., Xu, Z., Liu, W., & Zhang, Y. (2014). The impact of climate change on runoff in the Yarlung Tsangpo River basin in the Tibetan Plateau. *Stochastic Environmental Research and Risk Assessment*, *28*(3), 517–526. https://doi.org/10.1007/s00477-013-0769-z

Li, Z., & Jin, J. (2017). Evaluating climate change impacts on streamflow variability based on a multisite multivariate GCM downscaling method in the Jing River of China. *Hydrology and Earth System Sciences*, *21*(11), 5531–5546. https://doi.org/10.5194/hess-21-5531-2017

Liang, X., Lettenmaier, D. P., Wood, E. F., & Burges, S. J. (1994). A simple hydrologically based model of land surface water and energy fluxes for general circulation models. *Journal of Geophysical Research: Atmospheres*, *99*(D7), 14415–14428. https://doi.org/10.1029/94JD00483

Lin, G.-F., Chang, M.-J., & Wu, J.-T. (2017). A hybrid statistical downscaling method based on the classification of rainfall patterns. *Water Resources Management*, *31*, 377–401. https://doi.org/10.1007/s11269-016-1532-2

Longobardi, A., & Villani, P. (2010). Trend analysis of annual and seasonal rainfall time series in the Mediterranean area. *International Journal of Climatology*, *30*(10), 1538–1546. https://doi.org/10.1002/joc.2001

Lutz, A. F., ter Maat, H. W., Biemans, H., Shrestha, A. B., Wester, P., & Immerzeel, W. W. (2016). Selecting representative climate models for climate change impact studies: an advanced envelope-based selection approach. *International Journal of Climatology*, *36*(12), 3988–4005. https://doi.org/10.1002/joc.4608

Mall, R. K., Gupta, A., Singh, R., Singh, R. S., & Rathore, L. S. (2006). Water resources and climate change: An Indian perspective. *Current Science*, *90*(12), 1610–1626. https://www.jstor.org/stable/24091910

Mann, H. B. (1945). Nonparametric Tests Against Trend. *Econometrica*, *13*(3), 245–259. https://doi.org/10.2307/1907187

Masson-Delmotte, V. (2018). Global warming of 1.5° c: An IPCC Special Report on impacts of global warming of 1.5° c above pre-industrial levels and related global greenhouse gas emission pathways, in the contex of strengthening the global response to the thereat of blimate change, s. *(No Title)*.

Masson-Delmotte, V., Zhai, P., Pirani, A., Connors, S. L., Péan, C., Berger, S., Caud, N., Chen, Y., Goldfarb, L., & Gomis, M. I. (2021). Climate change 2021: the physical science basis. *Contribution of Working Group I to the Sixth Assessment Report of the Intergovernmental Panel on Climate Change*, *2*.

McMahon, T. A., Peel, M. C., & Karoly, D. J. (2015). *Assessment of precipitation and temperature data from CMIP3 global climate models for hydrologic simulation*. https://doi.org/10.5194/hess-19-361-2015

Mcsweeney, C. F., & Jones, R. G. (2016). CMIP5 GCMs used in ISI-MIP ? *Climate Services*, 1–6. https://doi.org/10.1016/j.cliser.2016.02.001

McSweeney, C. F., Jones, R. G., Lee, R. W., & Rowell, D. P. (2015). Selecting CMIP5 GCMs for downscaling over multiple regions. *Climate Dynamics*, *44*(11–12), 3237–3260. https://doi.org/10.1007/s00382-014-2418-8

Meehl, G. A., Covey, C., McAvaney, B., Latif, M., & Stouffer, R. J. (2005). Overview of the coupled model intercomparison project. *Bulletin of the American Meteorological Society*, *86*(1), 89–93. https://doi.org/10.1175/BAMS-86-1-89

Meenu, R., Rehana, S., & Mujumdar, P. P. (2013). Assessment of hydrologic impacts of climate change in Tunga-Bhadra river basin, India with HEC-HMS and SDSM. *Hydrological Processes*, *27*(11), 1572–1589. https://doi.org/10.1002/hyp.9220

Mirza, M. M. Q. (2003). Climate change and extreme weather events: Can developing countries adapt? *Climate Policy*, *3*(3), 233–248. https://doi.org/10.3763/cpol.2003.0330

Mishra, V. (2020). Long-term (1870–2018) drought reconstruction in context of surface water security in India. *Journal of Hydrology*, *580*, 124228.https://doi.org/10.1016/j.jhydrol.2019.124228

Mishra, V. (2022). *Multiday Precipitation Is a Prominent Driver of Floods in Indian River Basins Multi-day precipitation is a prominent driver of floods in Indian river basins*. *July*. https://doi.org/10.1029/2022WR032723

Mishra, V., Aaadhar, S., Shah, H., Kumar, R., Pattanaik, D. R., & Tiwari, A. D. (2018). The Kerala flood of 2018: combined impact of extreme rainfall and reservoir storage. *Hydrology and Earth System Sciences Discussions*, *September*, 1–13. https://doi.org/10.5194/hess-2018-480

Mishra, V., Bhatia, U., & Tiwari, A. D. (2020). Bias-corrected climate projections for South Asia from Coupled Model Intercomparison Project-6. *Scientific Data*, *7*(1), 1–13. https://doi.org/10.1038/s41597-020-00681-1

Mishra, V., & Lilhare, R. (2016). Hydrologic sensitivity of Indian sub-continental river basins to climate change. *Global and Planetary Change*, *139*, 78–96. https://doi.org/10.1 016/j.gloplacha.2016.01.003

Mohan, T. S., & Rajeevan, M. (2017). Past and future trends of hydroclimatic intensity over the Indian monsoon region. *Journal of Geophysical Research*, *122*(2), 896–909. https://doi.org/10.1002/2016JD025301

Moriasi, D. N., Arnold, J. G., Van Liew, M. W., Bingner, R. L., Harmel, R. D., & Veith, T. L. (2007). Model evaluation guidelines for systematic quantification of accuracy in watershed simulations. *Transactions of the ASABE*, *50*(3), 885–900.

Moriasi, N. D., W. Gitau, M., Pai, N., & Daggupati, P. (2015). Hydrologic and Water Quality

Models: Performance Measures and Evaluation Criteria. *Transactions of the ASABE*, *58*(6), 1763–1785. https://doi.org/10.13031/trans.58.10715

Mukherjee, S., Aadhar, S., Stone, D., & Mishra, V. (2018). Increase in extreme precipitation events under anthropogenic warming in India. *Weather and Climate Extremes*, *20*(March), 45–53. https://doi.org/10.1016/j.wace.2018.03.005

Nanditha, J. S., & Mishra, V. (2022). Multiday Precipitation Is a Prominent Driver of Floods in Indian River Basins. *Water Resources Research*, *58*(7), 1–17. https://doi.org /10.1029/2022WR032723

Narsimlu, B., Gosain, A. K., & Chahar, B. R. (2013). Assessment of Future Climate Change Impacts on Water Resources of Upper Sind River Basin, India Using SWAT Model. *Water Resources Management*, *27*(10), 3647–3662. https://doi.org/10.1007/s11269-013-0371-7

Nashwan, M. S., & Shahid, S. (2019). A novel framework for selecting general circulation models based on the spatial patterns of climate. *International Journal of Climatology*, *n/a*(n/a). https://doi.org/10.1002/joc.6465

Ndhlovu, G. Z., & Woyessa, Y. E. (2020). Modelling impact of climate change on catchment water balance, Kabompo River in Zambezi River Basin. *Journal of Hydrology: Regional Studies*, *27*(December 2019), 100650. https://doi.org/10.1016/j.ejrh.2019.100650

Neitsch, S. ., Arnold, J. ., Kiniry, J. ., & Williams, J. . (2011). Soil & Water Assessment Tool Theoretical Documentation Version 2009. *Texas Water Resources Institute*, 1–647. https://doi.org/10.1016/j.scitotenv.2015.11.063

Ngai, S. T., Tangang, F., & Juneng, L. (2017). Bias correction of global and regional simulated daily precipitation and surface mean temperature over Southeast Asia using quantile mapping method. *Global and Planetary Change*, *149*, 79–90. https://doi.org/10.10 16/j.gloplacha.2016.12.009

Nikam, B. R., Garg, V., Jeyaprakash, K., Gupta, P. K., Srivastav, S. K., Thakur, P. K., & Aggarwal, S. P. (2018). Analyzing future water availability and hydrological extremes in the Krishna basin under changing climatic conditions. *Arabian Journal of Geosciences*, *11*(19). https://doi.org/10.1007/s12517-018-3936-1

Nilawar, A. P., & Waikar, M. L. (2019). Impacts of climate change on streamflow and sediment concentration under RCP 4.5 and 8.5: A case study in Purna river basin, India. *Science of The Total Environment*, *650*, 2685–2696. https://doi.org/10.1016/j.scitotenv.2018.09.334

Noor, M., Ismail, T., Shahid, S., Nashwan, M. S., & Ullah, S. (2019). Development of multi-model ensemble for projection of extreme rainfall events in Peninsular Malaysia. *Hydrology Research*, *50*(6), 1772–1788. https://doi.org/10.2166/nh.2019.097

O'Neill, B. C., Tebaldi, C., Van Vuuren, D. P., Eyring, V., Friedlingstein, P., Hurtt, G., Knutti, R., Kriegler, E., Lamarque, J. F., Lowe, J., Meehl, G. A., Moss, R., Riahi, K., & Sanderson, B. M. (2016). The Scenario Model Intercomparison Project (ScenarioMIP) for CMIP6. *Geoscientific Model Development*, *9*(9), 3461–3482. https://doi.org/10.51 94/gm d-9-3461-2016

Pai, D. S., Sridhar, L., Rajeevan, M., Sreejith, O. P., Satbhai, N. S., & Mukhopadhyay, B. (2014). Development of a new high spatial resolution (0.25× 0.25) long period (1901–2010) daily gridded rainfall data set over India and its comparison with existing data sets over the region. *Mausam*, *65*(1), 1–18.

Pandey, B. K., Khare, D., Kawasaki, A., & Meshesha, T. W. (2021). Integrated approach to simulate hydrological responses to land use dynamics and climate change scenarios employing scoring method in upper Narmada basin, India. *Journal of Hydrology*, *598*(November 2020), 126429. https://doi.org/10.1016/j.jhydrol.2021.126429

Pandey, B. K., Khare, D., Kawasaki, A., & Mishra, P. K. (2019). Climate Change Impact Assessment on Blue and Green Water by Coupling of Representative CMIP5 Climate Models with Physical Based Hydrological Model. *Water Resources Management*, *33*(1), 141–158. https://doi.org/10.1007/s11269-018-2093-3

Pankaj, K. R., & Asis, M. (2013). Water Resources in India under Changed Climate Scenario. *Asis Mazumdar / International Journal of Engineering Research and Applications (IJERA)*, *3*(1), 954–961. www.ijera.com

Perkins, S. E., Pitman, A. J., Holbrook, N. J., & McAneney, J. (2007). Evaluation of the AR4 Climate Models' Simulated Daily Maximum Temperature, Minimum Temperature, and Precipitation over Australia Using Probability Density Functions. *Journal of Climate*,

20(17), 4356–4376. https://doi.org/10.1175/JCLI4253.1

Piani, C., Weedon, G. P., Best, M., Gomes, S. M., Viterbo, P., Hagemann, S., & Haerter, J. O. (2010). Statistical bias correction of global simulated daily precipitation and temperature for the application of hydrological models. *Journal of Hydrology*, *395*(3–4), 199–215. https://doi.org/10.1016/j.jhydrol.2010.10.024

Pour, S. H., Shahid, S., & Chung, E. (2018). State Key Laboratory of Hydrology-Water Resources and Hydraulic Engineering , Nanjing SC. *Atmospheric Research*, #pagerange#. https://doi.org/10.1016/j.atmosres.2018.06.006

Pour, S. H., Shahid, S., Chung, E. S., & Wang, X. J. (2018). Model output statistics downscaling using support vector machine for the projection of spatial and temporal changes in rainfall of Bangladesh. *Atmospheric Research*, *213*(December 2017), 149–162. https://doi.org/10.1016/j.atmosres.2018.06.006

Press, W. H., Teukolsky, S. A., Vetterling, W. T., & Flannery, B. P. (1996). *Numerical Recipes: The Art of Scientific Computing with IBM PC or Macintosh*. Cambridge University Press.

Rajeevan, M., Bhate, J., & Jaswal, A. K. (2008). Analysis of variability and trends of extreme rainfall events over India using 104 years of gridded daily rainfall data. *Geophysical Research Letters*, *35*(18), 1–6. https://doi.org/10.1029/2008GL035143

Rajeevan, M., Bhate, J., Kale, J. D., & Lal, B. (2006). High resolution daily gridded rainfall data for the Indian region: Analysis of break and active monsoon spells. *Current Science*, *91*(3), 296–306. https://www.jstor.org/stable/24094135

Raju, K S., & Nagesh Kumar, D. (2015). Ranking general circulation models for India using TOPSIS. *Journal of Water and Climate Change*, *6*(2), 288–299. https://doi.org/10.2166/wcc.2014.074

Raju, K S., & Nagesh Kumar, D. (2016). Selection of global climate models for India using cluster analysis. *Journal of Water and Climate Change*, *7*(4), 764–774. https://doi.org/10.2166/wcc.2016.112

Raju, K S, & Nagesh kumar D. (2014). Ranking of global climate models for India using multicriterion analysis. *Climate Research*, *60*(2), 103–117. DOI: https://doi.org/10.3

354/cr01222

Raju, K S, Sonali, P., & Nagesh kumar D. (2017). *Ranking of CMIP5-based global climate models for India using compromise programming*. 563–574. https://doi.org/10.1007 /s00704-015-1721-6

Randall, D. A., Wood, R. A., Bony, S., Colman, R., Fichefet, T., Fyfe, J., Kattsov, V., Pitman, A., Shukla, J., Srinivasan, J., Ronald, S., Sumi, A., & Taylor, K. E. (2007). Climate Models and Their Evaluation. In *Climate Change 2007: The Physical Science Basis. Contribution of Working Group I to the fourth Assessment Report of the Intergovernmen tal Panel ond climate Change*.

Rathinasamy, M., Khosa, R., Adamowski, J., ch, S., Partheepan, G., Anand, J., & Narsimlu, B. (2014). Wavelet-based multiscale performance analysis: An approach to assess and improve hydrological models. *Water Resources Research*, *50*(12), 9721–9737. https://do i.org/10.1002/2013WR014650

Reshmidevi, T. V., Nagesh Kumar, D., Mehrotra, R., & Sharma, A. (2018). Estimation of the climate change impact on a catchment water balance using an ensemble of GCMs. *Journal of Hydrology*, *556*, 1192–1204. https://doi.org/10.1016/j.jhydrol.2017.02.016

Riahi, K., van Vuuren, D. P., Kriegler, E., Edmonds, J., O'Neill, B. C., Fujimori, S., Bauer, N., Calvin, K., Dellink, R., Fricko, O., Lutz, W., Popp, A., Cuaresma, J. C., KC, S., Leimbach, M., Jiang, L., Kram, T., Rao, S., Emmerling, J., … Tavoni, M. (2017). The Shared Socioeconomic Pathways and their energy, land use, and greenhouse gas emissions implications: An overview. *Global Environmental Change*, *42*, 153–168. /https://doi.or g/10.1016/j.gloenvcha.2016.05.009

Roy, S. Sen, & Balling, R. C. (2004). Trends in extreme daily precipitation indices in India. *International Journal of Climatology*, *24*(4), 457–466. https://doi.org/10.1002/joc.995

Ruan, Y., Yao, Z., Wang, R., & Liu, Z. (2018). Ranking of CMIP5 GCM Skills in Simulating Observed Precipitation over the Lower Mekong Basin, Using an Improved Score-Based Method. In *Water* (Vol. 10, Issue 12). https://doi.org/10.3390/w10121868

Sachindra, D. A., Huang, F., Barton, A. F., & Perera, B. J. C. (2014). Multi-model ensemble approach for statistically downscaling general circulation model outputs to precipitation.

Quarterly Journal of the Royal Meteorological Society, *140*(681), 1161–1178. https://doi.org/10.1002/qj.2205

Sadhwani, K., Eldho, T. I., & Karmakar, S. (2023). Investigating the influence of future landuse and climate change on hydrological regime of a humid tropical river basin. *Environmental Earth Sciences*, *82*(9), 1–19. https://doi.org/10.1007/s12665-023-10891-6

Sahoo, S., Dhar, A., Debsarkar, A., & Kar, A. (2018). Impact of water demand on hydrological regime under climate and LULC change scenarios. *Environmental Earth Sciences*, *77*(9), 1–19. https://doi.org/10.1007/s12665-018-7531-2

Salman, S. A., Shahid, S., Ismail, T., Al-Abadi, A. M., Wang, X., & Chung, E.-S. (2019). Selection of gridded precipitation data for Iraq using compromise programming. *Measurement*, *132*, 87–98. https://doi.org/10.1016/j.measurement.2018.09.047

Salman, S. A., Shahid, S., Ismail, T., & Wang, X. (2018). Selection of climate models for projection of spatiotemporal changes in temperature of Iraq with uncertainties. *Atmos pheric Research*. https://doi.org/10.1016/j.atmosres.2018.07.008

Sanchez-Gomez, E., Somot, S., & Déqué, M. (2009). Ability of an ensemble of regional climate models to reproduce weather regimes over Europe-Atlantic during the period 1961-2000. *Climate Dynamics*, *33*(5), 723–736. https://doi.org/10.1007/s00382-008-0502-7

Sarma, J.., 2011. Impact of High Rinfall/Floods on Groundwater Resources in the Krishna River Basin (During 1999-2009).

Sarthi, P., Kumar, P., & Ghosh, S. (2016). Possible future rainfall over Gangetic Plains (GP), India, in multi-model simulations of CMIP3 and CMIP5. Theoretical and Applied Climatology, 124(3–4), 691–701. https://doi.org/10.1007/s00704-015-1447-5

Sen, P. K. (1968). Estimates of the regression coefficient based on Kendall's tau. *Journal of the American Statistical Association*, *63*(324), 1379–1389.

Sheffield, J., & Wood, E. F. (2008). Projected changes in drought occurrence under future global warming from multi-model, multi-scenario, IPCC AR4 simulations. *Climate Dynamics*, *31*(1), 79–105. https://doi.org/10.1007/s00382-007-0340-z

Shiru, M. S., Shahid, S., Chung, E. S., Alias, N., & Scherer, L. (2019). A MCDM-based

framework for selection of general circulation models and projection of spatio-temporal rainfall changes: A case study of Nigeria. *Atmospheric Research*, *225*, 1–16. https://doi.org/10.1016/j.atmosres.2019.03.033

Shreem, S. S., Abdullah, S., & Nazri, M. Z. A. (2016). Hybrid feature selection algorithm using symmetrical uncertainty and a harmony search algorithm. *International Journal of Systems Science*, *47*(6), 1312–1329. https://doi.org/10.1080/00207721.2014.924600

Singh, D., Gupta, R. D., & Jain, S. K. (2015). Study of daily extreme temperature indices over sutlej basin, N-W Himalayan Region, India. *Global Nest Journal*, *17*(2), 301–311. https://doi.org/10.30955/gnj.001520

Singh, G. R., Jain, M. K., & Gupta, V. (2019). Spatiotemporal assessment of drought hazard, vulnerability and risk in the Krishna River basin, India. *Natural Hazards*, *99*(2), 611–635. https://doi.org/10.1007/s11069-019-03762-6

Sinha, R. K., & Eldho, T. I. (2018). Effects of historical and projected land use/cover change on runoff and sediment yield in the Netravati river basin, Western Ghats, India. *Environmental Earth Sciences*, *77*(3), 1–19. https://doi.org/10.1007/s12665-018-7317-6

Sinha, R. K., Eldho, T. I., & Subimal, G. (2020). Assessing the impacts of land use/land cover and climate change on surface runoff of a humid tropical river basin in Western Ghats, India. *International Journal of River Basin Management*, *0*(0), 1–38. https://doi.org/ 10.1 080/15715124.2020.1809434

Snyder, R. L., Moratiel, R., Song, Z., Swelam, A., Jomaa, I., & Shapland, T. (2011). Evapotranspiration response to climate change. *Acta Horticulturae*, *922*(May 2021), 91–98. https://doi.org/10.17660/ActaHortic.2011.922.11

Tabari, H., Paz, S. M., Buekenhout, D., & Willems, P. (2021). Comparison of statistical downscaling methods for climate change impact analysis on precipitation-driven drought. *Hydrology and Earth System Sciences*, *25*(6), 3493–3517. https://doi.org/10.5194/hess-25-3493-2021

Talchabhadel, R., Aryal, A., Kawaike, K., Yamanoi, K., & Nakagawa, H. (2021). A comprehensive analysis of projected changes of extreme precipitation indices in West Rapti River basin, Nepal under changing climate. *International Journal of Climatology*,

41(S1), E2581–E2599. https://doi.org/10.1002/joc.6866

Talchabhadel, R., Karki, R., Thapa, B. R., Maharjan, M., & Parajuli, B. (2018). Spatio-temporal variability of extreme precipitation in Nepal. *International Journal of Climatology*, *38*(11), 4296–4313. https://doi.org/10.1002/joc.5669

Tebaldi, C., & Knutti, R. (2007). The use of the multi-model ensemble in probabilistic climate projections. *Philosophical Transactions of the Royal Society A: Mathematical, Physical and Engineering Sciences*, *365*(1857), 2053–2075. https://doi.org/1 0.1098/ rsta.200 7.2076

Teutschbein, C., & Seibert, J. (2012). Bias correction of regional climate model simulations for hydrological climate-change impact studies: Review and evaluation of different methods. *Journal of Hydrology*, *456–457*, 12–29. https://doi.org/10.1016/j.jhydrol.2012 .05.052

Theil, H. (1992). *A Rank-Invariant Method of Linear and Polynomial Regression Analysis*. *3*(1950), 345–381. https://doi.org/10.1007/978-94-011-2546-8_20

Tiwari, P. R., Kar, S. C., Mohanty, U. C., Kumari, S., Sinha, P., Nair, A., & Dey, S. (2014). Skill of precipitation prediction with GCMs over north India during winter season. *International Journal of Climatology*, *34*(12), 3440–3455. https://doi.org/10.1002/joc.3 921

Trenberth, K. E., Fasullo, J. T., & Mackaro, J. (2011). Atmospheric moisture transports from ocean to land and global energy flows in reanalyses. *Journal of Climate*, *24*(18), 4907–4924. https://doi.org/10.1175/2011JCLI4171.1

van Pelt, S. C., Beersma, J. J., Buishand, T. A., van den Hurk, B. J. J. M., & Schellekens, J. (2015). Uncertainty in the future change of extreme precipitation over the Rhine basin: the role of internal climate variability. *Climate Dynamics*, *44*(7–8), 1789–1800. https:/ /doi.org/10.1007/s00382-014-2312-4

Wang, M., Zhang, L., & Baddoo, T. D. (2016). Hydrological Modeling in A Semi-Arid Region Using HEC-HMS. *Journal of Water Resource and Hydraulic Engineering*, *5*(3), 105–115. https://doi.org/10.5963/jwrhe0503004

Wang, S., Kang, S., Zhang, L., & Li, F. (2008). Modelling hydrological response to different land-use and climate change scenarios in the Zamu River basin of northwest China. *Hydrological Processes*, *22*(14), 2502–2510. https://doi.org/10.1002/hyp.6846

Woldemeskel, F. M., Sharma, A., Sivakumar, B., & Mehrotra, R. (2014). A framework to quantify GCM uncertainties for use in impact assessment studies A framework to quantify GCM uncertainties for use in impact assessment studies. *JOURNAL OF HYDROLOGY*, *519*(November 2017), 1453–1465. https://doi.org/10.1016/j.jhydrol.2014.09.025

Woldesenbet, T. A., Elagib, N. A., Ribbe, L., & Heinrich, J. (2018). Catchment response to climate and land use changes in the Upper Blue Nile sub-basins, Ethiopia. *Science of the Total Environment*, *644*, 193–206. https://doi.org/10.1016/j.scitotenv.2018.06.198

Wood, A. W., Leung, L. R., Sridhar, V., & Lettenmaier, D. P. (2004). Hydrologic implications of dynamical and statistical approaches to downscaling climate model outputs. *Climatic Change*, *62*(1–3), 189–216. https://doi.org/10.1023/B:CLIM.0000013685.99609.9e

Wu, Y., & Zhang, A. (2004). Feature selection for classifying high-dimensional numerical data. *Proceedings of the 2004 IEEE Computer Society Conference on Computer Vision and Pattern Recognition, 2004. CVPR 2004.*, *2*, II–II.

WWAP, U. (2012). *World Water Assessment Programme: The United Nations World Water Development Report 4: Managing Water under Uncertainty and Risk*. Paris: UNESCO.

Xie, P., Chen, M., & Shi, W. (2010). CPC unified gauge-based analysis of global daily precipitation. *Preprints, 24th Conf. on Hydrology, Atlanta, GA, Amer. Meteor. Soc*, *2*.

Xing, W., & Wang, B. (2017). Predictability and prediction of summer rainfall in the arid and semi-arid regions of China. *Climate Dynamics*, *49*(1–2), 419–431. https://doi.org/10.1007/s00382-016-3351-9

Xu, C. (1999). Climate change and hydrologic models: A review of existing gaps and recent research developments. *Water Resources Management*, *13*(5), 369–382. https://doi.org/10.1023/A:1008190900459

Ye, D. Z., & Chen, P. Q. (1992). *Global change in China: a preliminary study*. Meteorological Press, Beijing (In Chinese.).

Zhang, H., & Huang, G. H. (2013). Development of climate change projections for small watersheds using multi-model ensemble simulation and stochastic weather generation. *Climate Dynamics*, *40*(3–4), 805–821. https://doi.org/10.1007/s00382-012-1490-1

Zhang, L., Nan, Z., Yu, W., & Ge, Y. (2016). Hydrological Responses to Land-Use Change Scenarios under Constant and Changed Climatic Conditions. *Environmental Managemen t*, *57*(2), 412–431. https://doi.org/10.1007/s00267-015-0620-z

Zhang, X., Alexander, L., Hegerl, G. C., Jones, P., Tank, A. K., Peterson, T. C., Trewin, B., & Zwiers, F. W. (2011). Indices for monitoring changes in extremes based on daily tempera ture and precipitation data. *Wiley Interdisciplinary Reviews: Climate Change*, *2*(6), 851–870. https://doi.org/10.1002/wcc.147

PUBICATIONS FROM THE RESEARCH

1. **Anil, S.,** Manikanta, V., & Pallakury, A. R. (2021). Unravelling the influence of subjectivity on ranking of CMIP6 based climate models: A case study. International Journal of Climatology, 1–19. https://doi.org/10.1002/joc.7164
2. **Anil, S.,** & Anand Raj, P. (2022). Deciphering the projected changes in CMIP-6 based precipitation simulations over the Krishna River Basin. Journal of Water and Climate Change, 13(3), 1389–1407. https://doi.org/10.2166/wcc.2022.399
3. **Anil, S.,** & Anand Raj, P. (2023), "An exhaustive investigation of changes in projected extreme precipitation indices and streamflows using CMIP6 climate models: A case study". Journal of Earth System Science – Accepted
4. **Suram Anil**, Anand Raj P, Vamsi Krishna Vema; Catchment response to climate change under CMIP6 scenarios: a case study of the Krishna River Basin. Journal of Water and Climate Change 2024; jwc2024442. https://doi.org/10.2166/wcc.2024.442
5. **Anil, S.,** & Anand Raj, P., (2023), "Investigating projected impacts of climate and land use/land cover changes on hydrological responses Tungabhadra basin, KRB, India" paper draft is under correction.

Conference Presentations

1. **Anil, S.,** & Anand Raj, P., (2019), "Climate change impact on Maneru River basin using SWAT", International Conference on Hydraulics, Water Resources, & Coastal Engineering, Osmania University Hyderabad. 18-20 Dec.